Role of the NADPH oxidase NOX4 in hepatocyte proliferation

Macarena Herranz Itúrbide

Role of the NADPH oxidase Nox4 in hepatocyte proliferation. Relevance on liver regeneration

Report presented by

Macarena Herranz Itúrbide

To obtain the title of

Doctor of Philosophy (Ph.D.)

Supervised by:

Isabel Fabregat, PhD

Judit López, PhD

TGF-β and cancer group

Bellvitge Biomedical Research Institute (IDIBELL) - ONCOBELL Program

Doctoral Program in Biomedicine (University of Barcelona)

Abbreviations

ADAMTSL2	A disintegrin and metalloproteinase with thrombospondin repeats-like 2
ALK-5	Activin receptor-like kinase 5
AR	Amphiregulin
BEC	Biliary epithelial cells
BET	Bromodomain and extraterminal
BMP	Bone Morphogenic Protein
BSA	Bovine serum albumin
CAF	Cancer Associated Fibroblast
CCl$_4$	Carbon tetrachloride
CD36	Cluster of differentiation 36
CDK	Cyclin dependent kinase
CGD	Chronic granulomatous disease
CIP	CDK-interacting protein
CKI	Cdk inhibitors
Co-SMAD	Cooperating SMAD
D.A.B.	Diaminobenzidine
DAMPs	Damage-Associated Molecular Patterns
DAPI	4 ',6-diamidino-2-fenilindol
DEG	Differentially Expressed Genes
DEN	Diethylnitrosamine
DH	Dehydrogenase
DMN	Dimethylnitrosamine
ECM	Extracellular matrix
ECM1	Extracellular matrix protein 1
EDTA	Ethylenediaminetetraacetic acid
EGF	Epidermal Growth Factor
EGFR	Epidermal growth factor receptor
EMT	Epithelial-to-Mesenchymal Transition
ER	Endoplasmic reticulum
ERK1/2	Extracellular signal-regulated kinase 1 and 2
FAD	Flavine adenine dinucleotide
FBS	Fetal bovine serum
FFA	Free fatty acids
FOXO	Forkhead box O
GDF	Growth and differentiation factors

GF	Growth factor
GO	Gene Ontology
GPC3	Glypican 3
GPx	Glutathione peroxidase
GSH	Glutathione
GSSG	Glutathione disulphide
h	Hours
H&E	Hematoxylin and Eosin
HB-EGF	Heparin binding EGF-like growth factor
HCC	Hepatocellular Carcinoma
HGF	Hepatocyte Growth Factor
HIF-1α	Hypoxia-Inducible Factor 1α
HNF4α	Hepatocyte nuclear factor 4 alpha
HPASMC	Human pulmonary artery smooth muscle cells
HRP	Horseradish Peroxidase
HSC	Hepatic stellate cells
HSP27	Heat shock protein 27
HUVEC	Human umbilical vein endothelial cell
HUCMSC	Human umbilical cord mesenchymal stem cells
I-SMAD	Inhibitory SMAD
IGF	Insulin-like growth factor
IHC	Immunohistochemistry
IL-6	Interleukin-6
ILK	Integrin Linked Kinase
JNK	c-Jun terminal kinase
KC	Kupffer cell
LAP	Latency-Associated Peptide
LLC	Large latent complex
LPS	Lipopolysaccharides
LSEC	Liver sinusoidal endothelial cells
LTBP	Latent TGF-β binding protein
M6P/IGFII-R	Mannose-6-phosphate/type II insulin-like growth factor receptor
MAPK	Mitogen-activated protein kinase
MFB	Myofibroblast
MMP	Matrix metalloprotease

mTOR	Mammalian target of rapamycin
NADPH	Nicotinamide adenine dinucleotide phosphate
NASH	Non-alcoholic steatohepatitis
NF-κB	Nuclear factor-kappa B
NICD	Notch1 intracellular domain
NOX	Nicotinamide adenine dinucleotide phosphate (NADPH) oxidase
NOXA1	Nox activator 1
NOXO1	Nox organizer 1
Nrf2	Nuclear factor-erythroid 2 related factor 2
OCT	Optimal Cutting Temperature
PAMPs	Pathogen-Associated Molecular Patters
PBS	Phosphate-buffered saline
PBS-T	PBS-Tween
PCR	polymerase chain reaction
PDK4	Pyruvate Dehydrogenase Kinase 4
PFA	paraformaldehyde
PGC-1β	Peroxisome proliferation-activated receptor γ coactivator 1-β
PH	Partial hepatectomy
PI3K	Phosphatidylinositol-3-kinase
Poldip2	Polymerase-δ-interacting protein 2
PPAR	Peroxisome proliferation-activated receptor
pRb	retinoblastoma protein phosphorylation
PTP	Protein tyrosine phosphatases
RGD	Arginine-glycine-aspartate
ROS	Reactive oxygen species
RT	Reverse transcription
RT	Room Temperature
SARA	Smad anchor for receptor activation
SBE	SMAD-binding elements
SDS	Sodium Dodecyl Sulfate
SEC	Sinusoidal Endothelial Cells
SEM	Standard Error of the Mean
SOD	Superoxide dismutase
STAT3	Signal transducer and activator of transcription 3
TACE	Tumor necrosis factor-α-converting enzyme

TG	Triglycerides
TGF-α	Transforming growth factor-alpha
TGF-β	Transforming growth factor-beta
TGF-β RI	Transforming growth factor-beta Receptor I
TGF-β RII	Transforming growth factor-beta Receptor II
TNFR1	TNF receptor 1
TNF-α	Tumor necrosis factor-alpha
uPA	Urokinase plasminogen activator
uPA-R	Urokinase plasminogen activator receptor
VEOIBD	Very early-onset inflammatory bowel disease
VLDL	Very-low-density lipoprotein
VSMC	Vascular smooth muscle cell
RT-qPCR	Real Time Quantitative Polymerase Chain Reaction
R-SMAD	Receptor-associated SMAD
Rb	Retinoblastoma
WB	Western Blot
WT	Wild Type
TRIS	Tris(hydroxymethyl)aminomethane

Table of contents

I. Introduction

1. The liver

1.1. Liver anatomy

The liver is the **largest internal organ** in the human body, accounting for approximately 2 to 3% of average body weight. The liver has **numerous vital functions**, and its highly organized structure is important to carry out all these functions (Abdel-Misih & Bloomston, 2010; Abu Rmilah et al., 2019; Spear et al., 2006).

The human liver is grossly divided into left and right lobes by the falciform filament, but surgically, it can be divided into 8 segments. The upper surface of the liver is called the facies diaphragmatica, whereas the lower surface is called visceral surface. In mice and rats, the liver is divided into 4 lobes: median (or middle), left, right and caudate. All of them, except the left, are further subdivided into two or more parts. Mice and humans have a gall bladder, but not rats (Abu Rmilah et al., 2019; Malarkey et al., 2005).

The main architectural unit of the liver is the **liver lobule**. Liver lobules are roughly hexagonal structures, with a central vein in the center of the lobule and a portal triad of vessels in each of the six corners. The portal triad is comprised of portal vein, bile duct, and hepatic artery (**Figure I**). The portal vein, which comes from the large intestine, spleen and pancreas, supplies about 70-75% of the blood flow and 40% of the oxygen, and the hepatic artery supplies 25-30% of the blood flow and 60% of the oxygen. Hepatocytes form cords and arrange radially around the central vein. They are the major parenchymal cells of the liver and account for almost 80% of liver volume (Abdel-Misih & Bloomston, 2010; Abu Rmilah et al., 2019; Malarkey et al., 2005; Si-Tayeb et al., 2010). Apart from hepatocytes, the liver is composed of other cell types, including biliary epithelial cells (BECs) or cholangiocytes, hepatic stellate cells (HSCs), Kupffer cells (KCs) and liver sinusoidal endothelial cells (LSECs). Each of these cell types have a different embryological origin and possesses unique functions, which in cooperation regulate hepatic vital functions (Trefts et al., 2017).

The hepatocytes are polarized epithelial cells. The basolateral surfaces of the hepatocyte face the LSECs, and the narrow region between these two cell types is known as space of Disse. LSECs form fenestrated plates at the sinusoidal lumen, with pores ranging in size from 50–180 nm in humans or 50–280 nm in mice and rats. This organization facilitates exchange of proteins and particles between plasma and the cells of the liver, while maintaining some barrier functions. Sinusoidal blood flow, coming from the portal vein and the hepatic artery, is finally collected into central veins, then into larger hepatic veins, and

finally lead to the vena cava. In the apical surface of hepatocytes, tight junctions between neighboring hepatocytes generate a canaliculus that collect bile, which is carried to the bile ducts, and subsequently transported for storage in the gall bladder. Cholangiocytes, which are the second most abundant population of the liver, have an epithelial function in the lumen of the bile ducts. In the case of HSCs, they can exist in a quiescent or activated state. When quiescent, they store vitamin A in lipid droplets. Upon liver damage and subsequent activation, stellate cells proliferate, lose their vitamin A stores and produce collagen, process that contributes to scarring of the liver. The transition region between the canaliculus and intrahepatic bile ducts is called the canal of Hering, narrow channels that are lined by hepatocytes and cholangiocytes. Interestingly, the canals of Hering contain a small population of cells called Oval cells, which are resident stem cells in the adult liver. They can function as progenitor cells for both hepatocytes and cholangiocytes. Finally, KCs represents 15 % of liver cells and they are the resident macrophage population. They exert its phagocytic function in the sinusoidal lining, where they are located. KCs are able of recognizing pathogenic stimuli introduced through the portal circulation, such as aged red blood cells and microbes, and can attain pro- or anti-inflammatory roles in liver wound healing depending on several factors (Malarkey et al., 2005; Si-Tayeb et al., 2010; Spear et al., 2006; Trefts et al., 2017).
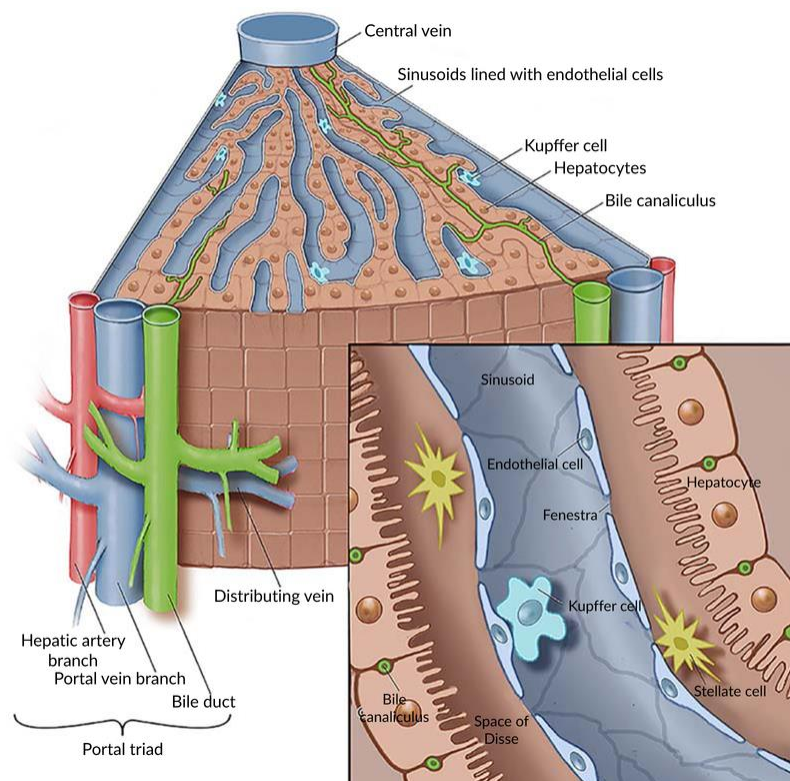
Figure I. Microscopic anatomy of liver showing the central vein, the portal triad and the different hepatic cells (Abu Rmilah et al., 2019).

In addition, **extracellular matrix** (ECM) plays an important role in the regulation and modulation of hepatic functions. Between 5 and 10% of the hepatic ECM is collagen. Apart from collagen, the ECM has numerous components such as matrix metalloproteinases; glycoproteins like laminin, fibronectin, vitronectin, undulin and nidogen (entactin); proteoglycans such as heparan sulfate; as well as cytokines and growth factors such as Transforming Growth Factor-β (TGF-β) and Hepatocyte Growth Factor (HGF) (Kang et al., 2012; Malarkey et al., 2005).

1.2. Liver functions

The liver is a critical hub for many biological processes, including macronutrient metabolism, blood volume regulation, immune system support, endocrine control of growth signaling pathways, lipid and cholesterol homeostasis, and the detoxification of xenobiotic compounds. Over the course of evolution, all these functions have been combined in a single organ, the liver, which is conserved in all vertebrates. This section highlights some of its numerous functions (Leiskau & Baumann, 2017; Trefts et al., 2017).

- *Proteins.* The liver accounts for 85-90 % of circulating protein volume. Albumin, which regulates blood volume, is the most abundant of these secreted proteins. Within others, the liver also secretes transferrin, acute phase proteins that indicate inflammation, blood coagulation factors, and protease inhibitors. Additionally, the liver plays a role in protein and glycoprotein degradation and metabolism of amino acids, generating the highly toxic metabolite ammonia. The urea cycle is largely responsible for its removal.

- *Carbohydrates.* The liver has an important role in maintaining blood glucose. In a fed state, glucose is taken up by the hepatocytes from portal blood, and it is used as a precursor for glycogen synthesis for storage and pyruvate via glycolysis. In this state, insulin increases, which induces glycogen synthase, and glucagon (that stimulates gluconeogenesis) decreases. By contrast, in a fasting state, insulin decreases and glucagon increases; this shifts the liver to glucose output which requires glycogen breakdown and gluconeogenesis.

- *Lipids.* The liver obtains fatty acids from the blood from chylomicron remnants, and by *de novo* synthesis from glucose when hepatic glycogen stores are complete. These fatty acids are esterified to triglycerides (TGs) and stored in lipid droplets in hepatocytes. Those fatty acids that are not converted to TGs or used in the synthesis of other molecules, are used as energy source trough oxidative pathways.

  Cholesterol is a main component of all cell membranes and is necessary to produce steroid hormones and bile acids. The liver can uptake cholesterol from

lipoproteins and chylomicrons, or synthesize *de novo* by HMG-CoA reductase. In the liver, cholesterol is stored as cholesterol ester or "free" cholesterol.

Very-low-density lipoprotein (VLDLs) particles are secreted by the liver and carry TGs and cholesterol to other tissues. When the synthesis of TGs exceeds the capacity of the liver to export or the internal metabolism, a fatty liver disease is developed.

- *Exocrine function.* Bile is produced in hepatocytes (75%) and cholangiocytes (25%), and it is stored in the gallbladder. The bile facilitates the elimination of many compounds, including drugs, toxins, and waste products, cholesterol and bilirubin, and it also supplies bile salts to the intestine for the emulsification and absorption of dietary lipids and fat-soluble vitamins.

- *Endocrine function*. The liver plays an active role in endocrine regulation by producing several hormones. Within others, it produces the mitogenic polypeptide hormones insulin-like growth factor (IGF), angiotensinogen (important in the renin–angiotensin–aldosterone system) or thrombopoietin (stimulating platelet production).

- *Drug metabolism (xenobiotic metabolism).* Xenobiotics are absorbed by the gastrointestinal tract and reach the liver trough the portal vein. They are neutralized into nontoxic metabolites via the cytochrome P450 family enzymes, and then, they are conjugated with hydrophilic products (e.g., glucuronic acid or glutathione) to increase the water solubility. Once rendered hydrophilic, the drug metabolites are further metabolized or directly excreted through the bile or the kidneys (Abu Rmilah et al., 2019; Leiskau & Baumann, 2017; Trefts et al., 2017).

It is important to highlight that the lobular organization of the liver has functional significance. Oxygenated blood from the hepatic artery mixes with nutrient-enriched blood from the portal circulation before flowing over the cells of the lobule and draining into the central vein. As blood progresses across the lobule, it becomes deoxygenated and metabolic products are secreted from cells. This generates a number of gradients including oxygen, hormones, nutrients, and waste products, and results in a compartmentalization of functions based on localization. This phenomenon is termed 'metabolic zonation' and typically divide the lobule into three distinct 'zones' (**Figure II A**). For example, increased oxidative metabolism occurs in areas with higher blood oxygen content; periportal hepatocytes are also specialized in glycogenolysis and gluconeogenesis; and centrilobular hepatocytes are active in glycolysis and glycogen synthesis (from glucose) (**Figure II B**). Interestingly, this hepatic zonation exists on a flexible spectrum. For example, in response to damage or loss of function, hepatocytes from Zone 1 can assume the functional attributes

of Zone 2. Moreover, not only the hepatocytes present gradients of gene and protein activity, but gradients also exist for SECs, KCs, HSCs, and the matrix in the space of Disse (Fausto & Campbell, 2003; Malarkey et al., 2005; Trefts et al., 2017).
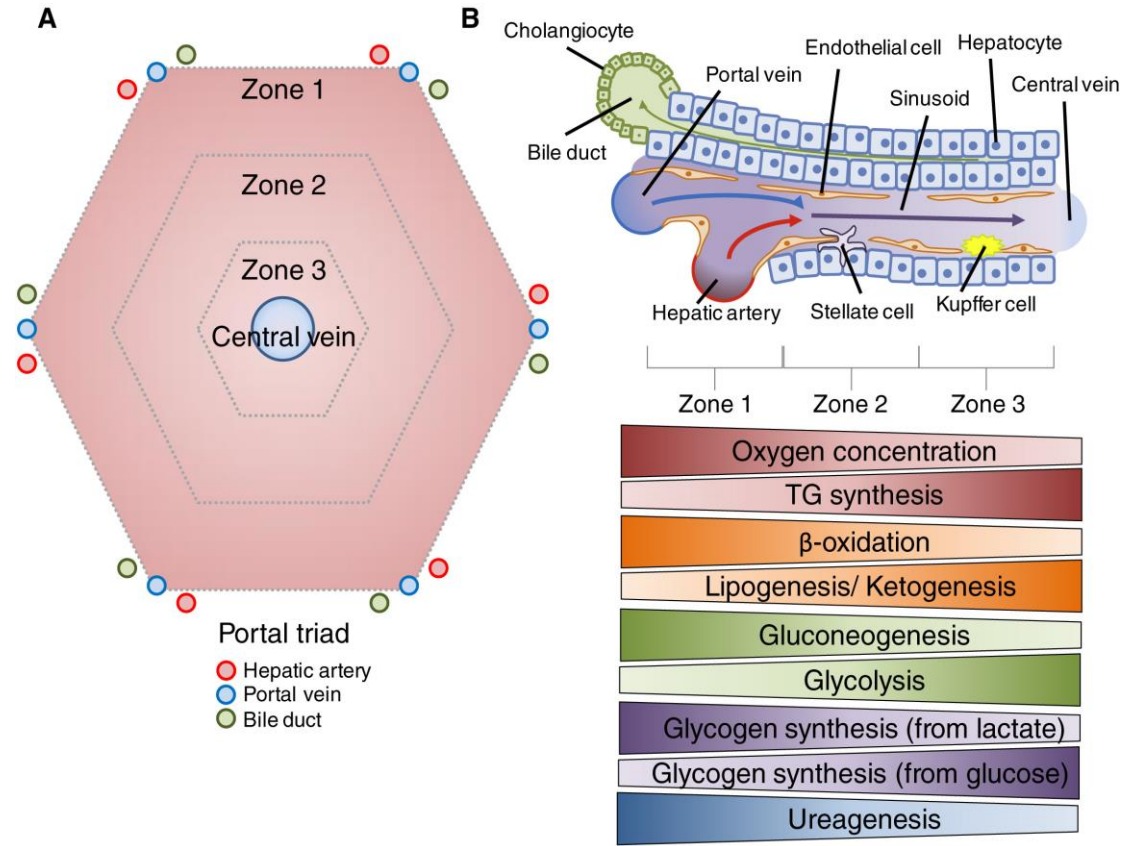
Figure II. A) Geometric representation of the hepatic lobule. **B)** Schematic representation of a sinusoid and the corresponding zonation of some metabolic processes across the sinusoid (Trefts et al., 2017).

2. Liver regeneration

In the Greek mythology, Prometheus stole the fire from Zeus and gave it to the mankind. As a punishment, Prometheus was tied up with a chain to the mountain Caucasus and an eagle ate his liver every single day. However, the following day, the liver was completely restored. This ancient myth is the oldest anecdote highlighting the incredible regenerative ability of the liver. Considering that the liver is an **indispensable center** for digestion, absorption, metabolism, and purification of many nutrients and substances in the body, liver regeneration (LR) safeguards all these functions in vertebrate organisms, from fish to mammals. Despite liver parenchymal cells (hepatocytes) are usually in a quiescent state in the adult liver, they are able to proliferate in a tightly regulated manner in response to different stimuli or injuries (López-Luque & Fabregat, 2018; Michalopoulos, 2020; Michalopoulos & Bhushan, 2021; Ozaki, 2020).

In contrast to what happens to other organs such as pancreas, kidneys or lungs, that will slightly increase if a big portion of the organ is lost, the liver is the only solid organ that regenerate to ensure that liver-to-body weight ratio is always at 100% of what is required for body homeostasis. Liver size changes in several situations, i.e., it increases during pregnancy and decreases in cachexia or after severe loss of body weight, but the "**hepatostat**" guarantee the stability of liver size in relation to body size (López-Luque & Fabregat, 2018; Michalopoulos, 2017, 2020; Michalopoulos & Bhushan, 2021).

The words "liver regeneration" could indicate that the liver can restore exactly the same disappeared lobules, but instead, the process is actually a "compensatory hyperplasia and hypertrophy". The cells in the remnant tissue simply proliferate and/or increase in size to restore the original liver mass (Kang et al., 2012; López-Luque & Fabregat, 2018; Miyaoka & Miyajima, 2013).

2.1. Models to study liver regeneration

Several experimental models have been described to induce liver regeneration. Loss of liver mass can be chemically induced by administration of hepatotoxic chemicals (carbon tetrachloride (CCl4), D-galactosidase or acetaminophen), bacterial particles (lipopolysaccharides (LPS)), and virus (López-Luque & Fabregat, 2018; Mao et al., 2014). However, the most commonly and best-studied model is the surgical procedure two-thirds (2/3) partial hepatectomy (PH) in rodents, which was first described in rats by Higgins and Anderson (Higgins & Anderson, 1931). Due to the multi-lobe structure of the liver, the left and median lobes are easily removed by a surgical intervention, and the remaining liver grow

in size to restore an aggregate equivalent to the mass of the lost tissue. The 2/3 or 70% PH is the most preferred for several reasons: (a) It does not require an advanced surgical technique; (b) It is well tolerated in rodents without an important perioperative mortality; (c) It is not accompanied by massive necrosis or inflammation to the remaining lobes; and (d) The regenerative phenomena can be precisely timed, using as a reference point (time 0) the time of the performance of the 2/3 partial hepatectomy (PH) (Abu Rmilah et al., 2019; Michalopoulos, 2010). In the mouse, 50% of the lost liver volume is recovered in 2-3 days after 2/3 PH, but it takes more than several weeks for a complete recovery. This phenomenon suggest that the liver always try to maintain minimal function for sustaining life, but once the minimal function necessary for survival is achieved, the regenerative process slows down (Ozaki, 2020).

2.2. Cellular and molecular mechanisms of Liver Regeneration

In a physiological situation, when liver functions are compromised following PH or after chemical insults, liver mass is replaced by replication of existing hepatocytes, which is the quickest and more efficient way of LR (Fausto, 2004). The regenerative ability of hepatocytes and cholangiocytes are normally characterized by **phenotypically fidelity**, but when proliferation of one of the two cell types is impaired, both hepatocytes and cholangiocytes behave as facultative stem cells and can transdifferentiate into each other to restore normal liver structure (Michalopoulos & Bhushan, 2021).

Cell size increase is the first response of hepatocytes to recover after PH. In this way, as early as a few hours after 70% PH, an increase in hepatocytes' size takes place and peaks at 1 day. Then, from 1 to 2 days after 2/3 PH, hepatocytes transcriptional program change from a hypertrophic phase to a proliferative phase. Interestingly, when 30% liver resection model is performed, the liver mass recovery occurs due to a significant 1.5-fold increase in the hepatocyte size without undergoing cellular division (Miyaoka & Miyajima, 2013) (**Figure III**).

It is also outstanding that about 70% of adult hepatocytes are tetraploid (Miyaoka & Miyajima, 2013) and that, during proliferation, binuclear hepatocytes do not seem to undergo conventional cell division, but binuclear mother cells split the nuclei into two daughter cells (Tormos et al., 2015). By the end of LR, cellular ploidy (binucleated polyploid hepatocytes) decreases, while nuclear ploidy (mononucleated polyploid hepatocytes) increases, but the global ploidy spectrum remains the same (Donne et al., 2020).

Cytokines, growth factors (GFs) and metabolic signals are important mediators of LR after PH. There is an important redundancy between signals, and many of their signaling agents overlap in function. Therefore, loss of an individual gene rarely leads to complete inhibition of LR, but only an initial delay in the regenerative process (López-Luque & Fabregat, 2018; Riehle et al., 2011).
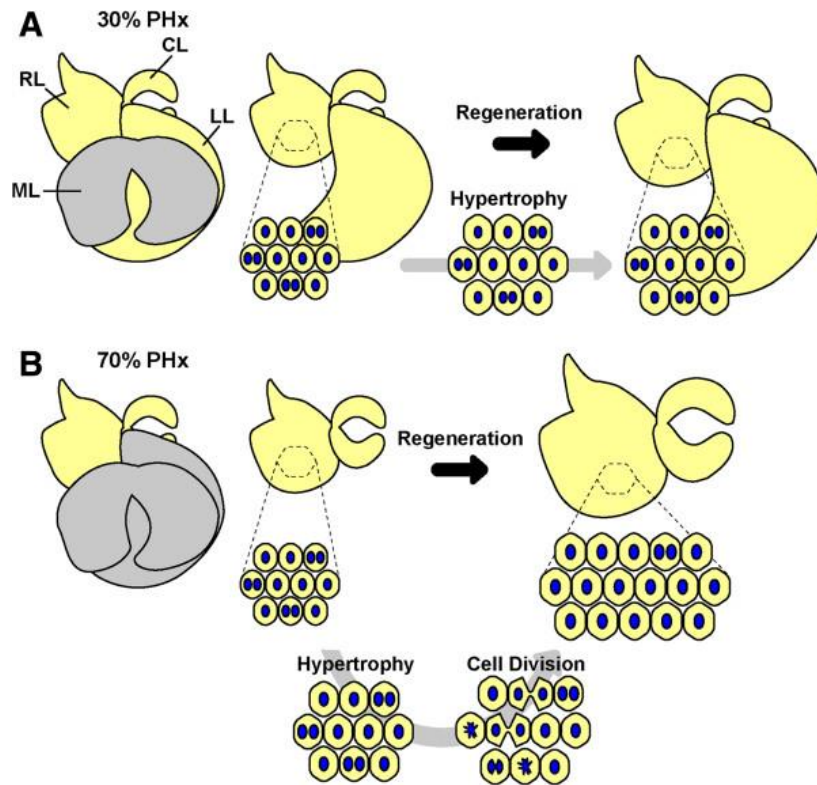
Figure III. Schematic representation of A) 30% and B) 70% Partial Hepatectomy (Miyaoka & Miyajima, 2013).

Hepatocyte regeneration proceed along **sequential phases**: initiation or "priming phase", which include overexpression of specific genes that prepare liver cells for replication; proliferation or "progression phase", when expansion of liver cells takes place; and "termination phase", when cell proliferation finishes preventing liver tissue overgrowth (**Figure IV**). These three phases are linked and they even share several mechanisms. Moreover, during the proliferative phase a complex remodeling of the parenchyma is required, which is known as fourth phase (López-Luque & Fabregat, 2018; Zimmermann, 2004).

Priming phase

The first phase is called, as previously mentioned, the "priming phase", and occurs in the first 4 hours after PH. Hepatocytes resting in a quiescence state (G_0 phase) can

quickly and synchronously enter the cell cycle upon stimulation, and undergo one to two rounds of replication before coming back to quiescence. They need to be **"primed"** to enter the cell cycle (G_1 phase) and respond to mitogens (Cienfuegos et al., 2014; López-Luque & Fabregat, 2018).

Hemodynamic changes are necessary for launching the liver regeneration process. After PH in rodents, each residual lobe of the liver retains its supply of hepatic artery and portal vein branches. Whereas the amount of arterial blood going into every lobe remains basically the same, the amount of portal vein blood going into each lobe increases theoretically threefold. The rise in portal blood pressure exerts a mechanical stress on the endothelial cells, which express an increase activity of urokinase plasminogen activator (uPA) 5 minutes after PH. Within 10 minutes, uPA mediates the conversion of plasminogen into plasmin, which in turn activates matrix metalloproteases (MMPs). Both plasmin and MMPs are involved in matrix remodeling and activation of many proteins from ECM, such as Hepatocyte Growth Factor (HGF). Moreover, migration of Notch1 intracellular domain (NICD) and β-catenin to hepatocyte nuclei occurs within 15-20 minutes after PH. Epidermal Growth Factor (EGF) coming from Brunner's glands of the duodenum, and insulin coming from pancreas enter the liver 1 hour after PH via portal vein (Abu Rmilah et al., 2019; Kang et al., 2012; Michalopoulos, 2010; Michalopoulos & Bhushan, 2021).

This process also depends on the interaction between hepatocytes and non-parenchymal cells (e.g., KCs and SECs) via cytokines. KCs are activated after recognition of Pathogen-Associated Molecular Patters (PAMPs) and Damage-Associated Molecular Patterns (DAMPs) released from necrotic cells after tissue injury, as well as lipopolysaccharide (LPS). KCs begin to produce and secrete tumor necrosis factor-alpha (TNF-α), which bind to TNF receptor 1 (TNFR1) on KCs surface, activating the nuclear factor-kappa B (NF-κB). Then, NF-κB binds to promoter region of *Il6* gene, inducing the production and secretion of interleukin-6 (IL-6) by activated KCs, which in turn binds IL-6 receptor on hepatocytes and leads to activation of the transcription factor signal transducer and activator of transcription 3 (STAT3), among other pathways. STAT-3 protein binds to the DNA activating several immediate-early response genes related to hepatocyte proliferation, such as c-Fos, c-Jun and c-Myc. Although these cytokines are not directly mitogenic to hepatocytes, they are critical to orchestrate the process of LR (Böhm et al., 2010; Cienfuegos et al., 2014; López-Luque & Fabregat, 2018; Ozaki, 2020).

Proliferation/progression phase

The second phase "progression or proliferation phase" corresponds to the transition **from G_1 to the completion of mitosis**. The cellular proliferation proceeds in a chronological sequence: hepatocytes divide first, followed by KCs, cholangiocytes and finally SECs (Abu Rmilah et al., 2019). In the case of hepatocytes, four waves of hepatocytes proliferation have been described. The first wave takes place from 24 to 60 hours after PH. The second one takes place from 60 to 84 hours, the third one from 84 to 108 hours, and the last one from 108 to 132 hours after PH. It is remarkable that the number of proliferating hepatocytes is gradually reduced as the liver recovers its mass (Zou et al., 2012).

After cytokines have triggered the G_0 to G_1 transition, cell cycle progression largely depends on growth factors. HGF and EGF are, by far, the most important initiators and augmenters of the proliferative phase during LR. As mention before, HGF is released from ECM after PH, but it is also newly synthesized by non-parenchymal cells, such as HSCs and SECs, and it exerts its mitogenic actions trough the c-Met receptor. Concomitantly, activation of the Epidermal growth factor receptor (EGFR) stimulate the progression of hepatocytes through the cell cycle during liver regeneration (Abu Rmilah et al., 2019; López-Luque & Fabregat, 2018), and mice expressing a truncated form of EGFR displayed lower and delayed proliferation and lower activation of proliferative signals (López-Luque et al., 2016). EGFR on hepatocytes is activated through different sources, including EGF, amphiregulin (AR), transforming growth factor-alpha (TGF-α) and heparin binding EGF-like growth factor (HB-EGF) (Riehle et al., 2011). c-Met and EGFR are receptor tyrosine kinases which activate multiple intracellular signaling pathways. Among them, Mitogen-activated protein kinase (MAPK), STAT3, Phosphatidylinositol-3-kinase (PI3K)/Akt and Extracellular signal-regulated kinase 1 and 2 (ERK1/2) are the most relevant for LR, which in turn regulate multiple transcription factors, such as c-Jun, c-Fos, c-Myc, NF-κB, STAT3 and C/EBPβ proteins. Beyond the compensatory mechanisms within the EGFR ligands, some studies suggest that both EGFR and c-Met may compensate for one another (López-Luque & Fabregat, 2018). In fact, Paranjpe et al. described that only the combined elimination of both receptors completely abolishes LR (Paranjpe et al., 2016).

Of special relevance for this work, related to the "proliferation/progression" phase of LR, is the **control of cell cycle**. Cell cycle is divided into four phases: G_1, S, G_2 and M phases. During G_1 phase, cells enlarge, whereas in S phase, DNA synthesis occur. G_2 phase is a gap prior to M phase or mitosis, when chromosome segregation and cytokinesis occur, giving rise to two daughter cells. In the case of rat and mouse, DNA synthesis has been

reported during 24 and 36 hours post-hepatectomy, respectively. After that, hepatocytes enter into mitosis at 48 hours post-PH. The cell cycle has three control checkpoints: restriction or "R" checkpoint, which determines the entry into late G_1 phase; and the two mitotic control checkpoints: the G_2/M, regulating the entrance in mitosis, and the metaphase-anaphase checkpoint. The bast majority of mitogens and growth factors, such as EGF, HGF and transforming growth factor-beta (TGF-β), regulate the rate of cell division in the "R" check point, when the cell is more sensitive to external factors. At that point, commitment occurs, and the cell no longer requires growth factors to complete the cell cycle (Blagosklonny & Pardee, 2002; Cienfuegos et al., 2014).

The progression of the cell cycle is tightly regulated by a highly conserved family of serine/threonine kinases. These enzymes are composed by a regulatory subunit (a cyclin) and a catalytic subunit (a cyclin dependent kinase or Cdk) (Ehrenfried et al., 1997). D-type cyclins associate with Cdk4/6 to regulate G_1 progression. This complex then phosphorylates the retinoblastoma protein (Rb), leading to E2F transcription and subsequent transcription of genes required for cell cycle progression. Then, binding of Cdk2 with Cyclin E is required for G_1/S transition. During the S and G_2 phases, Cdk2 is bound to Cyclin A, and in the late G_2 and early M, Cdk1 is bound to Cyclin A to mediate entry into M phase. Finally, mitosis is regulated by Cdk1 in complex with B-type cyclins. Furthermore, the kinase activity of Cdk/cyclin complexes is controlled by a plethora of Cdk inhibitors (CKIs), which are subdivided into two classes based on their Cdk specificity. On the one hand, the Ink4 family members ($p15^{INK4b}$, $p16^{INK4a}$, $p18^{INK4c}$ and $p19^{INK4d}$) primarily target Cdk4 and Cdk6. On the second hand, Cip/Kip family members ($p21^{Cip1}$, $p27^{Kip1}$ and $p57^{Kip2}$) inhibits all cyclin-bound CDKs (Blagosklonny & Pardee, 2002; Vermeulen et al., 2003).

Termination phase

The last step of liver regeneration is the "termination" phase. Once the original mass of the liver is restored, the **growth response must be terminated** to prevent the carcinogenic effect of the excess of proliferating cells. Therefore, liver regeneration must be a well-orchestrated process with a balance between mitogenic factors and proliferation-inhibiting factors. Curiously, the mechanisms underlying the termination phase remain poorly understood, but it seems that both extra- and intra-hepatic factors are involved in slowing down regeneration (Abu Rmilah et al., 2019; M. Liu & Chen, 2017; Ozaki, 2020).

TGF-β is one of the most recognized hepatocyte proliferation inhibitor and stop signal during liver regeneration. This cytokine is mainly secreted by non-parenchymal cells,

such as HSCs, KCs and platelets, and it can be expressed in regenerating hepatocytes (M. Liu & Chen, 2017). In early stages of regeneration, hepatocytes' proliferation must occur and TGF-β-induced antiproliferative effects are not needed (Karkampouna et al., 2012). TGF-β expression increases at 4 hours after PH, but regenerating hepatocytes are resistant to mitoinhibition-induced by TGF-β either by downregulation of receptors (Chart et al., 1995), norepinephrine protective action (Houck & Michalopoulos, 1989), up-regulation of transcriptional repressors SnoN and Ski (Macías-Silva et al., 2002), and up-regulation of anti-apoptotic and antioxidant signals (Herrera, Álvarez, et al., 2004). TGF-β reach a peak at 72 hours, when liver regeneration must finish and DNA synthesis stop (M. Liu & Chen, 2017). In this way, a perfect spaciotemporal orchestration of TGF-β signaling at different stages of the process is needed. Due to its relevance in this work, it will be further reviewed in Section 3.

Moreover, **activins** are members of the TGF-β superfamily and important mediators of termination of regeneration. Activin A is the variant most abundant and it is an inhibitor of initiation of DNA synthesis in hepatocytes. After rat liver injury or PH, Activin A receptors in hepatocytes are downregulated by 24 hours, and normalize at 72 hours, when DNA synthesis terminate (Böhm et al., 2010; Zimmermann, 2004). Interestingly, mice lacking components of the TGF-β signaling pathway, specifically *Tgfbr2*, present normal termination of LR, associated with increased Activin A signaling (Oe et al., 2004). This suggest that both TGF-β and activins collaborate in the termination phase of LR.

The **Integrin Linked Kinase** (ILK) is another protein involved in the termination phase. Liver-specific deletion of ILK provokes hepatomegaly and enhanced hepatocyte proliferation in mice, presenting an impaired termination of the process (Apte et al., 2009). **Glypican 3** (GPC3) increases at day 2 after PH, reaching maximal levels at day 5, and suppression of GPC3 in cultured rat hepatocytes enhances proliferation (B. Liu et al., 2009). Further, GPC3 overexpression in mice suppressed hepatocyte proliferation after PH (B. Liu et al., 2010), suggesting that GPC3 could be involved in the termination of LR. Moreover, **Hepatocyte nuclear factor 4 alpha** (HNF4α), which is a critical transcription factor (TF) involved in hepatic differentiation, is essential for termination of liver regeneration (Huck et al., 2019).

Finally, intra-hepatic levels of several growth factors and cytokines (e.g., IL-6 and HGF) decrease when LR proceeds (Ozaki, 2020), contributing also to the termination of regeneration. Altogether, a proper equilibrium of all these signals during the different phases might be a good determinant of the effectiveness of LR.

Parenchymal remodeling

ECM is partially degraded and remodeled at the beginning of LR, but it is restored along the process of regeneration. **ECM remodeling contributes to initiation** of proliferation by releasing locally available latent growth factors. During the proliferative phase, a reduction in the normal sinusoidal network is observed, concomitant with a partial loss of the space of Disse and a degradation of ECM through metalloproteinases. By 48 hours after PH, growing of small vessels, associated with synthesis of ECM proteins, the reconstitution of the space of Disse, and the repopulation of this space with HSCs, is observed. This parenchymal unit is oversized, and the completion of a normal volume demand termination and remodeling mechanisms (Kang et al., 2012; Michalopoulos, 2020; Zimmermann, 2004). Once again, TGF-β is necessary at the end of regeneration for induction of inflammation, epithelial-to-mesenchymal transition (EMT), as well as cell-cell interactions (Karkampouna et al., 2012; M. Liu & Chen, 2017).
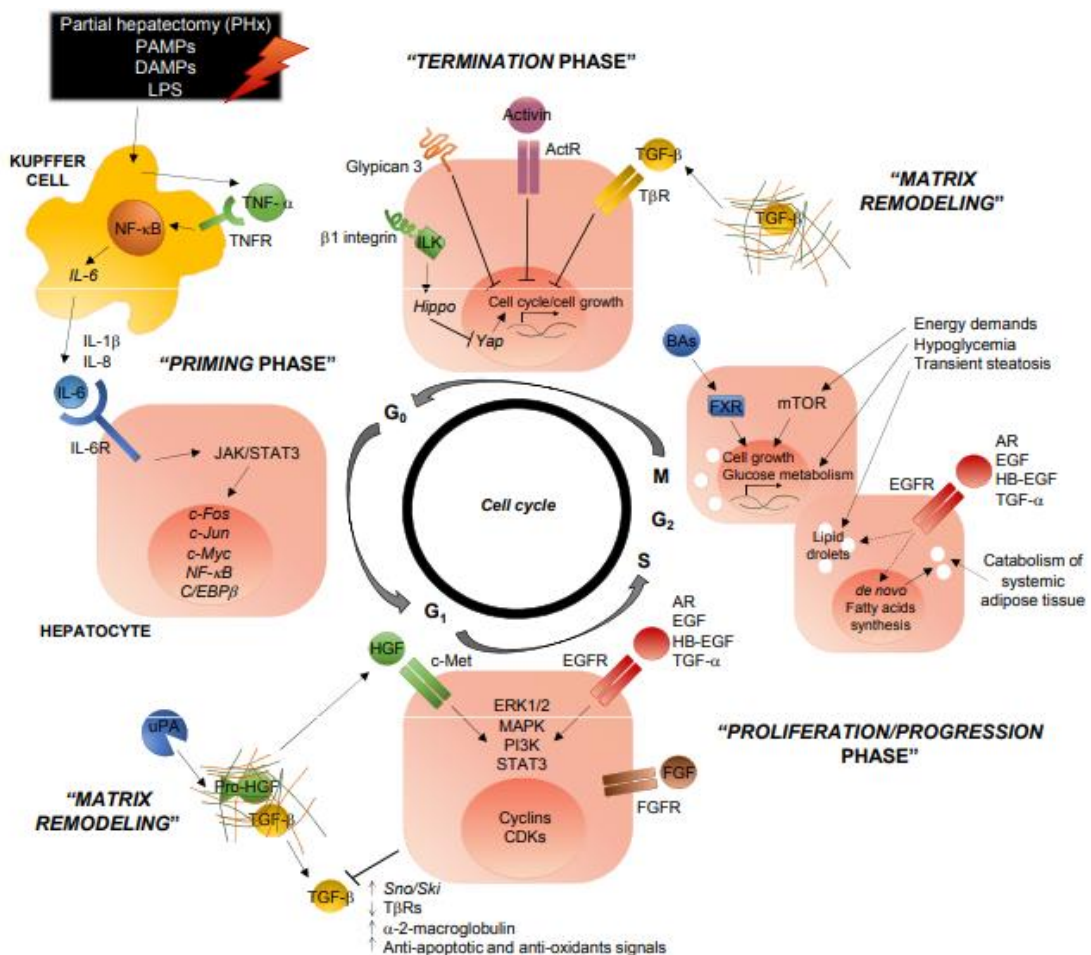
Figure IV. Liver regeneration based on hepatocyte proliferation. Four phases are represented: Priming, Proliferation/progression, Termination and Matrix remodeling (López-Luque & Fabregat, 2018)

Metabolic changes during Liver Regeneration

It is important to mention that rodents subjected to PH or exposed to toxic injury develop alteration in hepatic and systemic metabolism. The liver must regulate systemic energy levels while meeting its own demands needed for cell division. Within hours after PH, rodents developed **significant hypoglycemia** and decreased insulin levels, which results from the acute removal of 2/3 of hepatic glycogen content and gluconeogenic capacity (Huang & Rudnick, 2014; Mao et al., 2014). Interestingly, glucose supplementation suppresses both PH- (Simek et al., 1967; Weymann et al., 2009) and toxin-induced (Chanda & Mehendale, 1995) liver regeneration, associated with a disruption of many signaling events important for LR. Similarly, dietary caloric restriction accelerates cell proliferation in response to 70% PH (Cuenca et al., 2001). Altogether, the hypoglycemic response after liver damage seems to initiate the signals for regeneration. Hypoglycemic response is followed by a **systemic catabolic response** around 12 hours after PH, characterized by a decrease in lean- and adipose-tissue mass. The early regenerating liver present an important fat accumulation or "**transient steatosis**" after PH, which may result mainly from uptake of adipose-derived fat stores, and by a lower extent from *de novo* hepatic lipogenesis. These lipids serve as a substrate for energy production, especially trough β-oxidation of free fatty acids, or for membrane synthesis required for cellular proliferation. In fact, many studies have reported that decreased hepatic fat accumulation both pharmacological or genetically inhibit liver regeneration (Huang & Rudnick, 2014; Rudnick & Davidson, 2012). Moreover, bile acid metabolism is also altered: the remnant liver after PH excretes 2.5-fold more bile acids per gram liver than the control-operated mouse liver (Csanaky et al., 2009). Finally, translation is the control point that integrates nutrient levels with mitogenic signals, and many proteins involved are downstream of mammalian target of rapamycin (mTOR). As a result, the mTOR complex may regulate regeneration by modulating cell size and proliferation based on energy demands (Mao et al., 2014).

2.3. Liver regeneration in a clinical disease setting

In a clinical disease setting, liver regeneration is observed in conditions leading to a severe loss of hepatocytes. Chronic loss of hepatocytes is observed in infectious diseases (e.g., Hepatitis B and C viruses), chronic toxic conditions (e.g., metabolic diseases, alcohol, non-alcoholic steatohepatitis (NASH), storage diseases, hemochromatosis), ischemia reperfusion injury (which normally occur after liver transplantation) or chronic immune attacks (such as autoimmune hepatitis). Chronic loss of hepatocytes is accompanied by proliferation of the surviving cells, which may lead to development of neoplasia when

occurring in potentially genotoxic environments. Acute loss of hepatocytes, which is less common, can be caused by ingestion of toxins (e.g., attempted suicide by acetaminophen), trauma, or acute hepatitis. In all these situations, compensatory proliferation, hepatocytes' death and inflammation, which remove death cells and provide cytokines for repair, proceed in tandem (Michalopoulos, 2020). In fulminant hepatitis induced by drugs, the recovery of liver damage is expected after removal of the causative substances by hemofiltration and dialysis, and it may need supplementation of substances such as albumin and coagulation factors (Ozaki, 2020). Moreover, liver regeneration is also crucial since the liver resection is sometimes the best therapeutic option, as it happen in hepatic metastasis from colorectal cancer (Riddiough et al., 2021). Nevertheless, when the regenerative process is affected, it may lead to serious liver failure and a deterioration in a patient's general condition (Ozaki, 2020).

3. Transforming Growth Factor-beta (TGF-β)

Transforming Growth Factor-beta (TGF-β) are a family of polypeptides that play important roles in the regulation of embryogenesis and adult tissue homeostasis, but they are also implicated in pathophysiological mechanisms that are the basis of several diseases (Fabregat & Caballero-Díaz, 2018; Tzavlaki & Moustakas, 2020).

The human TGF-β family includes thirty-three genes which are grouped into the TGF-β subfamily and BMP subfamily. On the one hand, the TGF-β subfamily comprises three TGF-β ligands (TGF-β1, -β2 and -β3), two Activins (A and B), Nodal, and the growth and differentiation factors (GDF1, GDF3, GDF8 (also known as Myostatin), GDF9 and GDF11). On the other hand, the BMP subfamily includes 10 Bone Morphogenic Proteins (BMPs), several GDFs, and the anti-Mullerian hormone (Batlle & Massagué, 2019; Tzavlaki & Moustakas, 2020).

3.1. TGF-β Synthesis, Extracellular Deposition, and Activation

TGF-β is synthesized as a pro-hormone that includes a signal peptide, a large N-terminal region known as latency-associated peptide (LAP), and a short C-terminal sequence that will become the short mature ligand. TGF-β are synthesized by ribosomes attached to the endoplasmic reticulum (ER), where cleavage of the short signal sequence occurs. Then, the remaining polypeptide translocates to the lumen of the ER, where dimerization of pro-TGF-β occurs by three disulfide bonds: two in the LAP and one in the C-terminal, which corresponds to the mature active cytokine. Glycosylation of N-terminal region is known to support latency. In most of the cells, the dimeric pro-TGF-β crosslinks to the latent TGF-β binding proteins (LTBPs) again via disulfide bonds, forming the large latent complex (LLC). The LLC translocates from the ER lumen to cis- and then trans-Golgi cisternae, where furin proteases cleave at the junction of the prodomain with the mature peptide. The noncovalent bonds between them prevent the premature activation of the 25 kDa active TGF-β (Batlle & Massagué, 2019; Travis & Sheppard, 2014; Tzavlaki & Moustakas, 2020). The cleaved LLC is stored in secretory vesicles that undergo exocytosis and secrete LLC out of the cell, where N-terminal region of LTBP is covalently linked to the extracellular matrix (ECM). LLC crosslink to fibrillin and fibronectin (Santibanez, 2013; Tzavlaki & Moustakas, 2020)(**Figure V**). Mutations in Fibrillin 1 gene causes Marfan syndrome, a rare human disease caused by an excessive TGF-β signaling and characterized by joint laxity, skeletal deformities, and aortic aneurysms (Verstraeten et al., 2016).

TGF-β is synthesized in excess and its activation function as a rate-limiting step in its bioavailability (Santibanez et al., 2018). Several enzymatic and nonenzymatic mechanisms are implicated in the activation of TGF-β, including ECM proteases, such as matrix metalloproteases (MMPs), tolloid-like family of proteases, such as BMP-1, integrins, as well as heat, local acidification or reactive oxygen species (ROS), within others (Santibanez, 2013; Tzvlaki & Moustakas, 2020).

Figure V. Diagram showing the **biosynthesis** and extracellular matrix deposition of TGF-β (Tzvlaki & Moustakas, 2020).

One well known activation mechanism includes **BMP-1 and MMPs**. BMP-1 cleaves LTBP1, causing release of the latent complex, and then MMP2 cleaves LAP, releasing the mature TGF-β1 in mouse embryo fibroblast (Ge & Greenspan, 2006). **αv integrins** are also important mediators of TGF-β activation, through their interaction with the arginine-glycine-aspartate (RGD) integrin recognition motif present in the LAP (Batlle & Massagué, 2019; Tzvlaki & Moustakas, 2020). αvβ6 integrin, which interact with the actin cytoskeleton, exerts force and changes the conformation of the LLC from extended-closed to extended-open, allowing release of mature TGF-β from its latent complex (Dong et al., 2017; Shi et al., 2011). Moreover, it has been also recently described that αvβ8 binding to latent-TGF-β allows activation of TGF-β receptors without release and diffusion of mature TGF-β (Campbell et al., 2020). Another mechanism involves the mannose-6-phosphate/type II insulin-like growth factor receptor (**M6P/IGFII-R**) and urokinase plasminogen activator receptor (**uPA-R**). Latent-TGF-β1 binds to M6P/IGFII-R, which also complexes with uPA-R. Plasmin generated from plasminogen by the uPA/uPA-R system allows release of TGF-β1 through proteolytic cleavage of the N-terminal glycopeptide (Godár et al., 1999; Leksa et al., 2005).

3.2. TGF-β Signaling Pathway

Upon activation of the dimeric TGF-β from the latent form, TGF-β family members bind to transmembrane serine/threonine kinases, known as type I and type II receptors. The formation of a heterotetrametric complex of TGF-βRI, also known as activin receptor-like kinase 5 (ALK-5), and TGF-βRII, allow the initiation of the signal transduction cascade. Firstly, TGF-β binds to homodimeric TGF-βRII, which is constitutively active and acts as a high affinity receptor. This interaction produces a conformational adaptation between the ligand and TGF-βRII, and a new high-affinity binding site is formed for TGF-βRI in the interface of TGF-β and TGF-βRII. TGF-βRII phosphorylates serine residues in the juxtamembrane domain of the TGF-βRI, activating the type I receptor kinase. Activated TGF-βRI in turn phosphorylates its substrates: the SMAD family. Humans express eight SMAD proteins that can be classified into three groups: Receptor-associated SMADs (R-SMADs), Cooperating SMADs (Co-SMADs) and Inhibitory SMADs (I-SMADs). Among the R-SMADs, TGF-βRI phosphorylates SMAD1, SMAD5 and SMAD8 when the ligand is BMP subfamily, and it phosphorylates SMAD2 and SMAD3 at the carboxy-terminal after TGF-β, activins and nodal stimulation. Then, phosphorylated SMAD2 and SMAD3 associate with the Co-SMAD SMAD4, forming trimeric complexes that translocate to the nucleus to control the expression of target genes. SMAD3 and SMAD4 can directly bind on specific DNA

sequences (although with low affinity) known as SMAD-binding elements (SBEs), but SMAD complexes can also interact with a variety of DNA-binding partners to bind gene promoters. These binding partners are usually transcription factors that interact on one side with SMAD complexes and on the other with promoter regions (**Figure VI**). Furthermore, many SMAD cofactors promote the interaction with co-activators or co-repressors, which finally determine the transcriptional activity of SMADs. Moreover, initiation and propagation of TGF-β signaling can be counteracted by the activity of I-SMADs: SMAD6 and SMAD7. SMAD7 physically interact with TGF-βRI, inhibiting the phosphorylation of R-SMADs. Moreover, it recruits SMURF1/2 ubiquitin ligases to the TGF-βRI, promoting its ubiquitylation and subsequent degradation (Batlle & Massagué, 2019; Seoane, 2006; Tzavlaki & Moustakas, 2020). SMAD proteins consist of globular N-terminal and C-terminal domains connected by a linker region. The N-terminal or MH1 domain binds DNA, whereas the C-terminal or MH2 domain binds TGF-β receptors, other SMADs, cytoplasmic anchor proteins, lineage-specific DNA-binding cofactors, and chromatin modifiers (Macias et al., 2015).
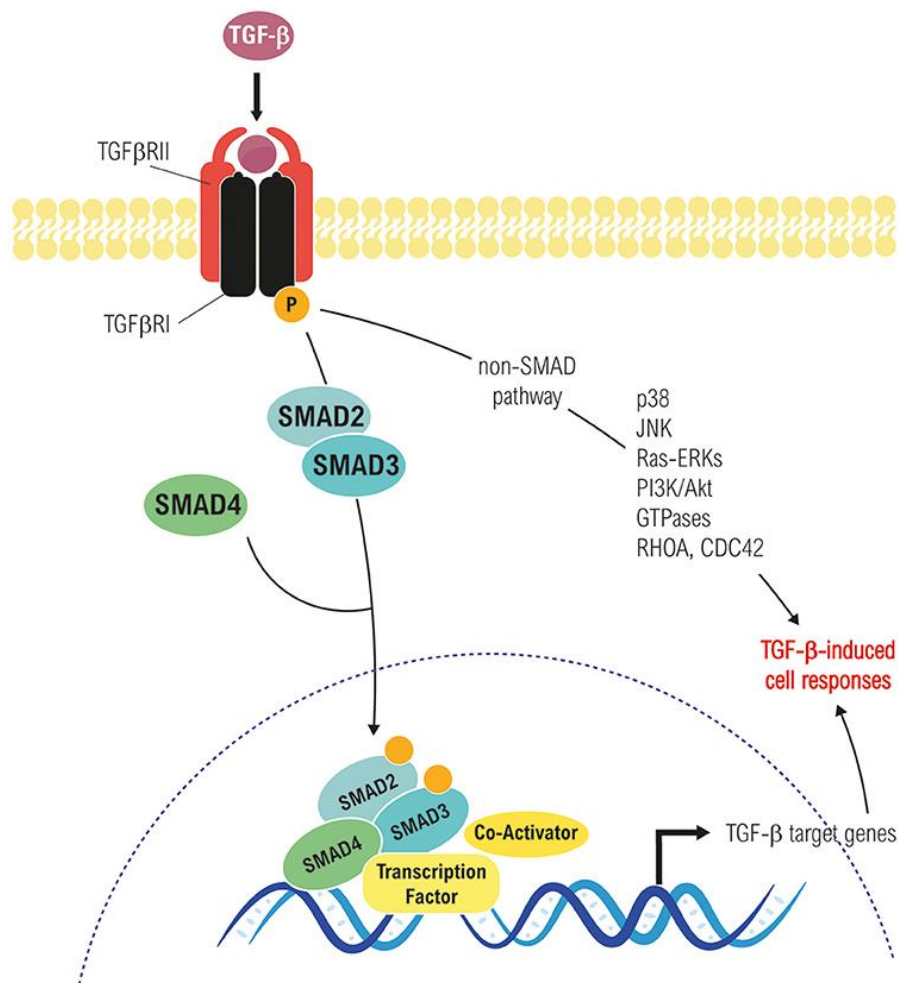
Figure VI. TGF-β signaling is transduced through Smad and non-Smad pathways (Fabregat & Caballero-Díaz, 2018).

On top of the canonical SMAD signaling, TGF-β is able to regulate non-SMAD effectors to mediate some of its downstream biological responses, including, mediators of cell survival (e.g., NF-kB, PI3K/Akt pathways), MAPK signaling pathways (ERK1/2, p38 MAPK, and JNK), as well as Rho GTPases like RhoA, Cdc42 and Rac1 (**Figure VI**) (Fabregat & Caballero-Díaz, 2018; Tzavlaki & Moustakas, 2020; Zhang, 2009).

3.3. TGF-β biological functions

TGF-β is secreted by several cell types and regulates many aspects of tissue and organ **homeostasis**, including morphogenesis and differentiation, proliferation, motility, adhesion, extracellular matrix production and programmed cell death, within others. In this section, we will summarize some of the functions exerted by TGF-β, specifically in liver, on which our group has focused its efforts during the last decades.

3.3.1. TGF-β and Growth Inhibition

In epithelial cells, as well as in neuronal and hematopoietic progenitor cells, TGF-β **inhibits progression of G_1 phase of the cell cycle** by the mobilization of cyclin-dependent kinase (CDK) inhibitors, through the canonical **Smad-signaling pathway**. The specific CDK inhibitors involved in the cytostatic response depend on the cell type. For example, in epithelial cells, TGF-β induces the expression of $p21^{cip1}$ (which inhibits Cyclin E/A-cdk2 complexes) and $p15^{ink4b}$ (which inhibits Cyclin D-cdk4/6 complexes). In this way, TGF-β prevents CDKs activation in the early G_1 phase, leading to inhibition of retinoblastoma protein (pRb) phosphorylation and cell cycle arrest. Equally important is **the TGF-β-induced downregulation of Myc** and ID1, 2 and 3, which are transcription factors involved in cellular proliferation and inhibition of differentiation, respectively. Therefore, TGF-β mediates a dual inhibitory effect on the cell cycle by inhibiting CDKs function and removing proliferative drivers. Many of the transcriptional complexes involved in the TGF-β cytostatic responses have been already elucidated. For instance, Smad3/4-FoxO transcriptional complex target the $p21^{cip1}$ promoter, whereas Smad3/4-FoxO-C/EBPβ bind to $p15^{ink4b}$ promoter, inducing transcriptional activation in both cases. Moreover, Smad3/4 complex together with E2F4/5 recognize a proximal element in the *MYC* promoter, and p107 recruits corepressors (Drabsch & ten Dijke, 2012; Massagué, 2008; Padua & Massagué, 2009). Apart from the Smad-induced cytostatic responses, it has been also described that TGF-β can also promote cell cycle arrest through **Smad-independent mechanisms**. For example, the binding of the TGF-βR complex to the regulatory subunit of PP2A promotes p70 S6 kinase dephosphorylation and inhibition, contributing to the TGF-β-induced cytostatic response

(Petritsch et al., 2000). In **hepatocyte**s, TGF-β can induce cell cycle arrest at low doses (Sánchez et al., 1996), and counteract proliferative signals induced by EGF (Carr et al., 1986).

Importantly, the TGF-β cytostatic effect is sometimes lost in tumoral cells, as it happens in colorectal, pancreatic, gastric, ovarian, and head and neck carcinomas. In certain cases, this is caused by the disruption of the TGF-β signaling due to inactivating mutations in components of the TGF-β pathway, such as mutations in Smad2 and 4, mutations in TGF-βRII, or with lower incidence, in TGF-βRI. Nevertheless, many other tumors, such as breast and prostate cancers, gliomas and melanomas, prefer to maintain the core signaling aspects but become resistant to the anti-proliferative response to TGF-β signaling (Padua & Massagué, 2009; Seoane, 2006). For instance, a group of gliomas present homozygous deletion of *p15INK4b* (Jen et al., 1994), whereas other cancers blunt the effects of CDK inhibitors by overexpressing c-MYC or Cyclin D1 (Massagué, 2008; Seoane, 2006). Furthermore, in some other cases the lack of the TGF-β anti-proliferative response is due to overactivation of non-Smad pathways. In fact, our group described that TGF-β induces survival signals through the transactivation of the EGFR pathway (further discussed in Section 3.3.3).

3.3.2. TGF-β and Apoptosis

In addition to its function controlling the cell cycle, TGF-β also participates in the maintenance of tissue homeostasis through its ability **to induce apoptosis.** Paradoxically, depending on the cell-type and the environmental factors, TGF-β can simultaneously induce **both pro-survival and pro-apoptotic signals**. Several Smad-dependent and -independent mechanisms have been described for a variety of cell lines, and these signals ultimately lead to activation of pro-apoptotic caspases and changes in expression, localization and activation of pro- and anti-apoptotic members of the **BCL-2 family** (Padua & Massagué, 2009).

In hepatocytes, TGF-β modulates the expression of different members of BCL-2 family. Some studies have shown that TGF-β induces downregulation of the anti-apoptotic protein Bcl-xL in rat fetal and TAMH hepatocytes (Franklin et al., 2003; Herrera, Fernández, et al., 2001). By contrast, fetal hepatocytes resistant to TGF-β presents higher expression of Bcl-xL (Valdés et al., 2004). Further, TGF-β also induces the up-regulation of pro-apoptotic proteins Bim and Bax in liver cells (Teramoto et al., 1998; J. Yu et al., 2008). TGF-β-induced apoptosis is coincident with **ROS production**. In fact, TGF-β-induced ROS

production is required to exert its pro-apoptotic role in hepatocytes (Sánchez et al., 1996) and it is also necessary for an efficient mitochondrial-dependent execution of apoptosis (Herrera, Fernández, et al., 2001; Herrera, Álvarez, et al., 2001). ROS levels depends on two different mechanisms: 1) the induction of a nicotinamide adenine dinucleotide phosphate (NADPH) oxidase (NOX) system, specifically induction of NOX4, to increase extra-mitochondrial ROS (Carmona-Cuenca et al., 2008; Herrera, Murillo, et al., 2004) or 2) downregulation of antioxidant genes and proteins (Franklin et al., 2003; Herrera, Murillo, et al., 2004). The implication of NOX4 in TGF-β-induced apoptosis will be later reviewed in Section 4.3.3.

3.3.3. TGF-β-mediated anti-suppressor signals. Crosstalk with the EGFR pathway.

As it has been previously mentioned, TGF-β can induce **survival signals**. Many studies have reported that TGF-β1 is overexpressed in various types of human cancer, which correlates with a poor prognostic (Fabregat et al., 2014). It seems that TGF-β suppresses the early stages of tumor development, but it later favors tumor progression when cells become resistant to its cytostatic effects (Fabregat et al., 2016). These antiapoptotic signals are in a great extent caused due to the activation of the EGFR pathway and c-Src phosphorylation (**Figure VII**). EGF counteracts TGF-β-induced cell death effects in hepatocytes (Carmona-Cuenca et al., 2006; Fabregat et al., 1996, 2000). In fact, blocking the EGFR signaling increases the apoptotic response to TGF-β (Murillo et al., 2005). This process requires activation of the PI3K/Akt axis to impair TGF-β-induced up-regulation of NOX4 and mitochondrial-dependent apoptosis (Carmona-Cuenca et al., 2006). Indeed, TGF-β is able to mediate the production of EGFR ligands, for which it requires the activity of the metalloprotease tumor necrosis factor-α-converting enzyme (TACE)/ADAM17, which is responsible for shedding of the EGF receptor ligands (Caja et al., 2007; Murillo et al., 2005). Caveolin-1 is required for the activation of TACE/ADAM17 by TGF-β in hepatocytes (Moreno-Càceres et al., 2014). Moreover, Clathrin expression is required for TGF-β -induced anti-apoptotic signals in liver tumor cells (Caballero-Díaz et al., 2020).

Moreover, our group has described that another member of the NADPH oxidase family, NOX1, plays an anti-apoptotic role the liver. In fact, TGF-β-induced activation of NOXes mediates upregulation of EGFR ligands through a NF-kB-dependent mechanism (Murillo et al., 2007). Furthermore, NOX1 promotes autocrine growth of liver tumor cells through the activation of the EGFR pathway via upregulation of TGF-α (Sancho & Fabregat,

2010). Moreover, Caveolin-1-dependent activation of the TACE/ADAM17 in hepatocytes requires activation of Src and NOX1 (Moreno-Càceres et al., 2016).

Interestingly, the ability of hepatocytes to survive to TGF-β depends on their differentiation status (Sanchez, 1999). Thus, rat adult hepatoma cells respond to TGF-β inducing survival signals, whereas adult hepatocytes do not (Caja et al., 2007).
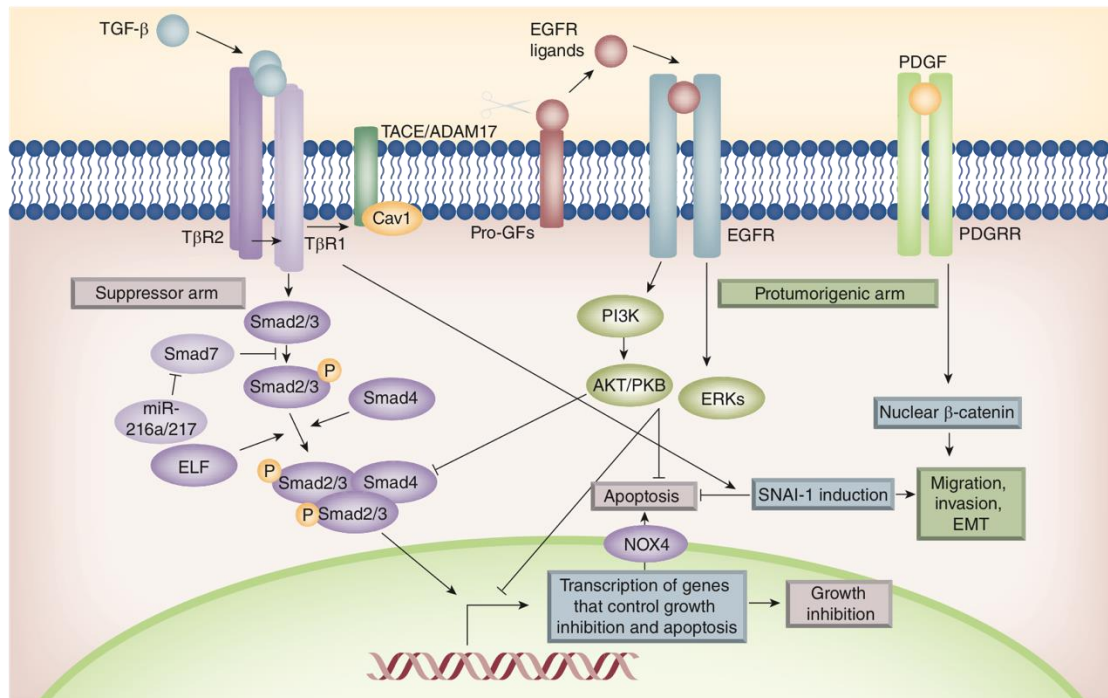
Figure VII. Diagram of the TGF-β crosstalk with EGFR and other growth factors, which may contribute to its pro-tumorigenic actions. The TGF-β-induced activation of EGFR in liver cells requires the activity of the metalloprotease TACE/ADAM17, which is responsible for the shedding of the EGF family of growth factors (Moreno-Càceres & Fabregat, 2015).

4. ROS and NADPH oxidase NOX4

4.1. Reactive oxygen species

Reactive oxygen species (ROS) are highly reactive molecules derived from molecular oxygen, generated by redox reactions or by electrophilic excitation. They can be classified into non- radical (e.g., H_2O_2, ROOH, O_3) and free radical species (e.g., O_2^-, -OH, ROO-). Within them, **hydrogen peroxide (H_2O_2)** is recognized as the major ROS in **redox regulation of biological activities** (Schröder, 2019; Sies & Jones, 2020).

The intracellular concentration of H_2O_2 is normally maintained under tight control. At low levels (< 10 nM), H_2O_2 is associated with the maintenance of physiological redox signaling, what is known as "**oxidative eustress**", while higher concentrations lead to the activation of adaptative stress responses, such as induction of Nrf2/Keap1 or NF-κB (**Figure VIII**). If concentration of H_2O_2 is supraphysiological (> 100 nM), ROS can damage DNA, lipids, and proteins, ultimately leading to growth arrest and cell death. This is known as "**oxidative distress**". Of notice, assessment of a given H_2O_2 concentration to the classification of eustress or distress may vary with cell type, with the level of complexity (i.e., comparison of isolated cell/tissue versus the whole organism), or with the duration of the exposure to H_2O_2 (Buvelot, Jaquet, et al., 2019; Sies, 2017; Sies & Jones, 2020).
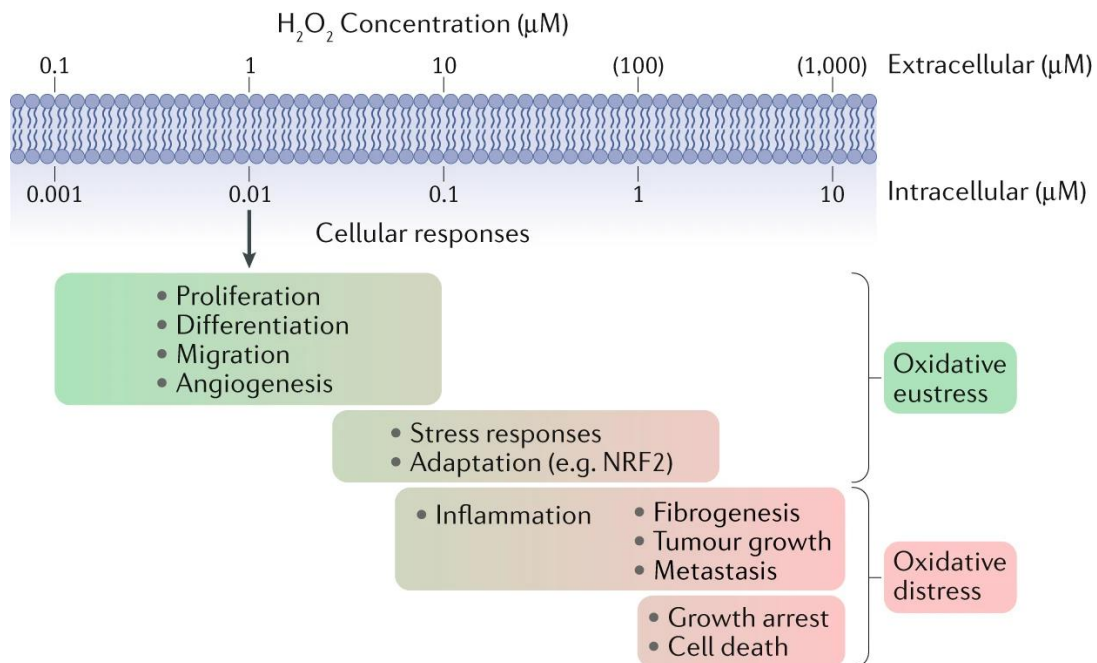
Figure VIII. Oxidative eustress and distress: estimated ranges and cellular responses (Sies & Jones, 2020).

4.1.1. ROS generation and regulation

The most important sources of $O_2^{\cdot-}$ and H_2O_2 are transmembrane NADPH oxidases (NOXs) (Bedard & Krause, 2007; Knock, 2019; Parascandolo & Laukkanen, 2019) and the mitochondrial electron transport chain (Murphy, 2009) (**Figure IX**).

Of special interest for this work is the production of H_2O_2 by NOXs. NOXs are located in different cellular components, which contributes to local generation of ROS. H_2O_2 is also produced by other oxidases present in the endoplasmic reticulum (ER) and peroxisomes, as well as by superoxide dismutases (SOD1–SOD3) from $O_2^{\cdot-}$ (Sies & Jones, 2020). Importantly, specific aquaporins called peroxiporins facilitate H_2O_2 to cross membranes (Bienert & Chaumont, 2014). This differential ROS production has functional significance: different proteins are redox-modified depending on the source (Sies & Jones, 2020).
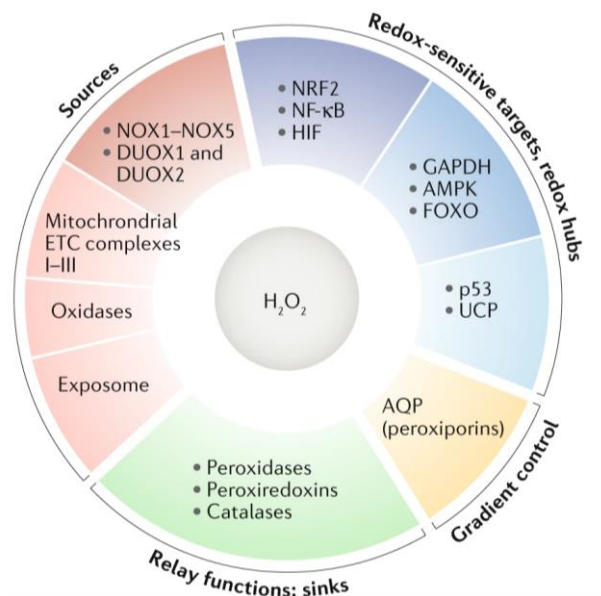
Figure IX. Key modulators and targets of H_2O_2. H_2O_2 sources (red), redox-sensitive targets and hubs (blue), aquaporins (yellow) and sinks (green) (Sies & Jones, 2020).

In physiological situations, ROS play important functions in maintaining cellular homeostasis, as they orchestrate host defense, cell growth and signaling. Nevertheless, if not properly controlled, ROS can rapidly accumulate in great amounts during oxidative stress situations (Liang et al., 2016). In order to maintain homeostasis in the liver, free radicals are scavenged by a powerful antioxidant system (**Figure IX**):

- **Enzymatic detoxification. Catalase** dismutates H_2O_2 to H_2O and O_2. **Glutathione peroxidase (GPx)** also detoxifies H_2O_2 in a reaction in which reduced glutathione

(GSH) is oxidized to glutathione disulphide (GSSG), that is then reduced back to GSH by glutathione reductase using NADPH as a co-factor.

- **Thioredoxins and peroxiredoxins** also function as redox sinks. These proteins contain numerous cysteine residues in a basal reduced-thiol anionic form that are rapidly oxidized by ROS.

- **Transcription factors.** Nuclear factor-erythroid 2 related factor 2 (**Nrf2**) translocates to the nucleus and binds to antioxidant response elements (ARE) in the promoters of antioxidant genes. Forkhead box O (**FOXO**) regulates SOD and catalase transcripts (Jiang & Török, 2014; Kalyanaraman, 2013; Lambeth & Neish, 2014; Sies & Jones, 2020).

4.2. NADPH oxidase family members

Nicotinamide adenine dinucleotide phosphate (NADPH) oxidases (NOXs) family is an important source of ROS in signal transduction (D. I. Brown & Griendling, 2009). In most mammals, seven isoforms of NOX have been described: NOX1-5 and two dual oxidases (DUOX1-2). They use NADPH as an electron donor to reduce oxygen to superoxide anion (O_2^-), according to the following reaction:

$$NADPH + 2O_2 \longleftrightarrow NADP^+ + 2O_2^- + H^+$$
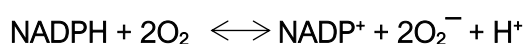
O_2^- is then converted to H_2O_2 either spontaneously or by enzymatic action. The first NOX identified and most studied isoform is NOX2. Due to its high level of expression in neutrophils and macrophages, NOX2 is known as "phagocyte NADPH oxidase" (Buvelot, Jaquet, et al., 2019). Increasingly sensitive detection methods developed during the 90s made clear that superoxide and hydrogen peroxide production was not only restricted to phagocytes, as other cells/tissues generated them (Lambeth & Neish, 2014). Since then, the expression of other mammalian NOX homologs has been found in various cell types and tissues. NOX are essential for maintaining their normal physiology and activity, and dysregulation in their expression and activation is related to oxidative stress and altered cellular responses, which may at the end lead to several pathological consequences such as cardiovascular diseases, cancer, diabetes, and neurodegenerative diseases (Waghela et al., 2021).

4.2.1. NOX structure and activation

NADPH oxidases are transmembrane flavoproteins that transport electrons across biological membranes to reduce oxygen to superoxide anion. In accordance with their preserved function, they share some structural properties: 1) the catalytic core of NOX enzymes contains six (seven for DUOX1–2) transmembrane α-helical domains; 2) they present a NADPH-binding site and a Flavine adenine dinucleotide (FAD)-binding site at the cytosolic C- terminus; 3) they contain four highly conserved heme-binding histidines, two in the third and two in the fifth transmembrane domain (Bedard & Krause, 2007; Brown & Griendling, 2009; Buvelot, Jaquet, et al., 2019). Differences between NOX family members are found in their NH_2-terminal structure, regulatory proteins and subunits (Buvelot, Jaquet, et al., 2019). Considering their mode of activation, NADPH oxidases can be grouped into three groups (**Figure X**):

- The first group of NOXs consists of NOX1, NOX2, and NOX3. The complex is formed by the NOX subunit and the p22^{phox}, which function as a maturation factor required for glycosylation and localization of the NOX subunit, stabilizing the NOX subunit. Of interest for NOX1-3, p22^{phox} has a proline rich region that serves as the docking site for regulatory subunits. In an inactive state, these cytosolic subunits remain dispersed in the cytosol, but upon activation, they assemble with transmembrane subunits to form an active enzyme component. Therefore, NOX1-3 activation depends on the binding of the membrane bound subunits with the small GTPase Rac and with cytosolic proteins. NOX1 and NOX3 bind NOXA1 (Nox activator 1) and NOXO1 (Nox organizer 1), whereas NOX2 binds p67^{phox}, p47^{phox} and p40^{phox}. NOXA1 and p67^{phox} are activators that require NOXO1 and p47^{phox}, respectively, as organizers. As a result of their activation, NOX1-3 generate O_2^- as a prime product.

- NOX5, DUOX1 and DUOX2, which are the calcium activated NOX, can be pooled into group 2. They are independent of cytosolic factors but instead have EF-hands calcium-binding motifs for Ca^{2+} sensing. NOX5 mainly produce O_2^-, but DUOX 1-2 have an extracellular peroxidase domain that allow them to produce H_2O_2.

- The third group of NOXs is only composed by NOX4. NOX4 associates with p22^{phox}, like group 1. However, NOX4 does not require any further cytosolic subunit and therefore is the only one constitutively active (Bedard & Krause, 2007; Brown & Griendling, 2009; Lambeth & Neish, 2014; Schröder, 2020; Waghela et al., 2021). Considering the relevance of NOX4 for the present work, it will be further reviewed in Section 4.3.
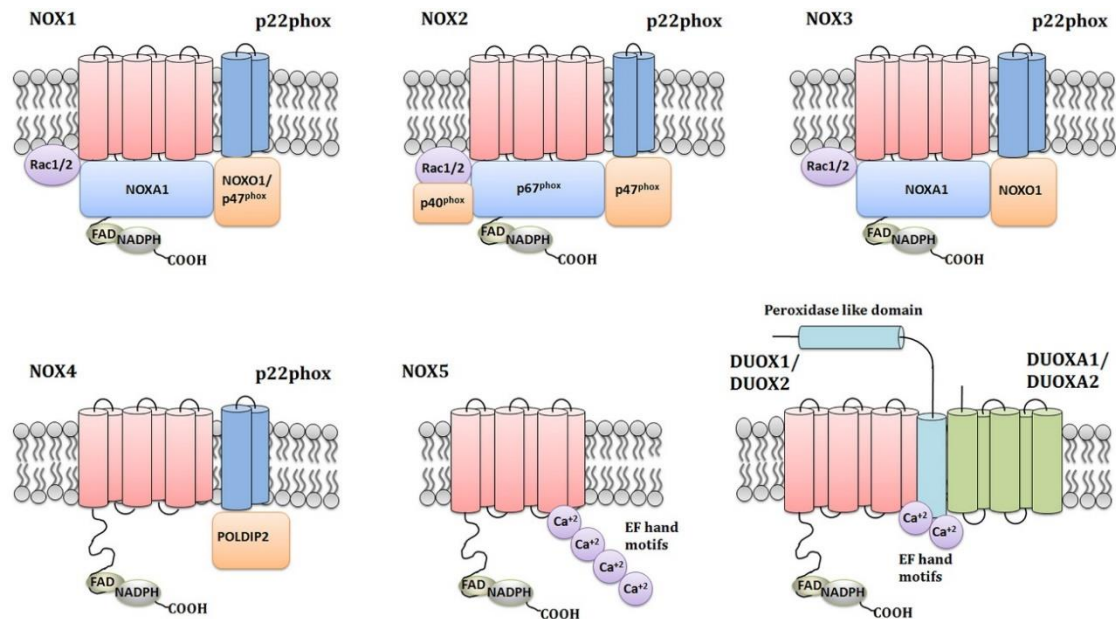
Figure X. Illustration of mammalian NADPH oxidase family structure (Waghela et al., 2021).

4.2.2. NOX functions in physiology and pathology

Besides those cases of a physiological function of NADPH oxidases, whose absence led to a namable disease (i.e., NOX2 and DUOX2), many functions of the family members are unclear. Nevertheless, NOXs play a role in prevention or as contributors to several diseases, although their exact role often remains to be defined (Schröder, 2020).

- **NOX1** presents high expression in the colon (Altenhöfer et al., 2015), and its lost in children predisposes to very early-onset inflammatory bowel disease (VEOIBD) (Hayes et al., 2015).

- **NOX2** presents high level of expression in neutrophiles and macrophages, although it is found in other cell lines. NOX2 in association with p47^{phox} and p67^{phox} are needed for a proper fist line host defense, known as "the oxidative burst": direct toxicity of ROS as well as modification of intracellular signaling in phagocytes allow the defense against infection. In fact, CGD (chronic granulomatous disease) is a disease provoked by disfunction or absence of one of the components of NOX2 complex, characterized by frequent infections by fungi and bacteria. The severe infections in these patients highlight the important role of NOX2 in host defense (Buvelot, Jaquet, et al., 2019; Schröder, 2020). In the liver, neutrophils promote the phenotypic conversion of pro-inflammatory to pre-resolving macrophages during liver repair through ROS-produced by NOX2 (Yang et al., 2019).

- **NOX3** is mainly expressed in the inner ear, and mutations in this gene leads to vestibular disfunctions and severe balance and spatial orientation defect

(Paffenholz, 2004). However, no such mutations have been detected in humans (Buvelot, Jaquet, et al., 2019).

- **NOX5** is mainly present in lymphoid tissue and testis (Altenhöfer et al., 2015). Importantly, NOX5 is not expressed in rats and mice, and therefore, the knowledge about NOX5 is limited. Its physiological function is not well understood, but it seems to contribute to vascular oxidative stress in coronary lesions, hypertension and stroke (Buvelot, Jaquet, et al., 2019).

- **DUOX1** and **DUOX2** are mainly expressed in thyroid and lung tissue (Altenhöfer et al., 2015). DUOX2 physiological role is to oxidize iodine for its incorporation into the thyroid hormone. If DUOX2 or its maturation partner DUOXA2 are not present, the formation of the hormone is reduced and subsequent diseases such as goiter and hypothyroidism develop (Schröder, 2020). In contrast, Duox1 mutations does not affect thyroid hormone synthesis (Buvelot, Jaquet, et al., 2019).

4.3. NOX4

NOX4 was discovered as an NADPH oxidase highly expressed in the kidney (Geiszt et al., 2000; Shiose et al., 2001), but it can also be found in other cell types, such as hepatocytes. The human *NOX4* gene is located on chromosome 11q14.2–q21 and it comprises 25 exons (Breitenbach et al., 2018; Buvelot, Jaquet, et al., 2019; Guo & Chen, 2015). So far, four splice variants have been described (Goyal et al., 2005). The primary sequence of NOX4 comprises 578 amino acids and NOX4 protein has a predicted molecular weight of 66.5 kDa (Guo & Chen, 2015).

4.3.1 NOX4 structure and activity

Similar to other members of NADPH oxidase family, NOX4 comprises 6 transmembrane domains connected by five loops (loops A–E), and a dehydrogenase (DH) domain at the cytosolic C- terminus (**Figure X**). While the A, C and E loops face extra-luminal space, where potentially produce ROS, the B and D loops face the cytoplasm (**Figure XI**) (Guo & Chen, 2015). It has been proposed that the E loop contains superoxide dismutase-like activity, allowing NOX4 to restrain single reduced O_2^- and reduce it further to H_2O_2. In fact, this activity can be prohibited by exchanging a single histidine residue in the E-loop (Takac et al., 2011). Nisimoto et al. observed that purified NOX4 forms 10% of O_2^- and 90% of H_2O_2 (Nisimoto et al., 2014). Moreover, electrons are transported by two non-identical heme groups that are coordinated by four conserved histidine residues located in the third and fifth transmembrane helices (Guo & Chen, 2015). As previously said, NOX4

enzymatic complex is only composed of NOX4 and p22^{phox}, and it does not need the binding of the cytosolic co-factors.
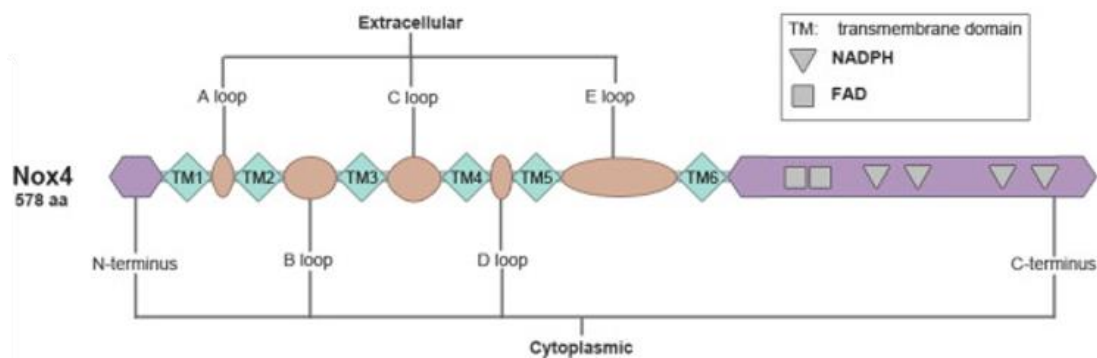
Figure XI. NOX4 protein domain (Adapted from Choi et al., 2014).

Considering that NOX4 has been generally thought to be constitutive active (Nisimoto et al., 2010), ROS production is mainly dependent on NOX4 transcriptional regulation (Serrander et al., 2007). In this way, several stimuli have been reported as NOX4 regulators, including hypoxia, hyperoxia, or shear stress (Buvelot, Jaquet, et al., 2019). Moreover, some transcription factors have been implicated in *Nox4* gene regulation in different cells, such as E2F, Nrf2, HIF-1α, NF-κB, oct-1, sp3 and sp1, c-jun, STAT3, by binding to the specific site of *Nox4* gene promoter (Guo & Chen, 2015). Interestingly, several groups have described that TGF-β signaling is an important inducer of NOX4 expression in smooth muscle cells (Sturrock et al., 2007), in breast epithelial cells (Boudreau et al., 2012), in pancreatic cancer cells (Hiraga et al., 2013) and in hepatocytes (Carmona-Cuenca et al., 2008) within others. Moreover, NOX4 activity could be enhanced by the binding of Polymerase-δ-interacting protein 2 (Poldip2) in the NOX4 enzymatic complex (Datla et al., 2014; Lyle et al., 2009). In contrast, a negative regulation of NOX4 could occur when Hic-5 associates with the ubiquitin ligase Cbl-c and HSP27. This interaction provokes NOX4 ubiquitination and subsequent decrease in ROS levels (Desai et al., 2014). In any case, the predominant controller of NOX4-dependent ROS formation is the expression level of the protein.

4.3.2. NOX4 intracellular localization

Considering that the enzyme is constitutively active, it has been speculated that its activity may depend on its cellular location (Breitenbach et al., 2018; Schröder, 2014). However, the identification of NOX4 intracellular localization is still a matter of discussion. On one hand, there are not good enough commercially available antibodies. On the other

hand, NOX4 localization may differ between cell types and differentiation state (Schröder, 2014). NOX4 localization has been reported in mitochondria (Block et al., 2009; Kuroda et al., 2010), in the endoplasmic reticulum (Buul et al., 2005), in mitochondria-associated membrane or MAM (Beretta et al., 2020), in focal adhesions (Hilenski et al., 2004), in the nucleus (Anilkumar et al., 2013; Kuroda et al., 2005), as well as in the plasma membrane (Block et al., 2009). Interestingly, four different splice isoforms (Nox4 B-E) have been identified and localized in different compartments of the cell. Two of them have dominant negative characteristics for ROS generation. While Nox4B lacks the first NADPH, Nox4C lacks all FADH and NADPH binding sites. The two other splice-variants, Nox4D and Nox4E, lack the transmembrane domains, suggesting that they are non-membrane associated isoforms. Nox4D contains all FADH and NADPH binding domains, showing the same rate of ROS generation than Nox4 prototype (Goyal et al., 2005). Taken together, it seems that Nox4 exists as several isoforms that may have different functions in ROS-related cell signaling depending on its sub-cellular location. Interestingly, changes in the localization of NOX4 have been related with the activation of the enzyme. For instance, insulin stimulates H_2O_2 production and a rapid surface localization of NOX4 in podocytes (Kim et al., 2012).

4.3.3. NOX4 functions in physiology and pathology

As it has been already explained, high level of ROS causes oxidative stress leading to many diseases, while lower level of ROS could serve as second messengers to induce a panel of intracellular signaling pathways involved in differentiation, cell proliferation, migration, among others (Guo & Chen, 2015). As one of the main endogenous H_2O_2 sources, NOX4 is involved in all these processes.

An important feature of NOX4 is that it is ubiquitously expressed: although is highly expressed in the kidney, it has also been also described in other cell types including smooth muscle cells, endothelial cells, fibroblasts, keratinocytes, osteoclasts, neurons, and hepatocytes (Paletta-Silva et al., 2013). The expression of NOX4 in those differentiated cells would suggest that NOX4 itself could be necessary for the process of **differentiation**. In fact, in vascular smooth muscle cell (VSMC), adipocytes and chondrocytes, it has been reported that NOX4 drives the differentiating process (Clempus et al., 2007; Kanda et al., 2011; Kim et al., 2010; Schröder et al., 2009). Differentiation of a cell reduces their motility and, somehow, appears to cause senescence. In relation with this, some studies suggest a role for NOX4 in **senescence**. Indeed, one of the first observation after the identification of the enzyme was that NIH3T3 fibroblasts overexpressing NOX4 developed signs of senescence (Geiszt et al., 2000). NOX4-induced senescence has been also described in the kidney, in

endothelial cells as well as nucleus pulposus cells (Baltanás et al., 2013; Feng et al., 2017; Schilder et al., 2009). On the contrary, Przybylska et al. reported that NOX4 downregulation leads to senescence of human vascular smooth muscle cells (Przybylska et al., 2016). This suggest that NOX4-induced senescence depends on the cell type.

Furthermore, evidence showed that NOX4 is implicated in promoting **cell migration**. Most of the studies have been done in relation with vascular smooth muscle cells (VSMCs)(Meng et al., 2008). In fact, it has been suggested that NOX4 could be associated with cytoskeletal structures, such as vinculin, in VSMCs (Hilenski et al., 2004). However, NOX4 represses epithelial-to-amoeboid transition and efficient tumor dissemination in hepatocellular carcinoma cells (Crosas-Molist et al., 2017). Finally, NOX4 is an inducible regulator of myocardial **angiogenesis**. NOX4-null mice developed contractile dysfunction, hypertrophy, and cardiac dilatation during exposure to chronic overload whereas NOX4-overxepressing mice were protected (M. Zhang et al., 2010). Further, Nox4 promotes endothelial angiogenic responses in human vascular endothelial cells (Datla et al., 2007).

Moreover, the implication of NOX4 in the regulation of **cell proliferation** has been reported in several studies. NOX4 promotes cell proliferation in multiple cell types, including VSMC (Menshikov et al., 2006), endothelial cells (Peshavariya et al., 2009), human pulmonary artery smooth muscle cells (Ismail et al., 2009), pulmonary artery adventitial fibroblasts (S. Li et al., 2008), skeletal muscle precursor cells (Mofarrahi et al., 2008) and gliomas cells (Shono et al., 2008). The underlying mechanisms mediating these effects depend on the cell type. For example, in endothelial cells, low level of NOX4-derived ROS activates mitogen-activated protein kinase (MAPK) family members including p38 MAPK, ERK and JNK/SAP kinases. NOX4-induced cell proliferation is mediated through TGF-β1 and Smad2/3 pathway in human pulmonary artery smooth muscle cell (Guo & Chen, 2015). In contrast, our group described that NOX4 silencing in untransformed hepatocytes and hepatocarcinoma cells increased cell proliferation, suggesting that NOX4 plays a negative role in liver cell proliferation (Crosas-Molist et al., 2014). Again, the role of NOX4 in cell proliferation seems to be cell type specific.

On the contrary, NOX4 has also been associated with **cell death.** Multiple publications reported that NOX4 mediates cell death, mainly through induction of apoptosis, in arterial smooth muscle cells (Pedruzzi et al., 2004), leukemia cells (McKallip et al., 2006), alveolar cells (Carnesecchi et al., 2011), endothelial cells (Tian et al., 2012), and cardiac myocyte (Ago et al., 2011), within others. Indeed, NOX4 inhibitor GLX7013114 counteracts human islet cell apoptosis *in vitro* (Wang et al., 2018). Apart from apoptosis, necrotic-cell

death induced by NOX4 has been described in human umbilical vein endothelial cells (HUVECs) (Simon & Fernández, 2009).

Importantly, some of these NOX4 effects are primarily induced by TGF-β. It has been mentioned that NOX4 mediates cell senescence. Indeed, it mediates TGF-β-induced senescence in the liver (Senturk et al., 2010). Regarding cell migration, NOX4 mediates TGF-β induced cytoskeletal changes in endothelial cells (Hu et al., 2005), and it also mediates TGF-β-induced epithelial-to-mesenchymal transition and migration of breast epithelial cells (Boudreau et al., 2012).

In some of these works, NOX4 is also mediating TGF-β-induced regulation of cell proliferation. For Instance, TGF-β treatment of human pulmonary artery smooth muscle cells (HPASMC) facilitates proliferation by upregulating NOX4 and ROS production, with transient oxidative inactivation of phosphatases and activation of growth signaling cascades (Sturrock et al., 2006). NOX4 also mediates TGF-β-induced phosphorylation of retinoblastoma protein (pRb), proliferation, and cell hypertrophy in airway smooth muscle cell (Sturrock et al., 2007).

Importantly for the work presented here, NOX4 also mediates TGF-β-induced cell death in liver cancer cells (Caja et al., 2009), hepatocytes (Carmona-Cuenca et al., 2008; Sancho et al., 2012), mouse hepatic oval cells (Martínez-Palacián et al., 2013), as well as in podocytes (Das et al., 2014) and endothelial cells (Yan et al., 2014). In the liver, NOX4 mediates TGF-β-induced apoptosis via the liver-specific tumor suppressor STAT5 and the modulation of the expression of key pro-apoptotic genes from the Bcl-2 family, such as PUMA, BIM and BMF (Caja et al., 2009; Yu et al., 2012). Knockdown of NOX4 attenuates TGF-β-induced caspase activation and cell death in rat hepatocytes (Carmona-Cuenca et al., 2008) and it also decreases ROS production, and a decreased expression level of Bcl-2 family members in hepatocellular carcinoma cells is observed (Caja et al., 2009). Accumulation of ROS produced by NOX4 in the mitochondria could lead to mitochondria dysfunction, mitochondrial swelling and cytochrome c release (Kuroda et al., 2010; Xu et al., 2013). Of note, the pro-apoptotic role of NOX4 can be attenuated after NOX1 activation, which promotes autocrine growth through the upregulation of the EGFR pathway in liver cells (Sancho & Fabregat, 2010).

Finally, NOX4 can induce myofibroblasts activation in some organs, such as pancreas (Masamune et al., 2008). Specifically, NOX4 plays a key role in TGF-β-induced myofibroblast activation in lung (Amara et al., 2010; Hecker et al., 2009), kidney (Bondi et al., 2010), heart (Cucoranu et al., 2005), prostate (Sampson et al., 2011), and also in the liver (Jiang et al., 2012; Sancho et al., 2012).

4.3.4. NOX4 in liver disease

In physiological situations, the amount of H_2O_2 is under a tight control by peroxiredoxins, glutathione peroxidases and catalase, as previously said (Sies & Jones, 2020). However, during chronic liver injury, this balanced is perturbed, leading to oxidative stress. This is a common feature in viral hepatitis, alcoholic and non-alcoholic steatohepatitis, liver fibrosis and cancer. Importantly, NOXs are expressed in both parenchymal and non-parenchymal hepatic cells. Major NOX isoforms in the liver are NOX1, NOX2, and NOX4. Thus, hepatocytes express NOX1, NOX2, NOX4, DUOX1 and DUOX2; HSCs and SECs express NOX1, NOX2 and NOX4; and KCs express the phagocyte NADPH oxidase NOX2 (**Figure XII**) (Jiang & Török, 2014; Liang et al., 2016; Paik et al., 2014).
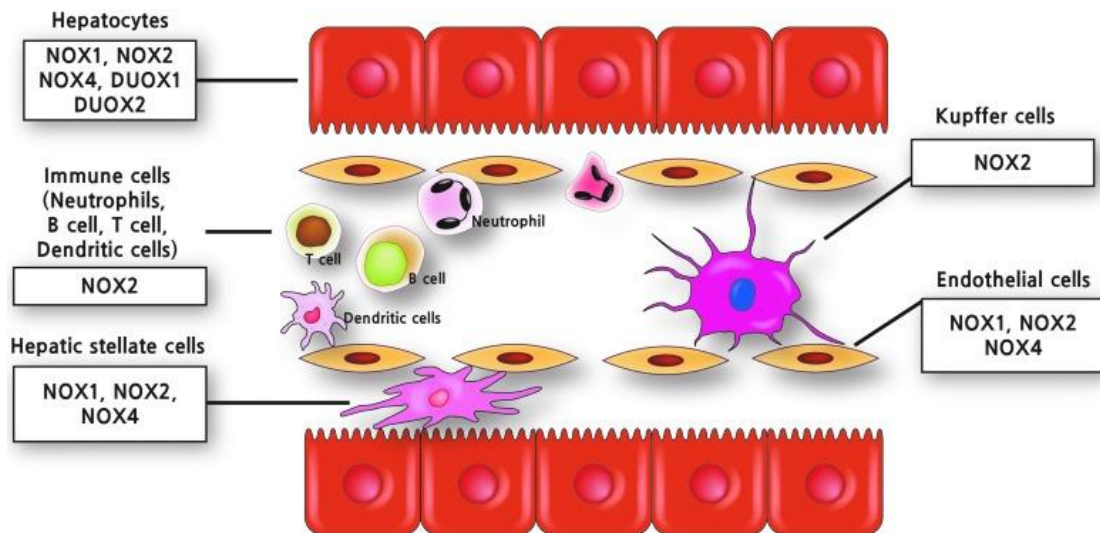
Figure XII. Cellular distribution of NOX isoforms in the liver (Paik et al., 2014).

Of relevance for this work is the role of NOX4 in **liver fibrosis**. NOX4 regulates oxidative stress in the liver and its levels are increased in fibrotic patients, both virus- or NASH-related (Bettaieb et al., 2015; Sancho et al., 2012), as well as in mice with diet-induced steatohepatitis (Bettaieb et al., 2015). On the one hand, it has been described by our group that TGF-β promotes **cell death** via NOX4 activation in hepatocytes and mouse hepatic oval cells (Carmona-Cuenca et al., 2008; Martínez-Palacián et al., 2013). Moreover, NOX4 is also required for FasL or TNFα-mediated apoptosis (Jiang et al., 2012). Hepatocyte cell death is a crucial and indirect event during fibrogenesis because apoptotic bodies derived from damaged hepatocytes can transdifferentiate HSCs to MFBs (Crosas-Molist & Fabregat, 2015).

In addition, one of the most studied mechanisms of fibrogenesis influenced by ROS is **myofibroblast activation**. Whereas high concentrations of ROS induce HSCs dead, non-

toxic levels of ROS stimulate the activation, proliferation, and collagen I production of HSCs (Paik et al., 2014). Importantly, activated HSCs have increased ROS-detoxifying capacity compared to quiescent HSCs, which protects them from ROS-induced cell death (Dunning et al., 2013). It was suggested that NOX could mediate TGF-β-induced myofibroblasts activation in some organs including the liver (**Figure XIII**). Indeed, TGF-β-induced HSCs activation is attenuated by NOX4 downregulation (Sancho et al., 2012). Accordingly, myofibroblast activation was shown to be inhibited by antioxidants in the liver(Abhilash et al., 2012; Foo et al., 2011). In fact, Hotta et al. reported that TGF-β-induced collagen production in myofibroblast is mediated by NOX4-derived ROS (Hotta et al., 2018). It is important to highlight that during fibrosis development the highest level of NOX4 expression is found in hepatocytes, followed by myofibroblast and HSCs (Sancho et al., 2012).

Not only NOX4, but also NOX1 and NOX2 play important roles in the progression of hepatic fibrosis (Cui et al., 2011; Jiang et al., 2010; Paik et al., 2011). Both NOX1 and NOX2 have been shown to induce profibrogenic genes in HSCs, and NOX1-/- and NOX2-/- mice show decreased hepatic fibrosis after CCl_4 treatment or bile duct ligation (Jiang et al., 2010; Paik et al., 2011). Furthermore, NOX5 mediates proliferation and activation of HSCs in response to TGF-β, via p38 MAPK (Andueza et al., 2018).

Considering the important role of **NOX-derived ROS in hepatic fibrogenesis**, the development of **pharmacological NOX inhibitors** is being assessed as potential anti-fibrotic therapeutics. Indeed, GKT137831, which is a dual NOX4/NOX1, decreases both the apparition of fibrogenic markers and hepatocyte apoptosis *in vivo* upon bile duct ligation and CCl_4 treatment (Aoyama et al., 2012; Jiang et al., 2012). Moreover, GKT137831 treatment prevents liver inflammation and lowered proliferative and pro-fibrotic genes after CCl_4 injection (Lan et al., 2015). Nevertheless, further studies are needed to better knowledge the physiological functions of NOX4 and the potential consequences of its inhibition.

Liver fibrosis can lead to cirrhosis, a condition that highly predisposes to develop **hepatocellular carcinoma**. The implication of NOX4 in cancer differs between tumors. While it is considered to be oncogenic in some tumors, such as non-small cell lung cancer (C. Zhang et al., 2014), colorectal cancer (Lin et al., 2017), gastric cancer (Tang et al., 2018) or pancreatic cancer (Witte et al., 2017), NOX4 acts as a tumor suppressor in liver cancer (in association with TGF-β). On the one hand, TGF-β-induced senescence in HCC cells is dependent on NOX4, p21^{cip1}, p15^{Ink4b} and ROS (Senturk et al., 2010). On the other hand, our group described that TGF-β activation of NOX4 promotes hepatocyte (Carmona-Cuenca et al., 2008) and hepatocellular carcinoma cells apoptosis, and overactivation of

the MEK/ERK pathway in liver tumor cells confers them resistance to the TGF-β -induced cell death through impairing NOX4 upregulation (Caja et al., 2009). We also reported that NOX4 silencing in HCC cells confers them higher tumorigenic potential, trough downregulation of p21^{cip1}, upregulation of cyclin D1 and nuclear localization of β-catenin (Crosas-Molist et al., 2014). Also, NOX4 is necessary for adhesion of the cell–cell and cell–matrix, leading to the suppression of epithelial-to-amoeboid transition and the inhibition of liver cancer progression via the decreased expression of *RhoC* and *Cdc42* (Crosas-Molist et al., 2017). In accordance, it has been recently described that deletion of NOX4 promotes colon carcinoma and fibrosarcoma tumor formation, concomitant with increased activity of AKT and lower recognition of DNA damage (Helfinger et al., 2021). Eun *et al*. reported that whereas HCC patients with high *NOX4* and *DUOX1* expression showed higher survival in association with genes that inhibit tumor progression, those patients with high *NOX1/2/5* showed poor prognoses and genes associated with cell survival and metastasis (Eun et al., 2017). Eun *et al*. later described that high nuclear NOX4 and low cytoplasmic NOX4 correlate with short overall survival in HCC patients (Eun et al., 2019) Finally, it has been described that TGF-β dependent activation of fibroblast to cancer associated fibroblasts (CAFs) is dependent on ROS produced by NOX4 (Hanley et al., 2018).
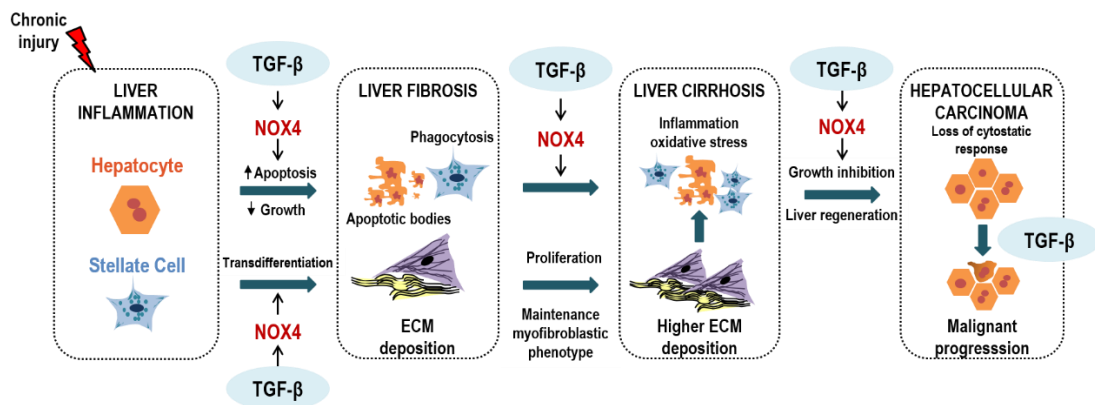
Figure XIII. NOX4 implication in different stages of liver chronic diseases. Early on, NOX4 induces apoptosis of hepatocytes and transdifferentiation of HSCs to myofibroblasts after a chronic injury, which leads to an inflammatory process and liver fibrosis. If chronic injury is maintained, liver fibrosis leads to liver cirrhosis, which is the previous step of Hepatocellular carcinoma. At that stage, NOX4 acts as a tumor suppressor during early stages, but once tumor cells acquire the capacity to overcome its cytostatic response, it acts as a pro-tumorigenic cytokine (Adapted from (Fabregat et al., 2016).

4.3.5. NOX targeting

Considering that the function of NOX in the regulation of many physiological functions remains poorly understood, the development of NOX inhibitors may help to uncover how NOX regulates these pathways. Moreover, regarding the role of NOX in the pathogenesis of many diseases, such as fibrotic diseases, neurodegenerative disorders, or cardiovascular diseases, NOX inhibitors have also a potential therapeutic purpose. Several NOX inhibitors have been identified, and for some pathological conditions, it has been demonstrated that pharmacological inhibition of NOX is beneficial. However, until the date, there are not specific NOX inhibitors, most compounds are **pan-NOX inhibitors**. Considering the role of ROS in physiological signaling processes, another form of imbalance deserves attention, i.e., reductive stress, which is the excess of reducing agents in a cell, leading to shortage of ROS. Therefore, instead of attempting to systematically scavenge ROS, it would be more effective to target specifically the source of pathophysiological relevant ROS (Altenhofer et al., 2012; Buvelot, Jaquet, et al., 2019; Schmidt et al., 2021). With that aim, some of the most known NOX inhibitors will be briefly reviewed:

- **Diphenyleneiodonium (DPI)** acts as a general flavoprotein inhibitor and thus inhibits many other enzymes apart from NOXs, such as eNOS, xanthine oxidase, and proteins of the mitochondrial electron transport chain. It is the most useful pharmacological tool for *in vitro* studies.

- **Apocynin.** It shows intrinsic antioxidant effects, that is, non-specific ROS scavenging properties. Importantly, apocynin activation results in the formation of a radical and thus apocynin can induce oxidative stress in the cell by itself.

- **VAS2870** is a triazolo pyrimidine. It was developed by the company Vasopharm GmbH as a NOX2 inhibitor. It directly modifies thiols like the ones in p47^{phox}, thus inhibiting both NOX1 and NOX2. Some studies also suggest that it can inhibit NOX4 and NOX5.

- **GKT compounds.** GKT136901 and GKT137831 (setanaxib or GKT-831), developed by GenKyoTex, potently inhibit NOX1 and NOX4, and partially NOX5 (50% inhibition of activity (IC_{50})). Their mode of action is unclear and is probably not restricted to direct NOX inhibition. Nevertheless, GKT inhibitors show promising results in several animal models of oxidative stress-induced disease. In fact, GKT137831is currently in a phase II clinical trial for the treatment of primary biliary cholangitis, idiopathic pulmonary fibrosis and kidney disease in type 1 diabetes (Altenhöfer et al., 2015; Brandes et al., 2014; Buvelot, Jaquet, et al., 2019; Schmidt et al., 2021).

- **GLX7013114.** GLX7013114 specifically inhibits NOX4 and it counteracts human islet cell death *in vitro* (Wang et al., 2018), and it has been used in preclinical studies.

Considering the interest in the development of NOX inhibitors to treat several pathologies, and specifically, taking into account the use of NOX4 inhibitors in the context of liver fibrosis, it seems indispensable to analyze which would be the consequences of using these compounds in liver physiology.

4.3.6. NOX4 Knock-out mice models

In contrast to NOX inhibitors, which have limited isoform selectivity, knockout mouse models allow to study the involvement of individual NOX isoforms in a given disease.

At least **four NOX4 knock-out** mouse models have been published to date. They differ in the genetic strategy that was applied to generate them. Thus, different exons were deleted, and constitutive, cell-specific or inducible cre/lox systems were used (Altenhofer et al., 2012). Deletion of exons 1 and 2 should delete the complete NOX4 protein (Helfinger et al., 2021; Rezende et al., 2017; Schröder et al., 2012; M. Zhang et al., 2010). Deletion of exon 4 leaves the first transmembrane domain of NOX4 (Carnesecchi et al., 2011; Y. Li et al., 2012). Another knock-out was generated by deleting exon 9 of NOX4 in cardiomyocytes, deleting the FAD binding domain and leaving a non-functional enzyme (Kuroda et al., 2010). Finally, the fourth published NOX4 knock-out mouse was generated by deleting exons 14 and 15, that encode to the NADPH binding domain (Kleinschnitz et al., 2010).

Interestingly, NOX4 gene deletion in mice does not affect the life span of the animals (Rezende et al., 2017), and they do not display a notable phenotype except for a moderate tendency for accelerated increase in weight (Y. Li et al., 2012).

4.4. NADPH oxidases and Regeneration

Although very little is known about the role of NADPH oxidases during liver regeneration, some studies have reported involvement of NADPH oxidases during tissue repair or regeneration after injury.

NOX1 is required for epithelial restitution following dextran sulfate sodium-induced colitis. NOX1 expression, as well as ROS production, increase in the colon crypt during the repair process, and NOX1 deficiency mice presented inhibition of proliferation, cell survival, migration, and terminal differentiation of crypt progenitor cells (Kato et al., 2016). With respect to NOX2, vitamin D improved vascular regeneration after carotid injury in a NOX2-dependent manner trough MAPK activation. Healing was lost in NOX2-/- mice, but not in NOX1-/- and NOX4-/- mice (Leisegang et al., 2016). Moreover, during nerve injury, NOX2 oxidizes PTEN, which promotes PI3K/Akt pathway activation and dorsal root ganglia

regenerative outgrowth (Hervera et al., 2018). Further, after spinal cord injury, enriched conditioning expands the regenerative ability of sensory neurons via neuronal PKC-STAT3-NOX2 signaling (De Virgiliis et al., 2020). Han et al. identified that Duox/Nox2 levels increase during zebrafish heart regeneration. H_2O_2, potentially generated from those NADPH oxidases, promotes heart regeneration by unleashing MAP kinase signaling through a de-repression mechanism (Han et al., 2014).

Regarding NOX4, some studies report a detrimental role of NOX4 during tissue repair. For instance, Cao et al. showed that HGF produced by endothelial cells mitigates profibrotic NOX4 expression in perivascular fibroblasts. Ectopic induction of endothelial cells-induced HGF in combination with NOX4 inhibitor GKT137831 stimulated regenerative integration of mouse and human parenchymal cells in chronically injured lung and liver (Cao et al., 2017). Furthermore, bromodomain and extraterminal (BET) inhibitor inactivate epigenetic reader proteins, such as Brd4, thus blocking the association of Brd4, H4K16ac, and p300 acetyltransferase with NOX4 promoter region. BET-induced NOX4 downregulation restores lung capacity and improve lung fibrosis resolution in aged mice (Sanders et al., 2020). By contrast, other groups proposed NOX4 as a pro-regenerative protein. For instance, NOX4 contributed to myoblast fusion and skeletal muscle regeneration after injury by cardiotoxin (Youm et al., 2019).

With respect to liver regeneration, Ueno et al. described that reactive oxygen species derived from a phagocytic-related NOX system are not essential for LR after PH. Knockout mice lacking Cybb (NOX2) presented a normal liver structure as well as normal TNF-α and IL-6 production after PH, and similar levels of hepatocyte DNA replication as those of WT mice (Ueno et al., 2006). Moreover, mice lacking the subunit gp91(phox) of NOX2 did not have altered acetaminophen-induced liver injury or recovery. In that model, neither Kupffer cells nor neutrophils are able to generate ROS, meaning that injury and clean-up functions are not dependent on NOX2-derived ROS production (Williams et al., 2014). Importantly, our grouped described that **NOX4 expression was downregulated under physiological proliferative situations** of the liver, such as **regeneration after PH**, as well as during pathological proliferative conditions, such as Diethylnitrosamine (DEN)-induced hepatocarcinogenesis (Crosas-Molist et al., 2014).

Reactive oxygen species scavengers have been administrated during liver regeneration. In general, antioxidant treatment improves liver regeneration, indicating that ROS could be deleterious during this process. Thus, α-tocopherol shows a beneficial effect on LR after PH on rats (Al Dohayan, 1999), and elevating levels of antioxidants with

edaravone in human umbilical cord mesenchymal stem cells (hUCMSCs) significantly improved hepatic functions and promoted host liver regeneration (Zeng, 2015). Moreover, rats treated with cerium oxide nanoparticles show a significant increase in LR after PH, and they presented a decreased early liver damage in response to acetaminophen treatment (Córdoba-Jover, 2019). Nevertheless, Bai *et al.* described that H_2O_2 promotes adult hepatocytes to transition from quiescence to proliferation in an ERK-dependent pathway, and they also reported an increase in H_2O_2 early after 2/3 PH (Bai et al., 2015).

Considering that liver regeneration occurs during both acute and chronic damage and the implication of NOX4 in fibrosis and HCC, it is important to know the role of NOX4 during liver regeneration. However, with the exception of some studies relating NOX4 and tissue repair, very little is known.

II. Hypothesis

Due to the role of NOX4 as mediator of fibrotic processes in the liver, there is an increasing interest in the development of NOX4 inhibitors, which could be used as a treatment to ameliorate fibrosis. However, whether NOX4 plays a role during liver regeneration is not known yet. Previous results indicate that expression of *Nox4* decreases in the model of liver regeneration after two-thirds partial hepatectomy in mice; and previous results from our group have demonstrated that in hepatocytes and liver tumor cells, NOX4 inhibits proliferation and mediates TGF-β-induced apoptosis. Taking all this into consideration, we hypothesize that deletion of *Nox4* could contribute to improve the proliferative process rate and mass recovery during liver regeneration after partial hepatectomy.

III. Objectives

The main objective of this thesis was **to study liver regeneration after two-thirds partial hepatectomy in murine models of *Nox4* deletion.**

Specific objectives:

Objective 1. *In vivo* analysis of the role of Nox4 during liver regeneration in experimental animal models. Analysis of the capacity of two different mice models with null expression of *Nox4* to regenerate the liver after two-thirds (2/3) partial hepatectomy (PH).

1.1 Analysis of the liver-to-body weight ratio and tissue recovery after 2/3 PH.

1.2 Analysis of cellular proliferation after 2/3 PH.

1.3 RNA-seq analysis to identify how Nox4 influences the liver regeneration transcriptomic program.

1.4 Analysis of the expression of growth factors related to liver regeneration, as well as growth suppressor pathways.

1.5 Potential role of Nox4 in controlling lipid metabolism and oxidative stress.

1.6 Analysis of liver regeneration after 2/3 PH in one-year-old mice.

Objective 2. *In vitro* analysis of the cellular and molecular mechanisms involved in the regulation of liver cell proliferation by Nox4 *in vitro*, by using hepatocytes isolated from WT and *Nox4* deleted mice models.

2.1 Analysis of cell proliferation in response to mitogens.

2.2 Response to TGF-β in terms of intracellular signaling and inhibition of cell proliferation.

IV. Materials and Methods

1. Animal experimentation

1.1. Ethics statement

All experiments complied with the EU Directive 2010/63/UE for animal experiments and the institution's guidelines (Ethical Committee for animal experimentation of IDIBELL) and were approved by the General Direction of Environment and Biodiversity, Government of Catalonia (experiments in NOX4-/- mice, #4589) and the Animal Care Committee of UC Davis (experiments in NOX4hepKO mice).

1.2. NOX4 Knock-out animal models

NOX4-/- (B6.129-Nox4tm1Kkr/J) mice generated in Dr. Karl-Heinz Krause's laboratory (Geneva, Switzerland), were obtained from Jackson Laboratories (JAX stock #022996) and housed at IDIBELL (Barcelona, Spain). In this model, a neomycin cassette replaces exon 4 of the *Nox4* gene, abolishing gene expression in these null/knockout mice (Carnesecchi et al., 2011)(**Figure 1**). C57BL/6J mice were used as Wild Type control mice.
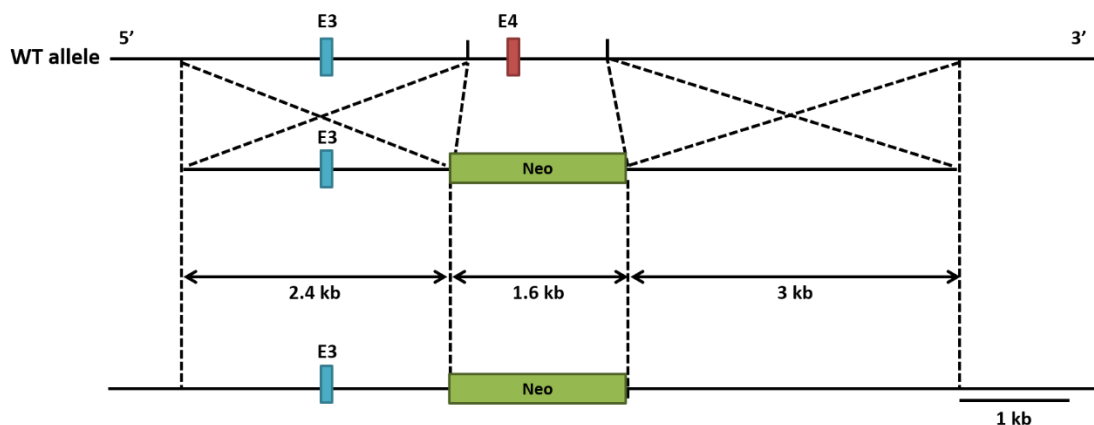
Figure 1. Diagram of the targeting vector (middle) designed to replace the *Hind*III fragment containing exon 4 of the *Nox4* gene in the wild-type (WT) allele (top) with a *neo* cassette (Neo). The predicted mutant allele generated by homologous recombination is shown (bottom). (Adapted from Carnesecchi et al., 2011).

Genotyping was assessed by polymerase chain reaction (PCR) as specified in the JAX protocol and explained later (Section 4.1), using specific primers that exclusively detect expression of *Nox4*. It was verified that the amplified region of the *Nox4* gene in NOX4-/- mice had a higher size (approximately 350bp) than the one from WT mice (228bp) due to the presence of the neomycin cassette (**Figure 2**).
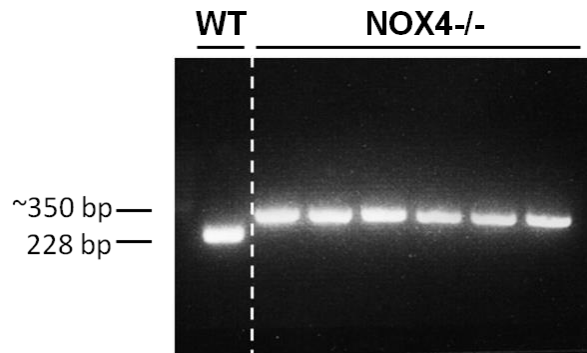
Figure 2. Validation of the experimental animal model B6.129-Nox4tm1Kkr/J (abbreviated NOX4-/-) mice. Study of *Nox4* gene by semi-quantitative PCR in 3-weeks old mice.

NOX4 hepatocyte-specific knockout (**NOX4hepKO**) mice on a C57BL/6J background were generated in Dr. Natalie J. Török's group (Bettaieb et al., 2015), and housed at University of California Davis (Sacramento, CA, USA). NOX4floxp+/+ mice with C57BL/6 background (from Dr. Brandes, Goethe University, Frankfurt, Germany) were generated by targeted deletion of the translation initiation site and exons 1 and 2 of the *Nox4* gene (Zhang et al., 2010). The NOX4floxp+/+ mice were bred with C57BL/6 Albumin-Cre mice (Jackson) to create NOX4 hepatocyte-specific knockout (NOX4hepKO) mice (**Figure 3**). NOX4floxp+/+ mice with C57BL/6 background were used as control animals (WT). We established a collaboration with Dr. Török for using these animals in our project.
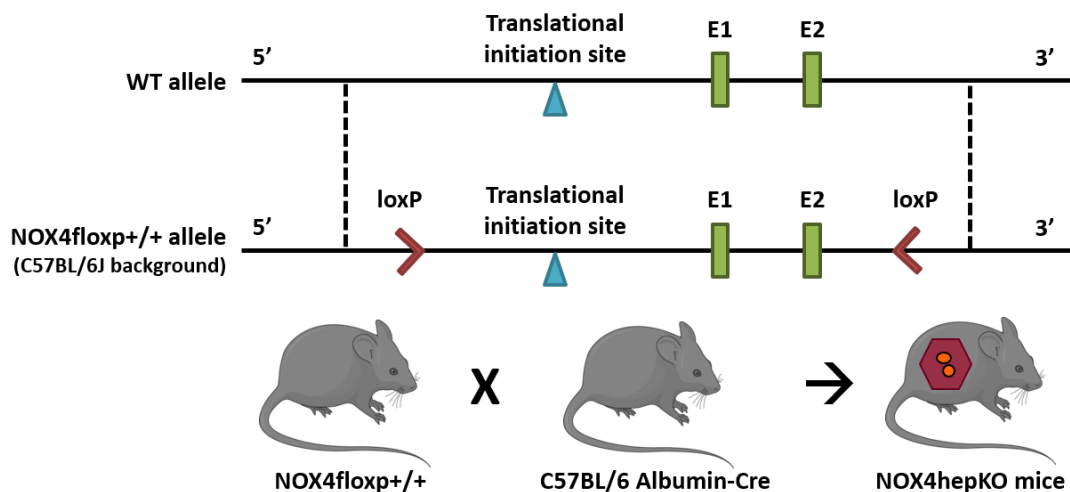
Figure 3. Diagram of the NOX4floxp+/+ allele (bottom), containing LoxP sites to target Translation initiation site and exon 1 and 2. Recombination between LoxP sites is catalyzed by Cre recombinase under the control of the mouse albumin promoter.

1.3. Partial hepatectomy

8 to 16-week-old male and female mice hosted under 12h light/dark cycles with free access to food and water were used in the study. Partial hepatectomies (PH) were performed by removal of two-thirds of the adult mouse liver, as described by Higgins and Anderson (Higgins & Anderson, 1931). Mice were anesthetized by isoflurane and subcutaneous injection of buprenorphine. Briefly, after cleaning the animal with 70% Ethanol, an incision was made just above the sternum bone and opened a little bit up and down. Next, a "V" incision was made on the muscle layer just delimiting the bone. By pushing with four fingers from down to up surrounding the opened area, the central and left lobe of the liver got out of the body. A ligature surrounding the two lobes was performed and the two lobes were removed simply by cutting them. Finally, both incisions were closed sewing them and mice were subcutaneously injected with meloxicam. Mice were euthanized at 6, 24, 36, 48 and 72 hours, 7 days and 4 weeks after surgery (**Figure 4**). Livers from SHAM-operated mice were used as control. Liver lobes were immediately frozen in liquid nitrogen for RNA and protein extraction, cryopreserved in optimal cutting temperature (OCT) compound or fixed in 4% paraformaldehyde (PFA) overnight and paraffin embedded for histological analysis (protocols below).
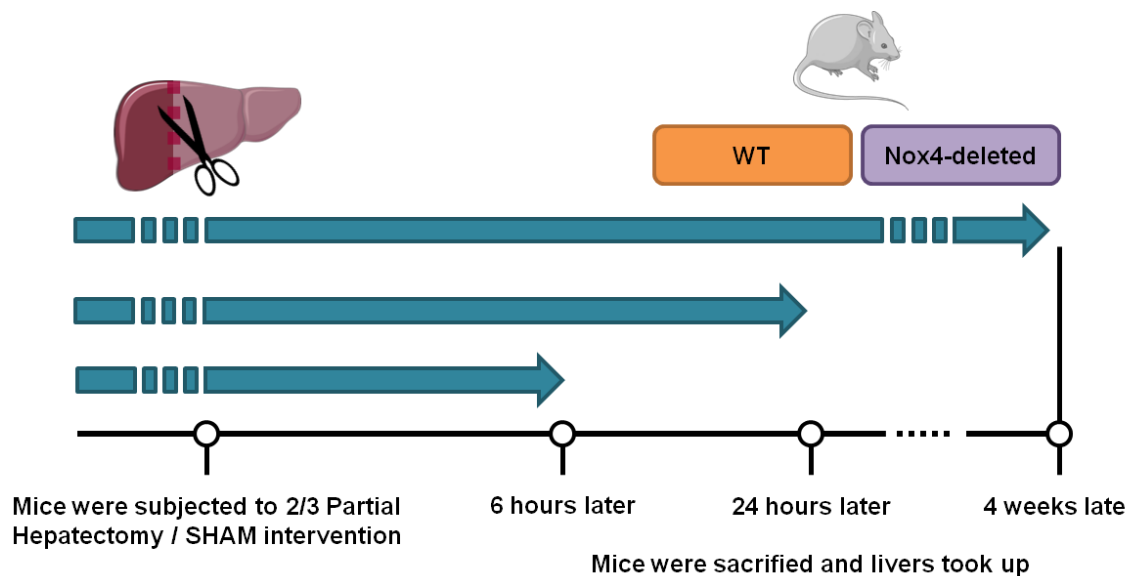
Figure 4. Schematic representation of the experimental schedule.

NOX4-/- partial hepatectomy experiments were performed by Judit López Luque, Daniel Caballero Díaz, Noel Pérez Fusté and Macarena Herranz Itúrbide in the IDIBELL (Barcelona, Spain). NOX4hepKO partial hepatectomy experiments were performed by Judit López Luque and Xiaosong Jiang in University of California Davis (Sacramento, CA, USA).

Number of animals used in the study was minimized for ethical reasons. Thus, for NOX4-/- model between 3-10 animals were used per time point (**Table 1** and **2**). For NOX4hepKO model between 2-3 animals per time point were analyzed (**Table 3**) and 2 different RNA extractions per animal liver tissue were done.

Table 1. Number of 8-12-weeks-old WT and NOX4-/- mice used in PH experiments.

	WT	NOX4-/-
SHAM	5	7
6 hours	3	10
24 hours	4	9
36 hours	5	6
48 hours	7	10
72 hours	6	7
7 days	6	7
4 weeks	5	4

Table 2. Number of 1-year-old WT and NOX4-/- mice used from in PH experiments.

	WT	NOX4-/-
SHAM	4	4
24 hours	5	5
48 hours	4	5
72 hours	3	4

Table 3. Number of 8-16-weeks-old NOX4floxp+/+ and NOX4hepKO mice used in PH experiments.

	NOX4floxp+/+	NOX4hepKO
SHAM	3	2
24 hours	2	3
36 hours	3	2
48 hours	2	3
72 hours	3	2

1.4. Isolation of primary hepatocytes

8 to 16-week-old male and female mice hosted under 12h light/dark cycles with free access to food and water were used in the study. Mice were anesthetized by intraperitoneal injection of xylazine and ketamine. After cleaning the animal with 70% Ethanol, an incision was made through the ventral midline and the viscera were displaced to the right to expose the inferior vena cava and the portal vein. The liver was perfused *in situ* with Solution I (**Table 4**) via the inferior vena cava, and immediately the portal vein was severed. Then, suprahepatic veins were clamped off. After washing the liver with Solution I, it was perfused with Collagenase solution (C5138, Sigma, Saint-Louis, MO, USA) (**Table 5**). Once perfusion was completed, the liver was carefully excised and placed in a Petri dish containing Solution III (**Table 6**). Glisson's capsule was cut to obtain disperse cells. This cell suspension was filtered through a 100-μm strainer and centrifuged twice at 70 ×g to eliminate non-parenchymal cells. Finally, number and viability of cells was quantified with a Neubauer chamber.

Isolation of NOX4-/- primary hepatocytes were performed by Ester González Sánchez and Macarena Herranz Itúrbide in the IDIBELL (Barcelona, Spain). Isolation of NOX4hepKO primary hepatocytes were performed by Judit López Luque and Xiaosong Jiang in University of California Davis (Sacramento, CA, USA).

Table 4. Solution I. After prepared, pH was adjusted 7.3-7.5.

Compound	Quantity
Hanks' Balance Salts (WO Calcium) (Sigma-Aldrich H2387)	
HEPES	2.38 g
NaHCO$_3$	0.35 g
EDTA	0.19 g
ddH$_2$O	1 L

Table 5. Solution II: Collagenase solution. After prepared, pH was adjusted 7.3-7.5.

Compound	Quantity
MEM (with Ca2+)	75mL
Collagenase IV	0.018 g *
BSA (180 mg/100 mg Collagenase)	0.324 g *

*For 2/3 hepatectomized mice, 0.06 g of collagenase and 0.108 g of BSA were used.

Table 6. Solution III. After prepared, pH was adjusted 7.3-7.5.

Compound	Quantity
Hanks' Balance Salts (Sigma- Aldrich H6136)	
HEPES	2.38 g
$NaHCO_3$	0.35 g
FBS	100 mL
BSA	2 g
ddH_2O	1 L

2. Cell culture

2.1. Culture conditions

After primary hepatocytes isolation, cells were plated in collagen I-treated plates with Williams'E medium (W4125, United Kingdom), supplemented with 15% Fetal bovine serum (FBS) (Gibco®), Bovine serum albumin (BSA) (0.2%), Insulin (1,8 uM) (I9278, Sigma-Aldrich, St. Louis, MO, USA), Hydrocortisone (100 uM) (H2270, Sigma-Aldrich, St. Louis, MO, USA), Penicillin (100U/mL) and Streptomycin (100μg/mL) and maintained in a humidified atmosphere of 37ºC, 5% CO_2.

2.2. Treatments used

For the experiments with NOX4hepKO primary hepatocytes, cells were serum-starved for 8h before treatment with fresh Williams'E medium supplemented with human recombinant TGF-β1 (2ng/ml) (Calbiochem, La Jolla, CA, USA), or 2 or 15% FBS.

For experiments with NOX4-/- primary hepatocytes, cells were serum-starved for 4 h and treated with fresh Williams'E medium supplemented with: FBS (2%), human recombinant TGF-β1 (2ng/ml) (616455, Calbiochem, La Jolla, CA, USA), Insulin (2μM), Hydrocortisone (100μM), EGF (20ng/mL) (E9644, Sigma-Aldrich, St. Louis, MO, USA), as indicated in the figures.

3. Analysis of cell proliferation

3.1. Crystal violet staining

Adherent cells detached after undergoing a toxic process, so crystal violet staining allows quantifying the number of cells that survive after a toxic process. It is useful as well for quantifying the changes in the cell number along time when cells are cultured under certain conditions. The method consists on cell staining with a colorant, crystal violet. Primary hepatocytes were seeded in 24-well plates and cultured under basal conditions or treated with FBS or TGF-β1.

After the time of culture required, cell medium was removed, cells were washed twice with Phosphate-buffered saline (PBS) and the remaining viable adherent cells were stained with 300µL/well of crystal violet solution (0.2%(w/v) in 2% ethanol) for 30 minutes. Following this, the staining solution was removed, and the wells were washed several times with distilled water until the dye excess was eliminated. The plate was air-dried, and the stained cells were lysed by adding 10% Sodium Dodecyl Sulfate (SDS) for 30 minutes, in motion. This led to a cellular rupture that released the dye incorporated by the remaining cells and stained the SDS proportionally to the number of still attached cells. By spectrophotometric analysis, the absorbance was measured in a wavelength of 595nm. Results were then calculated as the percentage of viable cells at the indicated times relative to time zero.

4. Analysis of gene expression

4.1. DNA isolation and semi-quantitative Polymerase Chain Reaction (PCR) of genomic DNA

To confirm the experimental animal model genotyping was performed. Mouse ear snips were obtained from 3-weeks old mice and they were incubated in PUNCH buffer (10mM NaOH, 1mM EDTA) at 99ºC for 10 minutes. Subsequently, the tubes were spinned at maximum speed to obtain the supernatant with the genomic DNA. PCR amplification was used for detection of the modified gene of *Nox4*. 2mL of each tissue sample supernatant was used per PCR reaction using the kit KAPAG2 Fast HotStart ReadyMix with loading dye PCR kit (Ref. B4KK5609, KAPA BIOSYSTEM, Boston, Massachusetts, USA) according to the manufacturer's instructions. PCR conditions were as follows: 94ºC for 2 minutes, 10x [94ºC for 20 s, 65ºC for 15 s, 68ºC for 10 s], 28x [94ºC for 15 s, 60ºC for 15 s, 72ºC for 10 s], 72ºC for 2 minutes and hold at 10ºC. NOX4-/- mice were genotyped using the primers (**Table 7**) and the instructions provided by Jackson Laboratories (**Table 8**). PCR products were analyzed in 1.5% agarose gels with ethidium bromide, and visualized using a Gel DOC 2000 (BioRad).

Table 7. Primers sequences used in semi-quantitative PCR for genotyping NOX4-/- mice.

Gene (mouse)	Primer (5'-3')
Nox4 *Common Forward primer (17665)*	GTGGTCCAACAGAACAACTGC
Nox4 *Wild Type Reverse primer (17666)*	CACAAGTCTCCTAGTCAAAAGTGA
Nox4 *Mutant Reverse primer (17814)*	AACGTCGTGACTGGGAAAAC

Table 8. Semi-quantitative PCR conditions.

Reaction component	Volume (µl)	Final concentration	Total volume (µl)
ddH2O	4.25		4.25
5X Kapa 2G HS buffer	2.40	1X	2.4
25nM MgCl2	0.96	2mM	0.96
10mM dNTPS-kapa	0.24	0.2mM	0.24
20µM 17665	0.30	0.5µM	0.3
20µM 17666	0.30	0.5µM	0.3
20µM 17814	0.30	0.5µM	0.3
5mM 10x Loading Dye	1.20	0.5mM	1.2
2.5 U/µl Kapa 2G HS taq polymerase	0.05	0.01U/µl	0.05
DNA	2.00		2

4.2. RNA isolation and Reverse Transcription

E.Z.N.A.® Total RNA Kit II (Omega bio-tek, Norcross, GA, USA) was used for total RNA isolation, following Manufacturer's protocol. For RNA isolation from culture cells, plates were washed with PBS. After 3 minutes incubation with trypsin, cells were collected and centrifuged at 2500rpm for 5 minutes. The pellet was resuspended in PBS and centrifuged again. Then, it was resuspended in 350uL RNA solv-Reagent with 20 μL/mL of β-Mercaptoethanol.

When RNA was isolated from tissues, small pieces of the frozen liver were mechanically fragmented with a tissue grinder and resuspended in 1mL of RNA solv-Reagent with 20 μL/mL of β-Mercaptoethanol.

Reverse transcription (RT) was carried out with random primers using 1μg of total RNA from each sample for complementary DNA synthesis using High Capacity RNA to cDNA Master Mix Kit (Thermo Fisher Scientific, Applied biosystems, Vilnius, Lithuania), according to the guidelines of manufacturer.

4.3. Real Time Quantitative PCR (RT-qPCR)

For quantitative real time PCR, cDNA was obtained as explained in the previous section. Expression levels were measured in duplicate in a LightCycler® 480 Real Time PCR System, using the LightCycler® 480 SYBR Green I Master Mix (Roche Diagnostics GmbH, Mannheim, Germany), in a 384-well plate, in a final volume of 20μL per duplicate. The PCR reaction was prepared using 5μL of SYBR Green I Master Mix, 1μL specific primers (5μM) (Table 9) and 1μL of cDNA (1:5 or 1:10 diluted depending on the gene of interest), and finally, it was added RNAse free water up to 10μL per each duplicate. Then, the plate was centrifuged at 1200 rpm for 2 minutes at 4ºC, and after that, it was introduced into the thermocycling machine. After that, manufacturer's protocols were followed to determine mRNA levels for each gene of interest and were normalized with *Rpl32* as a housekeeping gene.

Table 9. Mouse primers sequences used in a LightCycler 480 SYBR Green System quantitative PCR.

Gene	Forward (5'–3')	Reverse (5'–3')
Ccna2	GAATGTCAACCCCGAAAAACTG	TGCTCATCGTTTATAGGAAGGTC
Ccnb2	TCCTAAAGCCAAGAGCCATG	TGGTACTTTGGTGTTCTGAGG
Ccnd1	CATCTACACTGACAACTCTATCCG	TCTGGCATTTTGGAGAGGAAG
Myc	AGCCCCTAGTGCTGCATGA	TCCACAGACACCACATCAATTTC
Nox1	TCCATTTCCTTCCTGGAGTG	GCATTGGTGAGTGCTGTTGTTC
Nox2	TCCTATGTTCCTGTACCTTTGTG	GTCCCACCTCCATCTTGAATC
Nox4	AAAGCAAGACTCTACACATCACAT	AGTTGAGGGCATTCACCAAG
Rpl32	AACGTCAAGGAGCTGGAAG	GGGTTGGTGACTCTGATGG
Tgfb1	CCTGAGTGGCTGTCTTTGA	CGTGGAGTACATTATCTTTGCTG

5. RNA sequencing (RNA-seq)

Total RNA from *Mus musculus* was quantified by Qubit® RNA BR Assay kit (Thermo Fisher Scientific) and the RNA integrity was estimated by using RNA 6000 Nano Bioanalyzer 2100 Assay (Agilent). The RNA-seq libraries were prepared with KAPA Stranded mRNA-Seq Illumina® Platforms Kit (Roche) following the manufacturer´s recommendations. Briefly, 500 ng of total RNA was used for the poly-A fraction enrichment with oligo-dT magnetic beads, following the mRNA fragmentation. The strand specificity was achieved during the second strand synthesis performed in the presence of dUTP instead of dTTP. The blunt-ended double stranded cDNA was 3´adenylated and Illumina platform compatible adaptors with unique dual indexes and unique molecular identifiers (Integrated DNA Technologies) were ligated. The ligation product was enriched with 15 PCR cycles and the final library was validated on an Agilent 2100 Bioanalyzer with the DNA 7500 assay. The libraries were sequenced on HiSeq 4000 (Illumina) with a read length of 2x51bp+17bp+8bp using HiSeq 4000 SBS kit (Illumina) and HiSeq 4000 PE Cluster kit (Illumina), following the manufacturer's protocol for dual indexing. Image analysis, base calling and quality scoring of the run were processed using the manufacturer's software Real Time Analysis (RTA 2.7.7).

Reads obtained by RNA-seq were mapped against *Mus musculus* reference genome (GRCm38) using STAR software version 2.5.3a (Dobin et al., 2013) with ENCODE parameters for long reads. Annotated genes were quantified using RSEM version 1.3.0 (Li & Dewey, 2011) with default parameters and the annotation file from GENCODE version M15. Differential expression analysis was performed withDESeq2 v1.26.0 R package (Love et al., 2014), using a Wald test to compare the different time points between samples WT and NOX4-/-, and adjusting for sex. We considered differentially expressed genes (DEG) those with p-value adjusted <0.05 and absolute fold-change |FC|> 1.5. The heatmap was plotted with the 'pheatmap' R package using the shrunken log2 fold change of the DEG in each time point. Time course gene expression plots were generated using the normalized counts obtained with DESeq2 and the R package 'ggplot2'. A Gene Ontology (GO) term enrichment analysis was performed with the differentially expressed genes using the R package gProfileR v0.7.0 (Reimand et al., 2007), based on GO terms from the ENSEMBL database. Networks of protein-protein interactions were generated using the webtool STRING dB (https://string-db.org/).

6. Analysis of protein expression

6.1. Cell lysis

For protein lysis from cells in culture, cell plates were washed with PBS. After 3 minutes incubation with trypsin, cells were collected and centrifuged at 2500rpm for 5 minutes. The pellet was resuspended in PBS and centrifuged again. Then, it was resuspended in 60-100uL of RIPA Lysis Buffer (**Table 10**) and cell lysis took place during one hour with rotation at 4ºC. Subsequently, tubes were centrifuged at 13000rpm during 10 minutes at 4ºC, and the supernatants were collected in new eppendorf tubes and store at -80ºC until use.

Table 10. RIPA Lysis Buffer.

Sodium Deoxycholate	0.5%
TRIS-HCl pH 7.5	30mM
SDS	0.1%
Triton-X-100	1%
NaCl	150mM
EDTA	5mM
Glycerol	10%
PMSF	1mM
Leupeptin	5μg/mL
Na_3VO_4	0.1mM
DTT	0.5mM
β-Glycerolphosphate	20mM

When protein was isolated from tissues, small pieces of the tissue were mechanically fragmented with a tissue grinder, resuspended in 250μL of RIPA Lysis Buffer (**Table 10**) and transferred to an eppendorf tube. Afterwards, cell lysis took place during one hour with rotation at 4ºC. Subsequently, tubes were centrifuged at 13000rpm during 10 minutes at 4ºC, and the supernatants were collected in new eppendorf tubes and store at -80ºC until use.

6.2. Protein quantification by Bio-Rad commercial kit

Protein concentration was measured using the commercial kit Bio-Rad Protein Assay dye reagent concentrate (Bio-Rad Laboratories GmbH, Munich, Germany). For each measurement, a standard curve of protein concentration was prepared with Bovine Serum Albumin (BSA) in a range from 0 to 2μg/μL. The commercial solution was firstly diluted 1:5 in distilled water. Afterwards, 200μL of this solution were added to 10μL of diluted sample

(1:150 for liver lysates and 1:20 for primary hepatocytes), into a 96-well plate. Absorbance was measured in duplicates at 595 nm wavelength, without previous incubation.

6.3. Protein immunodetection by Western blot

Protein separation by their molecular weight was done by denaturalizing polyacrylamide gels. Protein samples were prepared by mixing 20-30 µg of protein with Laemmli loading buffer and were denaturalized by heating them at 95ºC during 5 minutes. Acrylamide gels were prepared depending on the protein of interest. For proteins with low molecular weight 12-15% acrylamide gels were prepared. Whereas for proteins with high molecular weight, 8-10% acrylamide gels were prepared. Once the gel was ready to be used, it was assembled into the gel holder and immersed into the tank, which was filled with an electrophoresis buffer (25 mM Tris; 192 mM glycine; 0.1% SDS (w/v); pH 8.3). Then, samples were carefully loaded into the gel, together with a molecular weight standard in order to know the molecular weight of the proteins studied. Finally, the samples were submitted to electrophoresis at a constant voltage of 100V.

Once the electrophoresis finished, proteins were transferred to a Nitrocellulose Blotting Membrane (GE Healthcare, Life Science, Germany) through the passage of electrical current using a wet equipment. Firstly, the nitrocellulose membrane was immersed into water for 1 minute in order to activate it. Then, the nitrocellulose membrane, the gel and the Wattman papers were soaked in transfer buffer (25 mM Tris; 192 mM Glycine; 20% Methanol (w/w); pH 8.3) for approximately 5 minutes, and the equipment was assembled as follows from bottom to top: 3 Wattman papers - nitrocellulose membrane - Acrylamide gel - 3 Wattman papers. An electrical current of 300 mA was applied during 45-75 minutes (depending on the protein of interest). After this time, the membrane was stained into a solution of 0.5% red Ponceau in 1% acetic acid to confirm that proteins were uniformly transferred into the membrane. Then, membrane was washed several times in PBS-T 0.05%.

For blotting the desired protein, the membrane was incubated in 5% of non-fat dry milk in PBS-T for one hour at RT, in order to block unspecific bindings. After this time, it was incubated with the primary antibody (see antibodies and conditions in **Table 11**) in 0.5 % milk in PBS-T overnight at 4°C in motion. After that, the membrane was washed 3 times during 10 minutes with PBS-T (0.05%), and subsequently incubated with the secondary antibody (from GE Healthcare: anti-Mouse (NA931V) and anti-Rabbit (NA934V), conjugated with Horseradish Peroxidase (HRP)) at a dilution of 1:2000 in 0.5% milk-PBS-T

during 1 hour at RT in motion. The membrane was washed again 3 times in PBS-T (0.05%). To detect the hybridation of the antibody, the membrane was incubated with ECL TM Western blotting detection reagent (GE Healthcare, Life Science, UK) and developed with ChemiDoc Gel Imaging System (BioRad). Densitometric analysis of protein bands' intensity was performed using ImageJ software (National Institutes of Health (NIH), Bethesda, MD, USA).

Table 11. Primary antibodies used for Western blotting.

Primary antibody	Reference	Working conditions
Mouse anti β-actin (Clone AC-15)	A5441 (Sigma-Aldrich)	1:5000
Mouse anti-Caveolin-1	610406 (BD- Biosciences)	1:800
Mouse anti-p21	sc-6246 (Santacruz)	1:1000
Rabbit anti-Myc	ab32072 (Abcam)	1:1000
Rabbit anti-M6PR	ab124767 (Abcam)	1:1000
Rabbit anti-phospho-Akt (Ser473)	4060 (Cell Signalling)	1:1000
Rabbit anti-phospho-p44/42 MAPK (Erk1/2) (Thr202/Tyr204)	9101 (Cell Signalling)	1:1000
Rabbit anti-phospho Smad2 (Ser465/467)	3108 (Cell Signalling)	1:1000
Rabbit anti-phospho Smad3 (Ser423/Ser425)	07-1389 (Millipore)	1:1000

7. Immunocytochemistry

7.1. Immunofluorescence in cultured cells

Epifluorescence microscopy studies were performed on cells seeded on gelatin-coated glass coverslips. To detect Ki67 (Ab1666, Abcam) and c-Myc (ab32072 (Abcam), cells were washed with PBS and fixed with 4% paraformaldehyde (PFA) in PBS 1X for 20 minutes. After washing 5 times with PBS, cells were permeabilized with 0.1% Triton-X-100 for 2 minutes. Prior to the incubation with the primary antibody, they were incubated with a blocking solution (1% BSA; 10% FBS; in PBS) during 1 hour at RT. Primary antibody was diluted 1:50 in PBS-BSA 1% and incubated during 1 hour at RT. Then, after 3 washes with PBS, samples were incubated with fluorescent-conjugated secondary antibody (anti-rabbit Alexa Fluor® 488 from Molecular Probes (Eugene, OR, USA)), using 1:200 dilution in PBS-BSA 1% during 1 hour at RT. Finally, cells were washed 2 times for 5 minutes each with PBS, adding DAPI in the third last wash for nuclear DNA staining for another 5 minutes. At the end, samples were embedded using MOWIOL® 4-88 reagent (Calbiochem, La Jolla, CA, USA). Cells were visualized in a Nikon eclipse 80i microscope with the appropriate filters, and representative images were taken with a Nikon DS-Ri1 digital camera and using NIS-Elements BR 3.2 (64-bit) software. For confocal microscopy studies, a Leica TSC SL spectral confocal microscope was used. In both cases, representative images were edited in Adobe Photoshop. ImageJ software (National Institutes of Health [NIH], Bethesda, MD, USA) was used to quantify different parameters.

8. Immunohistochemistry

8.1. Paraffin embedding

After weighed, fresh tissue was cleaned with PBS and then included in a cassette for paraffin embedding. Then, it was fixed with paraformaldehyde (4%) during 12-16 hours. After fixing the samples, they were washed 3-4 times with PBS, and sequentially immersed in PBS-30% saccharose, PBS-20% saccharose and PBS-10% saccharose. Then, tissue samples were dehydrated by bathing them in subsequent alcohols as indicated on **Table 12**. Finally, dehydrated samples were embedded in paraffin at 65ºC and taken to 4ºC for solidification.

Table 12. Samples dehydration for paraffin-embedding.

Step	Time
Rinse with tap water	30 minutes
Ethanol 70%	60 minutes
Ethanol 96%	60 minutes
Ethanol 96% (new)	60 minutes
Ethanol 96% (new)	Overnight
Ethanol 100%	60 minutes
Ethanol 100% (new)	90 minutes
Ethanol 100% (new)	90 minutes
Xylene	90 minutes
Xylene-Paraffin (50%, 65ºC)	90 minutes
Paraffin (65ºC)	Overnight

8.2. Hematoxylin and Eosin staining on paraffin-embedded tissues

Paraffin-embedded samples were cut into 4-µm-thick sections with a microtome and placed in poly-lysinated slides (for poly-lysing, slides were incubated for 20 minutes with poly-L-Lysine at 4ºC and overnight of air-drying at 37ºC). Then after, paraffin was removed and samples rehydrated. To do that, sample slides were placed at 50ºC during 30 minutes and then immersed in subsequent alcohols as indicated in **Table 13**. Next, sample slides were stained with Hematoxylin and Eosin (H&E) for tissue structure study or used for immunohistochemistry (IHC).

Table 13. Samples rehydration for H&E staining or Immunohistochemistry.

Step	Time
Xylene	10 minutes
Xylene (new)	10 minutes
Xylene (new)	10 minutes
Ethanol 100%	5 minutes
Ethanol 100% (new)	5 minutes
Ethanol 100% (new)	5 minutes
Ethanol 96%	5 minutes
Ethanol 96% (new)	5 minutes
Ethanol 96% (new)	5 minutes
Ethanol 70%	5 minutes
Distilled water	5 minutes

For H&E staining, Hematoxylin solution, Harris modified (Ref. HHS32, Sigma-Aldrich, St. Louis, MO), was used. Samples were stained for 1 minute and washed abundantly with tap water. Next, samples were stained with Eosin Y solution (Ref. 115935.0100, Merck) for 1 minute and washed again abundantly with tap water. Finally, samples were dehydrated soaking them in subsequent alcohols as indicated in **Table 14** and slides were mounted in D.P.X. mountant (Ref. 360294H, BDH Prolabo, Germany) for preservation.

Table 14. Samples dehydration after H&E staining or Immunohistochemistry.

Step	Time
Ethanol 70%	5 minutes
Ethanol 96%	5 minutes
Ethanol 96% (new)	5 minutes
Ethanol 96% (new)	5 minutes
Ethanol 100%	5 minutes
Ethanol 100% (new)	5 minutes
Ethanol 100% (new)	5 minutes
Xylene	10 minutes
Xylene (new)	10 minutes
Xylene (new)	10 minutes

8.3. Immunohistochemistry on paraffin-embedded tissues

For immunohistochemistry, after rehydration as indicated in **Table 13**, samples were rinsed during 5 minutes with distilled water and then covered with a mixture of citric acid (0.38mg/mL) and sodium citrate (2.45mg/mL), taken to boiling temperature and left boiling during 2 minutes to break the methylene bridges and expose the antigenic sites in order to allow the antibodies to bind. After that, samples were left immersed in this mixture for 20 minutes at RT (until the temperature is between 35-45ºC), and then rinsed during 5 minutes with distilled water. At this point, we proceeded to inactivate the endogenous peroxidases of the samples, in order to minimize the background, by incubating the slides in 3% hydrogen peroxide during 10 minutes and then washing them, first during 5 minutes in distilled water, and then in PBS-Tween (PBS-T) (0.1%) during 10 minutes. Afterwards, samples were covered during 2 hours in a wet chamber at RT in IHC-blocking solution: 2% BSA and 20% Fetal Bovine Serum (FBS) in PBS-T (0.1%). Then, slides were incubated overnight with primary antibody (**Table 15**) diluted in IHC-blocking solution, at 4ºC in a wet chamber.

Table 15. Primary antibodies used for Immunohistochemistry.

Primary antibody	Reference	Working conditions
Mouse anti-β-catenin	610154 (BD-Transduction)	1:100
Mouse anti-Caveolin-1	610406 (BD- Biosciences)	1:100
Mouse anti-TGF-β1	ab64715 (Abcam)	1:50
Rabbit anti-Ki67	Ab16667 (Abcam)	1:50
Rabbit anti-Myc	ab32072 (Abcam)	1:100
Rabbit anti-M6PR	ab124767 (Abcam)	1:100
Rabbit anti-phospho Histone 3 (Ser 10)	9701 (Cell Signalling)	1:100
Rabbit anti-Smad3 (clone EP568Y)	04-1035 (Millipore)	1:100

Next morning, slides were washed 3 times with PBS-Tween (0.1%) during 10 minutes and incubated during 1 hour with anti-rabbit secondary peroxidase-conjugated antibody (Ref. PK4001 for anti-rabbit and Ref. PK4002 for anti-mouse, Vectastain ABC KIT, Vector laboratories Inc., Burlingame, CA, USA) following the manufacturer's protocol. Afterwards, samples were washed 3 times with PBS-T (0.1%) during 10 minutes. Then, they were incubated in ABC (Vectastain ABC KIT, Vector laboratories Inc., Burlingame, CA, USA) solution for 30 minutes, following the manufacturer's indications, until developing the peroxidase staining with diluted Diaminobenzidine (D.A.B) (Ref. K3468, DAKO, Inc.,

Carpinteria, CA, USA). This last step lasted a maximum of 30 minutes, taking care not to obtain a saturated signal. Once we had acquired an optimum staining, the developing reaction was stopped by soaking the samples into tap water during 5 minutes.

The final steps consisted in a counterstaining with Mayer's Hematoxylin (Ref. HHS32, Sigma-Aldrich, St. Louis, MO, USA) and subsequent sample dehydration as indicated in **Table 14**, and mounting the slides in D.P.X. for preservation.

Tissues were visualized in a Nikon eclipse 80i microscope. Representative images were taken with a Nikon DS-Ri1 digital camera and using NIS-Elements BR 3.2 (64-bit) software. Representative images were edited in Adobe Photoshop software.

9. Lipid analysis

9.1. Oil Red O staining

For analysis of lipid content by Oil Red O solution (Ref. 01391, Sigma Aldrich, St. Louis, MO), OCT tissue-blocks from partial hepatectomy were cut into 10-μm-thick sections. Firstly, tissue sections were sequentially fixed with 4% PFA for 15 min, washed with distilled water, rinsed with 60% isopropanol and washed with distilled water again. After that, tissue slices were stained with freshly prepared Oil Red O working solution for 10 minutes at room temperature. The working solution of Oil Red O was prepared by diluting a stock solution, i.e. 0.5 g of Oil Red O in 100 ml of isopropanol, with distilled water at a ratio of 3:2 (v/v). After rinsing with 60% isopropanol and washing with distilled water for 5 minutes, tissues were stained with Hematoxylin and mounted in Mowiol.

Lipid droplets were visualized with a Nikon eclipse 80i microscope. Representative images were taken with a Nikon DS-Ri1 digital camera and using NIS-Elements BR 3.2 (64-bit) software. Representative images were edited in Adobe Photoshop software.

10. Statistical analyses

Data are represented as Mean ± Standard Error of the Mean (SEM). Differences between groups were compared using Student's t-test with Welch correction (when comparing two groups) or Two-way ANOVA with Tukey's multiple comparison post-hoc test (differences between groups considering two independent variables). Survival curves were estimated by Kaplan-Meier analysis, and significance was tested by the log-rank test. Statistical calculations were performed using GraphPad Prism software (GraphPad for Science Inc., San Diego, CA, USA). Differences were considered statistically significant when $p<0.05$.

V. Results

Analysis of the liver-to-body weight ratio and tissue recovery after two-thirds Partial Hepatectomy

In order to study the specific role of Nox4 during liver regeneration, NOX4-/- and NOX4hepKO mice (see Material & Methods section) were used to analyze the response to 2/3 PH. The majority of the analysis has been performed in the NOX4-/- model, were *Nox4* is deleted in all the cells of the body. The NOX4hepKO model, with *Nox4* deletion in hepatocytes specifically, has also been really useful for confirming some results as well as to study the effect of deleting *Nox4* in hepatocytes during proliferation.

We had previously reported that *Nox4* expression decreases after PH in C57BL/6 mice (Crosas-Molist et al., 2014). Here we confirmed that the decrease in *Nox4* mRNA levels also occurred in NOX4floxp+/+ mice, the WT mice used for breeding and obtaining the NOX4hepKO mice (**Figure 1**).
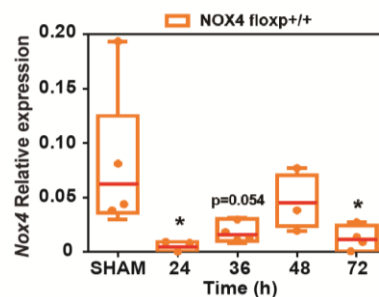

Figure 1. Nox4 levels decrease in NOX4floxp+/+ mice after PH. *Nox4* RT-qPCR analysis in livers from NOX4floxp+/+ (WT control of NOX4hepKO mice). Relative expression to *Rpl32* mRNA levels. Red bars represent the Median (n=3-6 per time point). Student's t test with Welch correction was used: *p < 0.05 compared to SHAM condition.

As a relevant control, we next analyzed how *Nox4* deletion affects the liver expression of other members of the *Nox* gene family. *Nox2* expression was not significantly different between WT and NOX4 deleted mice in any of the groups and its expression dropped, recovering later, in response to PH (**Figure 2**).
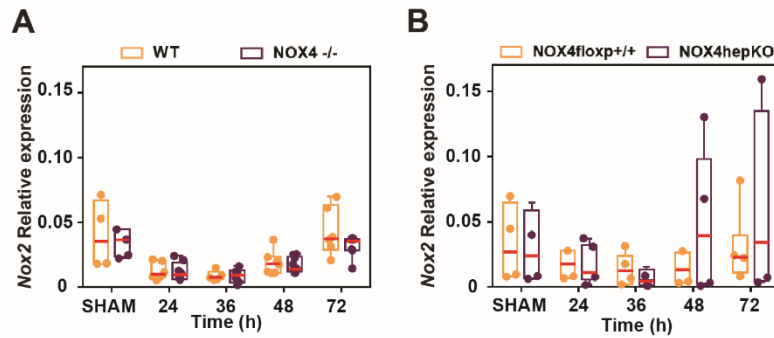
Figure 2. No differences in *Nox2* expression in livers after PH. *Nox2* RT-qPCR analysis in livers from **(A)** NOX4-/- and **(B)** NOX4hepKO mice and their respective WT controls. Relative expression to *Rpl32* mRNA levels. Red bars represent the Median.

Expression of *Nox1* was very low, barely detected by Real-Time PCR and with huge fluctuations among animals (**Figure 3**). These results indicate that the absence of *Nox4* expression is not compensated by differences in the expression of other members of the family.
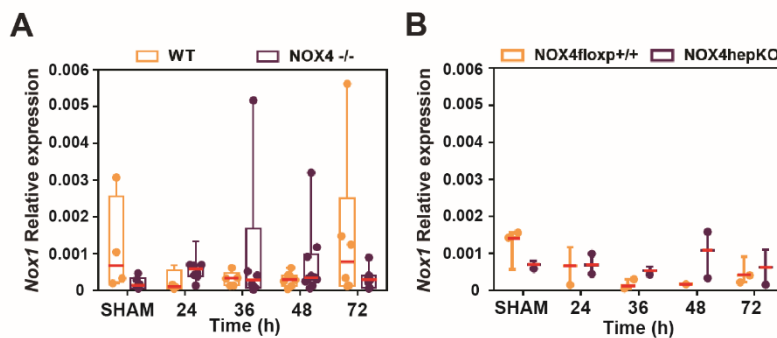

Figure 3. No differences in *Nox1* expression in livers after PH. *Nox1* RT-qPCR analysis in livers from **(A)** NOX4-/- and **(B)** NOX4hepKO mice and their respective WT controls. Relative expression to *Rpl32* mRNA levels. Red bars represent the Median.

Liver and body weights were recorded after PH, and the ratio of liver-to-body weight at the time of sacrifice was used as a parameter to evaluate the progression of LR. It was observed that liver recovery took place post hepatectomy in both WT and NOX4-/- mice (**Figure 4A**), and in NOX4floxp+/+ and NOX4hepKO mice (**Figure 4B**). However, we observed a significantly faster recovery in both NOX4-/- and NOX4hepKO mice when compared to the corresponding WT mice (**Figure 4A** and **B**). This faster recovery correlated with a significantly higher survival after PH in NOX4-/- mice (**Figure 4C**). Although the number of animals was too low to obtain statistical significance, a similar tendency was observed in NOX4hepKO mice (**Figure 4D**). Interestingly, a long-term analysis revealed that, at the end of the regenerative process (4 weeks), NOX4-/- liver reached a size that did not

overcome the initial one (**Figure 4A**). Therefore, Nox4 did not appear to be essential for the termination of liver regeneration.
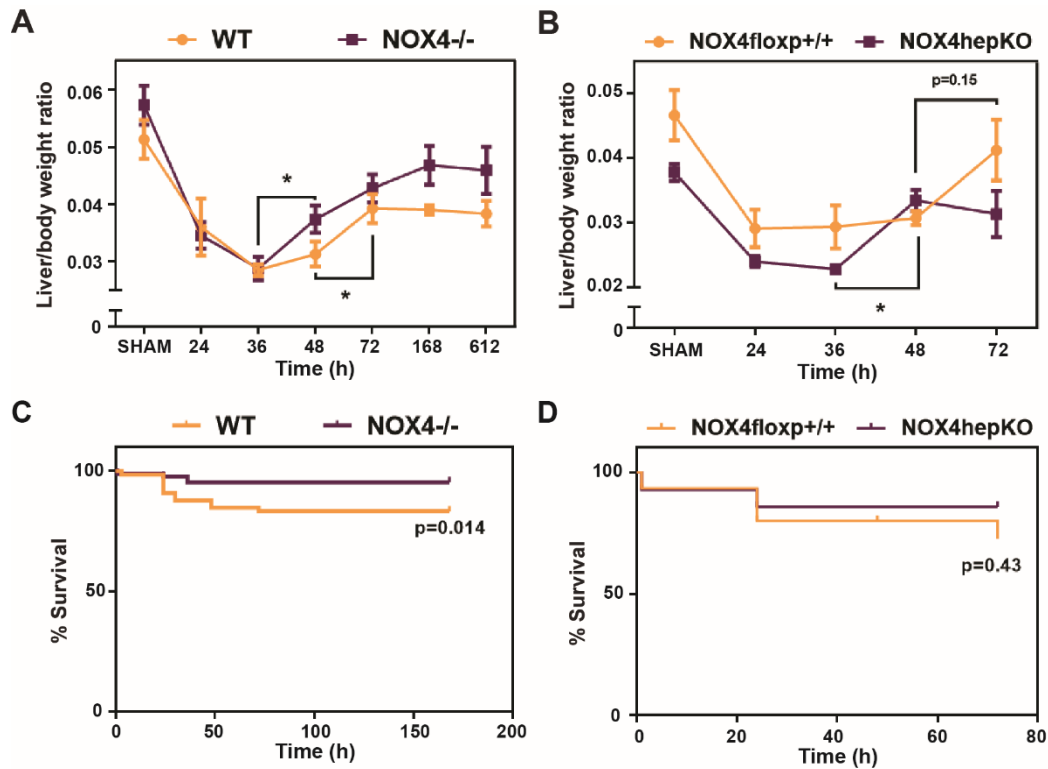

Figure 4. NOX4 deleted mice presented an earlier recovery of the liver-to-body weight ratio and higher survival after PH. Mice were subjected to PH and sacrificed at the indicated time points. **(A)** Liver/Body weight ratio was calculated for NOX4-/- and **(B)** NOX4hepKO mice and represented as mean ± SEM (n= 2-10 per time point). Student's t test with Welch correction was used: $*p<0.05$ compared to previous time point. **(C)** Kaplan-Meier curve of overall survival in NOX4-/- and **(D)** NOX4hepKO mice. Significance was tested by the log-rank test.

Considering that repopulation of the liver with newly generated liver cells is accommodated by massive tissue remodeling, we studied differences between WT and NOX4-/- livers at the histological level. We performed H&E staining and we observed that, at the beginning of the "progression phase" (i.e., 24-36 hours after PH), both genotypes presented a disorganized structure and they also presented the regenerative steatosis characteristic of the final G2/M phase of the hepatocyte cell cycle (López-Luque & Fabregat, 2018) (**Figure 5A**). Significant differences mainly occurred 48 hours post hepatectomy, when WT still presented a disorganized parenchyma and lipid droplets accumulation, but NOX4-/- livers presented an almost completely organized parenchyma and liver steatosis was already resolved (**Figure 5B**).

Importantly, 7 days and 4 weeks after PH, both WT and NOX4-/- showed a normal hepatic structure (**Figure 5C**), supporting the idea that Nox4 may not be essential for the termination of liver regeneration.
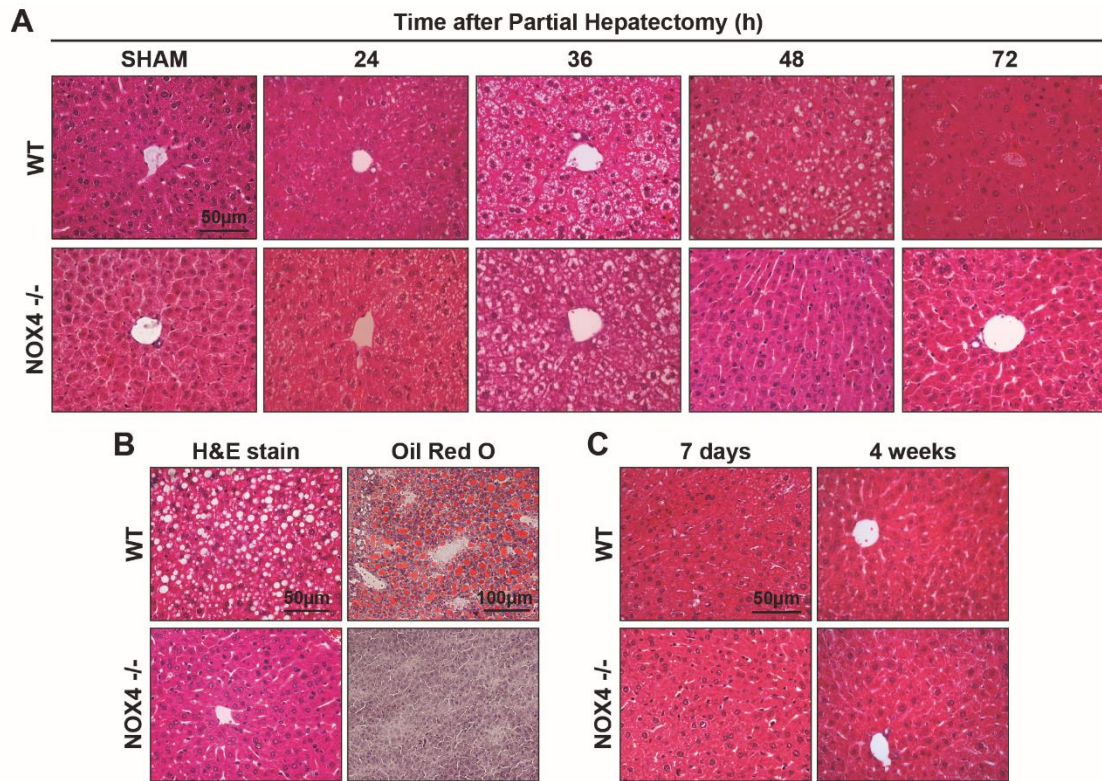

Figure 5. NOX4-/- mice presented an earlier recovery of the parenchymal structure and regenerative steatosis after 2/3 PH. (A) Hematoxylin and Eosin staining performed in paraformaldehyde-fixed and paraffin-embedded tissue sections. Representative 40x images are shown at different time points after PH. (B) H&E (left) and Oil Red O staining (right). Oil Red O staining was performed in frozen liver sections. Representative 20x images are shown. (C) H&E staining performed after 7 days and 4 weeks after PH.

H&E and Oil Red O staining also revealed an earlier recovery of the parenchymal structure in NOX4hepKO mice when compared with NOX4floxp+/+ mice (**Figure 6A and B**). 72 hours after PH, NOX4floxp+/+ still presented hepatic steatosis and a disorganized structure, whereas NOX4hepKO livers already recovered from lipid droplet accumulation and presented a normal parenchymal structure.

After that, considering that cell size increase is one of the first responses of hepatocytes to recover after PH (Miyaoka & Miyajima, 2013), we performed immunohistochemical analysis to quantify hepatocyte size. It was interesting to observe a transient higher size at 36 hours after PH in hepatocytes from NOX4-/- mice when compared to WT animals (**Figure 7A**), which was also noticed in NOX4hepKO at 24 and 72 hours after

PH, when compared to NOX4floxp+/+ (**Figure 7B**). This hypertrophy could contribute to the earlier recovery in the liver-to-body weight ratio in both models of NOX4 deleted mice.
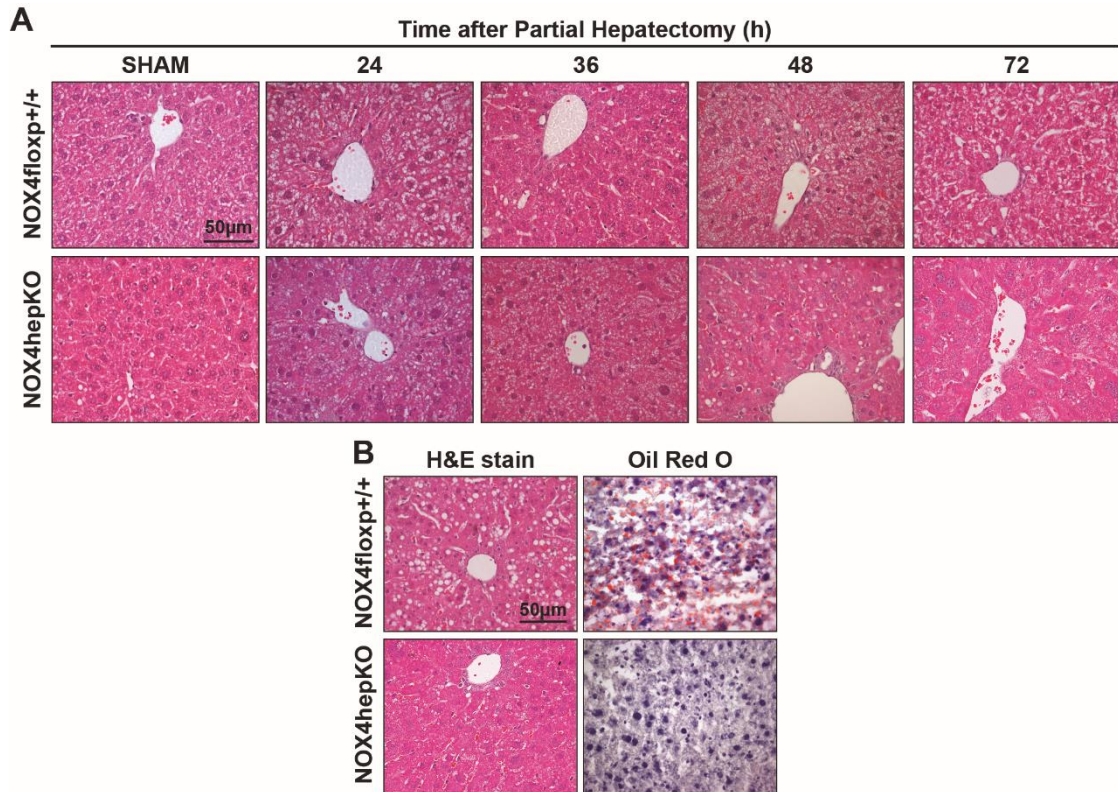

Figure 6. NOX4hepKO mice presented an earlier recovery of the parenchymal structure and regenerative steatosis after 2/3 PH. (A) Hematoxylin and Eosin staining performed in paraformaldehyde-fixed and paraffin-embedded tissue sections. Representative 40x images are shown at different time points after PH. (B) H&E (left) and Oil Red O staining (right). Oil Red O staining was performed in frozen liver sections. Representative 40x images are shown.

Kinetics of the recovery after PH varied between both models of animals, probably due to the different background and different environmental factors in the culture room (NOX4-/- mice were at IDIBELL in Barcelona; NOX4HepKO mice were at UC Davis, in CA). But it was clear that deletion of NOX4, either in the whole animal or in hepatocytes, induced an earlier recovery of the liver mass, parenchymal structure and regenerative steatosis, concomitant with a transient increase in hepatocyte size. Similar results were obtained in both NOX4-/- and NOX4HepKO mice and this would indicate that *Nox4* silencing has a higher impact on the hepatocyte responses to PH, which could be expected considering that the hepatocyte is the liver cell where *Nox4* expression is notably higher (Sancho et al., 2012).

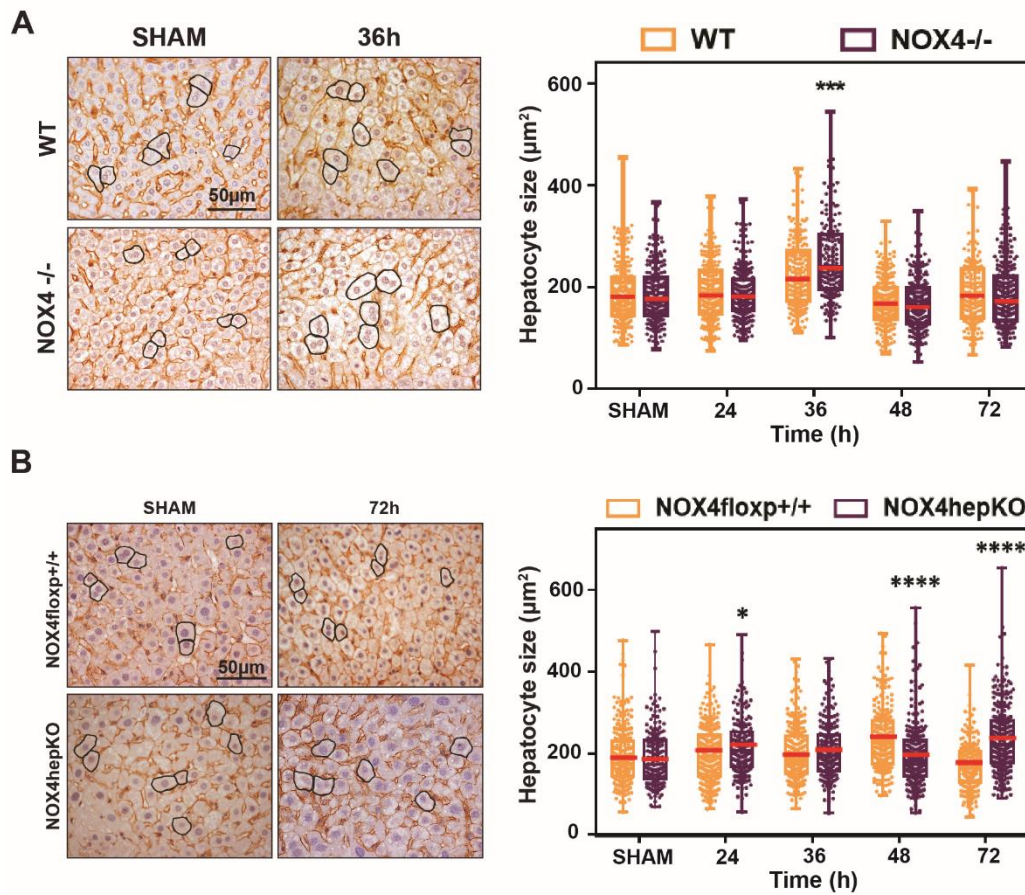Figure 7. NOX4 deleted hepatocytes presented higher hepatocyte size after PH. β-catenin immunostaining was performed in paraformaldehyde-fixed and paraffin-embedded tissue sections in (A) NOX4-/- and (B) NOX4hepKO mice (left) to quantify hepatocyte size (right). Red bars represent the Median. Student's t test with Welch correction was used: * p <0.05, *** p <0.001, **** p <0.0001 compared to WT.

Analysis of cellular proliferation in Nox4 deleted mice livers and primary hepatocytes

Considering that hepatocytes' proliferation constitutes one of the most important mechanisms in liver recovery after PH (Riehle et al., 2011), we decided to analyze this process. We performed immunohistochemistry analysis of Ki67, a proliferative marker present in the nucleus during all active phases of the cell cycle (Scholzen & Gerdes, 2000), in NOX4floxp+/+ and NOX4hepKO mice. Results revealed a significant increase in the number of stained hepatocytes at 48 and 72 hours after PH in NOX4hepKO when compared to NOX4floxp+/+ (**Figure 8**). Furthermore, NOX4hepKO hepatocytes reached the maximal DNA synthesis at 48 hours after PH, whereas NOX4floxp+/+ reached it at 72 hours.

Figure 8. NOX4hepKO livers presented higher liver proliferation after PH. Ki67 immunohistochemistry was performed in paraformaldehyde-fixed and paraffin-embedded tissue sections in NOX4floxp+/+ and NOX4hepKO mice (upper) and positive nuclei were quantified with ImageJ software (lower). Red bars represent the Median. Student's t test with Welch correction was used: *** $p < 0.001$, **** $p < 0.0001$ compared to NOX4floxp+/+.

We also performed immunohistochemistry analysis of phosphorylated Histone H3 in Ser10, a specific marker of G2/M phase cells (Juan et al., 1998). Results again indicated a significant increase in the number of stained hepatocytes at 48 and 72 hours after PH in NOX4hepKO when compared to NOX4floxp+/+ (**Figure 9**).
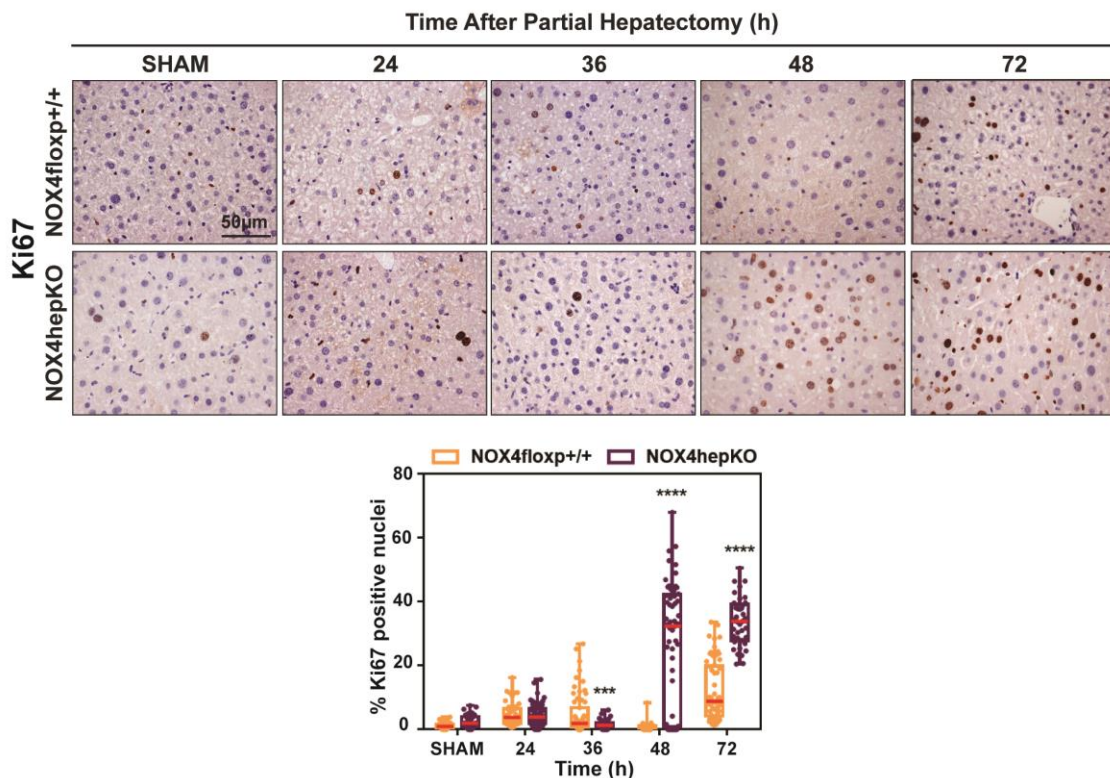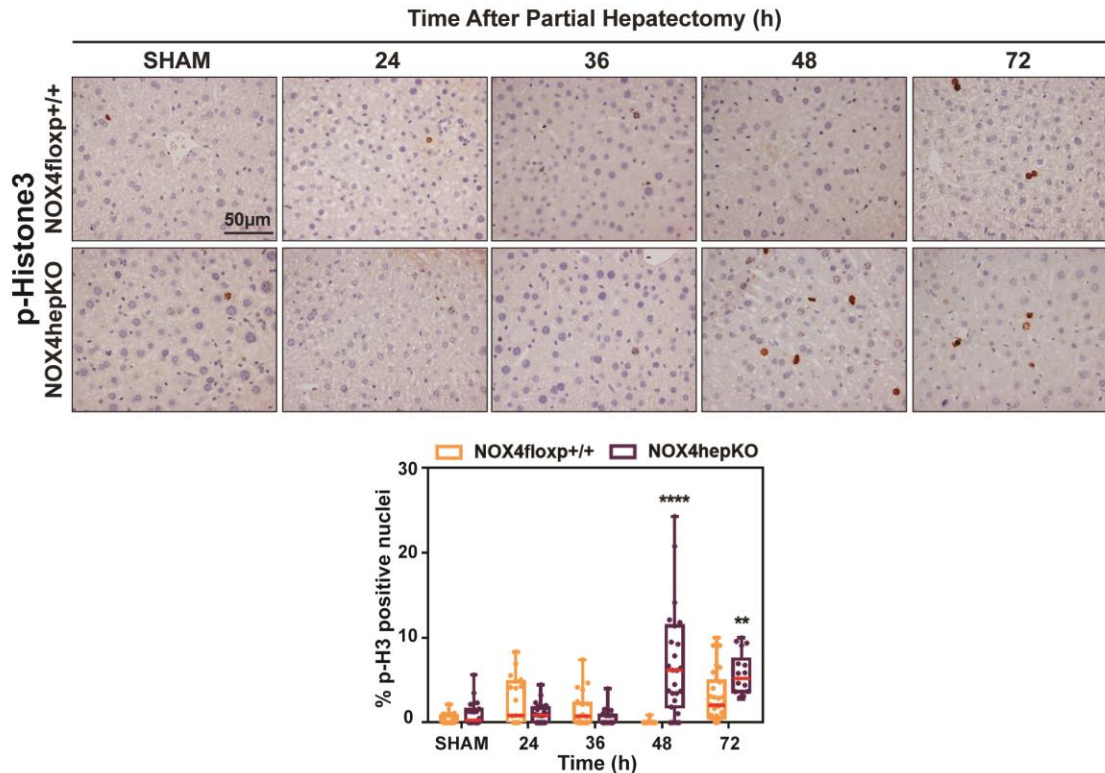
Figure 9. NOX4hepKO livers presented higher liver proliferation after PH. Phospho-Histone H3 immunohistochemistry was performed in paraformaldehyde-fixed and paraffin-embedded tissue sections in NOX4floxp+/+ and NOX4hepKO mice (upper) and positive nuclei were quantified with ImageJ software (lower). Red bars represent the Median. Student's t test with Welch correction was used: ** p <0.01, **** p <0.0001 compared to NOX4floxp+/+.

With the aim of better exploring the proliferative capacity of the NOX4 deleted hepatocytes, we isolated them from unhepatectomized mice and cultured them to evaluate the response to FBS.

Interestingly, very low concentrations of FBS (2 %) allowed NOX4hepKO cells to increase almost 40 % the number of viable cells in 24 hours, significantly higher than the increase observed in NOX4floxp+/+ control hepatocytes (**Figure 10A**). Then, to assess the progression of hepatocytes' proliferation at the molecular level, we analyzed cell cycle regulators by RT-qPCR. The increase in viable cells correlated with a much higher increase in the expression of Cyclin D1 (*Ccnd1*), Cyclin A2 (*Ccnd2*) and Cyclin B2 (*Ccnb2*) in NOX4hepKO primary hepatocytes, when compared to the NOX4floxp+/+ ones (**Figure 10B**). Similar results were obtained in NOX4-/- primary hepatocytes (**Figure 11**). Moreover, immunocytochemistry analysis of Ki67 in FBS-treated primary hepatocytes showed a higher number of Ki67 positive nuclei in NOX4-/- primary cells than in WT (**Figure 12**).
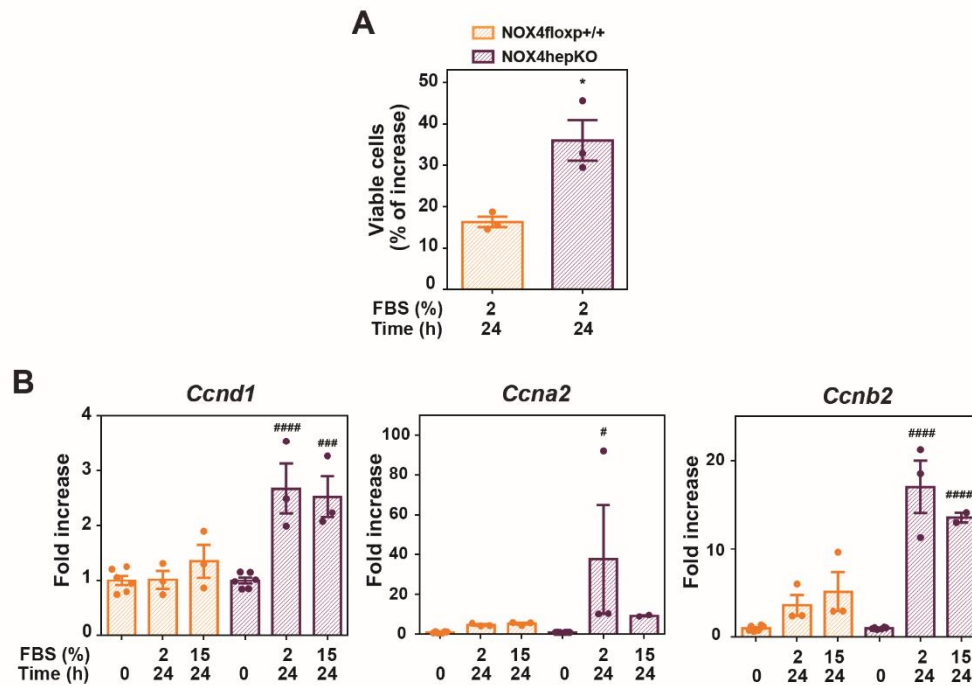
Figure 10. NOX4hepKO primary hepatocytes presented higher proliferation after FBS treatment. Primary hepatocytes isolated from NOX4floxp+/+ and NOX4hepKO mice were treated as indicated in the graph. **(A)** Viable cell number represented as % of increase versus 0 time. **(B)** RT-qPCR analysis of Cyclin D1 (*Ccnd1*), Cyclin A2 (*Ccna2*) and Cyclin B2 (*Ccnb2*). Relative expression to *Rpl32* gene. Mean ± SEM (n=3). Two-way ANOVA with Tukey's multiple comparison post-hoc test was used: * $p < 0.05$ compared to NOX4floxp+/+. # $p < 0.05$, ### $p < 0.001$, #### $p < 0.0001$ compared to untreated cells.

All these results suggest that the absence of *Nox4* expression primes hepatocytes for a faster and higher response to mitogenic signals.

Our group had previously described that Myc expression is required for an efficient liver regeneration in mice (Baena et al., 2005), as its deletion delays the recovery of the liver mass. In this regard, we observed that livers from NOX4-/- mice showed a higher increase in *Myc* expression 24 hours after PH, and both 24 and 36 hours after PH in NOX4HepKO livers (**Figure 13A**) when compared to the corresponding WT mice. Western blot and IHC analysis revealed significantly higher c-Myc protein levels and c-Myc positive nuclei 36 hours after PH in NOX4hepKO hepatocytes, which confirmed the differences observed at the mRNA level (**Figure 13B** and **C**).
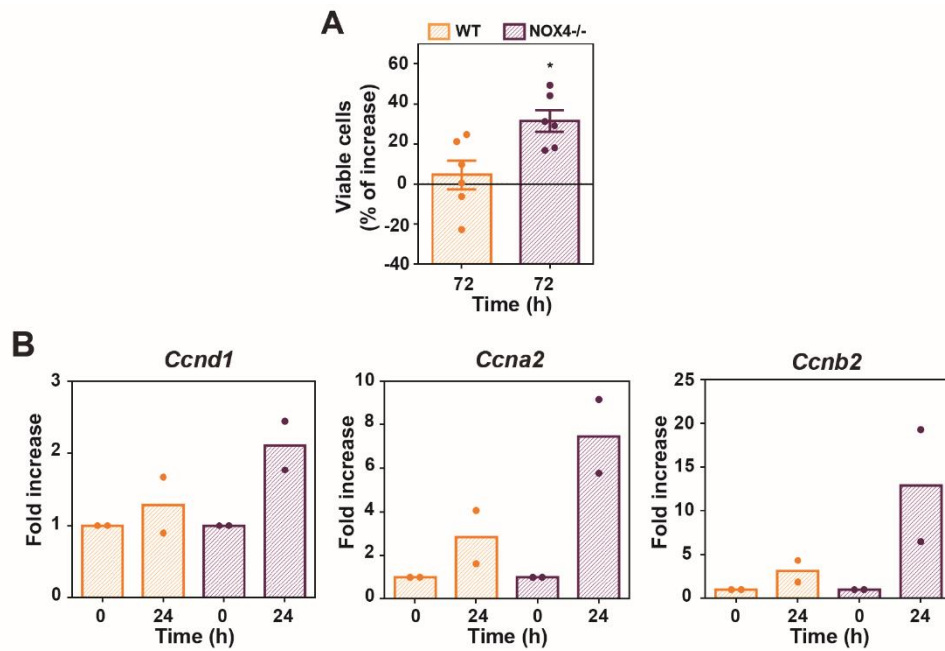
Figure 11. NOX4-/- primary hepatocytes presented higher proliferation after 2% FBS treatment. Primary hepatocytes isolated from WT and NOX4-/- were isolated and treated with 2% FBS for the time indicated in the graph. (A) Viable cell number represented as % of increase versus 0 time. Mean ± SEM (6 independent plates). Student's t test with Welch correction was used: *< p0.05 compared to WT cells. (B) RT-qPCR analysis of Cyclin D1 (Ccnd1), Cyclin A2 (Ccna2) and Cyclin B2 (Ccnb2). Relative expression to Rpl32 gene. Bars represent the Mean from 2 independent plates. A representative experiment (n = 3) is shown.
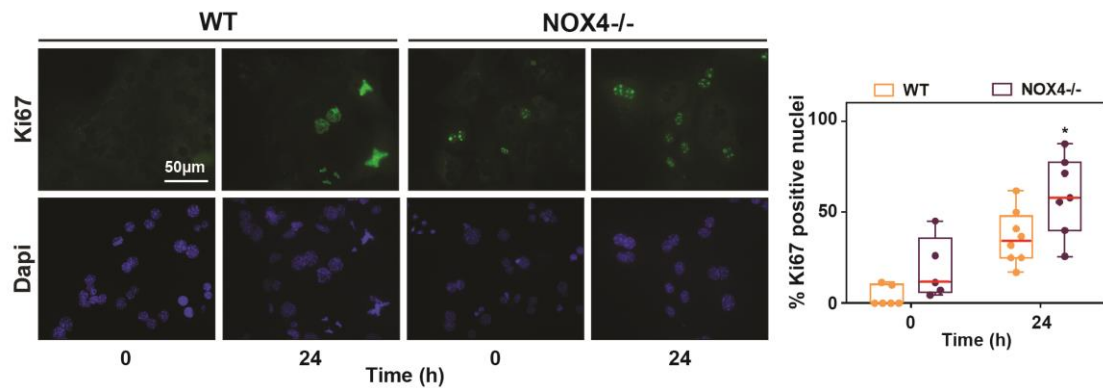
Figure 12. NOX4-/- primary hepatocytes presented higher percentage of Ki67 positive nuclei after 2% FBS treatment. Immunostaining of Ki67 (Green) and DAPI (blue) (left) and quantification of positive nuclei quantified with ImageJ software (right). Red bars represent the Median. Student's t test with Welch correction was used: *< p0.05 compared to WT cells.
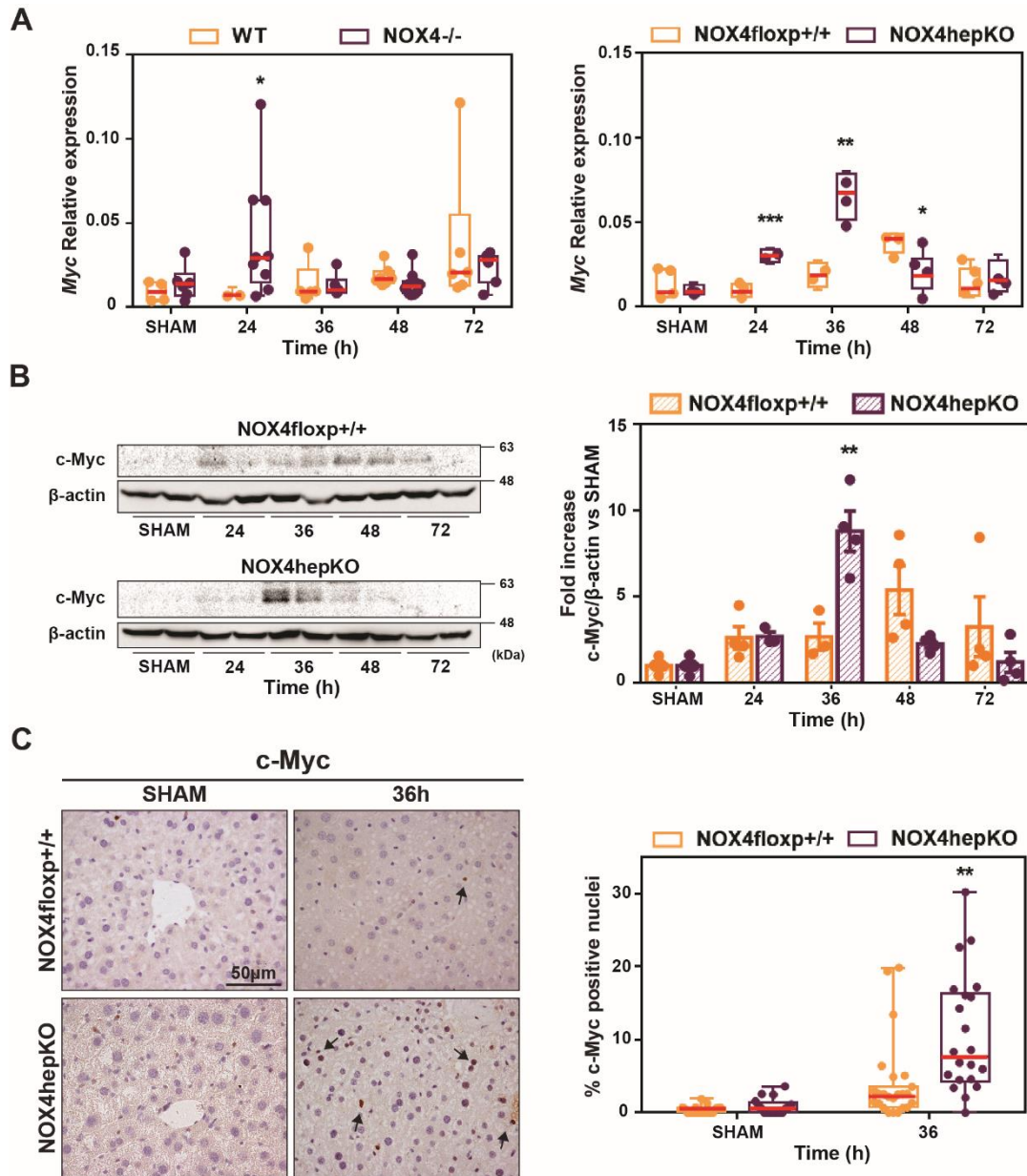
Figure 13. Higher levels of c-Myc were found in NOX4 deleted mice after PH. (A) RT-qPCR analysis of *Myc* in livers from NOX4-/- and NOX4hepKO mice and their respective WT controls. Relative expression to *Rpl32* gene. Red bars represent the Median (n= 4-10 per time point in NOX4-/- model; n=4-6 per time point in NOX4hepKO model). (B) Analysis of c-Myc by Western Blot in NOX4floxp+/+ and NOX4hepKO livers (left) and densitometry of the different experiments performed (right). Mean ± SEM (n=3-4 per time point). β-actin was used as a loading control. (C) c-Myc immunostaining in NOX4floxp+/+ and NOX4hepKO livers 36 h after PH (left) and positive nuclei quantified with ImageJ software (right). Red bars represent the Median. Student's t test with Welch correction was used: *p <0,05, ** < p 0.01, *** p <0.001 compared to WT controls.

Primary hepatocytes coming from WT and NOX4-/- mice 30 and 48 hours after PH were isolated and cultured. Interestingly, NOX4-/- primary hepatocytes isolated 30 hours

after PH and treated with FBS or a mitogenic mixture containing FBS, Insulin, Hydrocortisone and Epidermal Growth Factor showed much higher increase in *Myc* mRNA levels than WT primary culture (**Figure 14A**). These differences disappeared at 48 hours after PH, when the response was even higher in WT hepatocytes (**Figure 14B**). The increased *Myc* mRNA levels in response to mitogenic stimuli observed in NOX4-/- hepatocytes 30 hours after PH correlated with relevant differences in c-Myc protein levels and higher levels of intracellular signals that mediate hepatocyte proliferation, such as phospho-ERKs and phospho-Akt (**Figure 14C**).
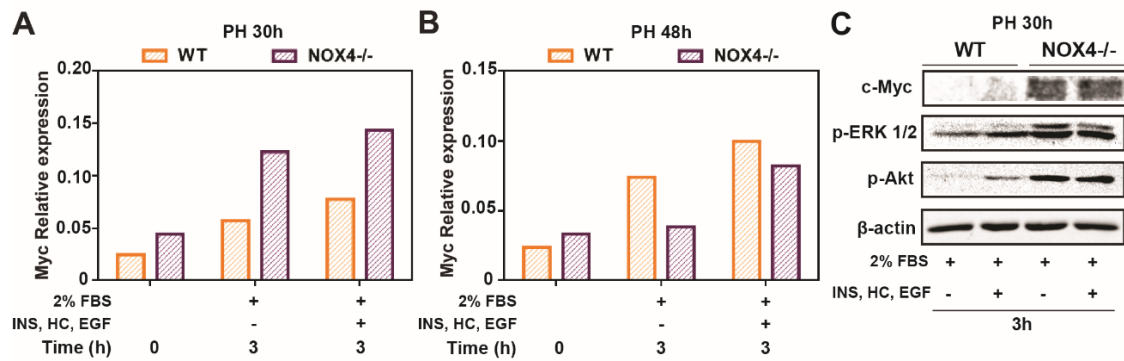
Figure 14. Induction of Myc expression in response to proliferative stimuli in WT and NOX4-/- regenerating hepatocytes 30 and 48 hours after PH. WT and NOX4-/- mice were subjected to PH. After 30 h or 48 h, primary hepatocytes were isolated and treated with 2% FBS or a mitogenic mixture containing 2% FBS, Insulin (INS, 2 µM), Hydrocortisone (HC, 100 µM) and Epidermal growth factor (EGF, 20 ng/mL). RT-qPCR analysis of *Myc* in primary hepatocytes after **(A)** 30 hours or **(B)** 48 hours after PH. Relative expression to *Rpl32* gene. **(C)** Analysis of c-Myc, p-ERK 1/2 and p-Akt by Western Blot in primary hepatocytes isolated 30 h after PH. β-actin was used as a loading control. Representative experiment is shown (n=2).

All these results suggest that acceleration of liver regeneration in NOX4 deleted mice correlates with higher expression of c-Myc at mRNA and protein levels.

RNA-seq analysis to identify how Nox4 influences the liver regeneration transcriptomic program

To better understand the molecular mechanisms that would justify the acceleration of liver regeneration and the differences in *Myc* expression found in NOX4 deleted mice, we performed RNA-seq analysis in collaboration with Beatriz Martín Mur, Marta Gut and Anna Esteve Codina, from CNAG-CRG (Centre for Genomic Regulation). We analyzed liver samples from WT and NOX4-/- mice at 6, 24, 48 and 168 hours after PH, and SHAM animals. Results revealed significant differences in gene expression between WT and NOX4-/-, particularly at 24 hours after PH (**Figure 15**).
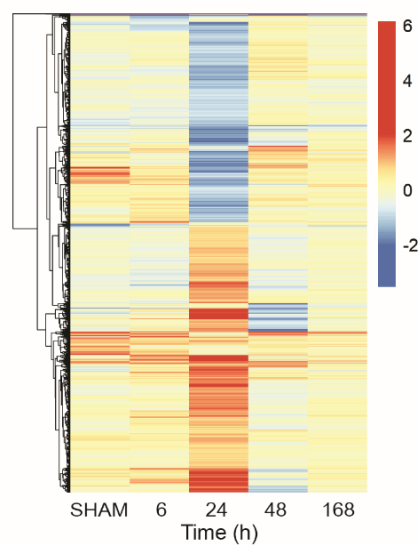
Figure 15. Transcriptomics RNA-seq analysis of livers after PH in WT and NOX4-/- mice. Heatmap showing all differentially expressed genes between NOX4-/- and WT mice in at least one time point (SHAM, 6, 24, 48 and 168 hours after PH).

The Gene Ontology (GO) enrichment analysis of the differentially expressed (DE) genes at 24 hours showed that one of the significantly enriched pathways is "response to oxygen-containing compound", in which *Nox4* is involved. The network representation of the top100 DE genes (based on adjusted p-value) that belong to the aforementioned pathway indicated a central role for *Myc* (**Figure 16**).

Myc expression appeared up-regulated at 6 hours after PH in both WT and NOX4-/- livers, but at 24 hours after PH was maintained at high levels only in NOX4-/- livers, whereas in WT livers decreased at basal levels (**Figure 17**). This differential expression pattern at 24 h was also observed in other relevant proliferation-related genes that appeared

in the enriched oxygen-response network connected to *Myc*, such as *Jund, Jun, Egr1, Sox9* and *Fosb,* among others (**Figure 17**).
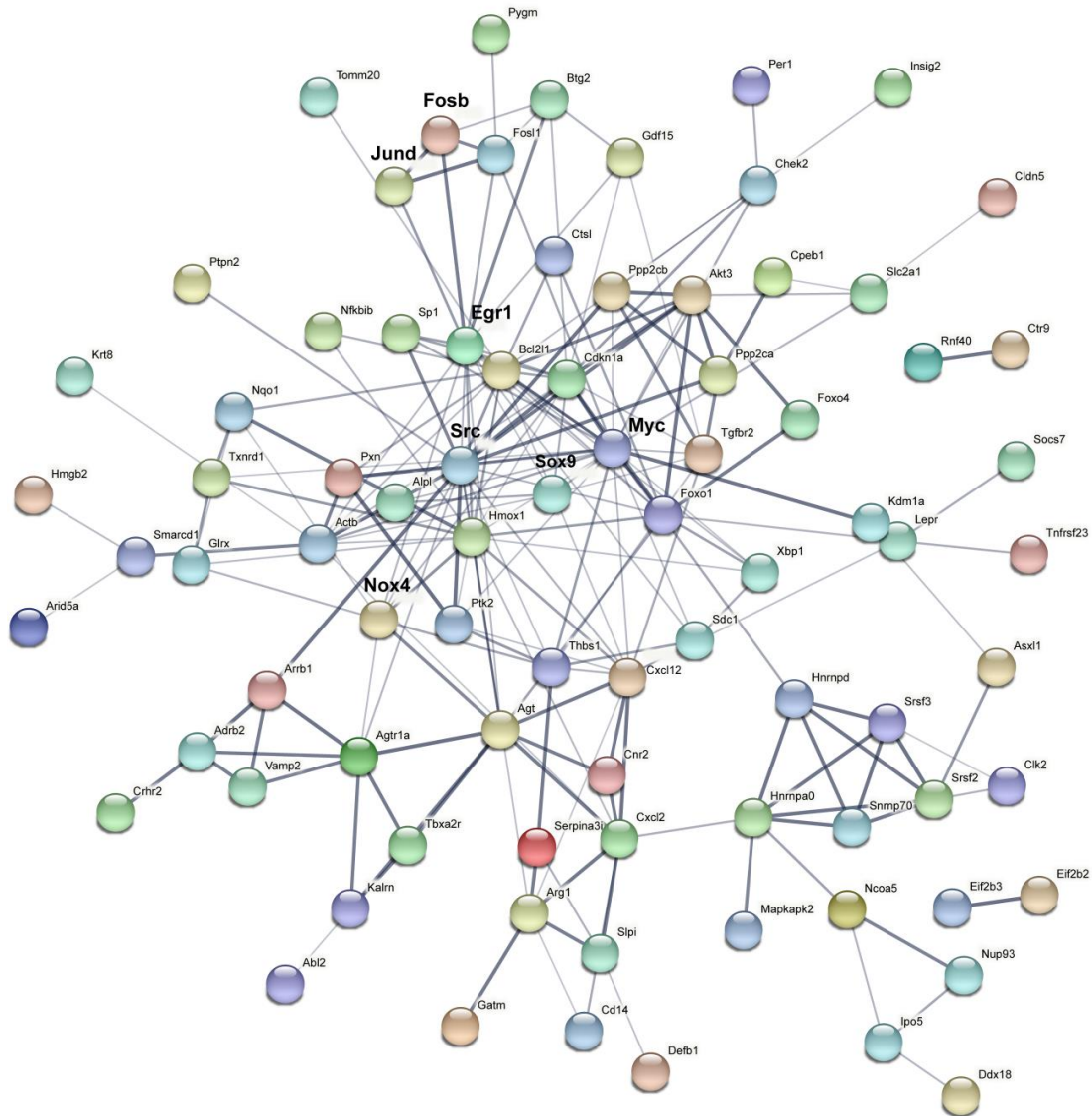
Figure 16. Protein-protein interactions network from RNA-seq analysis results of NOX4-/- vs WT livers 24 hours after PH. Network generated from the top100 differentially expressed genes (ranked by adjusted p-value) which belong to the GO pathway "response to oxygen-containing compound". The network is based on STRING database and predicts associations between groups of proteins.

Looking for mitogenic factors that showed changes in their expression, we found a significant difference in the expression of a member of the Epidermal Growth Factor Receptor (EGFR) family, the Heparin Binding EGF-like Growth Factor (*Hbegf* gene), whose expression was significantly higher at both 6 and 24 hours after PH in NOX4-/- mice (**Figure 18**). No significant differences were observed in the expression of Epidermal Growth Factor Receptor (*Egfr* gene) or its ligands Epidermal Growth Factor (EGF, *Egf* gene) and Transforming Growth Factor Alpha (TGF-alpha, *Tgfa* gene). We also analyzed the Met

receptor (*Met* gene) and its ligand, Hepatocyte Growth Factor (HGF, *Hgf* gene), but no significant differences were observed (**Figure 18**).
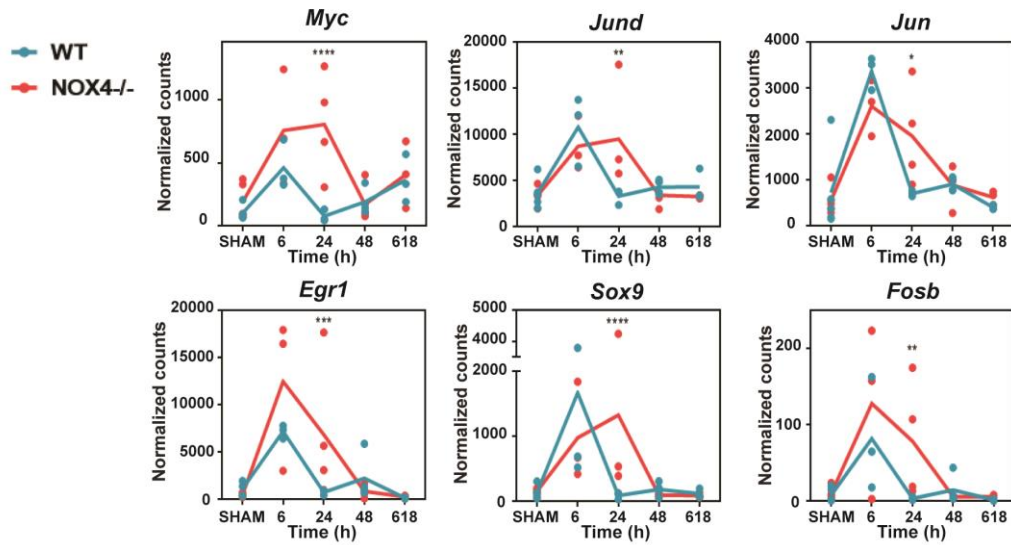
Figure 17. *Myc* and other proliferation-related transcription factors presented a differential expression along the time in WT and NOX4-/- mice. Transcriptomics RNA-seq analysis of livers after PH. Changes in gene expression over time. **p <0.01, ***p <0.001, ****p<0.0001 when compared changes in WT versus NOX4-/-.
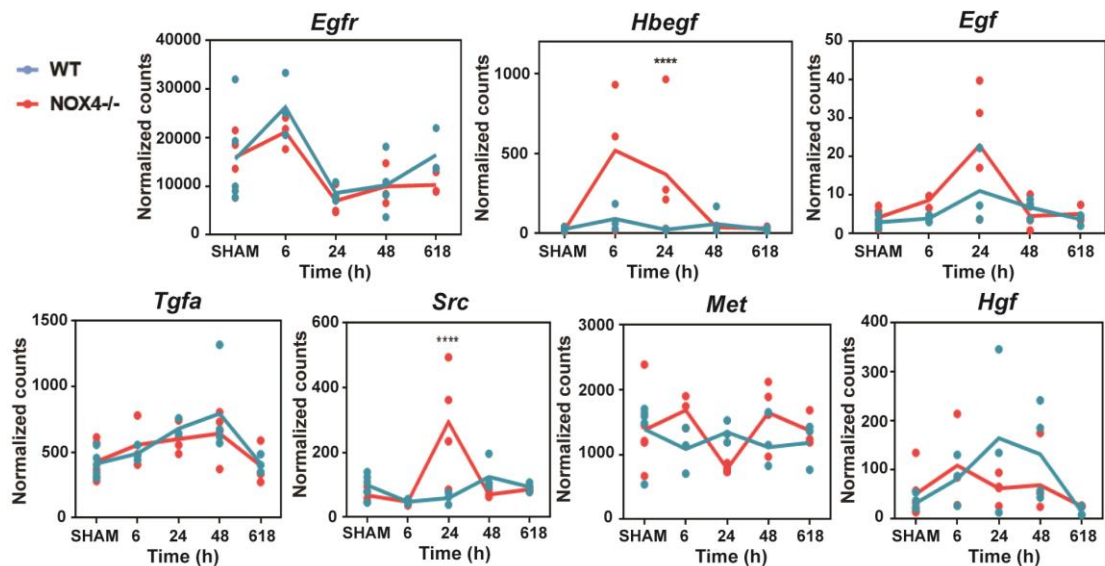
Figure 18. Changes in genes related to mitogenic pathways after PH. Transcriptomics RNA-seq analysis of livers after PH in WT and NOX4-/- mice. ****p<0.0001 when compared changes in WT versus NOX4-/-.

Interestingly, the top100 DE genes from the enriched oxygen-response network revealed a *Nox4 – Src – Myc axis*. In fact, *Src* expression significantly increased 24 hours after PH in NOX4-/- mice, whereas in WT mice no differences were observed (**Figure 18**).

Among the potential processes that regulate hepatocyte proliferation, the TGF-β pathway is one of the most significant negative regulators of the expression of *Myc* (Frederick et al., 2004). Coinciding with the transcriptional changes observed 24 hours after PH in NOX4-/- mice, we observed differences in the expression of the *Tgfb* gene family.

Tgfb1, the main isoform expressed in the liver (De Bleser et al., 1997), showed a significant reduction in its expression at 24 hours, when compared to WT mice (**Figure 19A**). In contrast, *Tgfb2* showed increased expression, although in absolute terms, the level of expression was much lower than that of *Tgfb1*. Expression of *Tgfb3* did not show significant differences.

It was proposed that a decrease in the expression of TGF-β receptors allow hepatocytes to escape from TGF-β-induced growth inhibition and apoptosis during liver regeneration (Chart et al., 1995). In our model, TGF-β RI did not show significant differences between WT and NOX4-/- (**Figure 19B**). In the case of TGF-β RII, its expression increased in WT at 6 hours to drop at 24 hours, but in NOX4-/- mice the increase at 6 hours was higher than in WT mice and its expression was maintained elevated at 24 hours.

Furthermore, considering that TGF-β is sequestered into the extracellular matrix in an inactive state, we focused our attention into genes that codify proteins whose function is related to the activation of the latent form of TGF-β1. *Adamtsl2* (a disintegrin and metalloproteinase with thrombospondin repeats-like 2), which interacts with latent TGF-β binding protein 1 (LTBP1) and anchors it in the extracellular matrix (Goff et al., 2009), showed a differential pattern of expression almost significant (adjusted p-value=0.068) in WT versus NOX4-/- mice (**Figure 19C**). Although its expression increased in WT at 6 hours to decrease at 24 hours, in NOX4-/- mice, the increase at 6 hours was higher than in WT mice and its expression was maintained high at 24 hours (**Figure 19C**).
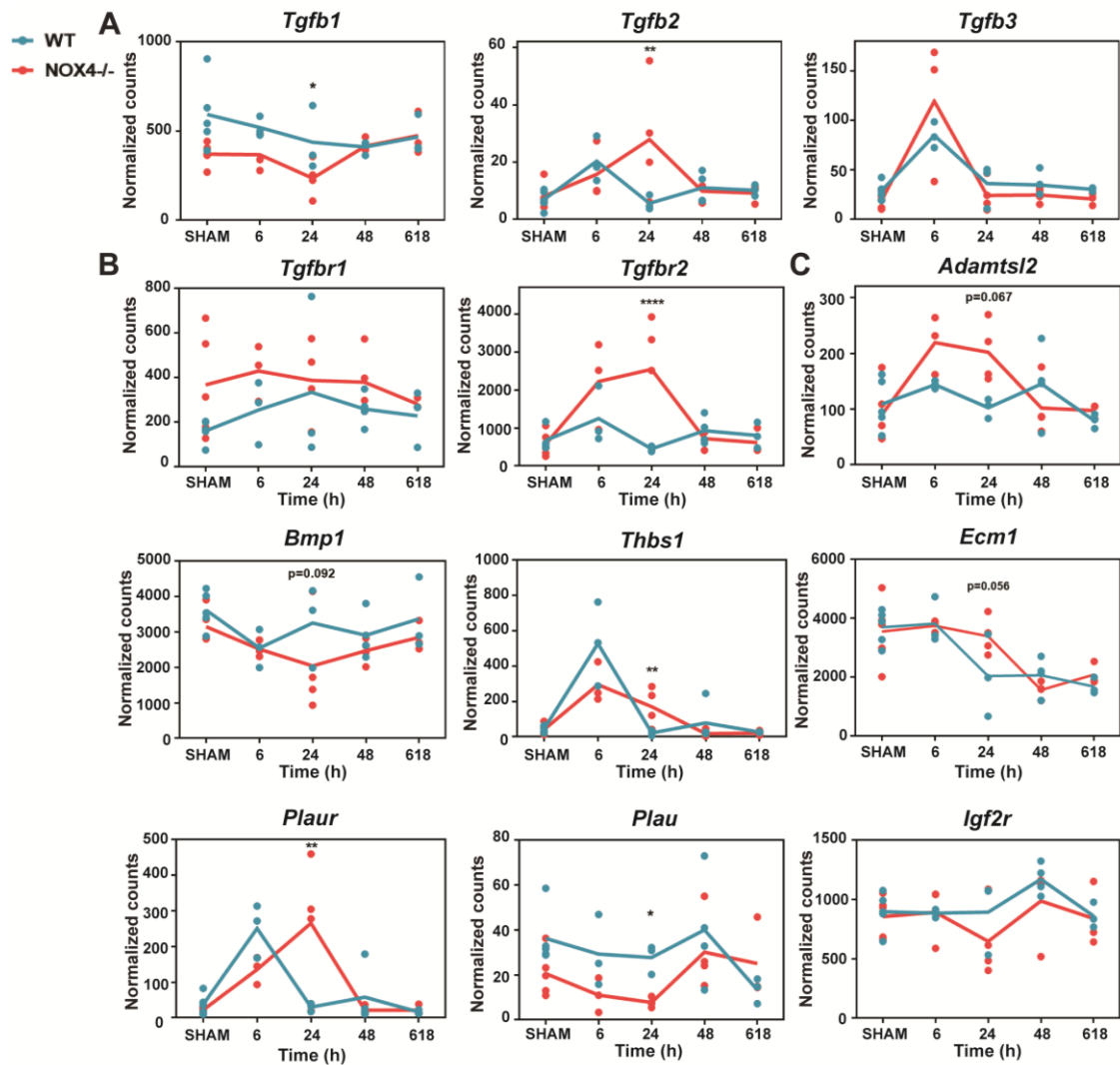
Figure 19. Differential activation of TGF-β may occur between WT and NOX4-/- livers.
Transcriptomics RNA-seq analysis of livers after PH. Changes in gene expression over time in **(A)** TGF-β ligands, **(B)** TGF-β receptors, and **(C)** genes involved in the activation of latent TGF-β1. $*p$ <0.05, $**p <0.01$, $****p<0.0001$.

Additionally, the expression of *Bmp1*, which cleaves LTBP1 from the extracellular matrix inducing TGF-β1 activation (Ge & Greenspan, 2006), was down-regulated at 6 hours after PH in both WT and NOX4-/- mice but, whereas in WT mice the levels returned to basal at 24 hours, in NOX4-/- mice continued down-regulated even at lower levels at 24 hours after PH (**Figure 19C**).

Thrombospondin-1 (TSP-1), is a matricellular protein also implicated in TGF-β activation *in vivo* (Crawford et al., 1998). We observed an increase in WT livers at 6 hours followed by a decrease at 24 hours. However, the induction was lower, and the decrease was less pronounced between 6 and 24 hours in NOX4-/- livers (**Figure 19C**).

Moreover, Extracellular matrix protein 1 (*Ecm1*) displayed a reduction in both WT and NOX4-/- livers, but this decrease occurred later, at 48 hours, in NOX4-/- mice. It has been described that ECM1 stabilizes latent-TGF-β in the extracellular matrix, preventing its activation (Fan et al., 2019).

The urokinase-type plasminogen activator system (uPA/uPAR) also participates in the activation of latent TGF-β1 from the extracellular matrix. uPA/uPAR converts plasminogen to plasmin, which in turn may promote the activation of latent TGF-β by proteolytic cleavage within the N-terminal region of the latency-associated peptide (LAP) (Lyons et al., 1990). In our model, urokinase-type plasminogen activator receptor (uPAR, *Plaur* gene) peaked later in the case of NOX4-/- livers, and urokinase-type plasminogen activator (uPA, *Plau* gene) presented lower levels in NOX4-/- mice.

Finally, Mannose 6-phosphate/insulin-like growth factor II receptor (M6P/IGFII-R) is overexpressed in hepatocytes during liver regeneration and it has been shown to be implicated in the maturation of latent pro-TGF-β (Villevalois-Cam et al., 2003). M6P/IGFII-R (*Igf2r* gene) presented a tendency of lower levels in NOX4-/- than in WT livers at 24 after PH, although difference was not significant (**Figure 19C**). M6P/IGFII-R was also analyzed by immunohistochemistry. 24 hours after PH M6PR seemed to be localized intracellularly in WT liver cells, whereas it was localized in the cellular membrane in NOX4-/- livers (**Figure 20**). The differences in its cellular location could be also responsible of the differences in TGF-β activation.
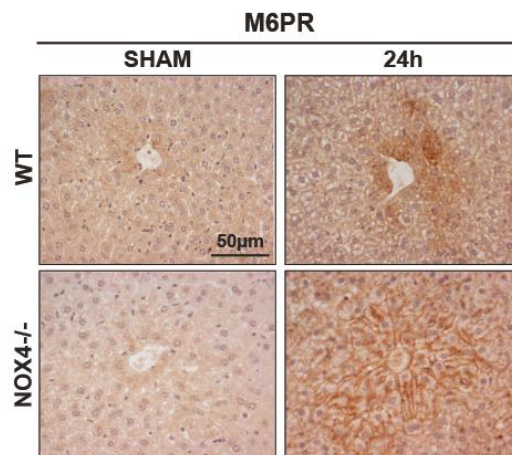
Figure 20. M6P/IGFII-R analysis in WT and NOX4-/- livers. M6P/IGFII-R immunostaining was performed in paraformaldehyde-fixed and paraffin-embedded tissue sections. Representative 40x images are shown.

In contrast, cell-surface integrins such as Integrin $\alpha_v\beta_6$ and Integrin $\alpha_v\beta_8$, and metalloproteases such as MMP2 and MMP9, did not present significant differences in the RNA-seq analysis (data not shown).

Altogether, the results indicated that the TGF-β pathway could be differentially activated along the time in WT and NOX4-/- mice, so we proceeded to analyze it more in detail.

TGF-β analysis in Nox4 deleted mice livers and primary hepatocytes

Immunohistochemistry analysis of the mature, active, form of TGF-β1 revealed that TGF-β1 staining considerably increased in WT liver tissues after PH, but this increase
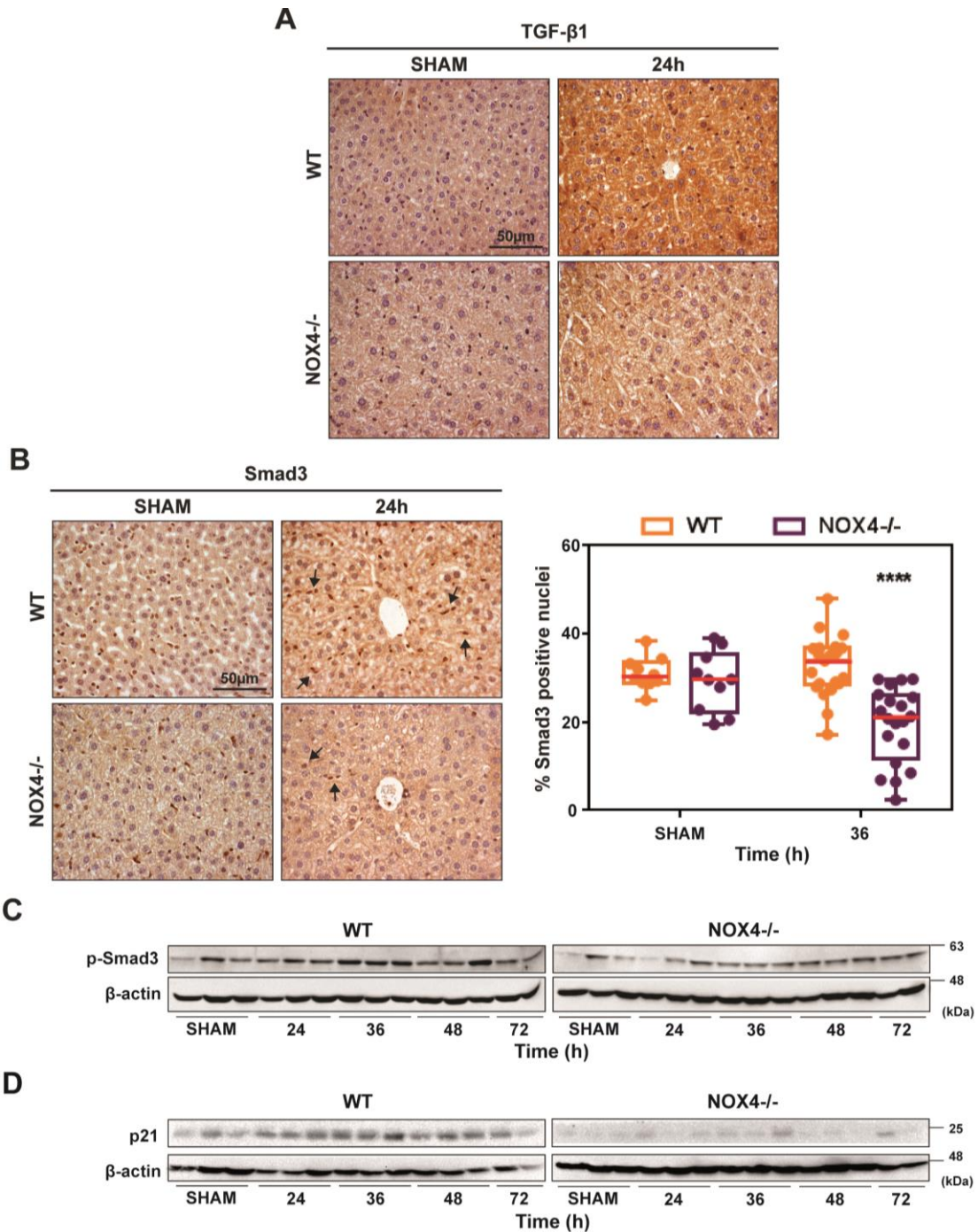
Figure 21. Lower activation of the TGF-β pathway in NOX4-/- livers after PH. **(A)** TGF-β1 and **(B)** Smad3 immunostaining was performed in WT and NOX4-/- mice. Arrows indicate Smad3 positive nuclei (left) and positive nuclei quantified with ImageJ software (right). Student's t test with Welch correction was used: **** p <0.0001 compared to WT. **(C)** Analysis of p-Smad3 and **(D)** p21 by Western Blot. β-actin was used as a loading control.

was significantly lower in NOX4-/- at 24 hours after PH (**Figure 21A**). The lower expression of TGF-β1 in NOX4-/- seemed to be reflected in a decrease in the activation of the TGF-β pathway. Indeed, analysis of Smad3 by immunohistochemistry revealed lower number of Smad3 positive nuclei in NOX4-/- than in WT (**Figure 21B**), and western blot analysis showed an increase in the levels of phospho-Smad3 after PH in WT mice that was delayed and attenuated in NOX4-/- (**Figure 21C**). Furthermore, we observed that one of the most relevant targets of TGF-β, the cyclin-CDK inhibitor p21, presented lower levels in NOX4-/- livers (**Figure 21D**).
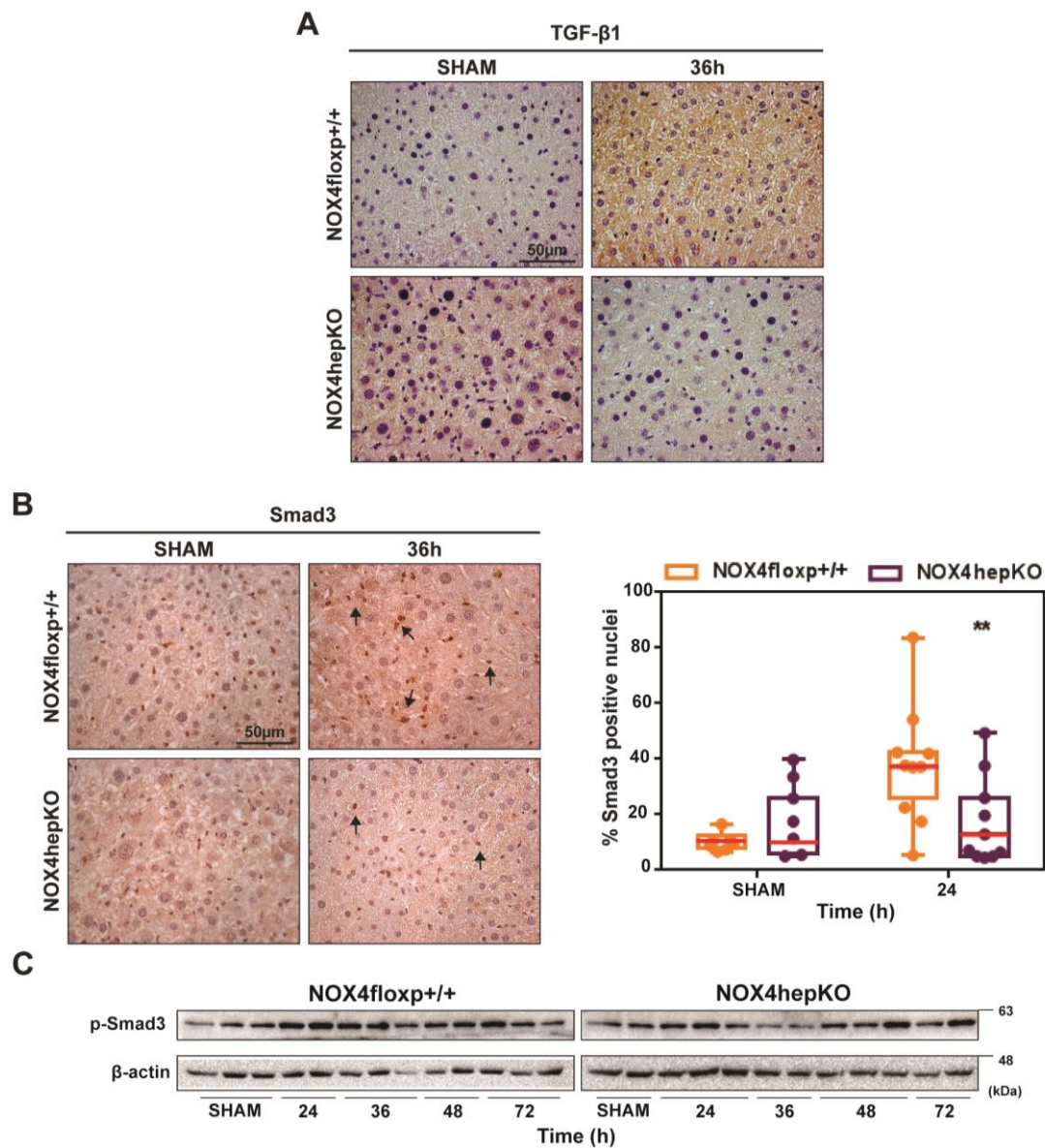
Figure 22. Lower activation of the TGF-β pathway NOX4hepKO livers after PH. (A) TGF-β1 and (B) Smad3 immunostaining was performed in NOX4floxp+/+ and NOX4hepKO mice. Arrows indicate Smad3 positive nuclei (left) and positive nuclei quantified with ImageJ software (right). Student's t test with Welch correction was used: **** p <0.0001 compared to NOX4floxp+/+. (C) Analysis of p-Smad3 by Western Blot. β-actin was used as a loading control.

Immunohistochemistry analysis of TGF-β1 also revealed that 36 hours after PH there was an increase in NOX4floxp+/+ liver tissues, but this increase was barely observed in NOX4HepKO (**Figure 22A**) and it correlated with a lower number of Smad3 positive nuclei (**Figure 22B**) and a delayed phosphorylation of Smad3 (**Figure 22C**) as observed in NOX4-/- model.

Previous results had demonstrated that deficiency in the liver of caveolin-1 impairs the TGF-β pathway and improves liver regeneration (Mayoral et al., 2010). Interestingly, concomitant with the alteration in the activation of the TGF-β pathway, we found lower expression of caveolin-1 in both models of NOX4 deficient mice versus the corresponding WT counterparts (**Figure 23**).

Taken together, these results indicated that the TGF- β1 pathway presented a transcriptional and functional attenuation *in vivo*.
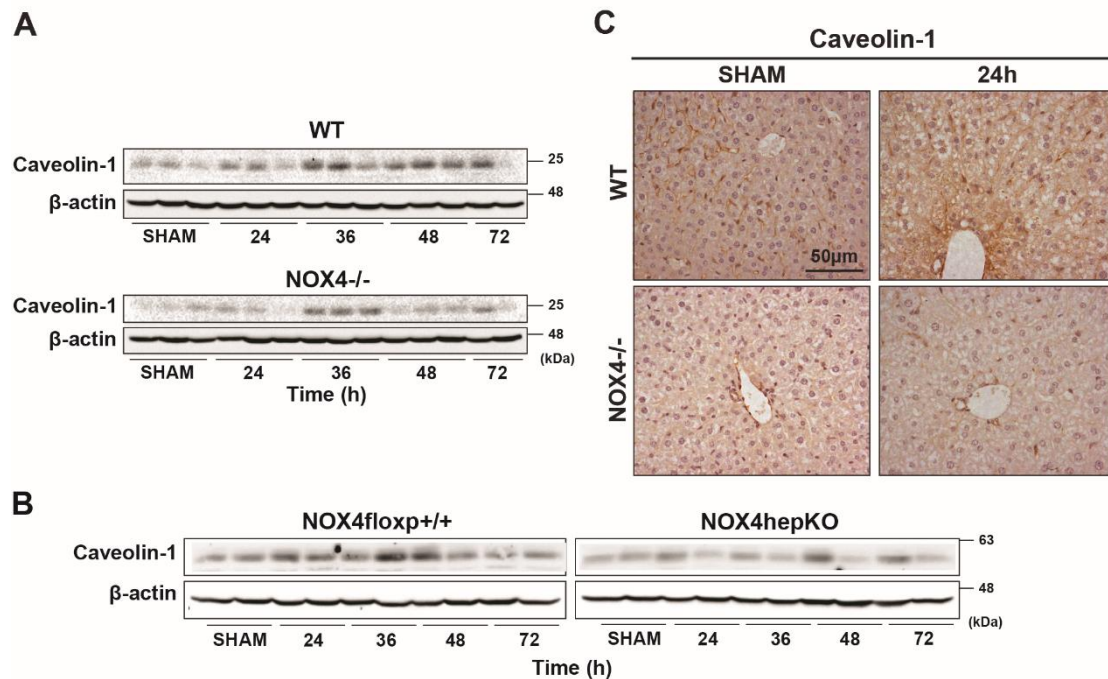
Figure 23. **Lower levels of Caveolin-1 pathway in NOX4 deleted mice after PH. (A)** Analysis of Caveolin-1 by Western Blot in NOX4-/- and **(B)** NOX4hepKO mice and their respective WT controls. β-actin was used as a loading control. **(C)** Caveolin-1 immunostaining was performed in paraformaldehyde-fixed and paraffin-embedded tissue sections in WT and NOX4-/- mice 24 hours after PH.

After that, we wondered whether or not NOX4-deficient cells were able to respond to active TGF- β1. To answer this question, primary hepatocytes were isolated from WT and NOX4-/- and were treated with 2% FBS in the absence or presence of TGF-β1 (2ng/mL) for the time indicated in the graphs.

Firstly, primary hepatocytes from WT and NOX4-/- mice were able to activate the TGF-β1 pathway in terms of Smad2 phosphorylation, both at 3 and 24 hours after treatment (**Figure 24A**). Moreover, we observed that 24 hours after treatment, primary hepatocytes presented phenotypical differences. TGF-β1-treated primary hepatocytes from both WT and NOX4/- mice lost their epithelial shape towards a fibroblast-like phenotype (**Figure 24B**).
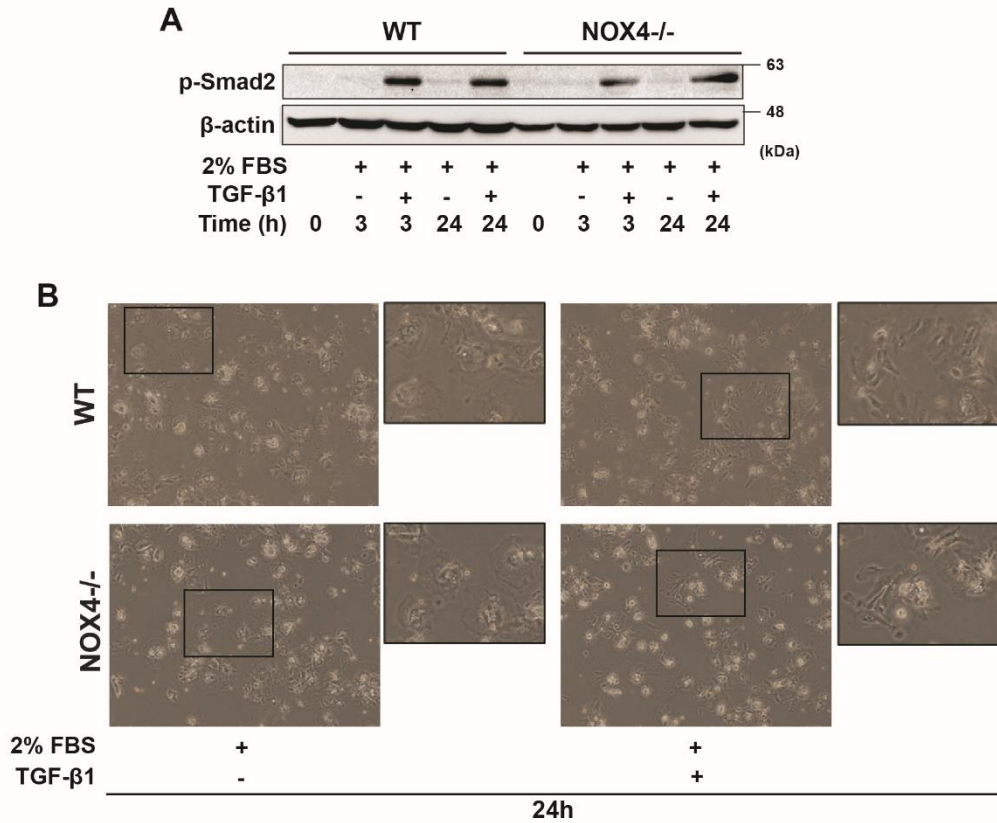
Figure 24. TGF-β1 treatment induced Smad2 phosphorylation and morphological changes in WT and NOX4-/- primary hepatocytes. (A) Analysis of p-Smad2 by Western Blot. β-actin was used as a loading control. A representative experiment (n=3) is shown. **(B)** Cell morphology analysis 24 hours after treatments of WT and NOX4-/- primary hepatocytes cultured on top of Collagen I. Representative bright-field images.

NOX4-deficient cells also demonstrated a correct response to exogenous TGF-β1 inhibiting FBS-induced increase in cell viability (**Figure 25A**) and cyclins expression (**Figure 25B**). Comparable results were observed in NOX4hepKO primary hepatocytes (data not shown).

Furthermore, Smad2 phosphorylation and decrease in cyclins was coincident with a decrease in the number or Ki67+ cells, regardless of *Nox4* expression (**Figure 26**).
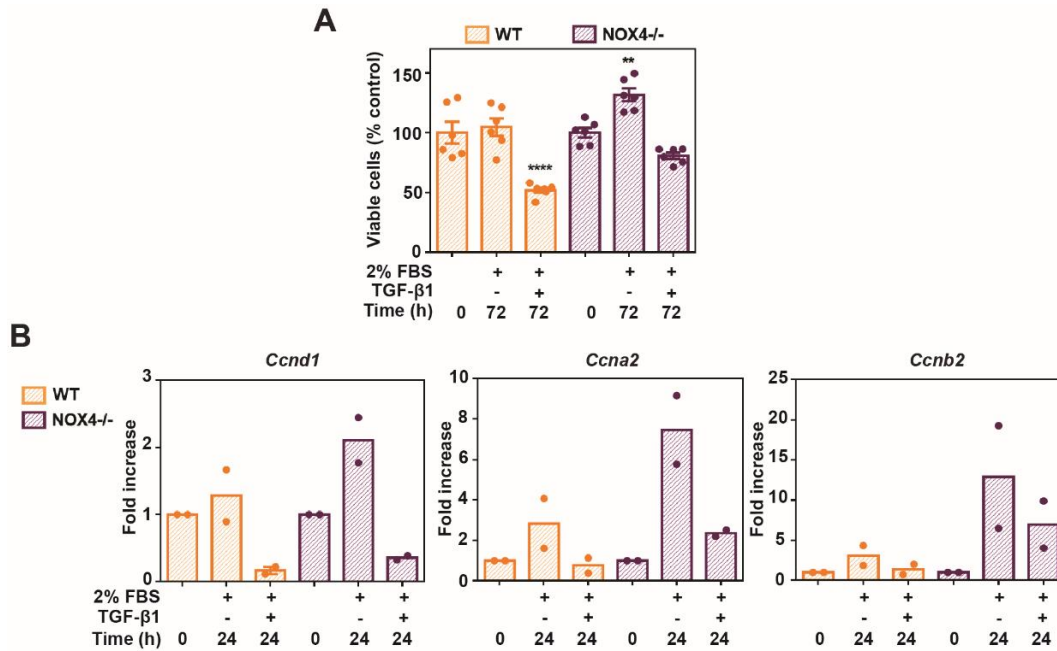
Figure 25. Decrease in proliferation was observed in WT and NOX4-/- primary hepatocytes after TGF-β1 treatment. (A) Viable cell number represented as % versus 0 time. Mean ± SEM (6 independent plates). ** < p 0.01, ****p<0.0001 compared to untreated cells. (B) RT-qPCR analysis of Cyclin D1 (*Ccnd1*), Cyclin A2 (*Ccna2*) and Cyclin B2 (*Ccnb2*). Relative expression to *Rpl32* gene. Bars represent the Mean from 2 independent plates. A representative experiment (n=3) is shown.
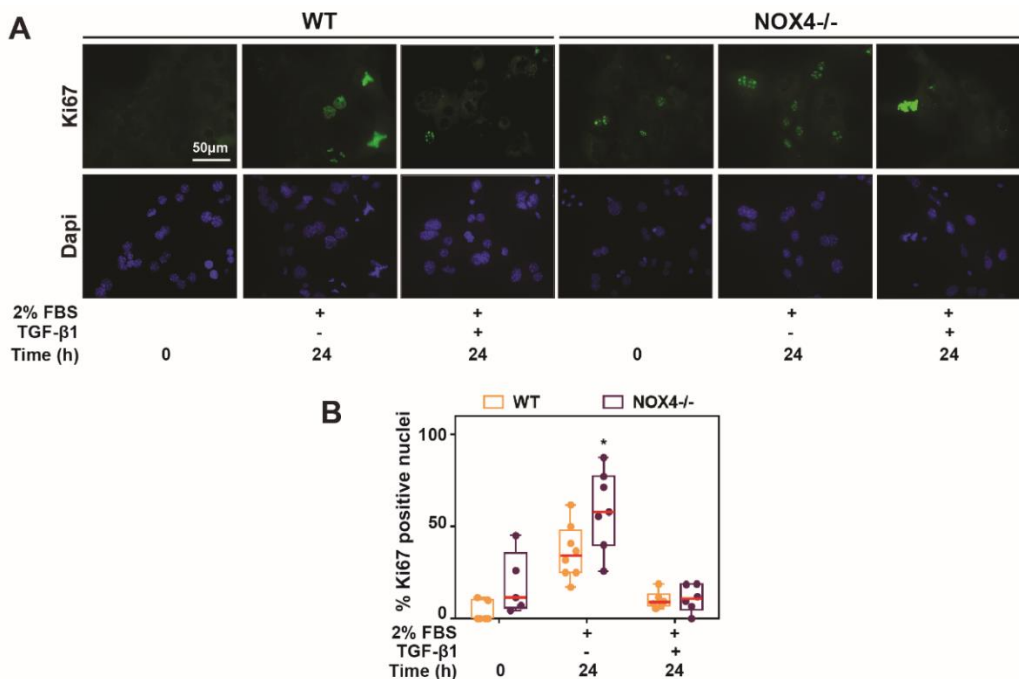
Figure 26. Decrease in Ki67+ nuclei in response to TGF-β1 treatment in WT and NOX4-/- primary hepatocytes. (A) Immunostaining of Ki67 (Green) and DAPI (blue) and (B) quantification of positive nuclei quantified with ImageJ software. Red bars represent the Median. Student's t test with Welch correction was used: *< p0.05 compared to WT cells.

24 hours after 2% FBS treatment, upregulation of c-Myc was observed in WT and NOX4-/- primary hepatocytes. c-Myc protein levels were higher at basal levels (**Figure 27 A**), as well as in response to FBS, in NOX4-/- hepatocytes (**Figure 27 A and B**). Moreover, the number of c-Myc positive nuclei after 2% FBS treatment was higher in NOX4-/- primary hepatocytes than in WT ones. Nevertheless, TGF-β1 showed identical capacity in inhibiting c-Myc upregulation in WT and in NOX4-/- primary hepatocytes (**Figure 27 A and B**).

Altogether, these results suggest that Nox4 is not required for TGF-β1-induced growth inhibition, nor for c-Myc downregulation.
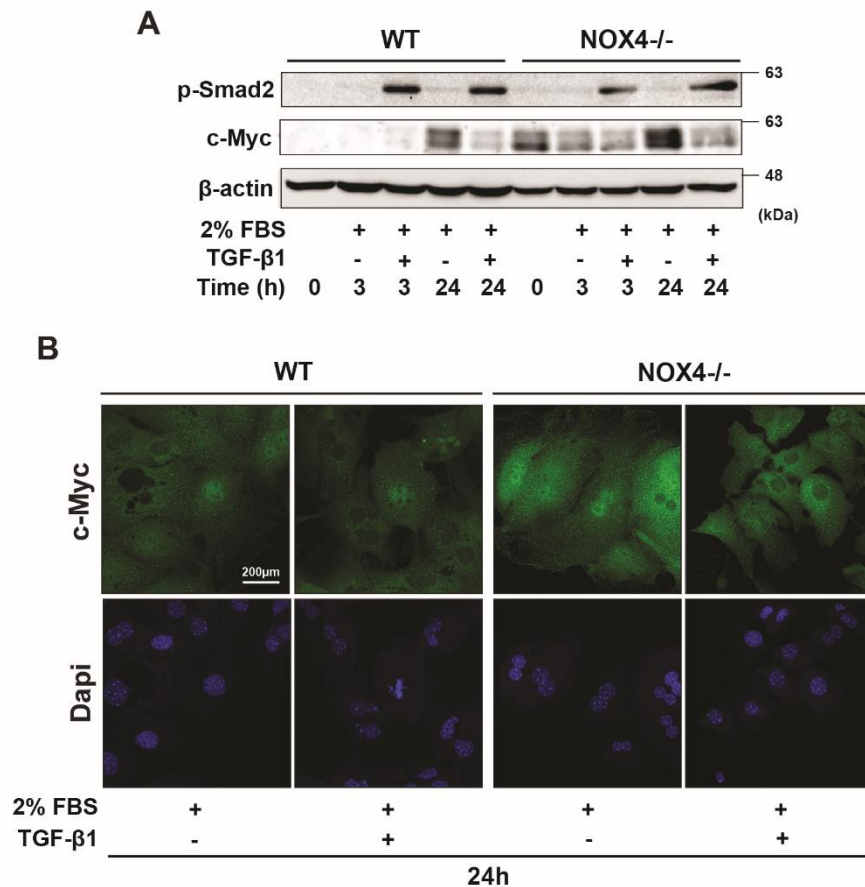
Figure 27. Decrease in c-Myc levels in response to TGF-β1 treatment in WT and NOX4-/- primary hepatocytes. (A) Analysis of p-Smad2 and c-Myc by Western Blot. β-actin was used as a loading control. A representative experiment is shown. **(B)** Immunostaining of c-Myc (Green) and DAPI (blue) was performed in WT and NOX4-/- mice to visualize the nuclear content.

Finally, within all the proteins that participate in the activation of the latent form of TGF-β1, Mannose 6-phosphate/insulin-like growth factor II receptor (M6P/IGFII-R) is localized inside the cell. Western blot analysis revealed that at time 0 hours, M6P/IGFII-R protein levels were higher in NOX4-/- primary hepatocytes than in WT ones (**Figure 28**).

Moreover, M6P/IGFII-R was induced at 3 and 24 hours in WT primary hepatocytes after both FBS and TGF-β1 treatment. However, this increase was barely observed in NOX4-/- primary hepatocytes at 3 hours after treatment, and levels dropped even more at 24 hours after treatment.
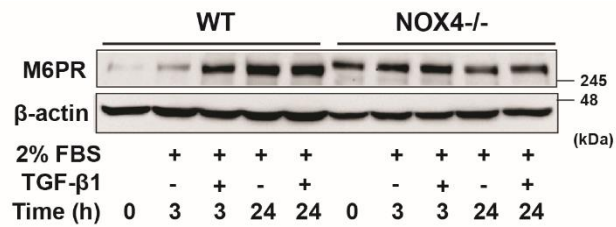
Figure 28. Induction of M6PR in WT primary hepatocytes in response to FBS and TGF-β1 treatment. Analysis of M6PR by Western Blot. β-actin was used as a loading control. A representative experiment is shown.

Potential role of Nox4 in controlling lipid metabolism and oxidative stress

Taking advantage of the data generated by the afore-described RNA-seq analysis, we decided to analyze metabolic and redox mediators that could be differentially expressed between WT and NOX4-/- mice.

It is well known that liver regeneration demands large amounts of simple substrates to cover energy and structural requirements, and so alterations in hepatic and systemic metabolism occur after PH. In this regard, we observed that at 36 hours after PH, WT and NOX4-/- presented lipid droplets, but this was resolved earlier, at 48 hours after PH, in NOX4-/- livers (**Figure 5**). Considering these differences, we decided to look for metabolic changes more in detail.

Peroxisome proliferation-activated receptor (PPAR) family are important metabolic regulators in the liver. PPAR-α (*Ppara* gene) did not shown significant differences between WT and NOX4-/- livers (**Figure 29**). However, *Cyp4a10* and *Cyp4a14*, which are PPAR-α target genes, presented an earlier induction at 6 hours after PH in NOX4-/- livers, when compared to WT (**Figure 29**). Another member of the PPAR family, PPAR- δ (*Ppard* gene), also presented higher levels at 24 hours after PH in NOX4-/- mice (**Figure 29**). In the case of PPAR-γ (*Pparg*), it did not present significant differences in our model (**Figure 29**). However, Peroxisome proliferation-activated receptor γ coactivator 1-β (PGC-1β, *Ppargc1b* gene), presented a significant increase in NOX4-/- livers at 6 and 24 hours after PH (**Figure 29**).

Cluster of differentiation 36 (CD36, *Cd36* gene), which mediates fatty acid uptake during liver regeneration, did not present significant differences between WT and NOX4-/- livers (**Figure 29**). Fatty acid synthase (*Fas* gene) and Glucose-6-phosphate dehydrogenase (*G6pdh* gene) neither presented significant differences (**Figure 29**).

Diacylglycerol O-acyltransferase 1 (*Dgat1*), which catalyzes the terminal step in triacylglycerol synthesis, presented higher levels in NOX4-/- at 24 hours after PH (**Figure 29**).

HMG-CoA reductase (*Hmgcr*) is key enzyme for cholesterol synthesis, which is one of the substrates required for liver regeneration (Zivna et al., 2002), and it presented an earlier and higher induction in NOX4-/- livers at 6 hours after PH, when compared to WT (**Figure 29**).

Pyruvate Dehydrogenase Kinase 4 (PDK4, *Pdk4* gene), another critical regulator of glucose and lipid metabolism, also presented significant differences. We found a significant upregulation at 24 hours after PH in NOX4-/- livers, when compared to WT (**Figure 29**).

Altogether, these results indicate that there could be a different metabolic response after PH between WT and NOX4-/- livers.
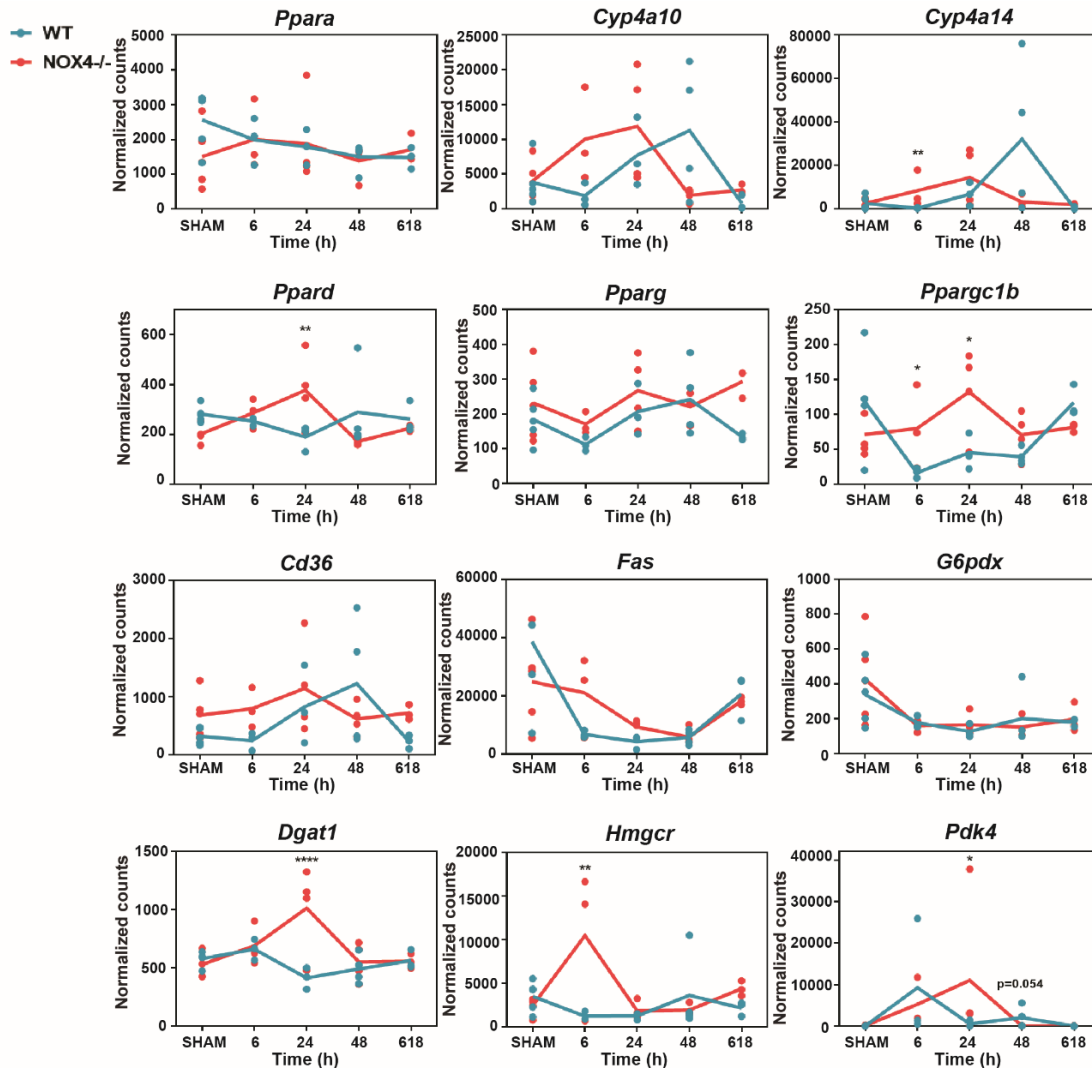
Figure 29. Metabolic changes during liver regeneration . Transcriptomics RNA-seq analysis of livers in WT and NOX4-/- mice. Changes in gene expression over time in genes implicated in regulation of hepatic metabolism. *p <0.05, **p <0.01, ****p<0.0001.

The liver is frequently subjected to oxidative stress, which has a negative impact on liver function and regeneration. Considering that the NADPH oxidase NOX4 participates in the redox balance of the cell, we thought that there could be differences in the redox status between WT and NOX4-/- after PH.

An important player in the defense against oxidative stress implicated in LR is the Nuclear factor erythroid 2-related factor 2, Nrf2 (*Nfe2l2* gene). Looking at the RNA-sequencing analysis, we observed that *Nfe2l2* presented a peak at 6 and 24 hours in NOX4-/- livers, which occurred later, at 48 hours, in WT mice. However, this difference was not significant (**Figure 30**).
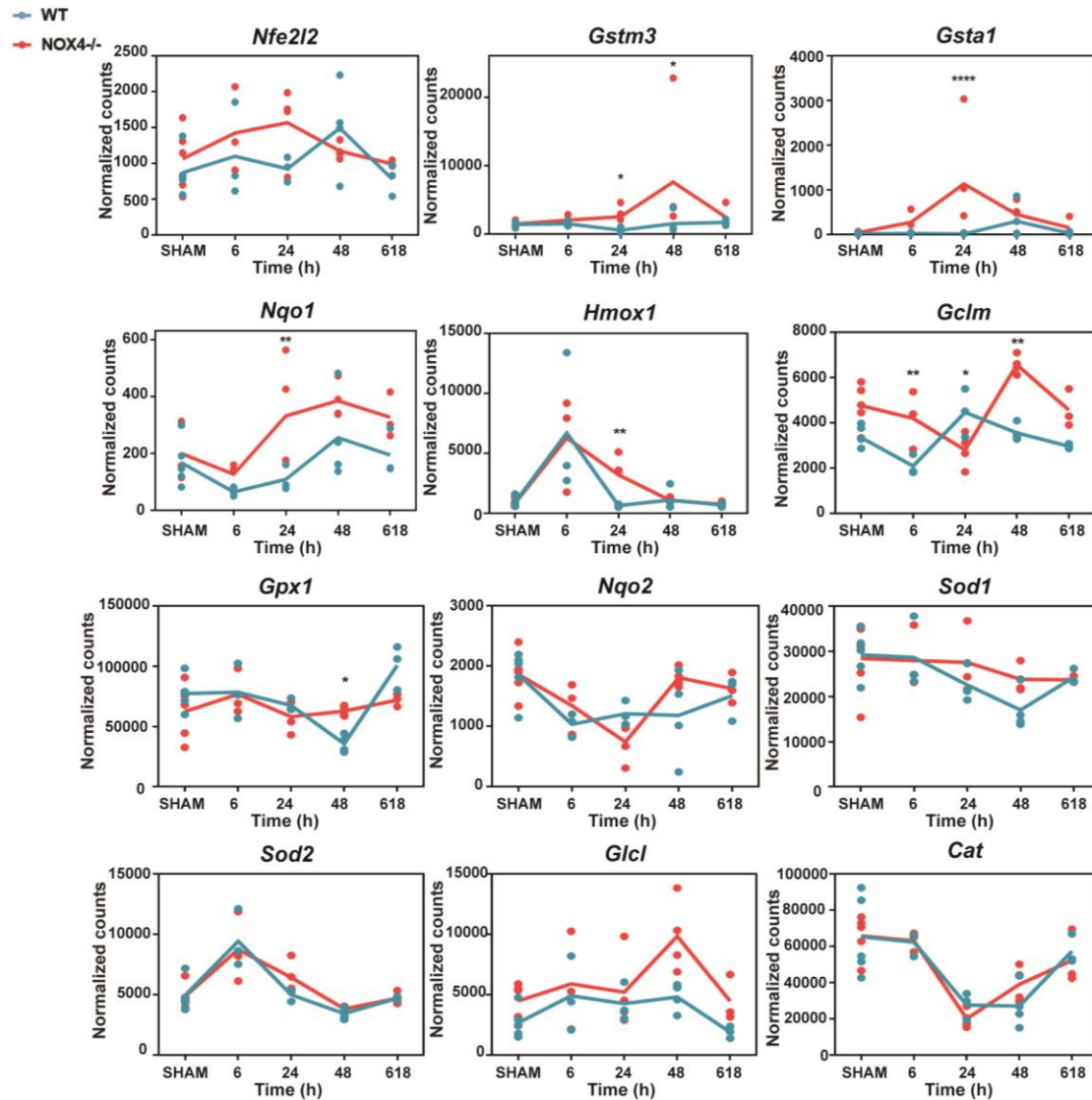
Figure 30. Role of Nox4 in the regulation of redox-related genes during liver regeneration. Transcriptomics RNA-seq analysis of livers after PH in WT and NOX4-/- mice. Changes in gene expression over time in genes implicated in regulation of redox balance. *p <0.05, **p <0.01, ****p<0.0001.

When we look at Nrf2 target genes, some of them presented differential expression along the time. Glutathione S-Transferase Mu 3 (*Gstm3*) showed higher levels at 24 and 48 hours after PH in NOX4-/- mice. Glutathione S-Transferase Alpha 1 (*Gsta1*), NAD(P)H Quinone Dehydrogenase 1 (*Nqo1*) and Heme Oxygenase 1 (*Hmox1*) presented higher

expression at 24 hours in NOX4-/- livers than in WT ones. In the case of Glutamate-Cysteine Ligase Modifier Subunit (*Gclm*), there was a decrease in WT at 6 hours, which occurred at 24 hours in NOX4-/-. Glutathione peroxidase 1 (*Gpx1)* presented a reduction in WT at 48 hours, which was lower and occurred earlier in NOX4-/- livers (**Figure 30**).

However, other target genes of Nrf2 such as NAD(P)H Quinone Dehydrogenase 2 (*Nqo2*), Superoxide Dismutase 1 and 2 (*Sod 1* and *Sod2*), Glutamate-Cysteine Ligase Catalytic Subunit (*Glcl*) and Catalase (*Cat*) did not presented significant differences between WT and NOX4-/- after PH (**Figure 30**).

Altogether, the results indicate that there are differences in the expression of some antioxidant genes between WT and NOX4-/- after two-thirds partial hepatectomy, although a timely regulated antioxidant response does not seem to be responsible for the earlier recovery of NOX4-/- after PH.

Analysis of liver regeneration after 2/3 PH in one-year-old mice

Considering that partial hepatectomy is an intervention that can be performed in elderly people, we performed a pilot experiment to explore liver regeneration in older mice. Firstly, we analyzed if *Nox4* levels decrease after partial hepatectomy in 1-year-old WT mice, as we had previously described in 8-16-weeks old mice (Crosas-Molist et al., 2014). *Nox4* expression decreased in WT mice at 24 hours after partial hepatectomy and then increased at 48 and 72 hours (**Figure 31A**).
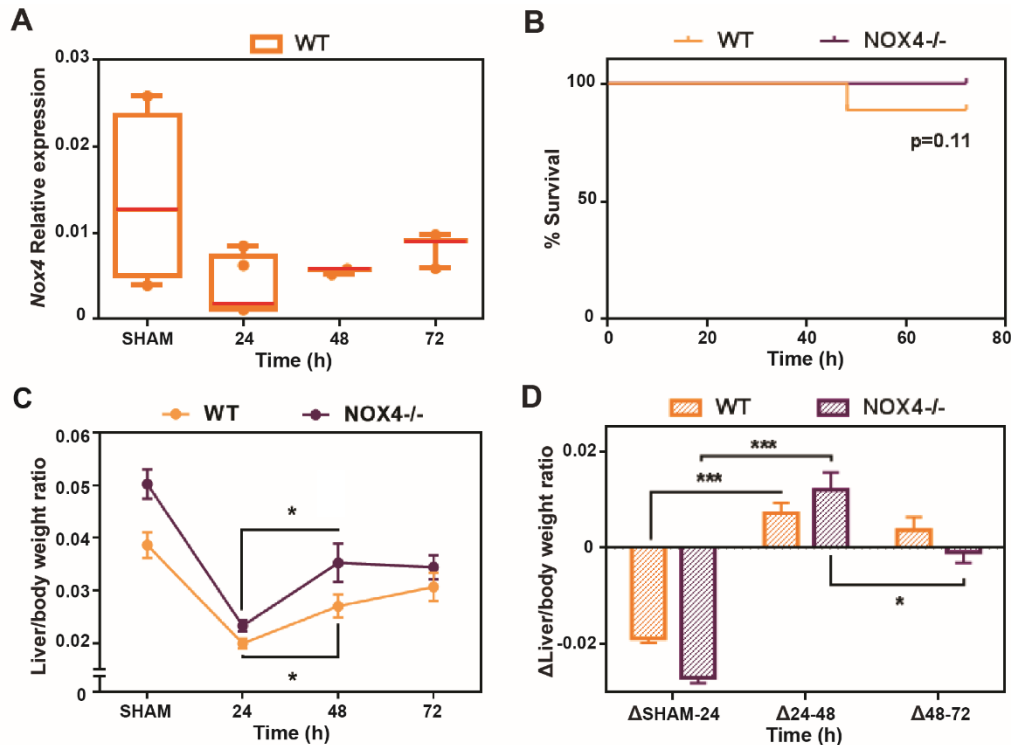
Figure 31. One-year old NOX4 deleted mice presented an earlier recovery of the liver-to-body weight ratio and higher survival after PH. Mice were subjected to PH and sacrificed at the indicated times. **(A)** RT-qPCR analysis of *Nox4* in livers from WT and NOX4-/- mice. Relative expression to *Rpl32* gene. Red bars represent the Median. **(B)** Kaplan-Meier curve of overall survival. **(C)** Liver/Body weight ratio was calculated for WT and NOX4-/- mice and represented as mean ± SEM. **(D)** Increment in liver-to-body weight ratio between timepoints. Data was expressed as mean ± SEM. Student's t test with Welch correction was used: *$p < 0.05$, ***$p < 0.001$ compared to previous time point.

After that, we analyzed mice survival after the surgeries. NOX4-/- mice presented a tendency to higher survival after PH than WT (**Figure 31B**). Liver to body weight ratio as well as the increment in the liver/body weight ratio were calculated, and we observed a more pronounced increase in the liver/body weight ratio in NOX4-/- mice than in WT counterparts between 24 and 48 hours (**Figure 31C** and **D**).

Then, we studied histological differences. Liver steatosis was perfectly observed in both WT and NOX4-/- livers at 48 hours after PH. However, at 72 hours after PH, NOX4-/- livers already recovered from lipid accumulation (**Figure 32**).
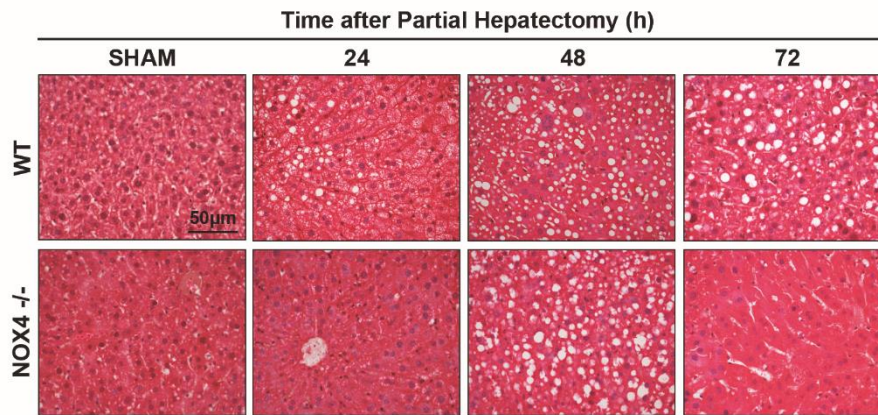
Figure 32. One-year old NOX4-/- mice presented an earlier recovery of the parenchymal structure and regenerative steatosis after 2/3 PH. Hematoxylin and Eosin staining performed in paraformaldehyde-fixed and paraffin-embedded tissue sections. Representative 40x images are shown at different time points after PH.

Afterwards, we wanted to study if the earlier recovery in NOX4-/- mice could be associated to the afore-mentioned increase in c-Myc levels. We found that c-Myc presented an upregulation after PH in both WT and NOX4-/- at the mRNA and protein level. Interestingly, 24 hours after PH two NOX4-/- mice presented higher levels of c-Myc than WT counterparts (**Figure 33A** and **B**).
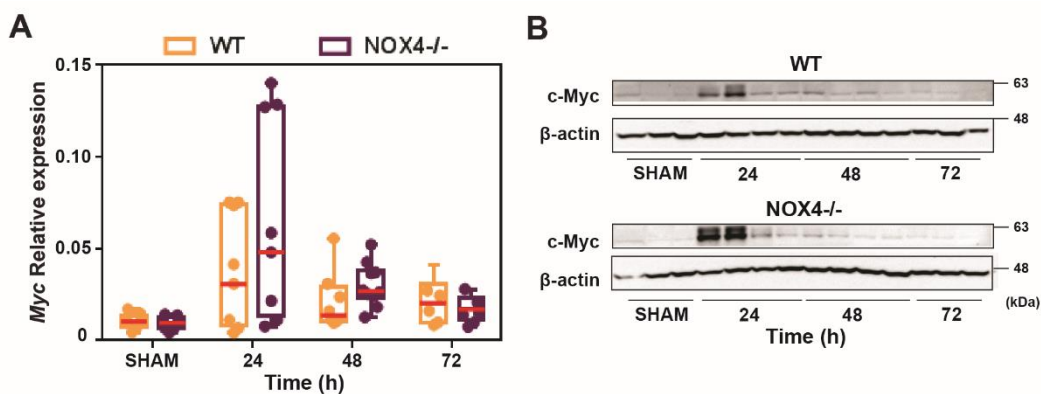
Figure 33. Higher levels of c-Myc were found in one-year old NOX4 deleted mice after PH. (A) RT-qPCR analysis of *Myc* in livers from WT and NOX4-/-. Relative expression to *Rpl32* gene. Red bars represent the Median. **(B)** Analysis of c-Myc by Western Blot in WT and NOX4-/- livers. β-actin was used as loading control.

Finally, considering the previous results in which the higher levels of c-Myc were accompanied by an attenuation of the TGF-β pathway, we decided to study the levels of p-

Smad3. Both WT and NOX4-/- presented an increase in Smad3 phosphorylation after PH. However, we observed that NOX4-/- livers presented lower levels of p-Smad3 than WT ones (**Figure 34**).
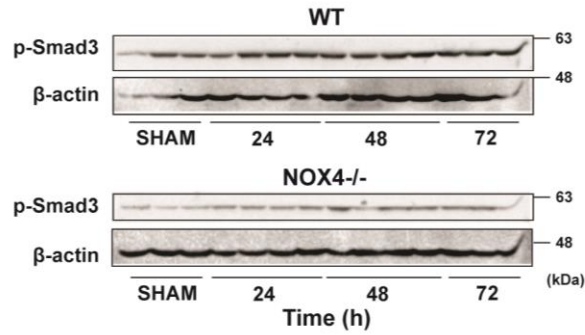
Figure 34. Lower levels of p-Smad3 were found in one-year old NOX4 deleted mice after PH. Analysis of c-Myc by Western Blot in WT and NOX4-/- livers. β-actin was used as loading control.

Taken together, the results indicate that NOX4 deletion also accelerates liver regeneration in 1-year-old mice.

VI. Discussion

Liver regeneration is a complex process that, despite extensive study, is not completely understood. Several signaling pathways, as well as interactions among different cell types, make the process extremely attractive to glean molecular insights into the self-renewal of mature cells, a property frequently associated with stem cells. Hepatocytes appear to be cell autonomous in deciding their replication fate, which depends on reprograming different molecular events in different cell types (Fausto et al., 2012). Results here support a role for Nox4 in negatively regulating liver regeneration, since deletion of its expression improved survival of mice, accelerated the recovery of the liver mass, as well as the liver parenchyma, and enhanced the process of hepatocyte proliferation, which correlated with a more efficient response of hepatocytes to mitogenic signals. Interestingly, similar results were observed in NOX4-/- (where *Nox4* is deleted in all the cell types of the organism) and the NOX4HepKO model (where *Nox4* is specifically deleted in hepatocytes), indicating that the relevant role of Nox4 during mice liver regeneration is mostly due to its function in hepatocytes. This is not surprising, since *Nox4* expression is two orders of magnitude higher in hepatocytes than in stellate cells, and even one order of magnitude higher than the expression in myofibroblasts, under fibrotic conditions (Sancho et al., 2012). In fact, NOX4 expression in the livers of NOX4HepKO mice was barely detectable, lower than 0.5% when compared to the corresponding WT mice (results not shown).

Nox4 expression is down-regulated after PH in mice, which is probably necessary for an efficient hepatocyte proliferation, due to its mitoinhibitory role (Crosas-Molist et al., 2014). Downregulation of Nox4 might occur by the increase in proliferative signals, since both EGF and HGF inhibit its expression (Cao et al., 2017; Carmona-Cuenca et al., 2006). In the experimental animal models used in this study, where *Nox4* gene expression is deleted, hepatocytes were more "primed" to respond to mitogenic signals in a fastest way.

An interesting aspect to be mentioned is that although an increase in the liver to body weight ratio was observed in NOX4-/- mice versus WT, long-term analysis revealed that proliferation was arrested. The liver reached a size that did not overcome the initial one and liver parenchyma structure was normal. This could be the consequence of the "hepatostat" regulation, which orchestrates growth and differentiation of all hepatic cell types towards body homeostasis. Many signals contribute to the termination of liver regeneration and maintenance of standard liver mass (Michalopoulos, 2017) and Nox4 does not appear to be essential for this process, which reinforces its potential as a therapeutic target in liver chronic diseases.

Trying to analyze the potential mechanism regulated by Nox4 that would make regeneration more efficient, we found a stronger activation of the c-Myc *in vivo*, as well as in hepatocytes in culture. c-Myc is a relevant regulator of the expression of cell-cycle related genes (Bretones et al., 2015) and it has been suggested that hepatocytes require upregulation of Myc after PH to efficiently exit G_0 (Baena et al., 2005). It is well known that hypertrophy without cell division precedes proliferation after two thirds PH and almost equally contribute to regeneration (Miyaoka et al., 2012). Interestingly, c- Myc not only regulates hepatocyte proliferation, but also cell size (Baena et al., 2005). Here, the increase in Myc expression in Nox4 deleted mice correlated with a significant increase in cell size at 24-36 h after PH and preceded the peak of cell proliferation.

RNA-seq analysis revealed significant differences at the transcriptional level after PH in NOX4-/- mice when compared to WT mice. The network of the top100 differentially expressed genes from the "response to oxygen-containing compound" pathway located *Myc* in a node of proliferation-related genes 24 hours after PH. The highest peak of *Myc* expression was coincident with a peak in *Jund* levels, and it has been reported that essential role of JunD in cell proliferation is mediated via MYC signaling in prostate cancer cells (Elliott et al., 2019). *Jun* gene, which codifies for c-Jun protein, also presented higher levels in NOX4-/- livers. This transcription factor has been proposed as a critical regulator of hepatocyte proliferation and survival during liver development and regeneration (Behrens et al., 2002). Early growth response (Egr)-1 (*Egr1*), which is a transcription factor required for timely cell-cycle entry and progression in hepatocytes after CCl_4 injection (Pritchard et al., 2011), also maintained higher levels in NOX4-/- at 24 hours after PH. Same pattern was observed in *Sox9,* whose expression allows periportal hepatocytes to behave as hybrid hepatocytes with ability to regenerate the liver after chronic hepatocyte-depleting injuries (Font-Burgada et al., 2015, p.). Finally, *Fosb*, a member of the Fos family which induce cell cycle entry by activating cyclin D1 (Brown et al., 1998), also presented the same pattern of expression.

Regarding mitogenic factors whose expression revealed changes, we found that *Hbegf*, which is a member of the EGFR ligands family, presented a significant increase in the expression at 24 hours after PH in NOX4-/- mice. It is known that HB-EGF links hepatocyte priming with cell cycle progression during liver regeneration (Mitchell, 2005) and transgenic expression of HB-EGF accelerates liver regeneration after 2/3 PH (Kiso et al., 2003). In spite of the fact that we did not find significant differences in other members of the

EGFR or Met family, it has been reported that HB-EGF has more potent protective and mitogenic effects for hepatocytes than HGF in liver regeneration (Khai et al., 2006).

All these transcriptional changes in proliferation-related genes mainly occur at 24 hours after partial hepatectomy, prior to hepatocyte proliferation and concomitant with higher *Myc* expression, and could contribute to the earlier recovery in NOX4-/- mice after two-thirds partial hepatectomy.

Evidence supports a role for TGF-β inhibiting *Myc* expression (Frederick et al., 2004). In hepatocytes, TGF-β1 inhibits growth and induces apoptosis in hepatocytes (Carr et al., 1986; Sánchez et al., 1996) and one of its earlier effects is downregulation of the mitogen-induced *Myc* early expression (Sanchez et al., 1995), without an effect on the expression of other proto-oncogenes, such as *Fos* or *Hras*. Here, we found that acceleration of liver regeneration and increased expression of *Myc* in both mice models of *Nox4* deletion could be explained, at least partially, due to attenuation of the TGF-β pathway. Different evidences support this hypothesis: 1) IHC analysis of TGF-β1 levels in hepatocytes revealed an increase shortly after PH in hepatocytes from WT mice in both models, as previously reported (Jirtle et al., 1991; Jakowlew et al., 1991); however this increase was attenuated, or even barely observed, in *Nox4* deleted mice; 2) Percentage of Smad3 positive nuclei, as a hallmark of TGF-β activation, was lower in liver tissues from *Nox4* deleted mice than in their corresponding WT mice; 3) Increase in phospho-Smad3 levels after PH was delayed in both NOX4-/- and NOX4HepKO mice.

TGF-β modulates the proliferation of hepatocytes through inhibition of DNA synthesis (Braun et al., 1988). However, it has been proposed that transient escape of regenerative hepatocytes from TGF-β-induced growth inhibition and apoptosis is achieved through reduction in the expression of TGF-β receptors I and II (Chart et al., 1995) and the acquisition of survival signals (Herrera, Álvarez, et al., 2004), within others. In this sense, we found that TGF-β type II receptor did not decrease, but even increased its levels after PH in NOX4-/- mice. Given that TGF-β type II receptor is the one that binds TGF-β, inducing phosphorylation and activation of TGF-β receptor I (Tzvlaki & Moustakas, 2020), we consider that upregulation of TGF-β RII could be a compensatory mechanism for the lower activation of TGF-β1 from the extracellular matrix. Nevertheless, a mitoinhibitory response to TGF-β is still present in regenerating hepatocytes, since intravenous TGF-β1/2 reversibly inhibits the proliferative response of liver to PH (Russell, 1988). Furthermore, inactivation of the TGF-β pathway by using liver-specific Tgfbr2 knock-out mouse results in an increased proliferative response after PH (Oe et al., 2004; Romero-Gallo et al., 2005), and inhibition

of TGF-β signaling also facilitates liver regeneration upon acute dimethylnitrosamine (DMN) or CCl$_4$-induced injury (Karkampouna et al., 2016; Masuda et al., 2020; Nakamura et al., 2004). Results here indicate that, in the absence of *Nox4* expression, the TGF-β pathway was attenuated in hepatocytes, which could contribute to the acceleration of the liver regeneration after partial hepatectomy.

Although it is well known that TGF-β upregulates NOX4 in stellate cells and hepatocytes (Carmona-Cuenca et al., 2008; Jiang et al., 2012; Sancho et al., 2012), it is less well recognized that NOX4 can reciprocally regulate TGF-β/SMAD signaling. The RNA-seq experiment revealed some potential mechanisms responsible for the attenuation of the TGF-β pathway. On one side, TGF-β ligands, which are mainly expressed in non-parenchymal liver cells, showed differences between WT and NOX4-/- mice. *Tgfb1* expression was significantly lower at 24 hours after PH in NOX4-/- mice when compared to WT mice. By contrast, another member of the family, *Tgfb2*, showed higher levels but its expression was much lower than that of *Tgfb1*. TGF-β2 upregulation correlates with fibrotic markers and play a prominent role in biliary liver diseases (Dropmann et al., 2016, 2020), but its expression during liver regeneration is 10 times lower than that of TGF-β1 (Jakowlew et al., 1991). Considering that Smad3 phosphorylation was clearly decreased in Nox4 deleted mice, the lower expression in *Tgfb1* appears to have a higher impact that the increase in *Tgfb2* expression.

On the other hand, Nox4 could be participating in the activation of TGF-β1. TGF-β1 is primarily synthesized by stellate cells in a latent form that is secreted and anchored in the extracellular membrane. That latent precursor must be cleaved by proteases to become activated. In fact, only activated TGF-β1 has the ability to inhibit cell proliferation after PH, but not latent TGF-β (Schrum et al., 2001), and loss of integrin αvβ8, which participate in TGF-β activation, accelerates liver regeneration (Greenhalgh et al., 2019).

Adamtsl2, which interacts with latent LTBP1 and anchors it to the ECM, showed an increase in its expression in NOX4-/- mice at 24 hours after PH. Mutations in ADAMTSL2 have been described in human diseases and lead to dysregulation of TGF-β signaling correlating with increase in active TGF-β1 (Goff et al., 2009). Furthermore, Bmp1 is a metalloproteinase that catalyze the cleavage of LTBP-1 from the ECM, releasing latent TGF-β bound to LTBP-1. Mice with null mutations in BMP-1 and the closely related tolloid1 (Tll1) protease increased LTBP1 accumulation and decreased phospho-Smad2/3 staining, suggesting defective activation of latent TGF-β (Ge & Greenspan, 2006). In agreement, the lower expression of Bmp1 at 24 hours after PH in NOX4-/- mice was concomitant with lower

levels of TGF-β1. Thrombospondin 1, which negatively regulates liver regeneration by participating in the activation of latent TGF-β, presented a higher induction in WT mice after PH. This induction is mediated by reactive oxygen species (ROS) in endothelial cells (Hayashi et al., 2013). Considering the results described above, TGF-β activation from the extracellular matrix could be attenuated in the absence of NOX4-/-.

Moreover, Extracellular matrix protein 1 (ECM1) stabilizes latent-TGF-β by interacting with integrins αV in the ECM, preventing activation of HSCs. Thus, hepatocyte-specific ECM1 Knock-out mice presented accelerated liver fibrosis in response to CCl₄, when compared with control mice (Fan et al., 2019). We observed that ECM1 declines after PH, but this decline occurred earlier in WT livers, allowing earlier TGF-β activation. ECM1 is mainly produced by hepatocytes, which could explain that both models of NOX4 deleted mice presented a downregulation of the pathway.

The transient increase in hepatocyte intracellular concentrations of TGF-β1 after PH, previously reported (Jirtle et al., 1991) and here observed, may also result from an increase in the expression (Rao et al., 2017) and/or an augmented uptake of the latent TGF-β1 into hepatocytes. Once inside the cell, mannose 6-phosphate/insulin-like growth factor II receptor (M6P/IGFII-R) directs latent-TGF-β to the intracellular pre-lysosomal/endosomal compartment where the mature TGF-β1 is activated by dissociation from the latent complex (Jirtle et al., 1991). Jirtle et al reported that M6P/IGFII-R co-localized with TGF-β1 both spatially and temporally in hepatocytes after partial hepatectomy. Even though we did not find significant differences in M6P/IGFII-R between WT and NOX4-/- livers at the mRNA level, we observed differences in the localization of the receptor. Whereas WT livers presented intracellular M6P/IGFII-R at 24 hours after PH, NOX4-/- had M6P/IGFII-R located at the extracellular membranes. Additionally, the increase in M6P/IGFII-R that is expected in cultured hepatocytes prior DNA replication (Villevalois-Cam et al., 2003) was observed in WT primary hepatocytes, but not in NOX4-/- primary hepatocytes.

Some studies have shown that M6P/IGFII-R interacts with urokinase-type plasminogen activator receptor (uPAR) to activate latent-TGF-β1. Plasmin generated from Plasminogen mediates release of TGF-β1 when uPAR is associated with M6PR (Godár et al., 1999). Moreover, activation of TGF-β1 is blocked by anti-uPA antibodies or by preventing uPA-uPAR interaction in co-cultures (Odekon et al., 1994). RNA-seq revealed that uPAR (*Plaur*) induction occurred later in NOX4-/- livers than in WT, and this was coincident with lower levels of uPA (*Plau* gene) and M6PR (*Igf2r* gene), which could also partially explain the lower activation of the TGF-β pathway *in vivo*.

Finally, Caveolin-1 is a protein located in lipid rafts at the cell membrane and involved in intracellular trafficking of receptors. Mayoral *et al.* reported that caveolin-1 -/- mice display an impairment of TGF-β signaling after PH and improve liver regeneration (Mayoral et al., 2010). We observed that NOX4-/- presented lower levels of caveolin-1 in NOX4-/- than WT, concomitant with a downregulation of the TGF-β signaling.

All these results reveal a mutual regulation between Nox4 and the TGF-β pathway: TGF-β1 is the main up-regulator of Nox4 expression and Nox4 could contribute to modulate the process of TGF-β1 activation. The mechanism by which Nox4 could be modulating the activation of TGF-β must be further studied.

Despite these *in vivo* observations, *in vitro* experiments in NOX4-/- hepatocytes indicated that they continue to respond to TGF-β1 in terms of growth inhibition, Smad2 phosphorylation or downregulation of *Myc* levels, maintaining its suppressor function. NOX4 does not appear to be required for TGF-β1-mediated Myc downregulation, which was proposed to be a SMAD dependent mechanism (Calonge & Massague, 1999; Frederick et al., 2004). Nox4 deletion increased the hepatocyte mitogenic response, as we had previously proposed (Crosas-Molist et al., 2014) and could modify the process of TGF-β1 activation *in vivo*, which increases the fastest and more efficient response of hepatocytes to mitogenic signals during liver regeneration. But the mechanism of response to extracellular TGF-β1 was not altered. It has been well described by our group that TGF-β mediates upregulation of NOX4 in hepatocytes and that that upregulation is necessary for its pro-apoptotic activity (Carmona-Cuenca et al., 2008; Sancho et al., 2012). However, Nox4 may not be necessary for TGF-β-induced growth inhibition. This could explain the arrest of proliferation *in vivo* long time (i.e., 4 weeks) after PH, when the expression/activation of TGF-β1, or other members of the family, increase.

It has been described that a marked steatosis develops in the regenerating liver to meet the increased energy demand for rapid cell proliferation and it is essential for the biosynthesis of membrane phospholipids (Zou et al., 2012). In fact, when hepatic adipogenesis and/or fat accumulation are suppressed pharmacological (Shteyer et al., 2004) or genetically (Gazit et al., 2010; Kohjima et al., 2013), liver regeneration is either impaired or inefficient. In this regard, we observed that 36 hours after PH, WT and NOX4-/- presented triglyceride accumulation, but this was resolved earlier, at 48 hours after PH, in NOX4-/- livers. Increased *de novo* hepatic fatty acid production and catabolism of systemic adipose tissue might be the main sources of the lipid that accumulates in the regenerating liver (Rudnick & Davidson, 2012). Fatty acid uptake during liver regeneration is mediated,

within others, by Cluster of differentiation 36 (CD36, *Cd36* gene). Although the difference was not significant, CD36 peaked earlier in NOX4-/- than in WT livers.

Mitochondrial oxidation of free fatty acids (FFA), coming from lipid droplets and hepatocytes uptake, is a rapid and efficient way of energy supply for proliferating cells during liver regeneration. Concomitant with the earlier recovery of lipid steatosis, a more efficient β-oxidation could be occurring in NOX4-/- mice. Several evidences support this hypothesis. Peroxisome proliferation-activated receptor- δ (*Ppard* gene) stimulates β-oxidation in the liver by an autophagy-lysosomal pathway involving AMPK/mTOR signaling (Tong et al., 2019). Peroxisome proliferation-activated receptor-α (PPAR-α, *Ppara* gene) enhance cell cycle progression and β-oxidation during liver regeneration (Xie et al., 2019). *Ppard* as well as PPAR-α target genes *Cyp4a10* and *Cyp4a14* in NOX4-/- livers presented an earlier induction in NOX4-/- livers. By contrast, PPAR-γ (*Pparg*) negatively regulates liver regeneration after PH (Cheng et al., 2018), but no differences were observed. Peroxisome proliferation-activated receptor γ coactivator 1-β (PGC-1β, *Ppargc1b* gene), which induce mitochondrial oxidative phosphorylation and fatty acid β-oxidation and protect against steatohepatitis (Bellafante et al., 2013), presented higher levels in NOX4-/- livers. c-Myc contributes to maintain normal lipid homeostasis in hepatocytes (Edmunds et al., 2016). Considering that Myc enhances fatty acid metabolism in several types of cancer (Casciano et al., 2020; Oliynyk et al., 2019), and Myc inhibition provokes accumulation of lipid droplets in cancer cells (Zirath et al., 2013), we speculate that overactivation of c-Myc in our model could explain, at least in part, the faster recovery of regenerative liver steatosis observed in NOX4-/- mice. In any case, further studies are needed to determine if a higher fatty acid oxidation is occurring in NOX4-/- livers and if this is caused by Myc upregulation.

Oxidative stress is crucial for many physiological and pathological processes, as reactive oxygen species (ROS) are known to regulate many different pathways. Considering that Nox4 is an NADPH oxidase that participate in the redox balance of the cell, we considered that there could be differences between WT and NOX4-/- livers after PH. The Keap1-Nrf2-ARE pathway is primordial in the regulation of various cellular processes, such as antioxidant defense or redox equilibrium, within others. Some studies have been conducted to investigate the role of Nrf2 during LR. Zou et al. described that Nrf-2 is indispensable for timely progression of hepatocytes trough the cell cycle during liver regeneration (Zou et al., 2015). Zou et al. also demonstrated that Nrf2 is implicated in maintaining hepatocytes in a fully differentiated state after PH (Zou et al., 2014). Moreover, Beyer et al described that Nrf2 deficient mice presented an impaired liver regeneration after partial hepatectomy (Beyer et al., 2008). Chan et al. recently described that

pharmacological activation of Nrf2 by administration of bardoxolone methyl (CDDO-Me) enhances LR in terms of recovery of liver volume and better liver function (Chan et al., 2021). By contrast, there are other studies, such as the one published by Köhler et al., which describe that activated Nrf2 impairs liver regeneration, resulting in a delay in hepatocyte proliferation and enhanced apoptosis (Köhler et al., 2014). In our model, we did not find significant differences in *Nrf2* between WT and NOX4-/-. Some of the target genes of Nrf2 were differentially expressed along the time between both models, but a differential redox response timely coordinated seems not to be the responsible for the acceleration of liver regeneration in NOX4-/-.

It is commonly known that age is an important determinant of both magnitude and timing of regenerative response after partial hepatectomy: the process is longer and the percentage of proliferating cells is lower in older animals (Fry et al., 1984). In fact, it has been described that patients over 60 years of age have higher mortality and morbidity after major liver resection (IJtsma et al., 2008). Therefore, we considered important to analyze the consequences of inhibiting Nox4 during liver regeneration in old mice. Rezende et al. reported that Nox4 has no impact on lifespan of mice and that *Nox4* mRNA levels dropped with age in lung mice (Rezende et al., 2017). We observed that Nox4 levels in the liver from 1-year-old mice were not so different from those observed in 8 to 16-weeks-old mice. We corroborated that *Nox4* levels decrease when hepatic cells proliferate, and then increase when liver regeneration must finish. Furthermore, we observed an earlier increment in the liver/body weight ratio, concomitant with higher survival and higher c-Myc levels in NOX4-/- mice. Altogether, inhibiting Nox4 in elder mice also benefits liver regeneration after 2/3 partial hepatectomy.

NOX4 has been proposed as a potential therapeutic target in human liver chronic diseases (Crosas-Molist & Fabregat, 2015), due to its role mediating TGF-β actions in liver fibrosis (Crosas-Molist et al., 2015). Results presented here would support the potential benefit of its inhibition also to favor liver regeneration from the remaining healthy hepatocytes. Nox4 does not appear to be essential for the termination of liver regeneration, which reinforces its potential as therapeutic target, without adverse effects. Nevertheless, considering that inhibiting NOX4 could be detrimental under preneoplastic conditions, Nox4 inhibition must be considered at early stages of chronic inflammation and fibrosis in the liver.
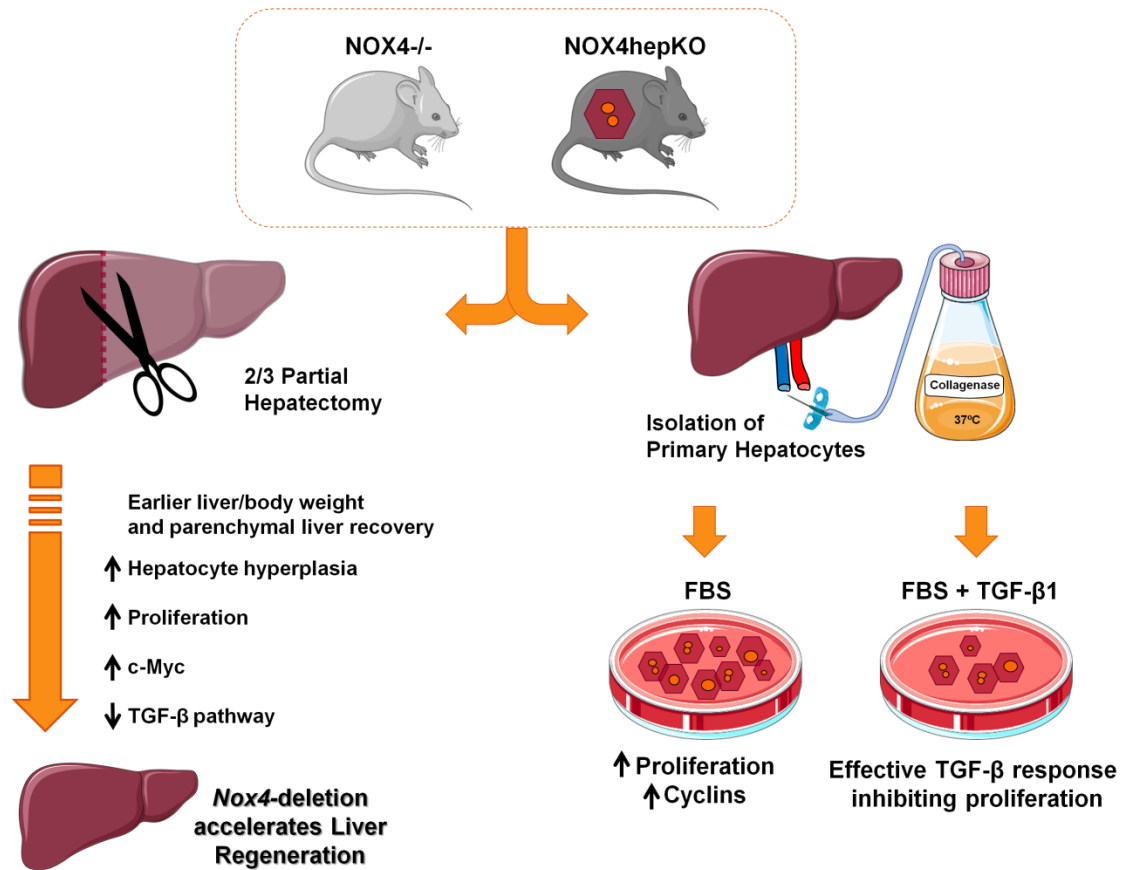
Figure 1. Summary diagram. Left: After partial hepatectomy, Nox4 deleted mice show earlier liver/body weight recovery, concomitant with higher hepatocyte hyperplasia and proliferation, upregulation of Myc and downregulation of the TGF-β pathway. **Right:** Primary hepatocytes from Nox4 deleted mice show higher proliferation in response to FBS, while maintaining TGF-β-induced growth inhibitory response (Graphical abstract performed with Servier Medical Art).

VII. Conclusions

1. *Nox4* deletion in mice induces an earlier liver-to-body weight and parenchymal structure recovery after two-thirds partial hepatectomy (PH).

2. *Nox4* deletion in hepatocytes induces an anticipation of proliferation after two-thirds PH.

3. *Nox4* deleted primary hepatocytes present higher proliferation upon FBS treatment, which correlates with higher levels of cyclins D1, A2 and B2.

4. Higher c-Myc expression is found in *Nox4* deleted mice after two-thirds PH. RNA-seq analysis located *Myc* in a node of regulation of proliferation gene expression.

5. RNA-seq analysis also reveals changes in genes involved in the activation of latent-TGF-β1, which correlates with transcriptional and functional attenuation of the TGF-β pathway.

6. *In vitro*, *Nox4* deleted hepatocytes maintain the capacity to respond to active TGF-β1 in terms of Smad2 phosphorylation and growth inhibition.

7. Earlier recovery from the regenerative steatosis is observed in *Nox4* deleted mice, which could be associated with a more efficient β-oxidation of free fatty acids.

8. One-year-old NOX4-/- mice display an earlier recovery from two-thirds PH, presenting similar features as those observed in younger mice.

References

Abdel-Misih, S. R. Z., & Bloomston, M. (2010). Liver Anatomy. *Surgical Clinics of North America*, *90*(4), 643–653.

Abhilash, P. A., Harikrishnan, R., & Indira, M. (2012). Ascorbic acid supplementation down-regulates the alcohol induced oxidative stress, hepatic stellate cell activation, cytotoxicity and mRNA levels of selected fibrotic genes in guinea pigs. *Free Radic Res*, *46*(2), 204–213.

Abu Rmilah, A., Zhou, W., Nelson, E., Lin, L., Amiot, B., & Nyberg, S. L. (2019). Understanding the marvels behind liver regeneration. *Wiley Interdisciplinary Reviews: Developmental Biology*, *8*(3), e340.

Ago, T., Kuroda, J., Pain, J., Fu, C., & Li, H. (2011). Upregulation of Nox4 by hypertrophic stimuli promotes apoptosis and mitochondrial dysfunction in cardiac myocytes. *Circ Res .*, *106*(7), 1253–1264.

Al Dohayan, A. (1999). The beneficial effect of alpha-tocopherol on liver regeneration after partial hepatectomy on rats. *Saudi J Gastroenterol*, *5*(3), 113–116.

Altenhofer, S., Kleikers, P. W. M., Radermacher, K. A., Scheurer, P., Hermans, J. J. R., Schiffers, P., Ho, H., & Wingler, K. (2012). The NOX toolbox: Validating the role of NADPH oxidases in physiology and disease. *Cell. Mol. Life Sci.*, *69*, 2327–2343.

Altenhöfer, S., Radermacher, K. A., Kleikers, P. W. M., Wingler, K., & Schmidt, H. H. H. W. (2015). Evolution of NADPH Oxidase Inhibitors: Selectivity and Mechanisms for Target Engagement. *Antioxidants & Redox Signaling*, *23*(5), 406–427.

Amara, N., Goven, D., Prost, F., Muloway, R., Crestani, B., & Boczkowski, J. (2010). NOX4/NADPH oxidase expression is increased in pulmonary fibroblasts from patients with idiopathic pulmonary fibrosis and mediates TGFb1-induced fibroblast differentiation into myofibroblasts. *Interstitial Lung Disease*, *65*, 733e738.

Andueza, A., Garde, N., García-Garzón, A., Ansorena, E., López-Zabalza, M. J., Iraburu, M. J., Zalba, G., & Martínez-Irujo, J. J. (2018). NADPH oxidase 5 promotes

proliferation and fibrosis in human hepatic stellate cells. *Free Radical Biology and Medicine*, *126*, 15–26.

Anilkumar, N., Jose, G. S., Sawyer, I., Santos, C. X. C., Sand, C., Brewer, A. C., Warren, D., & Shah, A. M. (2013). A 28-kDa Splice Variant of NADPH Oxidase-4 Is Nuclear-Localized and Involved in Redox Signaling in Vascular Cells. *Arteriosclerosis, Thrombosis, and Vascular Biology*, *33*(4).

Aoyama, T., Paik, Y.-H., Watanabe, S., Laleu, B., Gaggini, F., Fioraso-Cartier, L., Molango, S., Heitz, F., Merlot, C., Szyndralewiez, C., Page, P., & Brenner, D. A. (2012). Nicotinamide adenine dinucleotide phosphate oxidase in experimental liver fibrosis: GKT137831 as a novel potential therapeutic agent. *Hepatology*, *56*(6), 2316–2327.

Apte, U., Gkretsi, V., Bowen, W. C., Mars, W. M., Luo, J.-H., Donthamsetty, S., Orr, A., Monga, S. P. S., Wu, C., & Michalopoulos, G. K. (2009). Enhanced liver regeneration following changes induced by hepatocyte-specific genetic ablation of integrin-linked kinase. *Hepatology*, *50*(3), 844–851.

Baena, E., Gandarillas, A., Vallespinos, M., Zanet, J., Bachs, O., Redondo, C., Fabregat, I., Martinez-A., C., & de Alboran, I. M. (2005). C-Myc regulates cell size and ploidy but is not essential for postnatal proliferation in liver. *Proceedings of the National Academy of Sciences*, *102*(20), 7286–7291.

Bai, H., Zhang, W., Qin, X.-J., Zhang, T., Wu, H., Liu, J.-Z., & Hai, C.-X. (2015). Hydrogen Peroxide Modulates the Proliferation/Quiescence Switch in the Liver During Embryonic Development and Posthepatectomy Regeneration. *Antioxidants & Redox Signaling*, *22*(11), 921–937.

Baltanás, A., Solesio, M. E., Zalba, G., Galindo, M. F., Fortuño, A., & Jordán, J. (2013). The senescence-accelerated mouse prone-8 (SAM-P8) oxidative stress is

associated with upregulation of renal NADPH oxidase system. *Journal of Physiology and Biochemistry*, *69*(4), 927–935.

Batlle, E., & Massagué, J. (2019). Transforming Growth Factor-β Signaling in Immunity and Cancer. *Immunity*, *50*(4), 924–940.

Bedard, K., & Krause, K.-H. (2007). The NOX Family of ROS-Generating NADPH Oxidases: Physiology and Pathophysiology. *Physiological Reviews*, *87*(1), 245–313.

Behrens, A., Sibilia, M., & David, J.-P. (2002). Impaired postnatal hepatocyte proliferation and liver regeneration in mice lacking c-jun in the liver. *EMBO J.*, *2*(7), 1782–1790.

Bellafante, E., Murzilli, S., Salvatore, L., Latorre, D., Villani, G., & Moschetta, A. (2013). Hepatic-specific activation of peroxisome proliferator-activated receptor γ coactivator-1β protects against steatohepatitis. *Hepatology*, *57*(4), 1343–1356.

Beretta, M., Santos, C. X., Molenaar, C., Hafstad, A. D., Miller, C. C., Revazian, A., Betteridge, K., Schröder, K., Streckfuß-Bömeke, K., Doroshow, J. H., Fleck, R. A., Su, T., Belousov, V. V., Parsons, M., & Shah, A. M. (2020). Nox4 regulates InsP$_3$ receptor-dependent Ca^{2+} release into mitochondria to promote cell survival. *The EMBO Journal*, *39*(19).

Bettaieb, A., Jiang, J. X., Sasaki, Y., Chao, T.-I., Kiss, Z., Chen, X., Tian, J., Katsuyama, M., Yabe-Nishimura, C., Xi, Y., Szyndralewiez, C., Schröder, K., Shah, A., Brandes, R. P., Haj, F. G., & Török, N. J. (2015). Hepatocyte Nicotinamide Adenine Dinucleotide Phosphate Reduced Oxidase 4 Regulates Stress Signaling, Fibrosis, and Insulin Sensitivity During Development of Steatohepatitis in Mice. *Gastroenterology*, *149*(2), 468-480.e10.

Beyer, T. A., Xu, W., Teupser, D., auf dem Keller, U., Bugnon, P., Hildt, E., Thiery, J., Kan, Y. W., & Werner, S. (2008). Impaired liver regeneration in Nrf2 knockout mice:

Role of ROS-mediated insulin/IGF-1 resistance. *The EMBO Journal*, *27*(1), 212–223.

Bienert, G. P., & Chaumont, F. (2014). Aquaporin-facilitated transmembrane diffusion of hydrogen peroxide. *Biochimica et Biophysica Acta (BBA) - General Subjects*, *1840*(5), 1596–1604.

Blagosklonny, M. V., & Pardee, A. B. (2002). The Restriction Point of the Cell Cycle. *Cell Cycle*, *1*(2), 102–109.

Block, K., Gorin, Y., & Abboud, H. E. (2009). Subcellular localization of Nox4 and regulation in diabetes. *Proceedings of the National Academy of Sciences*, *106*(34), 14385–14390.

Böhm, F., Köhler, U. A., Speicher, T., & Werner, S. (2010). Regulation of liver regeneration by growth factors and cytokines. *EMBO Molecular Medicine*, *2*(8), 294–305.

Bondi, C. D., Manickam, N., Lee, D. Y., Block, K., Gorin, Y., Abboud, H. E., & Barnes, J. L. (2010). NAD(P)H Oxidase Mediates TGF-beta1–Induced Activation of Kidney Myofibroblasts. *J Am Soc Nephrol*, 10.

Boudreau, H. E., Casterline, B. W., Rada, B., Korzeniowska, A., & Leto, T. L. (2012). Nox4 involvement in TGF-beta and SMAD3-driven induction of the epithelial-to-mesenchymal transition and migration of breast epithelial cells. *Free Radical Biology and Medicine*, *53*(7), 1489–1499.

Brandes, R. P., Weissmann, N., & Schröder, K. (2014). Nox family NADPH oxidases: Molecular mechanisms of activation. *Free Radical Biology and Medicine*, *76*, 208–226.

Braun, L., Mead, J. E., Panzica, M., Mikumo, R., BELLt, G. I., & Fausto, N. (1988). Transforming growth factor f8 mRNA increases during liver regeneration: A possible paracrine mechanism of growth regulation. *Proc. Natl. Acad. Sci. USA*, *85*, 1539–1543.

Breitenbach, M., Rinnerthaler, M., Weber, M., Breitenbach-Koller, H., Karl, T., Cullen, P.,

Basu, S., Haskova, D., & Hasek, J. (2018). The defense and signaling role of

NADPH oxidases in eukaryotic cells: Review. *Wiener Medizinische Wochenschrift*,

168(11–12), 286–299.

Bretones, G., Delgado, M. D., & León, J. (2015). Myc and cell cycle control. *Biochimica et*

Biophysica Acta (BBA) - Gene Regulatory Mechanisms, *1849*(5), 506–516.

Brown, D. I., & Griendling, K. K. (2009). Nox proteins in signal transduction. *Free Radical*

Biology and Medicine, *47*(9), 1239–1253.

Brown, J. R., Nigh, E., Lee, R. J., Ye, H., Thompson, M. A., Saudou, F., Pestell, R. G., &

Greenberg, M. E. (1998). Fos Family Members Induce Cell Cycle Entry by

Activating Cyclin D. *Molecular and Cellular Biology*, *18*, 11.

Buul, J. D. V., Fernandez-Borja, M., Anthony, E. C., & Hordijk, P. L. (2005). Expression

and Localization of NOX2 and NOX4 in Primary Human Endothelial Cells.

Antioxidants & Redox Signaling, *7*(3–4), 308–317.

Buvelot, H., Jaquet, V., & Krause, K.-H. (Eds.). (2019). *Mammalian NADPH Oxidases*

(1982nd ed., Vol. 2019). Springer New York.

http://link.springer.com/10.1007/978-1-4939-9424-3

Caballero-Díaz, D., Bertran, E., Peñuelas-Haro, I., Moreno-Càceres, J., Malfettone, A.,

López-Luque, J., Addante, A., Herrera, B., Sánchez, A., Alay, A., Solé, X.,

Serrano, T., Ramos, E., & Fabregat, I. (2020). Clathrin switches transforming

growth factor-β role to pro-tumorigenic in liver cancer. *Journal of Hepatology*,

72(1), 125–134.

Caja, L., Ortiz, C., Bertran, E., Murillo, M. M., Miró-Obradors, M. J., Palacios, E., &

Fabregat, I. (2007). Differential intracellular signalling induced by TGF-β in rat adult

hepatocytes and hepatoma cells: Implications in liver carcinogenesis. *Cellular*

Signalling, *19*(4), 683–694.

Caja, L., Sancho, P., Bertran, E., Iglesias-Serret, D., Gil, J., & Fabregat, I. (2009). Overactivation of the MEK/ERK Pathway in Liver Tumor Cells Confers Resistance to TGF-β–Induced Cell Death through Impairing Up-regulation of the NADPH Oxidase NOX4. *Cancer Research*, *69*(19), 7595–7602.

Calonge, M. J., & Massague, J. (1999). Smad4/DPC4 Silencing and Hyperactive Ras Jointly Disrupt Transforming Growth Factor-beta Antiproliferative Responses in Colon Cancer Cells. *J Biol Chem*, *274*(47), 33637–33643.

Campbell, M. G., Cormier, A., Ito, S., Seed, R. I., Bondesson, A. J., Lou, J., Marks, J. D., Baron, J. L., Cheng, Y., & Nishimura, S. L. (2020). Cryo-EM Reveals Integrin-Mediated TGF-β Activation without Release from Latent TGF-β. *Cell*, *180*(3), 490-501.e16.

Cao, Z., Ye, T., Sun, Y., Ji, G., Shido, K., Chen, Y., Luo, L., Na, F., Li, X., Huang, Z., Ko, J. L., Mittal, V., Qiao, L., Chen, C., Martinez, F. J., Rafii, S., & Ding, B.-S. (2017). Targeting the vascular and perivascular niches as a regenerative therapy for lung and liver fibrosis. *Science Translational Medicine*, *9*(405), eaai8710.

Carmona-Cuenca, I., Herrera, B., Ventura, J.-J., Roncero, C., Fernández, M., & Fabregat, I. (2006). EGF blocks NADPH oxidase activation by TGF-β in fetal rat hepatocytes, impairing oxidative stress, and cell death. *Journal of Cellular Physiology*, *207*(2), 322–330.

Carmona-Cuenca, I., Roncero, C., Sancho, P., Caja, L., Fausto, N., Fernández, M., & Fabregat, I. (2008). Upregulation of the NADPH oxidase NOX4 by TGF-beta in hepatocytes is required for its pro-apoptotic activity. *Journal of Hepatology*, *49*(6), 965–976.

Carnesecchi, S., Deffert, C., Donati, Y., Basset, O., Hinz, B., Preynat-Seauve, O., Guichard, C., Arbiser, J. L., Banfi, B., Pache, J.-C., Barazzone-Argiroffo, C., &

Krause, K.-H. (2011). A Key Role for NOX4 in Epithelial Cell Death During Development of Lung Fibrosis. *Antioxidants & Redox Signaling*, *15*(3), 607–619.

Carr, B. I., Hayashi, I., Branum, E. L., & Moses, H. L. (1986). Inhibition of DNA Synthesis in rat hepatocytes by Platelet-derived Type beta Transforming Growth Factor. *Cancer Research*, *46*, 2330–2334.

Casciano, J. C., Perry, C., Cohen-Nowak, A. J., Miller, K. D., Vande Voorde, J., Zhang, Q., Chalmers, S., Sandison, M. E., Liu, Q., Hedley, A., McBryan, T., Tang, H.-Y., Gorman, N., Beer, T., Speicher, D. W., Adams, P. D., Liu, X., Schlegel, R., McCarron, J. G., … Schug, Z. T. (2020). MYC regulates fatty acid metabolism through a multigenic program in claudin-low triple negative breast cancer. *British Journal of Cancer*, *122*(6), 868–884.

Chan, B. K. Y., Elmasry, M., Forootan, S. S., Russomanno, G., Bunday, T. M., Zhang, F., Brillant, N., Starkey Lewis, P. J., Aird, R., Ricci, E., Andrews, T. D., Sison-Young, R. L., Schofield, A. L., Fang, Y., Lister, A., Sharkey, J. W., Poptani, H., Kitteringham, N. R., Forbes, S. J., … Copple, I. M. (2021). Pharmacological Activation of Nrf2 Enhances Functional Liver Regeneration. *Hepatology*, hep.31859.

Chanda, M., & Mehendale, H. (1995). Nutritional impact on the final outcome of liver injury inflicted by model hepatotoxicants: Effect of glucose loading. *FASEB J.*, *9*(12), 240–245.

Chart, R. S., Price, D. T., Sue, S. R., Meyers, W. C., & Jirtle, R. L. (1995). Down-regulation of transforming growth factor beta receptor type I, II, and III during liver regeneration. *The American Journal of Surgery*, *169*(1), 126–132.

Cheng, Z., Liu, L., Zhang, X.-J., Lu, M., Wang, Y., Assfalg, V., Laschinger, M., von Figura, G., Sunami, Y., Michalski, C. W., Kleeff, J., Friess, H., Hartmann, D., & Hüser, N. (2018). Peroxisome Proliferator-Activated Receptor gamma negatively regulates

liver regeneration after partial hepatectomy via the HGF/c-Met/ERK1/2 pathways. *Scientific Reports*, *8*(1), 11894.

Choi, J., Corder, N. L. B., Koduru, B., & Wang, Y. (2014). Oxidative stress and hepatic Nox proteins in chronic hepatitis C and hepatocellular carcinoma. *Free Radical Biology and Medicine*, *72*, 267–284.

Cienfuegos, J., Rotellar, F., Baixauli, J., Martínez-Regueira, F., Pardo, F., & Hernández-Lizoáin, J. (2014). Liver regeneration—The best kept secret. A model of tissue injury response. *Rev Esp Enferm Dig .*, *196*(3), 171–194.

Clempus, R. E., Sorescu, D., Dikalova, A. E., Pounkova, L., Jo, P., Sorescu, G. P., Lassègue, B., & Griendling, K. K. (2007). Nox4 Is Required for Maintenance of the Differentiated Vascular Smooth Muscle Cell Phenotype. *Arteriosclerosis, Thrombosis, and Vascular Biology*, *27*(1), 42–48.

Córdoba-Jover, B. (2019). Cerium oxide nanoparticles improve liver regeneration after acetaminophen-induced liver injury and partial hepatectomy in rats. *J Nanobiotechnol*, *17*, 12.

Crawford, S. E., Stellmach, V., Murphy-Ullrich, J. E., Ribeiro, S. M. F., Lawler, J., Hynes, R. O., & Boivin, G. P. (1998). Thrombospondin-1 Is a Major Activator of TGFbeta1 In Vivo. *Cell*, *93*, 159–1170.

Crosas-Molist, E., Bertran, E., Rodriguez-Hernandez, I., Herraiz, C., Cantelli, G., Fabra, À., Sanz-Moreno, V., & Fabregat, I. (2017). The NADPH oxidase NOX4 represses epithelial to amoeboid transition and efficient tumour dissemination. *Oncogene*, *36*(21), 3002–3014.

Crosas-Molist, E., Bertran, E., Sancho, P., López-Luque, J., Fernando, J., Sánchez, A., Fernández, M., Navarro, E., & Fabregat, I. (2014). The NADPH oxidase NOX4 inhibits hepatocyte proliferation and liver cancer progression. *Free Radical Biology and Medicine*, *69*, 338–347.

Crosas-Molist, E., & Fabregat, I. (2015). Role of NADPH oxidases in the redox biology of liver fibrosis. *Redox Biology*, *6*, 106–111.

Csanaky, I. L., Aleksunes, L. M., Tanaka, Y., & Klaassen, C. D. (2009). Role of hepatic transporters in prevention of bile acid toxicity after partial hepatectomy in mice. *American Journal of Physiology-Gastrointestinal and Liver Physiology*, *297*(3), G419–G433.

Cucoranu, I., Clempus, R., Dikalova, A., Phelan, P. J., Ariyan, S., Dikalov, S., & Sorescu, D. (2005). NAD(P)H Oxidase 4 Mediates Transforming Growth Factor-β1–Induced Differentiation of Cardiac Fibroblasts Into Myofibroblasts. *Circulation Research*, *97*(9), 900–907.

Cuenca, A. G., Cress, W. D., Good, R. A., Marikar, Y., & Engelman, R. W. (2001). Calorie Restriction Influences Cell Cycle Protein Expression and DNA Synthesis during Liver Regeneration. *Experimental Biology and Medicine*, *226*(11), 1061–1067.

Cui, W., Matsuno, K., Iwata, K., Ibi, M., Matsumoto, M., Zhang, J., Zhu, K., Katsuyama, M., Torok, N. J., & Yabe-Nishimura, C. (2011). NOX1/nicotinamide adenine dinucleotide phosphate, reduced form (NADPH) oxidase promotes proliferation of stellate cells and aggravates liver fibrosis induced by bile duct ligation. *Hepatology*, *54*(3), 10.

Das, R., Xu, S., Quan, X., Nguyen, T. T., Kong, I. D., Chung, C. H., Lee, E. Y., Cha, S.-K., & Park, K.-S. (2014). Upregulation of mitochondrial Nox4 mediates TGF-β-induced apoptosis in cultured mouse podocytes. *American Journal of Physiology-Renal Physiology*, *306*(2), F155–F167.

Datla, S. R., McGrail, D. J., Vukelic, S., Huff, L. P., Lyle, A. N., Pounkova, L., Lee, M., Seidel-Rogol, B., Khalil, M. K., Hilenski, L. L., Terada, L. S., Dawson, M. R., Lassègue, B., & Griendling, K. K. (2014). Poldip2 controls vascular smooth muscle cell migration by regulating focal adhesion turnover and force polarization.

American Journal of Physiology-Heart and Circulatory Physiology, *307*(7), H945–H957.

Datla, S. R., Peshavariya, H., Dusting, G. J., Mahadev, K., Goldstein, B. J., & Jiang, F. (2007). Important Role of Nox4 Type NADPH Oxidase in Angiogenic Responses in Human Microvascular Endothelial Cells In Vitro. *Arteriosclerosis, Thrombosis, and Vascular Biology*, *27*(11), 2319–2324.

De Bleser, P., Niki, T., Rogiers, V., & Geerts, A. (1997). Transforming growth factor-beta gene expression in normal and fibrotic rat liver. *J Hepatol*, *26*(4), 886–893.

De Virgiliis, F., Hutson, T. H., Palmisano, I., Amachree, S., Miao, J., Zhou, L., Todorova, R., Thompson, R., Danzi, M. C., Lemmon, V. P., Bixby, J. L., Wittig, I., Shah, A. M., & Di Giovanni, S. (2020). Enriched conditioning expands the regenerative ability of sensory neurons after spinal cord injury via neuronal intrinsic redox signaling. *Nature Communications*, *11*(1), 6425.

Desai, L. P., Zhou, Y., Estrada, A. V., Ding, Q., Cheng, G., Collawn, J. F., & Thannickal, V. J. (2014). Negative Regulation of NADPH Oxidase 4 by Hydrogen Peroxide-inducible Clone 5 (Hic-5) Protein. *Journal of Biological Chemistry*, *289*(26), 18270–18278.

Dobin, A., Davis, C. A., Schlesinger, F., Drenkow, J., Zaleski, C., Jha, S., Batut, P., Chaisson, M., & Gingeras, T. R. (2013). STAR: Ultrafast universal RNA-seq aligner. *Bioinformatics*, *29*(1), 15–21.

Dong, X., Zhao, B., Iacob, R. E., Zhu, J., Koksal, A. C., Lu, C., Engen, J. R., & Springer, T. A. (2017). Force interacts with macromolecular structure in activation of TGF-β. *Nature*, *542*(7639), 55–59.

Donne, R., Saroul-Aïnama, M., Cordier, P., Celton-Morizur, S., & Desdouets, C. (2020). Polyploidy in liver development, homeostasis and disease. *Nature Reviews Gastroenterology & Hepatology*, *17*(7), 391–405.

Drabsch, Y., & ten Dijke, P. (2012). TGF-β signalling and its role in cancer progression and metastasis. *Cancer and Metastasis Reviews*, *31*(3–4), 553–568.

Dropmann, A., Dediulia, T., Breitkopf-Heinlein, K., Korhonen, H., Janicot, M., Weber, S. N., Thomas, M., Piiper, A., Bertran, E., Fabregat, I., Abshagen, K., Hess, J., Angel, P., Coulouarn, C., Dooley, S., & Meindl-Beinker, N. M. (2016). TGF-β1 and TGF-β2 abundance in liver diseases of mice and men. *Oncotarget*, *7*(15), 19499–19518.

Dropmann, A., Dooley, S., Dewidar, B., Hammad, S., Dediulia, T., Werle, J., Hartwig, V., Ghafoory, S., Woelfl, S., Korhonen, H., Janicot, M., Wosikowski, K., Itzel, T., Teufel, A., Schuppan, D., Stojanovic, A., Cerwenka, A., Nittka, S., Piiper, A., … Meindl-Beinker, N. M. (2020). TGF-β2 silencing to target biliary-derived liver diseases. *Gut*, *69*(9), 1677–1690.

Dunning, S., ur Rehman, A., Tiebosch, M. H., Hannivoort, R. A., Haijer, F. W., Woudenberg, J., van den Heuvel, F. A. J., Buist-Homan, M., Faber, K. N., & Moshage, H. (2013). Glutathione and antioxidant enzymes serve complementary roles in protecting activated hepatic stellate cells against hydrogen peroxide-induced cell death. *Biochimica et Biophysica Acta (BBA) - Molecular Basis of Disease*, *1832*(12), 2027–2034.

Edmunds, L. R., Otero, P. A., Sharma, L., D'Souza, S., Dolezal, J. M., David, S., Lu, J., Lamm, L., Basantani, M., Zhang, P., Sipula, I. J., Li, L., Zeng, X., Ding, Y., Ding, F., Beck, M. E., Vockley, J., Monga, S. P. S., Kershaw, E. E., … Prochownik, E. V. (2016). Abnormal lipid processing but normal long-term repopulation potential of *myc-/-* hepatocytes. *Oncotarget*, *7*(21).

Ehrenfried, J. A., Ko, T. C., Thompson, E. A., & Evers, B. M. (1997). Cell cycle-mediated regulation of hepatic regeneration. *Surgery*, *122*(5), 927–935.

Elliott, B., Millena, A. C., Matyunina, L., Zhang, M., Zou, J., Wang, G., Zhang, Q., Bowen, N., Eaton, V., Webb, G., Thompson, S., McDonald, J., & Khan, S. (2019). Essential role of JunD in cell proliferation is mediated via MYC signaling in prostate cancer cells. *Cancer Letters*, *448*, 155–167.

Eun, H. S., Cho, S. Y., Joo, J. S., Kang, S. H., Moon, H. S., Lee, E. S., Kim, S. H., & Lee, B. S. (2017). Gene expression of NOX family members and their clinical significance in hepatocellular carcinoma. *Scientific Reports*, *7*(1), 11060.

Eun, H. S., Chun, K., Song, I.-S., Oh, C.-H., Seong, I.-O., Yeo, M.-K., & Kim, K.-H. (2019). High nuclear NADPH oxidase 4 expression levels are correlated with cancer development and poor prognosis in hepatocellular carcinoma. *Pathology*, *51*(6), 579–585.

Fabregat, I., & Caballero-Díaz, D. (2018). Transforming Growth Factor-β-Induced Cell Plasticity in Liver Fibrosis and Hepatocarcinogenesis. *Frontiers in Oncology*, *8*, 357.

Fabregat, I., Fernando, J., Mainez, J., & Sancho, P. (2014). TGF-beta Signaling in Cancer Treatment. *Current Pharmaceutical Design*, *20*(17), 2934–2947.

Fabregat, I., Herrera, B., Fernández, M., Álvarez, A. M., Sánchez, A., Roncero, C., Ventura, J.-J., Valverde, Á. M., & Benito, M. (2000). Epidermal Growth Factor Impairs the Cytochrome C/Caspase-3 Apoptotic Pathway Induced by Transforming Growth Factorβ in Rat Fetal Hepatocytes Via a Phosphoinositide 3-Kinase–Dependent Pathway. *Hepatology*, *32*(3), 528–535.

Fabregat, I., Moreno-Càceres, J., Sánchez, A., Dooley, S., Dewidar, B., Giannelli, G., ten Dijke, P., & the IT-LIVER Consortium. (2016). TGF-β signalling and liver disease. *The FEBS Journal*, *283*(12), 2219–2232.

Fabregat, I., Sanchez, A., Alvarez, A. M., Toshikazu Nakamura, & Benito, M. (1996). Epidermal growth factor, but not hepatocyte growth factor, suppresses the

apoptosis induced by transforming growth factor-beta in fetal hepatocytes in primary culture. *FEBS Letters*, *384*(1), 14–18.

Fan, W., Liu, T., Chen, W., Hammad, S., Longerich, T., Hausser, I., Fu, Y., Li, N., He, Y., Liu, C., Zhang, Y., Lian, Q., Zhao, X., Yan, C., Li, L., Yi, C., Ling, Z., Ma, L., Zhao, X., … Sun, B. (2019). ECM1 Prevents Activation of Transforming Growth Factor b, Hepatic Stellate Cells, and Fibrogenesis in Mice. *Gastroenterology*, *157*(5), 1352–1367.

Fausto, N. (2004). Liver regeneration and repair: Hepatocytes, progenitor cells, and stem cells. *Hepatology*, *39*(6), 1477–1487.

Fausto, N., & Campbell, J. S. (2003). The role of hepatocytes and oval cells in liver regeneration and repopulation. *Mechanisms of Development*, *120*(1), 117–130.

Fausto, N., Campbell, J. S., & Riehle, K. J. (2012). Liver regeneration. *Journal of Hepatology*, *57*(3), 692–694.

Feng, C., Zhang, Y., Yang, M., Lan, M., Liu, H., Huang, B., & Zhou, Y. (2017). Oxygen-Sensing Nox4 Generates Genotoxic ROS to Induce Premature Senescence of Nucleus Pulposus Cells through MAPK and NF-κ B Pathways. *Oxidative Medicine and Cellular Longevity*, *2017*, 1–15.

Font-Burgada, J., Shalapour, S., Ramaswamy, S., Hsueh, B., Rossell, D., Umemura, A., Taniguchi, K., Nakagawa, H., Valasek, M. A., Ye, L., Kopp, J. L., Sander, M., Carter, H., Deisseroth, K., Verma, I. M., & Karin, M. (2015). Hybrid Periportal Hepatocytes Regenerate the Injured Liver without Giving Rise to Cancer. *Cell*, *162*(4), 766–779.

Foo, N.-P., Lin, S.-H., Lee, Y.-H., Wu, M.-J., & Wang, Y.-J. (2011). A-Lipoic acid inhibits liver fibrosis through the attenuation of ROS-triggered signaling in hepatic stellate cells activated by PDGF and TGF-beta. *Toxicology*, 8.

Franklin, C. C., Rosenfeld-Franklin, M. E., White, C., Kavanagh, T. J., & Fausto, N. (2003). TGFβ1-induced suppression of glutathione antioxidant defenses in hepatocytes: Caspase-dependent posttranslational and caspase-independent transcriptional regulatory mechanisms. *The FASEB Journal*, *17*(11), 1–23.

Frederick, J. P., Liberati, N. T., Waddell, D. S., Shi, Y., & Wang, X.-F. (2004). Transforming Growth Factor-beta-Mediated Transcriptional Repression of c-myc Is Dependent on Direct Binding of Smad3 to a Novel Repressive Smad Binding Element. *Molecular and Cellular Biology*, *24*, 14.

Fry, M., Silber, J., Loeb, L., & Martin, M. (1984). Delayed and reduced cell replication and diminishing levels of DNA polymerase-α in regenerating liver of aging mice. *Journal of Cellular Physiology*, *118*(3), 225–232.

Gazit, V., Weymann, A., Hartman, E., Finck, B. N., Hruz, P. W., Tzekov, A., & Rudnick, D. A. (2010). Liver regeneration is impaired in lipodystrophic fatty liver dystrophy mice. *Hepatology*, *52*(6), 2109–2117.

Ge, G., & Greenspan, D. S. (2006). BMP1 controls TGFβ1 activation via cleavage of latent TGFβ-binding protein. *Journal of Cell Biology*, *175*(1), 111–120.

Geiszt, M., Kopp, J. B., Varnai, P., & Leto, T. L. (2000). Identification of Renox, an NAD(P)H oxidase in kidney. *Proceedings of the National Academy of Sciences*, *97*(14), 8010–8014.

Godár, S., Horejsi, V., Weidle, U., B R Binder, B., Hansmann, C., & Stockinger, H. (1999). M6P/IGFII-receptor complexes urokinase receptor and plasminogen for activation of transforming growth factor-β1. *Eur. J. Immunol.*, *29*, 1004–1013.

Goff, C. L., Morice-Picard, F., Dagoneau, N., Wang, L. W., Crow, Y. J., Bauer, F., Flori, E., Prost-Squarcioni, C., Krakow, D., Ge, G., Greenspan, D. S., Bonnet, D., Le, M., Munnich, A., Apte, S. S., & Cormier-Daire, V. (2009). ADAMTSL2 mutations in

geleophysic dysplasia demonstrate a role for ADAMTS-like proteins in TGF-β bioavailability regulation. *Nat Genet.*, *40*(9), 1119–1123.

Goyal, P., Weissmann, N., Rose, F., Grimminger, F., Schäfers, H. J., Seeger, W., & Hänze, J. (2005). Identification of novel Nox4 splice variants with impact on ROS levels in A549 cells. *Biochemical and Biophysical Research Communications*, *329*(1), 32–39.

Greenhalgh, S. N., Matchett, K. P., Taylor, R. S., Huang, K., Li, J. T., Saeteurn, K., Donnelly, M. C., Simpson, E. E. M., Pollack, J. L., Atakilit, A., Simpson, K. J., Maher, J. J., Iredale, J. P., Sheppard, D., & Henderson, N. C. (2019). Loss of Integrin αvβ8 in Murine Hepatocytes Accelerates Liver Regeneration. *The American Journal of Pathology*, *189*(2), 258–271.

Guo, S., & Chen, X. (2015). The human Nox4: Gene, structure, physiological function and pathological significance. *Journal of Drug Targeting*, *23*(10), 888–896.

Han, P., Zhang C, Chuan-Yun Li, Heping Cheng, Jing-Wei Xiong, & Xiao-Hai Zhou. (2014). Hydrogen peroxide primes heart regeneration with a derepression mechanism. *Cell Research*, *24*(9), 17.

Hanley, C. J., Mellone, M., Ford, K., Thirdborough, S. M., Mellows, T., Frampton, S. J., Smith, D. M., Harden, E., Szyndralewiez, C., Bullock, M., Noble, F., Moutasim, K. A., King, E. V., Vijayanand, P., Mirnezami, A. H., Underwood, T. J., Ottensmeier, C. H., & Thomas, G. J. (2018). Targeting the Myofibroblastic Cancer-Associated Fibroblast Phenotype Through Inhibition of NOX4. *JNCI: Journal of the National Cancer Institute*, *110*(1), 109–120.

Hayashi, H., Sakai, K., Baba, H., & Sakai, T. (2013). Thrombospondin-1 is a novel negative regulator of liver regeneration after partial hepatectomy via TGF-β1 activation in mice. *Hepatology*, *55*(5), 20.

Hayes, P., Dhillon, S., O'Neill, K., Thoeni, C., Hui, K. Y., Elkadri, A., Guo, C. H., Kovacic, L., Aviello, G., Alvarez, L. A., Griffiths, A. M., Snapper, S. B., Brant, S. R., Doroshow, J. H., Silverberg, M. S., Peter, I., McGovern, D. P. B., Cho, J., Brumell, J. H., … Knaus, U. G. (2015). Defects in Nicotinamide-adenine Dinucleotide Phosphate Oxidase Genes NOX1 and DUOX2 in Very Early Onset Inflammatory Bowel Disease. *Cellular and Molecular Gastroenterology and Hepatology*, *1*(5), 489–502.

Hecker, L., Vittal, R., Jones, T., Jagirdar, R., Luckhardt, T. R., Horowitz, J. C., Pennathur, S., Martinez, F. J., & Thannickal, V. J. (2009). NADPH oxidase-4 mediates myofibroblast activation and fibrogenic responses to lung injury. *Nature Medicine*, *15*(9), 1077–1081.

Helfinger, V., Freiherr von Gall, F., Henke, N., Kunze, M. M., Schmid, T., Rezende, F., Heidler, J., Wittig, I., Radeke, H. H., Marschall, V., Anderson, K., Shah, A. M., Fulda, S., Brüne, B., Brandes, R. P., & Schröder, K. (2021). Genetic deletion of Nox4 enhances cancerogen-induced formation of solid tumors. *Proceedings of the National Academy of Sciences*, *118*(11), e2020152118.

Herrera, B., Álvarez, A. M., Beltrán, J., Valdés, F., Fabregat, I., & Fernández, M. (2004). Resistance to TGF-β-induced apoptosis in regenerating hepatocytes: TGF-β-APOPTOSIS IN REGENERATING HEPATOCYTES. *Journal of Cellular Physiology*, *201*(3), 385–392. https://doi.org/10.1002/jcp.20078

Herrera, B., Álvarez, Alberto. M., Sánchez, A., Fernández, M., Roncero, C., Benito, M., & Fabregat, I. (2001). Reactive oxygen species (ROS) mediates the mitochondrial-dependent apoptosis induced by transforming growth factor ß in fetal hepatocytes. *The FASEB Journal*, *15*(3), 741–751.

Herrera, B., Fernández, M., Alvarez, A., Roncero, C., Benito, M., Gil, J., & Fabregat, I. (2001). Activation of caspases occurs downstream from radical oxygen species

production, Bcl-xL down-regulation, and early cytochrome C release in apoptosis induced by transforming growth factor β in rat fetal hepatocytes. *Hepatology*, *34*(3), 548–556.

Herrera, B., Murillo, M. M., Álvarez-Barrientos, A., Beltrán, J., Fernández, M., & Fabregat, I. (2004). Source of early reactive oxygen species in the apoptosis induced by transforming growth factor-β in fetal rat hepatocytes. *Free Radical Biology and Medicine*, *36*(1), 16–26.

Hervera, A., De Virgilis, F., Palmisano, I., Zhou, L., & Di Giovanni, S. (2018). Reactive oxygen species regulate axonal regeneration through the release of exosomal NADPH oxidase 2 complexes into injured axons. *Nature Cell Biology*, *20*, 18.

Higgins, G., & Anderson, R. (1931). Experimental pathology of liver: Restoration of liver in white rat following partial surgical removal. *Arch Pathol*, *49*, 186–202.

Hilenski, L. L., Clempus, R. E., Quinn, M. T., Lambeth, J. D., & Griendling, K. K. (2004). Distinct Subcellular Localizations of Nox1 and Nox4 in Vascular Smooth Muscle Cells. *Arteriosclerosis, Thrombosis, and Vascular Biology*, *24*(4), 677–683.

Hiraga, R., Kato, M., Miyagawa, S., & Kamata, T. (2013). Nox4-derived ROS Signaling Contributes to TGF-β-induced Epithelial-mesenchymal Transition in Pancreatic Cancer Cells. *ANTICANCER RESEARCH*, *33*, 4431–4438.

Hotta, Y., Uchiyama, K., Takagi, T., Kashiwagi, S., Nakano, T., Mukai, R., Toyokawa, Y., Yasuda, T., Ueda, T., Suyama, Y., Murakami, T., Tanaka, M., Majima, A., Doi, T., Hirai, Y., Mizushima, K., Morita, M., Higashimura, Y., Inoue, K., … Itoh, Y. (2018). Transforming growth factor b1-induced collagen production in myofibroblasts is mediated by reactive oxygen species derived from NADPH oxidase 4. *Biochemical and Biophysical Research Communications*, *506*(3), 557–562.

Houck, K. A., & Michalopoulos, G. K. (1989). Altered responses of regenerating

    hepatocytes to norepinephrine and transforming growth factor type beta. *Journal*

    of Cellular Physiology, *141*(3), 503–509.

Hu, T., RamachandraRao, S. P., Siva, S., Valancius, C., Zhu, Y., Mahadev, K., Toh, I.,

    Goldstein, B. J., Woolkalis, M., & Sharma, K. (2005). Reactive oxygen species

    production via NADPH oxidase mediates TGF-β-induced cytoskeletal alterations in

    endothelial cells. *American Journal of Physiology-Renal Physiology*, *289*(4), F816–

    F825.

Huang, J., & Rudnick, D. A. (2014). Elucidating the Metabolic Regulation of Liver

    Regeneration. *The American Journal of Pathology*, *184*(2), 309–321.

Huck, I., Gunewardena, S., Espanol-Suner, R., Willenbring, H., & Apte, U. (2019).

    Hepatocyte Nuclear Factor 4 Alpha Activation Is Essential for Termination of Liver

    Regeneration in Mice: Hepatology. *Hepatology*, *70*(2), 666–681.

IJtsma, A. J. C., Boevé, L. M. S., van der Hilst, C. S., de Boer, M. T., de Jong, K. P.,

    Peeters, P. M. J. G., Gouw, A. S. H., Porte, R. J., & Slooff, M. J. H. (2008). The

    Survival Paradox of Elderly Patients After Major Liver Resections. *Journal of*

    Gastrointestinal Surgery, *12*(12), 2196–2203.

Ismail, S., Sturrock, A., Wu, P., Cahill, B., Norman, K., Huecksteadt, T., Sanders, K.,

    Kennedy, T., & Hoidal, J. (2009). NOX4 mediates hypoxia-induced proliferation of

    human pulmonary artery smooth muscle cells: The role of autocrine production of

    transforming growth factor-β1 and insulin-like growth factor binding protein-3. *Am*

    J Physiol Lung Cell Mol Physiol, *296*, L489–L499.

Jakowlew, S. B., Danielpour, D., Wu, J., Roberts, A. B., & Fausto, N. (n.d.). Transforming

    growth factor-a (TGF-,B) isoforms in rat liver regeneration: Messenger RNA

    expression and activation of latent TGF-,8. *Cell Regulation*, 14.

Jen, J., Harper, J. W., Bigner, S. H., Bigner, D. D., Papadopoulos, N., & Markowitz, S. (1994). Deletion ofpl6 and pl5 Genes in Brain Tumors. *Cancer Research*, *54*, 6353–6358.

Jiang, J. X., Chen, X., Serizawa, N., Szyndralewiez, C., Page, P., Schröder, K., Brandes, R. P., Devaraj, S., & Török, N. J. (2012). Liver fibrosis and hepatocyte apoptosis are attenuated by GKT137831, a novel NOX4/NOX1 inhibitor in vivo. *Free Radical Biology and Medicine*, *53*(2), 289–296.

Jiang, J. X. & Török, NJ. (2014). NADPH Oxidases in Chronic Liver Diseases. *Advances in Hepatology*, *2014*, 1–8.

Jiang, J. X., Venugopal, S., Serizawa, N., Chen, X., Scott, F., Li, Y., Adamson, R., Devaraj, S., Shah, V., Gershwin, M. E., Friedman, S. L., & Török, N. J. (2010). Reduced Nicotinamide Adenine Dinucleotide Phosphate Oxidase 2 Plays a Key Role in Stellate Cell Activation and Liver Fibrogenesis In Vivo. *Gastroenterology*, *139*(4), 1375-1384.e4.

Jirtle, R. L., Carr, B. I., & Scott, C. D. (1991). Modulation of insulin-like growth factor-II/mannose 6-phosphate receptors and transforming growth factor-beta 1 during liver regeneration. *Journal of Biological Chemistry*, *266*(33), 22444–22450.

Juan, G., Traganos, F., James, W. M., Ray, J. M., Roberge, M., Sauve, D. M., Anderson, H., & Darzynkiewicz, Z. (1998). Histone H3 phosphorylation and expression of cyclins A and B1 measured in individual cells during their progression through G2 and mitosis. *Cytometry*, *32*, 71–77.

Kalyanaraman, B. (2013). Teaching the basics of redox biology to medical and graduate students: Oxidants, antioxidants and disease mechanisms. *Redox Biology*, *1*(1), 244–257.

Kanda, Y., Hinata, T., Kang, S. W., & Watanabe, Y. (2011). Reactive oxygen species mediate adipocyte differentiation in mesenchymal stem cells. *Life Sciences*, *89*(7–8), 250–258.

Kang, L.-I., Mars, W., & Michalopoulos, G. (2012). Signals and Cells Involved in Regulating Liver Regeneration. *Cells*, *1*(4), 1261–1292.

Karkampouna, S., Goumans, M.-J., ten Dijke, P., Dooley, S., & Kruithof-de Julio, M. (2016). Inhibition of TGFβ type I receptor activity facilitates liver regeneration upon acute CCl4 intoxication in mice. *Archives of Toxicology*, *90*(2), 347–357.

Karkampouna, S., ten Dijke, P., Dooley, S., & Kruithof-de Julio, M. (2012). TGFβ signaling in liver regeneration. *Curr Pharm Des* ., *18*(27), 4103–4113.

Kato, M., Marumo, M., Nakayama, J., Matsumoto, M., Yabe-Nishimura, C., & Kamata, T. (2016). The ROS-generating oxidase Nox1 is required for epithelial restitution following colitis. *Exp. Anim.*, *65*(3), 197–205.

Khai, N. C., Takahashi, T., Ushikoshi, H., Nagano, S., Yuge, K., Esaki, M., Kawai, T., Goto, K., Murofushi, Y., Fujiwara, T., Fujiwara, H., & Kosai, K. (2006). In vivo hepatic HB-EGF gene transduction inhibits Fas-induced liver injury and induces liver regeneration in mice: A comparative study to HGF. *Journal of Hepatology*, 9.

Kim, E. Y., Anderson, M., & Dryer, S. E. (2012). Insulin increases surface expression of TRPC6 channels in podocytes: Role of NADPH oxidases and reactive oxygen species. *American Journal of Physiology-Renal Physiology*, *302*(3), F298–F307.

Kim, K. S., Choi, H. W., Yoon, H. E., & Kim, I. Y. (2010). Reactive Oxygen Species Generated by NADPH Oxidase 2 and 4 Are Required for Chondrogenic Differentiation. *Journal of Biological Chemistry*, *285*(51), 40294–40302.

Kiso, S., Kawata, S., Tamura, S., Inui, Y., Yoshida, Y., Sawai, Y., Umeki, S., Ito, N., Yamada, A., Miyagawa, I., Higashiyama, S., Iwawaki, T., Saito, M., Taniguchi, N., Matsuzawa, Y., & Kohno, K. (2003). Liver Regeneration in Heparin-Binding EGF-

like Growth Factor Transgenic Mice After Partial Hepatectomy. *Gastroenterology*, *124*(3), 7.

Kleinschnitz, C., Grund, H., Wingler, K., Armitage, M. E., Jones, E., Mittal, M., Barit, D., Schwarz, T., Geis, C., Kraft, P., Barthel, K., Schuhmann, M. K., Herrmann, A. M., Meuth, S. G., Stoll, G., Meurer, S., Schrewe, A., Becker, L., de Angelis, H., … Weissmann, N. (2010). Post-Stroke Inhibition of Induced NADPH Oxidase Type 4 Prevents Oxidative Stress and Neurodegeneration. *PLoS Biology*, *8*(9), 13.

Knock, G. A. (2019). NADPH oxidase in the vasculature: Expression, regulation and signalling pathways; role in normal cardiovascular physiology and its dysregulation in hypertension. *Free Radical Biology and Medicine*, *145*, 385–427.

Kohjima, M., Tsai, T.-H., Tackett, B. C., Thevananther, S., Li, L., Chang, B. H.-J., & Chan, L. (2013). Delayed liver regeneration after partial hepatectomy in adipose differentiation related protein-null mice. *Journal of Hepatology*, *59*(6), 1246–1254.

Köhler, U. A., Kurinna, S., Schwitter, D., Marti, A., Schäfer, M., Hellerbrand, C., Speicher, T., & Werner, S. (2014). Activated Nrf2 impairs liver regeneration in mice by activation of genes involved in cell-cycle control and apoptosis. *Hepatology*, *60*(2), 670–678.

Kuroda, J., Ago, T., Matsushima, S., Zhai, P., Schneider, M. D., & Sadoshima, J. (2010). NADPH oxidase 4 (Nox4) is a major source of oxidative stress in the failing heart. *Proceedings of the National Academy of Sciences*, *107*(35), 15565–15570.

Kuroda, J., Nakagawa, K., Yamasaki, T., Nakamura, K., Takeya, R., Kuribayashi, F., Imajoh-Ohmi, S., Igarashi, K., Shibata, Y., Sueishi, K., & Sumimoto, H. (2005). The superoxide-producing NAD(P)H oxidase Nox4 in the nucleus of human vascular endothelial cells: Nox4 as a nuclear NAD(P)H oxidase. *Genes to Cells*, *10*(12), 1139–1151.

Lambeth, J. D., & Neish, A. S. (2014). Nox Enzymes and New Thinking on Reactive

    Oxygen: A Double-Edged Sword Revisited. *Annual Review of Pathology:*

    Mechanisms of Disease, *9*(1), 119–145.

Lan, T., Kisseleva, T., & Brenner, D. A. (2015). Deficiency of NOX1 or NOX4 Prevents

    Liver Inflammation and Fibrosis in Mice through Inhibition of Hepatic Stellate Cell

    Activation. *PLOS ONE*, *10*(7), 19.

Leisegang, M. S., Babelova, A., Wong, M. S. K., Helfinger, V., Weißmann, N., Brandes, R.

    P., & Schröder, K. (2016). The NADPH Oxidase Nox2 Mediates Vitamin D-Induced

    Vascular Regeneration in Male Mice. *Endocrinology*, *157*(10), 9.

Leiskau, C., & Baumann, U. (2017). Structure, Function, and Repair of the Liver. In D. A.

    Kelly (Ed.), *Diseases of the Liver and Biliary System in Children* (pp. 1–17). John

    Wiley & Sons, Ltd.

Leksa, V., Godar, S., Schiller, H. B., Fuertbauer, E., Muhammad, A., Slezakova, K.,

    Horejsi, V., Steinlein, P., Weidle, U. H., Binder, B. R., & Stockinger, H. (2005).

    TGF-β-induced apoptosis in endothelial cells mediated by M6P/IGFII-R and mini-

    plasminogen. *Journal of Cell Science*, *118*(19), 4577–4586.

Li, B., & Dewey, C. N. (2011). RSEM: Accurate transcript quantification from RNA-Seq

    data with or without a reference genome. *BMC Bioinformatics*, *12*(1), 323.

Li, S., Tabar, S. S., Malec, V., Eul, B. G., Klepetko, W., Weissmann, N., Grimminger, F.,

    Seeger, W., Rose, F., & Hänze, J. (2008). NOX4 Regulates ROS Levels Under

    Normoxic and Hypoxic Conditions, Triggers Proliferation, and Inhibits Apoptosis in

    Pulmonary Artery Adventitial Fibroblasts. *ANTIOXIDANTS & REDOX SIGNALING*,

    10(10), 12.

Li, Y., Mouche, S., Sajic, T., Veyrat-Durebex, C., Supale, R., Pierroz, D., Ferrari, S., Negro,

    F., Hasler, U., Feraille, E., Moll, S., Meda, P., Deffert, C., Montet, X., Krause, K.-H.,

& Szanto, I. (2012). Deficiency in the NADPH oxidase 4 predisposes towards diet-induced obesity. *International Journal of Obesity*, *36*(12), 1503–1513.

Liang, S., Kisseleva, T., & Brenner, D. A. (2016). The Role of NADPH Oxidases (NOXs) in Liver Fibrosis and the Activation of Myofibroblasts. *Frontiers in Physiology*, *7*.

Lin, X.-L., Yang, L., Fu, S.-W., Lin, W.-F., Gao, Y.-J., Chen, H.-Y., & Ge, Z.-Z. (2017). Overexpression of NOX4 predicts poor prognosis and promotes tumor progression in human colorectal cancer. *Oncotarget*, *8*(20), 33586–33600.

Liu, B., Bell, A. W., Paranjpe, S., Bowen, W. C., Khillan, J. S., Luo, J.-H., Mars, W. M., & Michalopoulos, G. K. (2010). Suppression of liver regeneration and hepatocyte proliferation in hepatocyte-targeted glypican 3 transgenic mice. *Hepatology*, *52*(3), 1060–1067.

Liu, B., Paranjpe, S., Bowen, W. C., Bell, A. W., Luo, J.-H., Yu, Y.-P., Mars, W. M., & Michalopoulos, G. K. (2009). Investigation of the Role of Glypican 3 in Liver Regeneration and Hepatocyte Proliferation. *The American Journal of Pathology*, *175*(2), 717–724.

Liu, M., & Chen, P. (2017). Proliferation-inhibiting pathways in liver regeneration. *Molecular Medicine Reports*, *16*(1), 23–35.

López-Luque, J., Caballero-Díaz, D., Martinez-Palacián, A., Roncero, C., Moreno-Càceres, J., García-Bravo, M., Grueso, E., Fernández, A., Crosas-Molist, E., García-Álvaro, M., Addante, A., Bertran, E., Valverde, A. M., González-Rodríguez, Á., Herrera, B., Montoliu, L., Serrano, T., Segovia, J.-C., Fernández, M., … Fabregat, I. (2016). Dissecting the role of epidermal growth factor receptor catalytic activity during liver regeneration and hepatocarcinogenesis. *Hepatology*, *63*(2), 604–619.

López-Luque, J., & Fabregat, I. (2018). Revisiting the liver: From development to regeneration - what we ought to know! *The International Journal of Developmental Biology*, *62*(6-7–8), 441–451.

Love, M. I., Huber, W., & Anders, S. (2014). Moderated estimation of fold change and dispersion for RNA-seq data with DESeq2. *Genome Biology*, *15*(12), 550.

Lyle, A. N., Deshpande, N. N., Taniyama, Y., Seidel-Rogol, B., Pounkova, L., Du, P., Papaharalambus, C., Lassègue, B., & Griendling, K. K. (2009). Poldip2, a Novel Regulator of Nox4 and Cytoskeletal Integrity in Vascular Smooth Muscle Cells. *Circulation Research*, *105*(3), 249–259.

Lyons, R. M., Gentry, L. E., Purchio, A. E., & Moses, H. L. (1990). Mechanism of Activation of Latent Recombinant Transforming Growth Factor by Plasmin. *The Journal of Cell Biology*, *10*, 7.

Macias, M. J., Martin-Malpartida, P., & Massagué, J. (2015). Structural determinants of Smad function in TGF-β signaling. *Trends in Biochemical Sciences*, *40*(6), 296–308.

Maćias-Silva, M., Li, W., Leu, J. I., Crissey, M. A. S., & Taub, R. (2002). Up-regulated Transcriptional Repressors SnoN and Ski Bind Smad Proteins to Antagonize Transforming Growth Factor-β Signals during Liver Regeneration. *Journal of Biological Chemistry*, *277*(32), 28483–28490.

Malarkey, D. E., Johnson, K., Ryan, L., Boorman, G., & Maronpot, R. R. (2005). New Insights into Functional Aspects of Liver Morphology. *Toxicologic Pathology*, *33*(1), 27–34.

Mao, S. A., Glorioso, J. M., & Nyberg, S. L. (2014). Liver regeneration. *Translational Research*, *163*(4), 352–362.

Martínez-Palacián, A., del Castillo, G., Suárez-Causado, A., García-Álvaro, M., Morena-Frutos, D. de la, Fernández, M., Roncero, C., Fabregat, I., Herrera, B., & Sánchez,

A. (2013). Mouse Hepatic Oval Cells Require Met-Dependent PI3K to Impair TGF-β-Induced Oxidative Stress and Apoptosis. *PLoS ONE*, *8*(1), e53108.

Masamune, A., Watanabe, T., Kikuta, K., Satoh, K., & Shimosegawa, T. (2008). NADPH oxidase plays a crucial role in the activation of pancreatic stellate cells. *Am J Physiol Gastrointest Liver Physiol*, *294*, 10.

Massagué, J. (2008). TGFβ in Cancer. *Cell*, *134*(2), 215–230.

Masuda, A., Nakamura, T., Mitsuhiko, A., Iwamoto, H., Sakaue, T., Tanaka, T., Suzuki, H., Koga, H., & Torimura, T. (2020). Promotion of liver regeneration and anti-fibrotic effects of the TGF-β receptor kinase inhibitor galunisertib in CCl4-treated mice. *Int J Mol Med .*, *46*(1), 427–438.

Mayoral, R., Bosca, L., & Martín-Sanz, P. (2010). *Impairment of Transforming Growth Factor _ Signaling in Caveolin-1-deficient Hepatocytes*. *285*(6), 10.

McKallip, R. J., Jia, W., Schlomer, J., Warren, J. W., Nagarkatti, P. S., & Nagarkatti, M. (2006). Cannabidiol-Induced Apoptosis in Human Leukemia Cells: A Novel Role of Cannabidiol in the Regulation of p22 [phox] and Nox4 Expression. *Molecular Pharmacology*, *70*(3), 897–908.

Meng, D., Lv, D.-D., & Fang, J. (2008). Insulin-like growth factor-I induces reactive oxygen species production and cell migration through Nox4 and Rac1 in vascular smooth muscle cells. *Cardiovascular Research*, *80*(2), 299–308.

Menshikov, M., Plekhanova, O., Cai, H., Chalupsky, K., Parfyonova, Y., Bashtrikov, P., Tkachuk, V., & Berk, B. C. (2006). Urokinase Plasminogen Activator Stimulates Vascular Smooth Muscle Cell Proliferation Via Redox-Dependent Pathways. *Arteriosclerosis, Thrombosis, and Vascular Biology*, *26*(4), 801–807.

Michalopoulos, G. K. (2010). Liver Regeneration after Partial Hepatectomy. *The American Journal of Pathology*, *176*(1), 2–13.

Michalopoulos, G. K. (2017). Hepatostat: Liver regeneration and normal liver tissue

      maintenance. *Hepatology*, *65*(4), 1384–1392.

Michalopoulos, G. K. (2020). Liver Regeneration. In I. M. Arias, H. J. Alter, J. L. Boyer, D.

      E. Cohen, D. A. Shafritz, S. S. Thorgeirsson, & A. W. Wolkoff (Eds.), *The Liver* (1st

      ed., pp. 566–584). Wiley.

Michalopoulos, G. K., & Bhushan, B. (2021). Liver regeneration: Biological and

      pathological mechanisms and implications. *Nature Reviews Gastroenterology &*

      Hepatology, *18*(1), 40–55.

Mitchell, C., Nivison, M., Jackson, L., Fox, R., Lee, D., Campbell, J., & Fausto, N. (2005).

      Heparin-binding Epidermal Growth Factor-like Growth Factor Links Hepatocyte

      Priming with Cell Cycle Progression during Liver Regeneration. *The Journal of*

      Biological Chemistry, *280*(4), 7.

Miyaoka, Y., Ebato, K., Kato, H., Arakawa, S., Shimizu, S., & Miyajima, A. (2012).

      Hypertrophy and Unconventional Cell Division of Hepatocytes Underlie Liver

      Regeneration. *Current Biology*, *22*(13), 1166–1175.

Miyaoka, Y., & Miyajima, A. (2013). To divide or not to divide: Revisiting liver regeneration.

      Cell Division, *8*(1), 8.

Mofarrahi, M., Brandes, R. P., Gorlach, A., Hanze, J., Terada, L. S., Quinn, M. T., Mayaki,

      D., Petrof, B., & Hussain, S. N. A. (2008). Regulation of Proliferation of Skeletal

      Muscle Precursor Cells By NADPH Oxidase. *ANTIOXIDANTS & REDOX*

      SIGNALING, *10*, 16.

Moreno-Càceres, J., Caja, L., Mainez, J., Mayoral, R., Martín-Sanz, P., Moreno-Vicente,

      R., del Pozo, M. Á., Dooley, S., Egea, G., & Fabregat, I. (2014). Caveolin-1 is

      required for TGF- β -induced transactivation of the EGF receptor pathway in

      hepatocytes through the activation of the metalloprotease TACE/ADAM17. *Cell*

      Death & Disease, *5*(7), e1326–e1326.

Moreno-Càceres, J., & Fabregat, I. (2015). Apoptosis in liver carcinogenesis and
chemotherapy. *Hepatic Oncology*, *2*(4), 381–397.

Moreno-Càceres, J., Mainez, J., Mayoral, R., Martín-Sanz, P., Egea, G., & Fabregat, I.
(2016). Caveolin-1-dependent activation of the metalloprotease TACE/ADAM17 by
TGF-β in hepatocytes requires activation of Src and the NADPH oxidase NOX1.
The FEBS Journal, *283*(7), 1300–1310.

Murillo, M. M., Carmona-Cuenca, I., del Castillo, G., Ortiz, C., Roncero, C., Sánchez, A.,
Fernández, M., & Fabregat, I. (2007). Activation of NADPH oxidase by
transforming growth factor-β in hepatocytes mediates up-regulation of epidermal
growth factor receptor ligands through a nuclear factor-κB-dependent mechanism.
Biochemical Journal, *405*(2), 251–259.

Murillo, M. M., Castillo, G. del, Sánchez, A., Fernández, M., & Fabregat, I. (2005).
Involvement of EGF receptor and c-Src in the survival signals induced by TGF-β1
in hepatocytes. *Oncogene*, *24*(28), 4580–4587.

Murphy, M. P. (2009). How mitochondria produce reactive oxygen species. *Biochemical
Journal*, *417*(1), 1–13.

Nakamura, T., Ueno, T., Sakamoto, M., Sakata, R., Torimura, T., Hashimoto, O., Ueno, H.,
& Sata, M. (2004). Suppression of transforming growth factor-β results in
upregulation of transcription of regeneration factors after chronic liver injury.
Journal of Hepatology, *41*(6), 974–982.

Nisimoto, Y., Diebold, B. A., Cosentino-Gomes, D., & Lambeth, J. D. (2014). Nox4: A
Hydrogen Peroxide-Generating Oxygen Sensor. *Biochemistry*, *53*(31), 5111–
5120.

Nisimoto, Y., Jackson, H. M., Ogawa, H., Kawahara, T., & Lambeth, J. D. (2010).
Constitutive NADPH-Dependent Electron Transferase Activity of the Nox4
Dehydrogenase Domain. *Biochemistry*, *49*(11), 2433–2442.

Odekon, L. E., Blasi, F., & Rifkin, D. B. (1994). Requirement for receptor-bound urokinase in plasmin-dependent cellular conversion of latent TGF-? To TGF-? *Journal of Cellular Physiology*, *158*(3), 398–407.

Oe, S., Lemmer, E. R., Conner, E. A., Factor, V. M., Levéen, P., Larsson, J., Karlsson, S., & Thorgeirsson, S. S. (2004). Intact signaling by transforming growth factor β is not required for termination of liver regeneration in mice. *Hepatology*, *40*(5), 1098–1105.

Oliynyk, G., Ruiz-Pérez, M. V., Sainero-Alcolado, L., Dzieran, J., Zirath, H., Gallart-Ayala, H., Wheelock, C. E., Johansson, H. J., Nilsson, R., Lehtiö, J., & Arsenian-Henriksson, M. (2019). MYCN-enhanced Oxidative and Glycolytic Metabolism Reveals Vulnerabilities for Targeting Neuroblastoma. *IScience*, *21*, 188–204.

Ozaki, M. (2020). Cellular and molecular mechanisms of liver regeneration: Proliferation, growth, death and protection of hepatocytes. *Seminars in Cell & Developmental Biology*, *100*, 62–73.

Padua, D., & Massagué, J. (2009). Roles of TGFβ in metastasis. *Cell Research*, *19*(1), 89–102.

Paffenholz, R. (2004). Vestibular defects in head-tilt mice result from mutations in Nox3, encoding an NADPH oxidase. *Genes & Development*, *18*(5), 486–491.

Paik, Y.-H., Iwaisako, K., Seki, E., Inokuchi, S., Schnabl, B., Österreicher, C. H., Kisseleva, T., & Brenner, D. A. (2011). The nicotinamide adenine dinucleotide phosphate oxidase (NOX) homologues NOX1 and NOX2/gp91phox mediate hepatic fibrosis in mice. *Hepatology*, *53*(5), 1730–1741.

Paik, Y.-H., Kim, J., Aoyama, T., De Minicis, S., Bataller, R., & Brenner, D. A. (2014). Role of NADPH Oxidases in Liver Fibrosis. *Antioxidants & Redox Signaling*, *20*(17), 2854–2872.

Paletta-Silva, R., Rocco-Machado, N., & Meyer-Fernandes, J. (2013). NADPH Oxidase

    Biology and the Regulation of Tyrosine Kinase Receptor Signaling and Cancer

    Drug Cytotoxicity. *International Journal of Molecular Sciences*, *14*(2), 3683–3704.

Paranjpe, S., Bowen, W. C., Mars, W. M., Orr, A., Haynes, M. M., DeFrances, M. C., Liu,

    S., Tseng, G. C., Tsagianni, A., & Michalopoulos, G. K. (2016). Combined

    systemic elimination of MET and epidermal growth factor receptor signaling

    completely abolishes liver regeneration and leads to liver decompensation: Liver

    Injury/Regeneration. *Hepatology*, *64*(5), 1711–1724.

Parascandolo, A., & Laukkanen, M. O. (2019). Carcinogenesis and Reactive Oxygen

    Species Signaling: Interaction of the NADPH Oxidase NOX1–5 and Superoxide

    Dismutase 1–3 Signal Transduction Pathways. *Antioxidants & Redox Signaling*,

    30(3), 443–486.

Pedruzzi, E., Guichard, C., Ollivier, V., Driss, F., Fay, M., Prunet, C., Marie, J.-C., Pouzet,

    C., Samadi, M., Elbim, C., O'Dowd, Y., Bens, M., Vandewalle, A., Gougerot-

    Pocidalo, M.-A., Lizard, G., & Ogier-Denis, E. (2004). NAD(P)H Oxidase Nox-4

    Mediates 7-Ketocholesterol-Induced Endoplasmic Reticulum Stress and Apoptosis

    in Human Aortic Smooth Muscle Cells. *Molecular and Cellular Biology*, *24*(24),

    10703–10717.

Peshavariya, H., Dusting, G. J., Jiang, F., Halmos, L. R., Sobey, C. G., Drummond, G. R.,

    & Selemidis, S. (2009). NADPH oxidase isoform selective regulation of endothelial

    cell proliferation and survival. *Naunyn-Schmiedeberg's Archives of Pharmacology*,

    380(2), 193–204.

Petritsch, C., Beug, H., Balmain, A., & Oft, M. (2000). TGF-beta inhibits p70 S6 kinase via

    protein phosphatase 2A to induce G1 arrest. *Genes & Development*, *14*, 3093–

    3101.

Pritchard, M. T., Malinak, R. N., & Nagy, L. E. (2011). Early growth response (EGR)-1 is required for timely cell-cycle entry and progression in hepatocytes after acute carbon tetrachloride exposure in mice. *American Journal of Physiology-Gastrointestinal and Liver Physiology*, *300*(6), G1124–G1131.

Przybylska, D., Janiszewska, D., Goździk, A., Bielak-Zmijewska, A., Sunderland, P., Sikora, E., & Mosieniak, G. (2016). NOX4 downregulation leads to senescence of human vascular smooth muscle cells. *Oncotarget*, *7*(41), 66429–66443.

Rao, S., Zaidi, S., Banerjee, J., Jogunoori, W., Sebastian, R., Mishra, B., Nguyen, B.-N., Wu, R.-C., White, J., Deng, C., Amdur, R., Li, S., & Mishra, L. (2017). Transforming growth factor-β in liver cancer stem cells and regeneration. *Hepatology Communications*, *1*(6), 477–493.

Reimand, J., Kull, M., Peterson, H., Hansen, J., & Vilo, J. (2007). g:Profiler—A web-based toolset for functional profiling of gene lists from large-scale experiments. *Nucleic Acids Research*, *35*(suppl_2), W193–W200.

Rezende, F., Schürmann, C., Schütz, S., Harenkamp, S., Herrmann, E., Seimetz, M., Weißmann, N., & Schröder, K. (2017). Knock out of the NADPH oxidase Nox4 has no impact on life span in mice. *Redox Biology*, *11*, 312–314.

Riddiough, G. E., Jalal, Q., Perini, M. V., & Majeed, A. W. (2021). Liver regeneration and liver metastasis. *Seminars in Cancer Biology*, *71*, 86–97.

Riehle, K. J., Dan, Y. Y., Campbell, J. S., & Fausto, N. (2011). New concepts in liver regeneration: New concepts in liver regeneration. *Journal of Gastroenterology and Hepatology*, *26*, 203–212.

Romero-Gallo, J., Sozmen, E. G., Chytil, A., Russell, W. E., Whitehead, R., Parks, W. T., Holdren, M. S., Her, M. F., Gautam, S., Magnuson, M., Moses, H. L., & Grady, W. M. (2005). Inactivation of TGF-β signaling in hepatocytes results in an increased proliferative response after partial hepatectomy. *Oncogene*, *24*(18), 3028–3041.

Rudnick, D. A., & Davidson, N. O. (2012). Functional Relationships between Lipid Metabolism and Liver Regeneration. *International Journal of Hepatology*, *2012*, 1–8.

Russell, W. E. (1988). Type beta transforming growth factor reversibly inhibits the early proliferative response to partial hepatectomy in the rat. *Cell Biology*, *85*(14), 5126–5130.

Sampson, N., Koziel, R., Zenzmaier, C., Bubendorf, L., & Plas, E. (2011). ROS Signaling by NOX4 Drives Fibroblast-to- Myofibroblast Differentiation in the Diseased Prostatic Stroma. *Mol Endocrinol*, *25*(3), 503–515.

Sanchez, A. (1999). Apoptotic Response to TGF-beta in Fetal Hepatocytes Depends upon Their State of Differentiation. *Experimental Cell Research*, *252*(2), 281–291.

Sanchez, A., Alvarez, A. M., Benito, M., & Fabregat, I. (1995). Transforming growth factor-beta modulates growth and differentiation of fetal hepatocytes in primary culture. *Journal of Cellular Physiology*, *165*(2), 398–405.

Sánchez, A., Álvarez, A. M., Benito, M., & Fabregat, I. (1996). Apoptosis Induced by Transforming Growth Factor- in Fetal Hepatocyte Primary Cultures: Involvement of reactive oxygen intermediates. *Journal of Biological Chemistry*, *271*(13), 7416–7422.

Sancho, P., & Fabregat, I. (2010). NADPH Oxidase NOX1 Controls Autocrine Growth of Liver Tumor Cells through Up-regulation of the Epidermal Growth Factor Receptor Pathway. *Journal of Biological Chemistry*, *285*(32), 24815–24824.

Sancho, P., Mainez, J., Crosas-Molist, E., Roncero, C., Fernández-Rodriguez, C. M., Pinedo, F., Huber, H., Eferl, R., Mikulits, W., & Fabregat, I. (2012). NADPH Oxidase NOX4 Mediates Stellate Cell Activation and Hepatocyte Cell Death during Liver Fibrosis Development. *PLoS ONE*, *7*(9), e45285.

Sanders, Y. Y., Lyv, X., Zhou, Q. J., Xiang, Z., Stanford, D., Bodduluri, S., Rowe, S. M., & Thannickal, V. J. (2020). Brd4-p300 inhibition downregulates Nox4 and accelerates lung fibrosis resolution in aged mice. *JCI Insight .*, *5*(14), 13.

Santibanez, J. F. (2013). Transforming Growth Factor-Beta and Urokinase-Type Plasminogen Activator: Dangerous Partners in Tumorigenesis—Implications in Skin Cancer. *ISRN Dermatology*, *2013*, 1–26.

Santibanez, J. F., Obradović, H., Kukolj, T., & Krstić, J. (2018). Transforming growth factor-β, matrix metalloproteinases, and urokinase-type plasminogen activator interaction in the cancer epithelial to mesenchymal transition: TGF-β, MMPs, and UPA Interplay in Cancer EMT. *Developmental Dynamics*, *247*(3), 382–395.

Schilder, Y. D. C., Heiss, E. H., Schachner, D., Ziegler, J., Reznicek, G., Sorescu, D., & Dirsch, V. M. (2009). NADPH oxidases 1 and 4 mediate cellular senescence induced by resveratrol in human endothelial cells. *Free Radical Biology and Medicine*, *46*(12), 1598–1606.

Schmidt, H. H. H. W., Ghezzi, P., & Cuadrado, A. (Eds.). (2021). *Reactive Oxygen Species: Network Pharmacology and Therapeutic Applications* (Vol. 264). Springer International Publishing. https://link.springer.com/10.1007/978-3-030-68510-2

Scholzen, T., & Gerdes, J. (2000). The Ki-67 protein: From the known and the unknown. *Journal of Cellular Physiology*, *182*, 311–322.

Schröder, K. (2014). NADPH Oxidases in Redox Regulation of Cell Adhesion and Migration. *Antioxidants & Redox Signaling*, *20*(13), 2043–2058.

Schröder, K. (2019). NADPH oxidase-derived reactive oxygen species: Dosis facit venenum. *Experimental Physiology*, *104*(4), 447–452.

Schröder, K. (2020). NADPH oxidases: Current aspects and tools. *Redox Biology*, *34*, 101512.

Schröder, K., Wandzioch, K., Helmcke, I., & Brandes, R. P. (2009). Nox4 Acts as a Switch Between Differentiation and Proliferation in Preadipocytes. *Arteriosclerosis, Thrombosis, and Vascular Biology*, *29*(2), 239–245.

Schröder, K., Zhang, M., Benkhoff, S., Mieth, A., Pliquett, R., Kosowski, J., Kruse, C., Luedike, P., Michaelis, U. R., Weissmann, N., Dimmeler, S., Shah, A. M., & Brandes, R. P. (2012). Nox4 Is a Protective Reactive Oxygen Species Generating Vascular NADPH Oxidase. *Circulation Research*, *110*(9), 1217–1225.

Schrum, L. W., Bird, M. A., Salcher, O., Burchardt, E.-R., Grisham, J. W., Brenner, D. A., Rippe, R. A., & Behrns, K. E. (2001). Autocrine expression of activated transforming growth factor-β_1 induces apoptosis in normal rat liver. *American Journal of Physiology-Gastrointestinal and Liver Physiology*, *280*(1), G139–G148.

Senturk, S., Mumcuoglu, M., Gursoy-Yuzugullu, O., Cingoz, B., Akcali, K. C., & Ozturk, M. (2010). Transforming growth factor-beta induces senescence in hepatocellular carcinoma cells and inhibits tumor growth. *Hepatology*, *52*(3), 966–974.

Seoane, J. (2006). Escaping from the TGF anti-proliferative control. *Carcinogenesis*, *27*(11), 2148–2156.

Serrander, L., Cartier, L., Bedard, K., Banfi, B., Lardy, B., Plastre, O., Sienkiewicz, A., Fórró, L., Schlegel, W., & Krause, K.-H. (2007). NOX4 activity is determined by mRNA levels and reveals a unique pattern of ROS generation. *Biochemical Journal*, *406*(1), 105–114.

Shi, M., Zhu, J., Wang, R., Chen, X., Mi, L., Walz, T., & Springer, T. A. (2011). Latent TGF-β structure and activation. *Nature*, *474*(7351), 343–349.

Shiose, A., Kuroda, J., Tsuruya, K., Hirai, M., Hirakata, H., Naito, S., Hattori, M., Sakaki, Y., & Sumimoto, H. (2001). A Novel Superoxide-producing NAD(P)H Oxidase in Kidney. *Journal of Biological Chemistry*, *276*(2), 1417–1423.

Shono, T., Yokoyama, N., Uesaka, T., Kuroda, J., Takeya, R., Yamasaki, T., Amano, T., Mizoguchi, M., Suzuki, S. O., Niiro, H., Miyamoto, K., Akashi, K., Iwaki, T., Sumimoto, H., & Sasaki, T. (2008). Enhanced expression of NADPH oxidase Nox4 in human gliomas and its roles in cell proliferation and survival: Nox4 Expression in Human Gliomas. *International Journal of Cancer*, *123*(4), 787–792.

Shteyer, E., Liao, Y., Muglia, L. J., Hruz, P. W., & Rudnick, D. A. (2004). Disruption of hepatic adipogenesis is associated with impaired liver regeneration in mice. *Hepatology*, *40*(6), 1322–1332.

Sies, H. (2017). Hydrogen peroxide as a central redox signaling molecule in physiological oxidative stress: Oxidative eustress. *Redox Biology*, *11*, 613–619.

Sies, H., & Jones, D. P. (2020). Reactive oxygen species (ROS) as pleiotropic physiological signalling agents. *Nature Reviews Molecular Cell Biology*, *21*(7), 363–383.

Simek, J., Chmelar, V., Mĕlka, J., Pazderka, & Charvát, Z. (1967). Influence of protracted infusion of glucose and insulin on the composition and regeneration activity of liver after partial hepatectomy in rats. *Nature*, *213*(5079), 910–911.

Simon, F., & Fernández, R. (2009). Early lipopolysaccharide-induced reactive oxygen species production evokes necrotic cell death in human umbilical vein endothelial cells. *J Hypertens*, *27*(6), 1202–1216.

Si-Tayeb, K., Lemaigre, F. P., & Duncan, S. A. (2010). Organogenesis and Development of the Liver. *Developmental Cell*, *18*(2), 175–189.

Spear, B. T., Jin, L., Ramasamy, S., & Dobierzewska, A. (2006). Transcriptional control in the mammalian liver: Liver development, perinatal repression, and zonal gene regulation. *Cellular and Molecular Life Sciences*, *63*(24), 2922–2938.

Sturrock, A., Cahill, B., Norman, K., Huecksteadt, T. P., Hill, K., Sanders, K., Karwande, S. V., Stringham, J. C., Bull, D. A., Gleich, M., Kennedy, T. P., & Hoidal, J. R. (2006).

Transforming growth factor-β1 induces Nox4 NAD(P)H oxidase and reactive oxygen species-dependent proliferation in human pulmonary artery smooth muscle cells. *American Journal of Physiology-Lung Cellular and Molecular Physiology*, *290*(4), L661–L673.

Sturrock, A., Huecksteadt, T. P., Norman, K., Sanders, K., Murphy, T. M., Chitano, P., Wilson, K., Hoidal, J. R., & Kennedy, T. P. (2007). Nox4 mediates TGF-β1-induced retinoblastoma protein phosphorylation, proliferation, and hypertrophy in human airway smooth muscle cells. *American Journal of Physiology-Lung Cellular and Molecular Physiology*, *292*(6), L1543–L1555.

Takac, I., Schröder, K., Zhang, L., Lardy, B., Anilkumar, N., Lambeth, J. D., Shah, A. M., Morel, F., & Brandes, R. P. (2011). The E-loop Is Involved in Hydrogen Peroxide Formation by the NADPH Oxidase Nox4. *Journal of Biological Chemistry*, *286*(15), 13304–13313.

Tang, C. T., Gao, Y. J., & Ge, Z. Z. (2018). *NOX4* , a new genetic target for anti-cancer therapy in digestive system cancer: NOX4 affects gastroenteric tumor growth. *Journal of Digestive Diseases*, *19*(10), 578–585.

Teramoto, T., Kiss, A., & Thorgeirsson, S. S. (1998). Induction of p53 and Bax during TGF-beta1 Initiated Apoptosis in Rat Liver Epithelial Cells. *Biochem Biophys Res Commun*, *251*(1), 5.

Tian, X. Y., Yung, L. H., Wong, W. T., Liu, J., Leung, F. P., Liu, L., Chen, Y., Kong, S. K., Kwan, K. M., Ng, S. M., Lai, P. B. S., Yung, L. M., Yao, X., & Huang, Y. (2012). Bone morphogenic protein-4 induces endothelial cell apoptosis through oxidative stress-dependent p38MAPK and JNK pathway. *Journal of Molecular and Cellular Cardiology*, *52*(1), 237–244.

Tong, L., Wang, L., Yao, S., Jin, L., Yang, J., Zhang, Y., Ning, G., & Zhang, Z. (2019). PPARδ attenuates hepatic steatosis through autophagy-mediated fatty acid oxidation. *Cell Death & Disease*, *10*(3), 197.

Tormos, A. M., Taléns-Visconti, R., & Sastre, J. (2015). Regulation of cytokinesis and its clinical significance. *Critical Reviews in Clinical Laboratory Sciences*, *52*(4), 159–167.

Travis, M. A., & Sheppard, D. (2014). TGF-β Activation and Function in Immunity. *Annual Review of Immunology*, *32*(1), 51–82.

Trefts, E., Gannon, M., & Wasserman, D. H. (2017). The liver. *Current Biology*, *27*(21), R1147–R1151.

Tzavlaki, K., & Moustakas, A. (2020). TGF-β Signaling. *Biomolecules*, *10*(3), 487.

Ueno, S., Campbell, J., & Fausto, N. (2006). Reactive Oxygen Species Derived From NADPH Oxidase System is Not Essential for Liver Regeneration After Partial Hepatectomy. *Journal of Surgical Research*, *136*(2), 6.

Valdés, F., Murillo, M. M., Valverde, Á. M., Herrera, B., Sánchez, A., Benito, M., Fernández, M., & Fabregat, I. (2004). Transforming growth factor-beta activates both pro-apoptotic and survival signals in fetal rat hepatocytes. *Experimental Cell Research*, *292*(1), 209–218.

Vermeulen, K., Van Bockstaele, D. R., & Berneman, Z. N. (2003). The cell cycle: A review of regulation, deregulation and therapeutic targets in cancer: *Cell cycle regulation and deregulation*. *Cell Proliferation*, *36*(3), 131–149.

Verstraeten, A., Alaerts, M., Van Laer, L., & Loeys, B. (2016). Marfan Syndrome and Related Disorders: 25 Years of Gene Discovery. *Human Mutation*, *37*(6), 524–531.

Villevalois-Cam, L., Rescan, C., Gilot, D., Ezan, F., Loyer, P., Desbuquois, B., Guguen-Guillouzo, C., & Baffet, G. (2003). The hepatocyte is a direct target for

transforming-growth factor b activation via the insulin-like growth factor II/mannose

6-phosphate receptor. *Journal of Hepatology*, *38*, 8.

Waghela, B. N., Vaidya, F. U., Agrawal, Y., Santra, M. K., Mishra, V., & Pathak, C. (2021).

Molecular insights of NADPH oxidases and its pathological consequences. *Cell*

Biochemistry and Function, *39*(2), 218–234.

Wang, X., Elksnis, A., Wikström, P., Walum, E., Welsh, N., & Carlsson, P.-O. (2018). The

novel NADPH oxidase 4 selective inhibitor GLX7013114 counteracts human islet

cell death in vitro. *PLOS ONE*, *13*(9), e0204271.

Weymann, A., Hartman, E., Gazit, V., Wang, C., Glauber, M., Turmelle, Y., & Rudnick, D.

A. (2009). P21 is required for dextrose-mediated inhibition of mouse liver

regeneration. *Hepatology*, *50*(1), 207–215.

Williams, C. D., Bajt, M. L., Sharpe, M. R., McGill, M. R., Farhood, A., & Jaeschke, H.

(2014). Neutrophil activation during acetaminophen hepatotoxicity and repair in

mice and humans. *Toxicology and Applied Pharmacology*, *275*(2), 122–133.

Witte, D., Bartscht, T., Kaufmann, R., Pries, R., Settmacher, U., Lehnert, H., & Ungefroren,

H. (2017). TGF-β1-induced cell migration in pancreatic carcinoma cells is RAC1

and NOX4-dependent and requires RAC1 and NOX4-dependent activation of p38

MAPK. *Oncology Reports*.

Xie, G., Yin, S., Zhang, Z., Qi, D., Wang, X., Kim, D., Yagai, T., Brocker, C. N., Wang, Y.,

Gonzalez, F. J., Wang, H., & Qu, A. (2019). Hepatocyte Peroxisome Proliferator–

Activated Receptor α Enhances Liver Regeneration after Partial Hepatectomy in

Mice. *The American Journal of Pathology*, *189*(2), 272–282.

Xu, Y., Ruan, S., Wu, X., Chen, H., Zheng, K., & Fu, B. (2013). Autophagy and apoptosis

in tubular cells following unilateral ureteral obstruction are associated with

mitochondrial oxidative stress. *International Journal of Molecular Medicine*, *31*(3),

628–636.

Yan, F., Wang, Y., Wu, X., Peshavariya, H. M., Dusting, G. J., Zhang, M., & Jiang, F.

    (2014). Nox4 and redox signaling mediate TGF-β-induced endothelial cell

    apoptosis and phenotypic switch. *Cell Death & Disease*, *5*(1), e1010–e1010.

Yang, W., Tao, Y., Wu, Y., Zhao, X., Ye, W., Zhao, D., Fu, L., Tian, C., Yang, J., He, F., &

    Tang, L. (2019). Neutrophils promote the development of reparative macrophages

    mediated by ROS to orchestrate liver repair. *Nature Communications*, *10*(1),

    1076.

Youm, T. H., Woo, S.-H., Kwon, E.-S., & Park, S. S. (2019). NADPH Oxidase 4

    Contributes to Myoblast Fusion and Skeletal Muscle Regeneration. *Oxidative*

    Medicine and Cellular Longevity, 12.

Yu, J. H., Zhu, B.-M., Riedlinger, G., Kang, K., & Hennighausen, L. (2012). The liver-

    specific tumor suppressor STAT5 controls expression of the reactive oxygen

    species-generating enzyme NOX4 and the proapoptotic proteins PUMA and BIM

    in mice. *Hepatology*, *56*(6), 2375–2386.

Yu, J., Zhang, L., Chen, A., Xiang, G., Wang, Y., Wu, J., Mitchelson, K., Cheng, J., &

    Zhou, Y. (2008). Identification of the gene transcription and apoptosis mediated by

    TGF-β-Smad2/3-Smad4 signaling. *Journal of Cellular Physiology*, *215*(2), 422–

    433.

Zeng, W., Xiao, J., Zheng, G., Xing, F., Tipoe, G., Wang, X., He, C., Chen, Z.-Y., & Liu, Y.

    (2015). Antioxidant treatment enhances human mesenchymal stem cell anti-stress

    ability and therapeutic efficacy in an acute liver failure model. *Scientific Reports*, *5*,

    17.

Zhang, C., Lan, T., Hou, J., Li, J., Fang, R., Yang, Z., Zhang, M., Liu, J., & Liu, B. (2014).

    NOX4 promotes non-small cell lung cancer cell proliferation and metastasis

    through positive feedback regulation of PI3K/Akt signaling. *Oncotarget*, *5*(12),

    4392–4405.

Zhang, M., Brewer, A. C., Schroder, K., Santos, C. X. C., Grieve, D. J., Wang, M.,
Anilkumar, N., Yu, B., Dong, X., Walker, S. J., Brandes, R. P., & Shah, A. M.
(2010). NADPH oxidase-4 mediates protection against chronic load-induced
stress in mouse hearts by enhancing angiogenesis. *Proceedings of the National
Academy of Sciences*, *107*(42), 18121–18126.

Zhang, Y. E. (2009). Non-Smad pathways in TGF-β signaling. *Cell Research*, *19*(1), 128–
139.

Zimmermann, A. (2004). Regulation of liver regeneration. *Nephrology Dialysis
Transplantation*, *19*(suppl_4), iv6–iv10.

Zirath, H., Frenzel, A., Oliynyk, G., Segerstrom, L., Westermark, U. K., Larsson, K.,
Munksgaard Persson, M., Hultenby, K., Lehtio, J., Einvik, C., Pahlman, S., Kogner,
P., Jakobsson, P.-J., & Arsenian Henriksson, M. (2013). MYC inhibition induces
metabolic changes leading to accumulation of lipid droplets in tumor cells.
Proceedings of the National Academy of Sciences, *110*(25), 10258–10263.

Zivna, H., Zivny, P., Palicka, V., & Simakova, E. (2002). *Influence of High Cholesterol Diet
and Pravastatin Sodium on the Initiation of Liver Regeneration in Rats After Partial
Hepatectomy*. *18*(1), 5.

Zou, Y., Bao, Q., Kumar, S., Hu, M., Wang, G.-Y., & Dai, G. (2012). Four Waves of
Hepatocyte Proliferation Linked with Three Waves of Hepatic Fat Accumulation
during Partial Hepatectomy-Induced Liver Regeneration. *PLoS ONE*, *7*(2), e30675.

Zou, Y., Hu, M., Lee, J., Nambiar, S. M., Garcia, V., Bao, Q., Chan, J. Y., & Dai, G.
(2015). Nrf2 is essential for timely M phase entry of replicating hepatocytes during
liver regeneration. *American Journal of Physiology-Gastrointestinal and Liver
Physiology*, *308*(4), G262–G268.

Zou, Y., Lee, J., Nambiar, S. M., Hu, M., Rui, W., Bao, Q., Chan, J. Y., & Dai, G. (2014).

Nrf2 Is Involved in Maintaining Hepatocyte Identity during Liver Regeneration.

PLoS ONE, *9*(9), e107423.

Appendix

Research Paper

NADPH oxidase 4 (Nox4) deletion accelerates liver regeneration in mice

M. Herranz-Itúrbide [a,b], J. López-Luque [a,b], E. Gonzalez-Sanchez [a,b,c], D. Caballero-Díaz [a,b], E. Crosas-Molist [a,1], B. Martín-Mur [d], M. Gut [d,e], A. Esteve-Codina [d], V. Jaquet [f,g], J.X. Jiang [h,2], N.J. Török [i], I. Fabregat [a,b,c,*]

[a] TGF-β and Cancer Group. Oncobell Program, Bellvitge Biomedical Research Institute (IDIBELL), L'Hospitalet de Llobregat, Barcelona, Spain
[b] Oncology Program, CIBEREHD, National Biomedical Research Institute on Liver and Gastrointestinal Diseases, Instituto de Salud Carlos III, Spain
[c] Department of Physiological Sciences, Faculty of Medicine and Health Sciences, University of Barcelona, Spain
[d] CNAG-CRG, Centre for Genomic Regulation, Barcelona Institute of Science and Technology, Barcelona, Spain
[e] Universitat Pompeu Fabra, Barcelona, Spain
[f] Department of Pathology and Immunology, Medical School, University of Geneva, Geneva, Switzerland
[g] RE.A.D.S Unit, Medical School, University of Geneva, Geneva, Switzerland
[h] Gastroenterology and Hepatology, UC Davis, Sacramento, CA, USA
[i] Department of Internal Medicine, Division of Gastroenterology and Hepatology, Stanford University, Stanford, CA, USA

ARTICLE INFO

ABSTRACT

Liver is a unique organ in displaying a reparative and regenerative response after acute/chronic damage or partial hepatectomy, when all the cell types must proliferate to re-establish the liver mass. The NADPH oxidase NOX4 mediates Transforming Growth Factor-beta (TGF-β) actions, including apoptosis in hepatocytes and activation of stellate cells to myofibroblasts. Aim of this work was to analyze the impact of NOX4 in liver regeneration by using two mouse models where *Nox4* was deleted: 1) general deletion of *Nox4* (NOX4−/−) and 2) hepatocyte-specific deletion of *Nox4* (NOX4hepKO). Liver regeneration was analyzed after 2/3 partial hepatectomy (PH). Results indicated an earlier recovery of the liver-to-body weight ratio in both NOX4−/− and NOX4hepKO mice and an increased survival, when compared to corresponding WT mice. The regenerative hepatocellular fat accumulation and the parenchyma organization recovered faster in NOX4 deleted livers. Hepatocyte proliferation, analyzed by Ki67 and phospho-Histone3 immunohistochemistry, was accelerated and increased in NOX4 deleted mice, coincident with an earlier and increased *Myc* expression. Primary hepatocytes isolated from NOX4 deleted mice showed higher proliferative capacity and increased expression of *Myc* and different cyclins in response to serum. Transcriptomic analysis through RNA-seq revealed significant changes after PH in NOX4−/− mice and support a relevant role for *Myc* in a node of regulation of proliferation-related genes. Interestingly, RNA-seq also revealed changes in the expression of genes related to activation of the TGF-β pathway. In fact, levels of active TGF-β1, phosphorylation of Smads and levels of its target p21 were lower at 24 h in NOX4 deleted mice. Nox4 did not appear to be essential for the termination of liver regeneration *in vivo*, neither for the *in vitro* hepatocyte response to TGF-β1 in terms of growth inhibition, which suggest its potential as therapeutic target to improve liver regeneration, without adverse effects.

1. Introduction

The NADPH oxidase (NOX) family has recently emerged as an important source of reactive oxygen species (ROS), which play relevant roles in signal transduction under both physiological and pathological situations [1]. The NOX4 isoform shows unique characteristics compared to other NOXes [2], since it produces large amounts of hydrogen peroxide (H_2O_2) constitutively, does not require GTPase Rac

for its activity and it is associated not only to cell membrane, but also to internal membranes, where H_2O_2 generation occurs [3]. In the liver, NOX4 plays relevant roles mediating Transforming Growth Factor-beta (TGF-β) actions in fibrosis and hepatocarcinogenesis [4,5]. We previously described that NOX4 mediates TGF-β1-induced myofibroblast activation, contributing to the development of liver fibrosis [6,7]. Indeed, there is an increasing interest in the development of NOX4 inhibitors as therapeutic tools for chronic liver diseases [8]. However, in hepatocytes and liver tumor cells, we found that NOX4 mediates TGF-β1-induced tumor suppressor actions, particularly apoptosis [9]. Furthermore, when NOX4 expression is knocked-down in hepatocellular carcinoma (HCC) cells, they acquire higher proliferative and migratory capacity *in vitro* and higher tumorigenic potential in *in vivo* xenografts in nude mice [10,11]. Interestingly, *NOX4* gene deletions were found in HCC patients, which correlate with a decrease in NOX4 protein levels [11].

Liver regeneration is the response to loss of hepatic tissue, which may occur as a result of toxic injury, exposure to infection, traumatic damage or surgical resection [12]. Hepatocytes are the major functional cells of the liver. Indeed, in most cases, the regenerative response is strongly triggered when there is a loss of hepatocytes at a large scale. Many genes are involved in liver regeneration, but the essential circuitry for the process involves the participation of cytokines, growth factors and metabolic networks [13]. Under normal conditions, all hepatic cells undergo one to three rounds of replication, but evidence strongly suggests that under conditions where the proliferation of hepatocytes or biliary cells is inhibited, they can act as facultative stem cells for each other and replenish the inhibited cellular compartment by a process of transdifferentiation [14]. Liver cell proliferation occurs also at any time in normal liver, although very few hepatocytes proliferate and the mechanisms involved in this slow process in the absence of liver injury are not well understood [15]. Partial hepatectomy is one of the most studied animal experimental models of liver regeneration [16]. The complexity of the signaling pathways initiating and terminating this process has provided paradigms for regenerative medicine and any aspect of the mechanisms involved continues to be under active investigation.

Very little is known about the role of NOXes during liver regeneration. However, considering the function of NOX4 in inhibiting hepatocyte proliferation, we previously reported that *Nox4* expression is downregulated after partial hepatectomy in mice [10]. The aim of this work was to understand more about the role of Nox4 in this process taking advantage of experimental mouse models were *Nox4* was deleted either in all cells or specifically in hepatocytes. The study is not only of interest because it provides an advanced understanding of the molecular mechanisms that regulate liver regeneration, but also to anticipate the potential of NOX4 inhibitors as therapeutic tools in human chronic liver pathologies.

2. Material and methods

2.1. Animal models

NOX4−/− (B6.129-Nox4tm1Kkr/J) mice, generated in Dr. Krause's Laboratory [17], were obtained from Jackson Laboratories (together with the corresponding C57BL/6J wild type (WT) mice) and housed at IDIBELL (Barcelona, Spain). *Nox4* hepatocyte-specific knockout (NOX4hepKO) mice on a C57BL/6J background were generated in Dr. Török's laboratory [18] and housed at University of California Davis (Sacramento, CA, USA). See Supplementary Fig. 1A for schematic description of the mouse models. 8 to 16-week-old male and female mice, hosted under 12 h light/dark cycle with free access to food and water were used in the study. All experiments complied with the EU Directive 2010/63/UE for animal experiments and the institution's guidelines (Ethical Committee for animal experimentation of IDIBELL) and were approved by the General Direction of Environment and

Biodiversity, Government of Catalonia (experiments in NOX4−/− mice, #4589) and the Animal Care Committee of UC Davis (experiments in NOX4hepKO mice).

2.2. Experimental model of liver regeneration

2/3 partial Hepatectomy (PH) was performed as described by Higgins and Anderson [19]. Mice were euthanized at different times after surgery, as indicated in the figures. Tissue samples were immediately frozen in liquid nitrogen, cryopreserved in optimal cutting temperature compound (OCT) or fixed in 4% paraformaldehyde (PFA) and paraffin-embedded for further analysis. SHAM operated mice were used as control. Number of animals used in the study were minimized for ethical reasons. Thus, for NOX4−/− model between 3-10 animals were used per timepoint. For NOX4hepKO model between 2-3 animals per timepoint were analyzed and 2 different RNA extractions per animal liver tissue were done.

2.3. Isolation of primary hepatocytes, cell culture and treatments

Primary hepatocytes from NOX4hepKO, NOX4−/− and the corresponding WT mice were isolated by collagenase (C5138, Sigma-Aldrich, St. Louis, MO) *in situ* perfusion as previously described [20], then cultured on collagen-coated plates using Williams'E medium (W4125, Sigma-Aldrich, St. Louis, MO, USA) supplemented with 10–15% Fetal Bovine Serum (FBS), Penicillin (100 U/ml), Streptomycin (100 μg/mL) and maintained in a humidified atmosphere of 37 °C, 5% CO_2. Between 20-36 h after isolation, cells were serum-starved for 4–8 h before incubation with fresh Williams'E medium supplemented with: FBS (2% or 15%), human recombinant TGF-β1 (2 ng/mL) (616455, Calbiochem, La Jolla, CA, USA), Insulin (2 μM) (I9278, Sigma-Aldrich, St. Louis, MO, USA), Hydrocortisone (100 μM) (H2270, Sigma-Aldrich, St. Louis, MO, USA), EGF (20 ng/mL) (E9644, Sigma-Aldrich, St. Louis, MO, USA), as indicated in the figures.

2.4. Western blot analysis

Protein extracts and western blotting procedures were carried out as previously described [21]. Briefly, samples were lysed in RIPA lysis buffer supplemented with a protease inhibitors cocktail (1 mM PMSF, 5 μg/mL Leupeptin, 0.1 mM Na_3VO_4, 0.5 mM DTT, 20 mM β-Glycerolphosphate) for 1 h at 4 °C. Protein was quantified with the Bio-Rad Protein Assay Dye Reagent Concentrate (Bio-Rad Laboratories, USA). Primary antibodies are summarized in Supplementary Table I. ECL Mouse IgG and Rabbit IgG, HRP-Linked antibodies (GE Healthcare, Buckinghamshire, UK) were used at 1:2000. Densitometric analysis was performed using ImageJ software (National Institutes of Health [NIH], Bethesda, MD, USA).

2.5. Analysis of cell viability

Viable cell numbers were determined by crystal violet staining. Cells were plated in 24-well plates. After treatments, culture medium was removed, cells were washed twice with PBS and then stained with crystal violet (0.2% w/v in 2% ethanol) for 30 min. Next, staining solution was removed, and cells were washed with PBS to remove dye excess before being lysed in 10% Sodium Dodecyl Sulphate (SDS) for 30 min. Absorbance was measured at 595 nm. Results were then calculated as the percentage of viable cells relative to time zero.

2.6. Immunofluorescence staining

For fluorescence microscopy studies, cells were plated on gelatin-coated glass coverslips. Primary hepatocytes were fixed with 4% PFA and permeabilized during 2 min with 0.1% Triton X-100. Cells were incubated with the primary antibody (Supplementary Table I) during

1 h, and then with a secondary anti-rabbit antibody coupled to Alexa Fluor 488 (Molecular Probes, Eugene, OR, USA) for 1 h. Nuclei were stained using DAPI (Sigma–Aldrich, Merck, Madrid, Spain). Cells were visualized in a Nikon eclipse 80i microscope and in a Leica TSC SL spectral confocal microscope. Representative images were taken and edited in Adobe Photoshop. ImageJ software (National Institutes of Health [NIH], Bethesda, MD, USA) was used to quantify positive nuclei.

2.7. Immunohistochemistry and histology analysis

Paraffin-embedded tissues were cut into 4-μm-thick sections. Hematoxylin and Eosin (H&E) staining and immunohistochemistry (IHC) analysis were performed using standard procedures [21]. For IHC assays, sections were incubated overnight at 4 °C with the corresponding primary antibodies. Binding was developed with the Vectastain ABC KIT rabbit or mouse (PK-4001 and PK-4002, Vector Laboratories Inc., Burlingame, CA, USA). Antibodies used and conditions are summarized in Supplementary Table I. Tissues were visualized in a Nikon Eclipse 80i microscope and representative images were taken with a Nikon DS-Ri1 digital camera. ImageJ software (National Institutes of Health [NIH], Bethesda, MD, USA) was used to quantify all the parameters.

2.8. Histological analysis of hepatic lipids

Hepatic lipid drops were analyzed using Oil Red O staining. 10-μm-thick tissue sections in OCT were sequentially fixed with 4% PFA, washed with distilled water, rinsed with 60% isopropanol and washed with distilled water again. Then tissues were stained with freshly prepared Oil Red O (O1391, Sigma Aldrich, St. Louis, MO, USA) working solution (3:2 v/v in distilled water) for 10 min at room temperature. After rinsing with 60% isopropanol and washing with distilled water for 5 min, tissues were stained with Hematoxylin and mounted in Mowiol. Lipid droplets were visualized with a Nikon eclipse 80i microscope and representative images were taken with a Nikon DS-Ri1 digital camera.

2.9. Analysis of gene expression

E.Z.N.A.® Total RNA Kit II (Omega bio-tek, Norcross, GA, USA) was used following manufacturer's protocol for total RNA isolation as previously described for tissues [21] and cells [22]. Reverse transcription (RT) was carried out with random primers using High Capacity RNA to cDNA Master Mix Kit (Applied Biosystems, Foster City, CA, USA). 1 μg of total RNA per sample was used. mRNA expression levels were determined in duplicates in a LightCycler® 480 Real Time PCR System, using the LightCycler® 480 SYBR Green I Master Mix (Roche Diagnostics GmbH, Mannheim, Germany). Gene expression was normalized to *Rpl32* mRNA content. See Supplementary Table II for primers sequences.

2.10. RNA sequencing (RNA-seq)

Total RNA from *Mus musculus* was quantified by Qubit® RNA BR Assay kit (Thermo Fisher Scientific) and the RNA integrity was estimated by using RNA 6000 Nano Bioanalyzer 2100 Assay (Agilent). The RNA-seq libraries were prepared with KAPA Stranded mRNA-Seq Illumina® Platforms Kit (Roche) following the manufacturer's recommendations. Briefly, 500 ng of total RNA was used for the poly-A fraction enrichment with oligo-dT magnetic beads, following the mRNA fragmentation. The strand specificity was achieved during the second strand synthesis performed in the presence of dUTP instead of dTTP. The blunt-ended double stranded cDNA was 3′adenylated and Illumina platform compatible adaptors with unique dual indexes and unique molecular identifiers (Integrated DNA Technologies) were ligated. The ligation product was enriched with 15 PCR cycles and the final library was validated on an Agilent 2100 Bioanalyzer with the DNA 7500 assay. The libraries were sequenced on HiSeq 4000 (Illumina) with a read length of 2x51bp+17bp+8bp using HiSeq 4000 SBS kit (Illumina) and HiSeq

4000 PE Cluster kit (Illumina), following the manufacturer's protocol for dual indexing. Image analysis, base calling and quality scoring of the run were processed using the manufacturer's software Real Time Analysis (RTA 2.7.7).

Reads obtained by RNA-seq were mapped against *Mus musculus* reference genome (GRCm38) using STAR software version 2.5.3a [23] with ENCODE parameters for long reads. Annotated genes were quantified using RSEM version 1.3.0 [24] with default parameters and the annotation file from GENCODE version M15. Differential expression analysis was performed withDESeq2 v1.26.0 R package [25], using a Wald test to compare the different time points between samples WT and NOX4−/−, and adjusting for sex. We considered differentially expressed genes (DEG) those with p-value adjusted <0.05 and absolute fold-change |FC|> 1.5. The heatmap was plotted with the 'pheatmap' R package using the shrunken log2 fold change of the DEG in each time point. Time course gene expression plots were generated using the normalized counts obtained with DESeq2 and the R package 'ggplot2'. A Gene Ontology (GO) term enrichment analysis was performed with the differentially expressed genes using the R package gProfileR v0.7.0 [26], based on GO terms from the ENSEMBL database. Networks of protein-protein interactions were generated using the webtool STRINGdb (https://string-db.org/).

2.11. Statistical analyses

Data are represented as Mean ± Standard Error of the Mean (SEM). Differences between groups were compared using Student's t-test with Welch correction (when comparing two groups) or Two-way ANOVA with Tukey's multiple comparison post-hoc test (differences between groups considering two independent variables). Survival curves were estimated by Kaplan-Meier analysis, and significance was tested by the log-rank test. Statistical calculations were performed using GraphPad Prism software (GraphPad for Science Inc., San Diego, CA, USA). Differences were considered statistically significant when p < 0.05.

3. Results

3.1. Nox4 deletion accelerated liver mass recovery and parenchymal structure

NOX4−/− and NOX4hepKO mice (see Material & Methods section) were used to analyze the response to 2/3 PH. We previously reported that *Nox4* expression decreases after PH in C57BL/6 mice [10]. Here we confirmed that decrease in *Nox4* mRNA levels also occurred in NOX4floxp+/+ mice, the WT mice used for breeding and obtaining the NOX4hepKO mice (Supplementary Fig. 1B). We next analyzed how *Nox4* deletion affects the liver expression of other members of the *Nox* gene family. *Nox2* expression was not significantly different between WT and KO mice in any of the groups and its expression decreased, recovering later, in response to PH (no significant differences between WT and KO mice, Supplementary Fig. 1C). Expression of *Nox1* was very low, barely detected by Real-Time PCR and with huge fluctuations among animals (Supplementary Fig. 1D). These results indicate that the absence of *Nox4* expression is not compensated by differences in the expression of other members of the family.

When the Liver/Body weight ratio was analyzed at different times after PH, we observed a significant earlier recovery in both NOX4−/− and NOX4hepKO mice when compared to the corresponding WT mice (Fig. 1A and Supplementary Fig. 2A), which correlated with significant higher survival after PH in NOX4−/− mice (Fig. 1B). Although number of animals was lower to obtain statistical significance, a similar tendency was observed in NOX4hepKO mice (Supplementary Fig. 2B). Kinetics of the recovery after PH varied in both models of animals, probably due to the different background and different environment in the animal room (NOX4−/− mice were at IDIBELL in Barcelona; NOX4HepKO mice were at UC Davis, in CA). But it was clear that deletion of NOX4, either in the
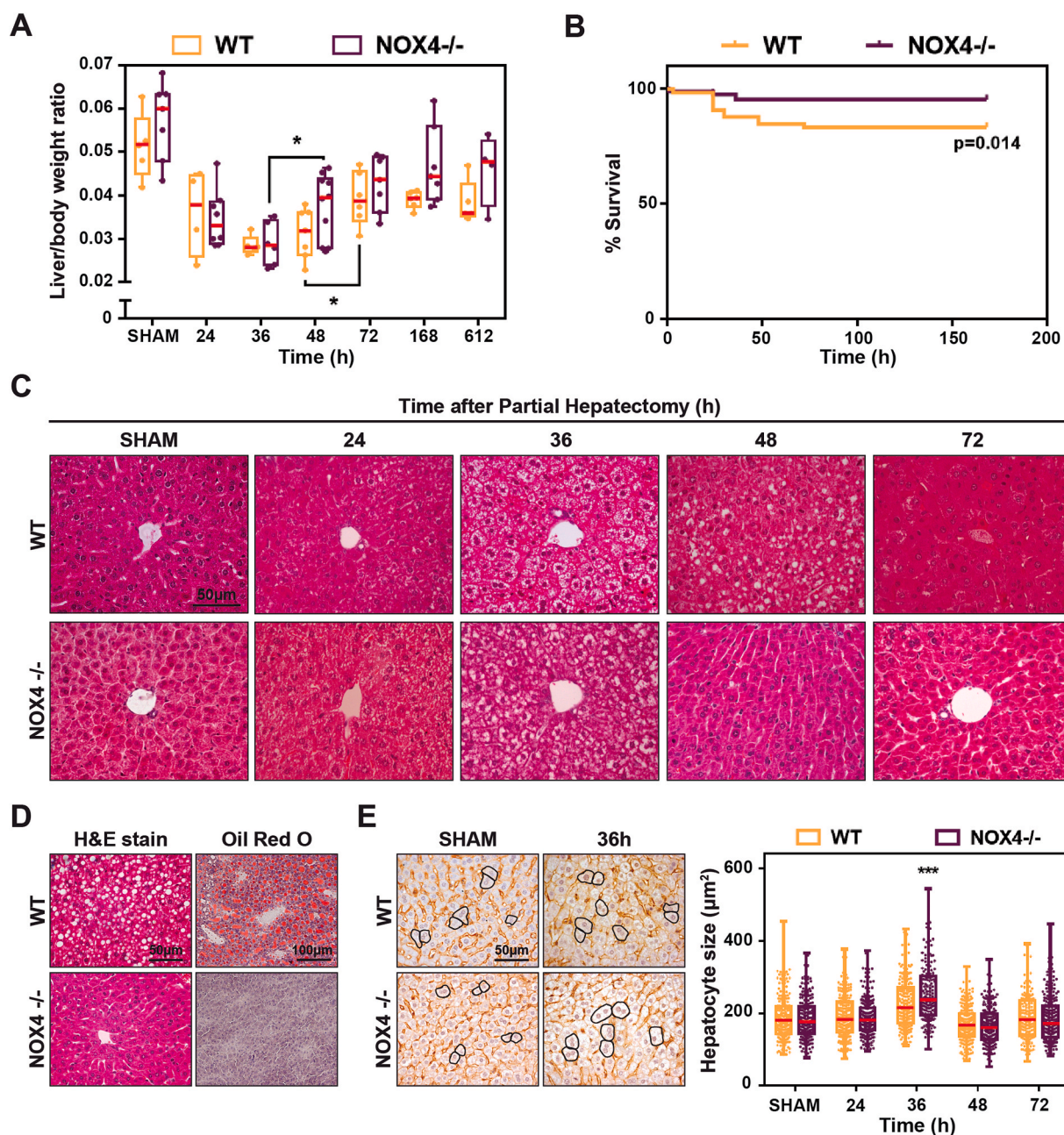
Fig. 1. Analysis of liver/body weight, mice survival and parenchymal structure in WT and NOX4−/− mice after 2/3 PH. (A) Mice were subjected to PH and sacrificed at the indicated times. Liver/Body weight ratio was calculated. Red bars represent the Median (n = 4–10 per time point). *p < 0.05 compared to previous time point. **(B)** Kaplan-Meier curve of overall survival in WT and NOX4−/− mice. **(C)** Representative images of Hematoxylin and Eosin (H&E) staining. **(D)** H&E (left) and Oil Red O staining (right). **(E)** β-catenin immunostaining performed (left) to quantify hepatocyte size (right). Red bars represent the Median. ***p < 0.001 compared to WT. (For interpretation of the references to colour in this figure legend, the reader is referred to the Web version of this article.)

whole animal or in the hepatocytes, induced an earlier recovery of the liver mass. H&E staining also revealed an earlier recovery of the parenchymal structure (Fig. 1C and Supplementary Fig. 2C). Liver steatosis, characteristic of the final G2/M phase of the hepatocyte cell cycle [12] was already resolved after 48 h in NOX4−/− mice, when maximal in WT yet (Fig. 1D). Furthermore, it was interesting to observe a transient higher size at 36 h after PH in hepatocytes from NOX4−/− mice when compared to WT animals, which was also noticed in NOX4hepKO at 24 and 72 h after PH, when compared to NOX4floxp+/+ (Fig. 1E and Supplementary Fig. 2D).

Altogether these results indicate that NOX4−/− and NOX4hepKO livers, after 2/3 PH, showed an earlier recovery of the liver parenchyma structure and regenerative steatosis, concomitant with a transient

increase in hepatocyte size. Similar results were obtained in both NOX4−/− and NOX4HepKO mice and this would indicate that *Nox4* silencing has a higher impact on the hepatocyte responses to PH, which could be expected considering that the hepatocyte is the liver cell where, under normal physiological conditions, *Nox4* expression is notably higher [6].

3.2. Accelerated and increased hepatocyte proliferation in NOX4hepKO mice after 2/3 PH

In order to analyze whether the proliferative response of the hepatocytes was altered in the absence of *Nox4* expression, we performed IHC analysis of Ki67, as a marker of a proliferative cell cycle, and

phospho-Histone3, as a more specific marker of G2/M phase, in the NOX4hepKO model. Results revealed a significant increase in the number of stained hepatocytes at 48 and 72 h after PH in NOX4hepKO when compared to NOX4floxp+/+ (Fig. 2A–B). Furthermore, NOX4-hepKO hepatocytes reached the maximal DNA synthesis at 48 h after PH, whereas NOX4floxp+/+ reached it at 72 h.

With the aim of better exploring the proliferative capacity of the hepatocytes, we isolated hepatocytes from unhepatectomized mice and cultured them to evaluate the response to FBS. Interestingly, very low concentrations of FBS (2%) allowed NOX4hepKO cells to increase almost 40% the number of viable cells in 24 h, significantly higher than the increase observed in NOX4floxp+/+ hepatocytes (Fig. 2C). This increase correlated with a much higher increase in the expression of Cyclin D1 (*Ccnd1*), Cyclin A2 (*Ccnd2*) and Cyclin B2 (*Ccnb2*) (Fig. 2D). Similar results were obtained in NOX4−/− isolated primary hepatocytes, correlating with increased Ki67 positive nuclei (Supplementary Figs. 3A–C).

These results indicate that the absence of *Nox4* expression primes hepatocytes for a faster and higher response to mitogenic signals.

3.3. Accelerated regeneration correlated with an earlier induction of *Myc* expression

We had previously described that *Myc* expression is required for an efficient liver regeneration in mice [27], as its deletion delays the recovery of the liver mass. Livers from NOX4−/− mice showed a higher increase in Myc expression 24 h after PH, and both 24 and 36 h after PH in NOX4HepKO livers (Fig. 3A) when compared to the corresponding WT mice. Western blot and IHC analysis revealed significantly higher c-Myc protein levels and c-Myc positive nuclei 36 h after PH in NOX4-hepKO hepatocytes, which confirmed the differences observed at the mRNA level (Fig. 3B–C). Interestingly, primary cultures of hepatocytes from WT and NOX4−/− mice 30 h after PH, showed much higher increase in *Myc* mRNA levels in NOX4−/− hepatocytes in response to FBS
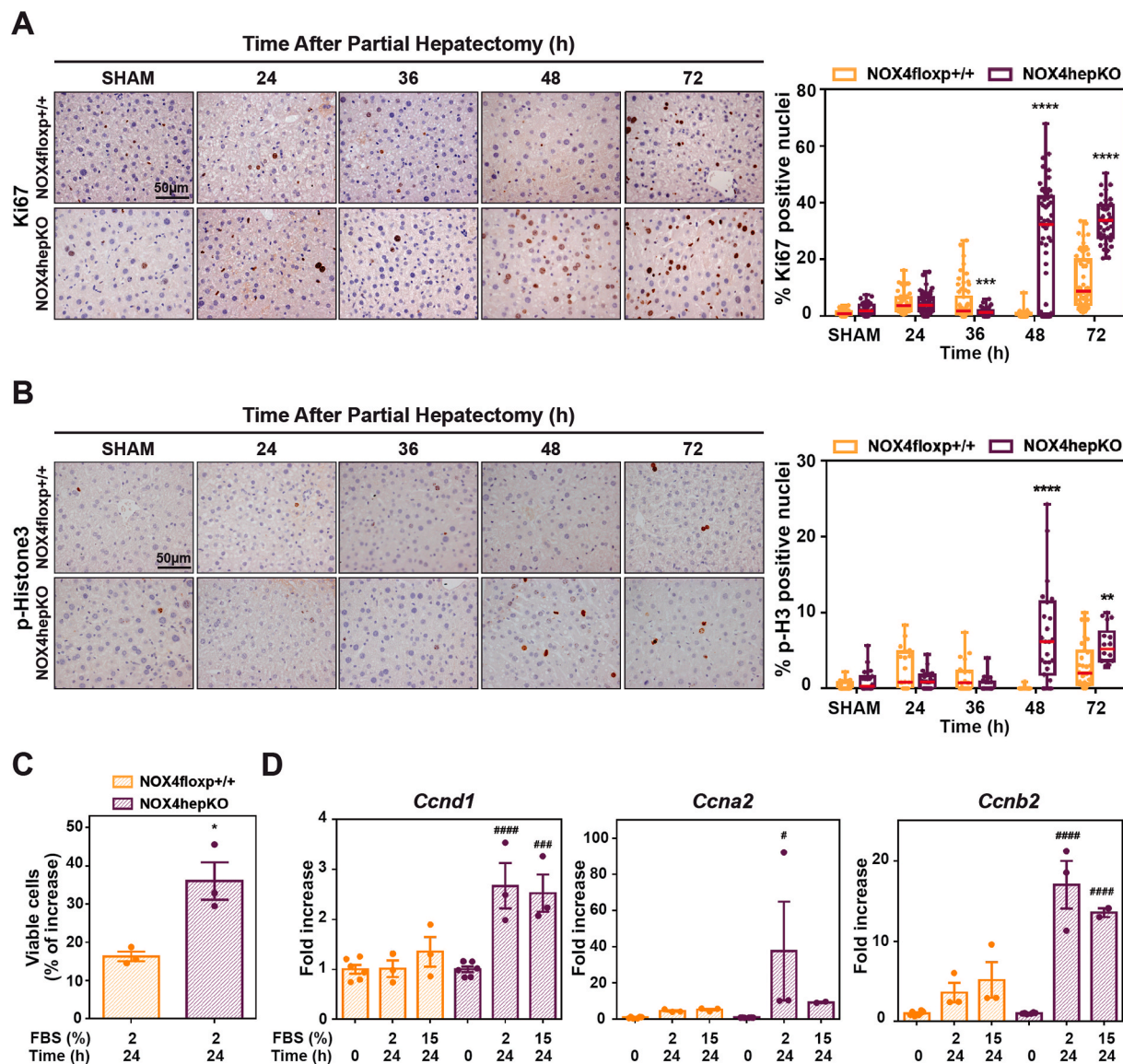

Fig. 2. Hepatocyte proliferation in NOX4floxp+/+ and NOX4hepKO analyzed in livers after PH and in cultured hepatocytes. (A) Ki67 and **(B)** p-Histone 3 immunostaining was performed in NOX4floxp+/+ and NOX4hepKO mice (left) and positive nuclei were quantified with ImageJ software (right). Red bars represent the Median. **p < 0.01, ***p < 0.001, ****p < 0.0001 compared to NOX4floxp+/+. **(C–D)** Primary hepatocytes isolated from NOX4floxp+/+ and NOX4hepKO mice were treated as indicated in the graph: C: Viable cell number represented as % of increase versus 0 time; D: RT-qPCR analysis of *Ccnd1*, *Ccna2* and *Ccnb2*. Relative expression to Rpl32 gene. In C and D, Mean ± SEM (n = 3). *p < 0.05 compared to NOX4floxp+/+ (C). #p < 0.05, ###p < 0.001, ####p < 0.0001 compared to untreated cells (D). (For interpretation of the references to colour in this figure legend, the reader is referred to the Web version of this article.)
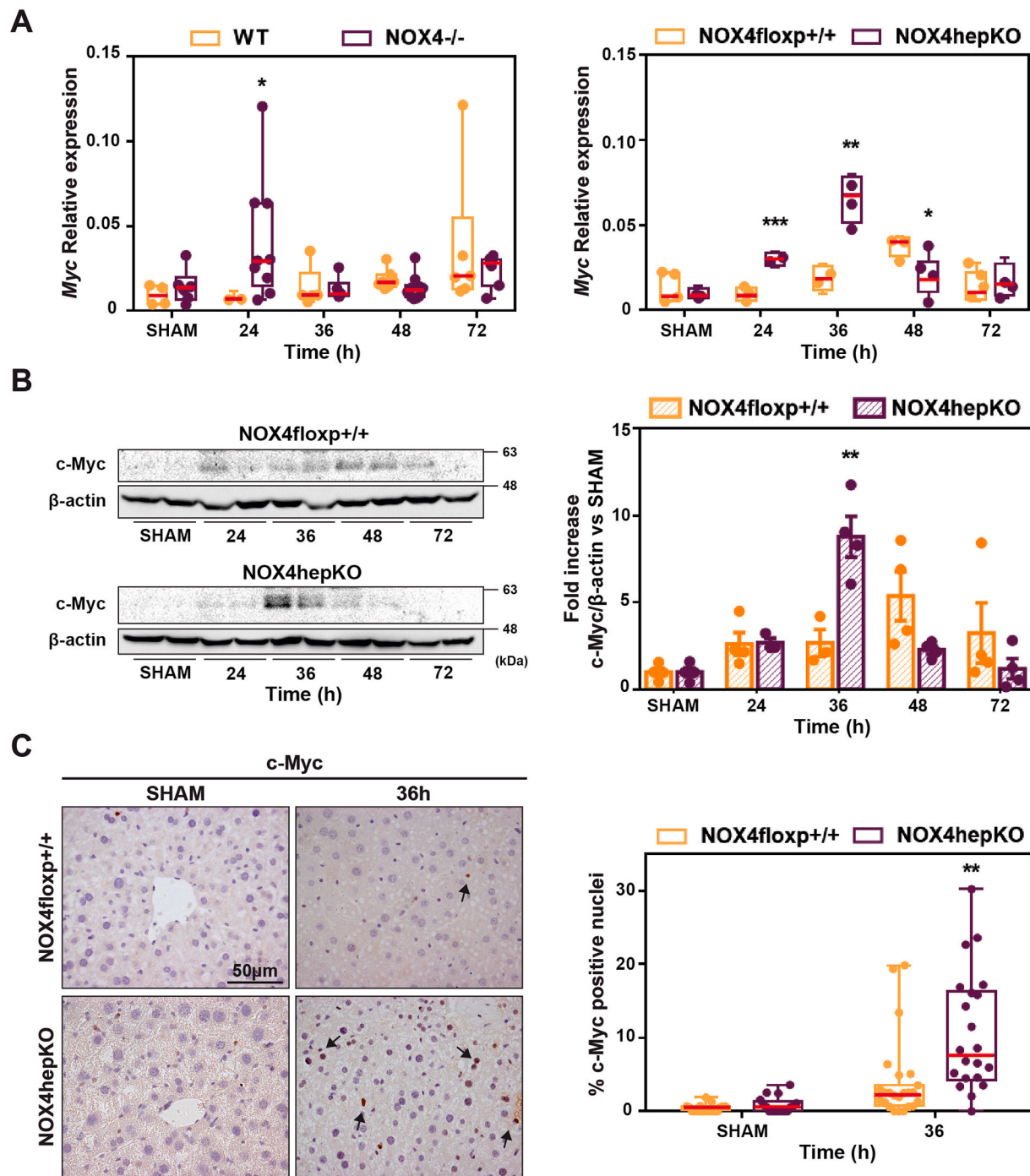
Fig. 3. Analysis of c-Myc expression in livers after PH. (A) RT-qPCR analysis of Myc in livers from NOX4−/− and NOX4hepKO mice and their respective WT controls. Relative expression to Rpl32 gene. Red bars represent the Median (n = 4–10 per time point in NOX4−/− model; n = 4–6 per time point in NOX4hepKO model). *p < 0,05, **p < 0.01, ***p < 0.001, compared to WT controls. **(B)** Analysis of c-Myc by Western Blot in NOX4floxp+/+ and NOX4hepKO livers (left) and densitometry of the different experiments performed (right): Mean ± SEM (n = 3–4 per time point). β-actin was used as a loading control. **(C)** c-Myc immunostaining in NOX4floxp+/+ and NOX4hepKO livers after 36 h PH (left); positive nuclei quantified with ImageJ software (right). Red bars represent the Median. ** < p 0.01 compared to NOX4floxp+/+. (For interpretation of the references to colour in this figure legend, the reader is referred to the Web version of this article.)

or a mitogenic mixture containing FBS, Insulin, Hydrocortisone and Epidermal Growth Factor (Supplementary Fig. 4A). These differences disappeared at 48 h after PH, where the response was even higher in the WT hepatocytes (Supplementary Fig. 4B). The increased *Myc* mRNA levels in response to mitogenic stimuli observed in NOX4−/− hepatocytes 30 h after PH correlated with relevant differences in c-Myc protein levels and higher increase in phospho-ERKs and phospho-Akt (Supplementary Fig. 4C).

All these results suggest that acceleration of liver regeneration in NOX4hepKO mice correlates with higher expression of Myc at mRNA and protein levels.

3.4. RNA-seq analysis revealed significant transcriptomic changes in NOX4−/− versus WT mice after PH

In order to better understand the molecular mechanisms that would

justify the acceleration of liver regeneration and the differences in Myc expression found in NOX4 deleted mice, we performed RNA-seq analysis of liver samples from WT and NOX4−/− mice at 6 h, 24 h, 48 h and 168 h after PH. Results revealed significant differences in gene expression between WT and NOX4−/−, particularly at 24 h after PH (Fig. 4A). The Gene Ontology (GO) enrichment analysis of the differentially expressed (DE) genes at 24 h showed that one of the significantly enriched pathways is "response to oxygen-containing compound", of which one of the genes involved is *Nox4*. The network representation of the top100 DE genes (based on adjusted p-value) that belong to the aforementioned pathway (Supplementary Fig. 5) indicated a central role for Myc, whose expression appeared up-regulated at 6 h after PH in both WT and NOX4−/− livers, but at 24 h after PH was maintained at high levels only in NOX4−/− livers, whereas in WT livers decreased at basal levels (Fig. 4B). This differential expression pattern at 24 h was also observed in other relevant proliferation-related genes that appeared in the enriched oxygen-response network connected to *Myc*, such as *Egr1*, *Sox9*, *Jund* and *Fosb*, among others (Fig. 4B and Supplementary Fig. 5). Looking for mitogenic factors whose expression revealed changes, we

only found a significant difference in the expression of a member of the Epidermal Growth Factor Receptor (EGFR) family, the Heparin Binding EGF-like Growth Factor (*Hbegf* gene), whose expression was significantly higher at both 6 and 24 h after PH in NOX4−/− mice (Fig. 4C). No significant differences were observed in the expression of other members of the EGFR family or in the Met/Hgf (Hepatocyte Growth Factor) pathway. Interestingly, the top100 DE genes from the enriched oxygen-response network revealed an axis Nox4 – Src – Myc. In fact, *Src* expression significantly increased at 24 h after PH in NOX4−/− mice, whereas in WT mice no differences were observed (Fig. 4C).

Among the potential processes that regulate hepatocyte proliferation, the TGF-β pathway is one of the most significant negative regulators of the expression of *Myc* [28]. Coincident with the transcriptional changes observed at 24 h after PH in NOX4−/− mice, we observed differences in the expression of the *Tgfb* gene family. *Tgfb1*, the main isoform expressed in the liver, showed a significant decrease in its expression at 24 h, when compared to WT mice (Fig. 4D). In contrast, *Tgfb2* showed increased expression, although in absolute terms, the level of expression is much lower than that of *Tgfb1*. Expression of *Tgfb3* did
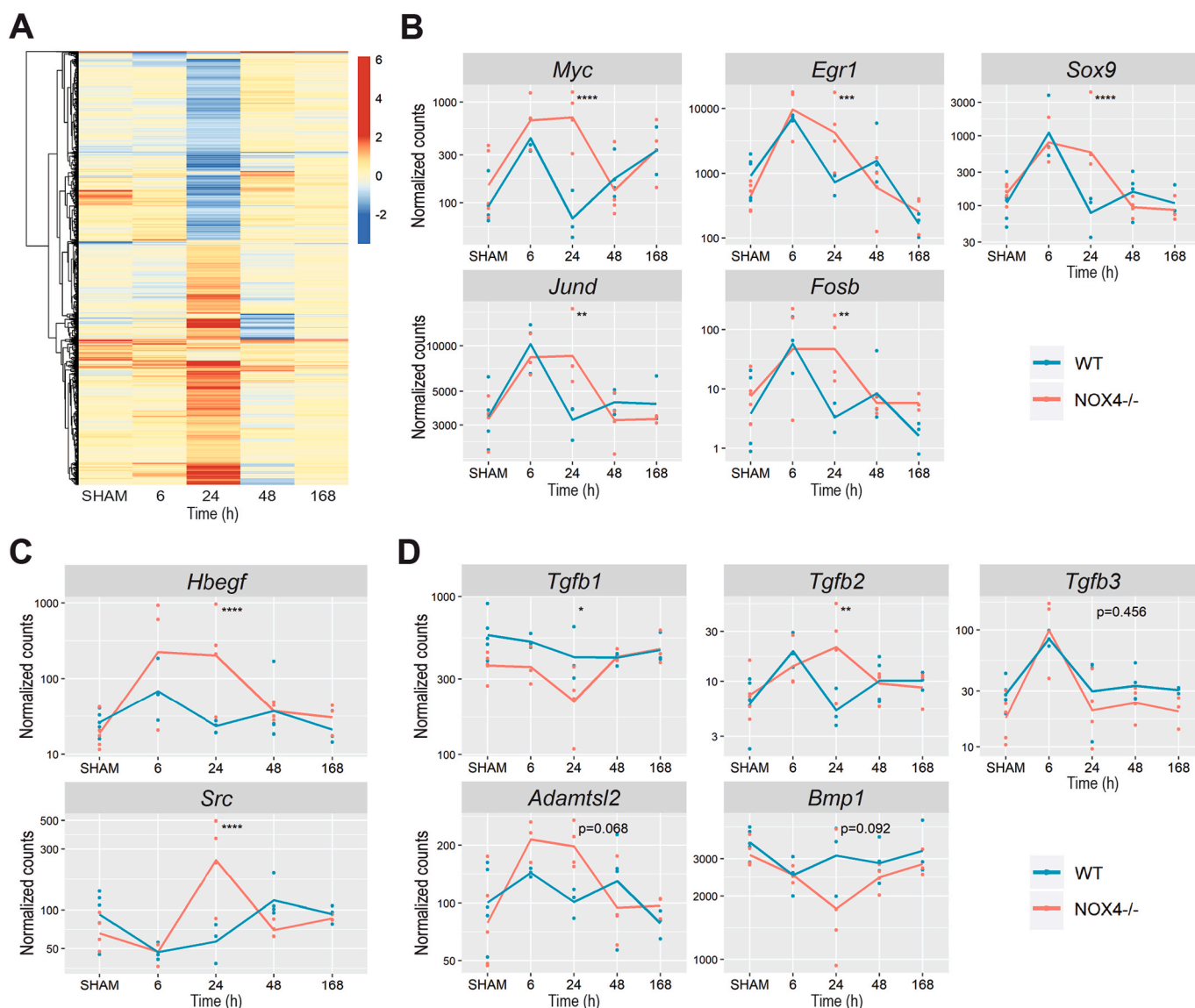

Fig. 4. Transcriptomics RNA-seq analysis of livers after PH in WT and NOX4−/− mice. (A) Heatmap showing all differentially expressed genes between NOX4−/− and WT mice in at least one time point (SHAM, 6 h, 24 h, 48 h and 168 h after PH). Changes in gene expression over time. *p < 0,05, **p < 0.01, ***p < 0.001, ****p < 0.00001. **(B)** *Myc* and other proliferation-related transcription factors; **(C)** Genes related to proliferation pathways; **D)** Genes related to the activation of the TGF-β pathway.

not show significant differences. Furthermore, we focused our attention into two genes that codify proteins whose function is related to the activation of the latent form of TGF-β1. *Adamtsl2* (a disintegrin and metalloproteinase with thrombospondin repeats-like 2), which interacts with latent TGF-β binding protein 1 (LTBP1) and anchors it in the extracellular matrix [29], showed a differential pattern of expression almost significant (adjusted p-value = 0.068) in WT versus NOX4−/− mice. Although its expression increased in WT at 6 h to decrease at 24 h, in NOX4−/− mice, the increase at 6 h was higher than in WT mice and its expression was maintained high at 24 h (Fig. 4D). Additionally, the

expression of Bmp1, which cleaves LTBPs inducing TGF-β1 activation [30], was down-regulated at 6 h after PH in both WT and NOX4−/− mice but, whereas in WT mice the levels returned to basal at 24 h, in NOX4−/− mice continued down-regulated even at lower levels at 24 h after PH (Fig. 4D). These results indicated that the TGF-β pathway could be differentially activated along the time in WT and NOX4−/− mice.
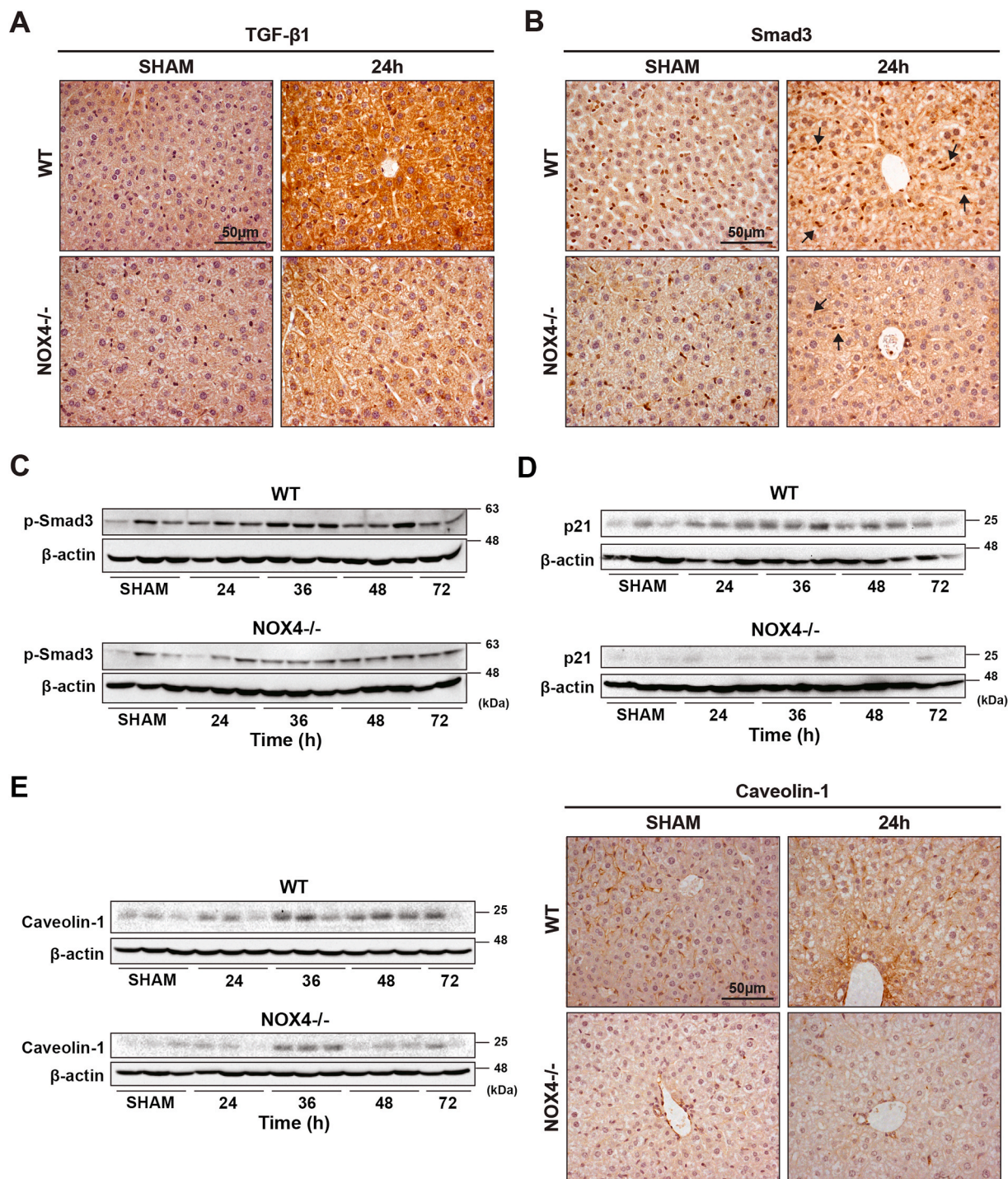

Fig. 5. Analysis of the TGF-β pathway in WT and NOX4−/− livers after PH. (A) TGF-β and **(B)** Smad3 immunostaining was performed in WT and NOX4−/− mice. Arrows indicate Smad3 positive nuclei. Analysis of p-Smad3 **(C)**, p21 **(D)** and caveolin-1 **(E)** by Western Blot (left). β-actin was used as a loading control. In **(E)**, on right, caveolin-1 immunostaining.

3.5. After PH, Nox4−/− and NOX4hepKO livers showed an earlier and increased attenuation of the TGF-β pathway

IHC analysis of the mature, active, form of TGF-β1 revealed that TGF-β1 staining considerably increased in WT liver tissues, but this increase was significantly lower in NOX4−/− and barely observed in NOX4-HepKO at 24 and 36 h after PH, respectively (Fig. 5A and Supplementary Fig. 6A, respectively). This correlated with lower number of Smad3 positive nuclei in NOX4−/− and NOX4HepKO, analyzed by IHC in liver tissues (Fig. 5B and Supplementary Fig. 6B). Western blot analysis revealed an increase in the levels of phospho-Smad3 after PH in both WT mice that was delayed and attenuated in NOX4−/− and NOX4HepKO mice (Fig. 5C and Supplementary Fig. 6C), correlating with decreased protein levels of one of its more relevant targets, p21, a cyclin-CDK

inhibitor (Fig. 5D). Previous results had demonstrated that deficiency in the liver of caveolin-1, a protein that is located in lipid rafts at the cell membrane and involved in intracellular trafficking of receptors, impairs the TGF-β pathway and improves liver regeneration [31]. Interestingly, concomitant with the alteration in the activation of the TGF-β pathway, we found lower expression of caveolin-1 in NOX4−/− mice when compared to WT mice (Fig. 5E).

Worthy to note that primary isolated hepatocytes from WT and NOX4−/− mice demonstrated a correct response to exogenous TGF-β1 inhibiting FBS-induced increase in cyclins expression and hepatocyte proliferation, analyzed as cell number or Ki67+ cells, regardless *Nox4* is expressed or not (Fig. 6A–C). Similar data were observed in primary hepatocytes from NOX4hepKO mice (results not shown). Levels of Smad2 phosphorylation in response to TGF-β1 were similar in WT and
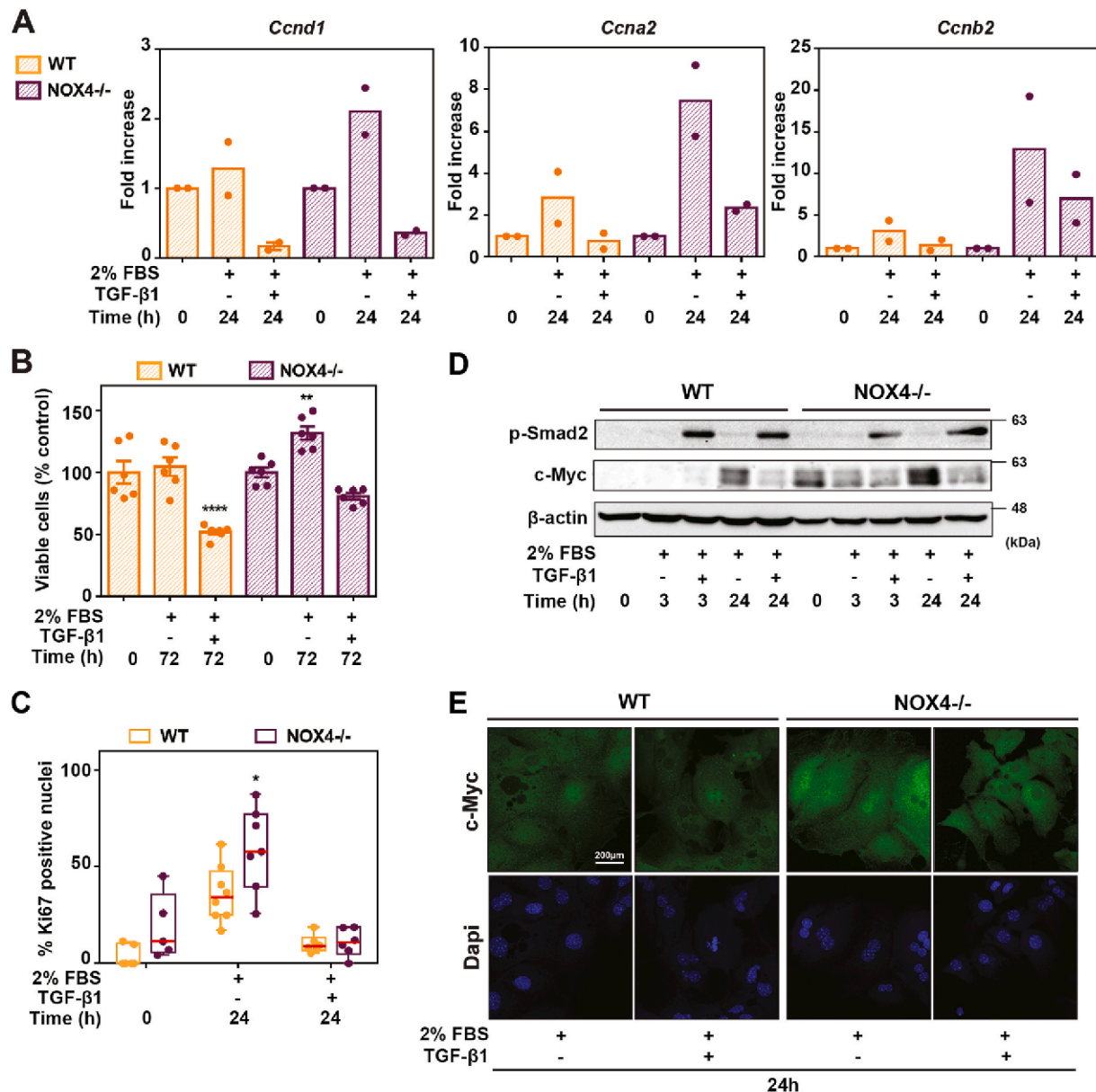

Fig. 6. Response of primary hepatocytes, isolated from WT and NOX4−/− livers, to TGF-β. Primary hepatocytes isolated from WT and NOX4−/− mice were treated with 2% FBS with or without TGF-β1 for the time indicated in each graph. A representative experiment (n = 3) is shown. **(A)** RT-qPCR analysis of *Ccnd1*, *Ccna2* and *Ccnb2*. Relative expression to *Rpl32* gene. Bars represent the Mean from 2 independent plates. **(B)** Viable cell number represented as % versus 0 time. Mean ± SEM (6 independent plates). ** < p 0.01, ****p < 0.00001 compared to untreated cells. **(C)** % of Ki67 positive nuclei. Red bars represent the Median. *< p 0.05 compared to WT cells. **(D)** Analysis of p-Smad2 and c-Myc by Western Blot. β-actin was used as a loading control. A representative experiment is shown. **(E)** c-Myc immunostaining was performed in WT and NOX4−/− mice to visualize the nuclear content. (For interpretation of the references to colour in this figure legend, the reader is referred to the Web version of this article.)

NOX4−/− hepatocytes (Fig. 6D). c-Myc levels were higher at basal levels, as well as in response to FBS, in NOX4−/− hepatocytes, but TGF-β1 showed identical capacity in inhibiting its up-regulation in WT and in NOX4−/− hepatocytes (Fig. 6D–E). These results suggest that *Nox4* is not required for TGF-β1-induced growth inhibition of cell cycle.

Altogether, *in vivo* results suggest that deletion of *Nox4* in mice accelerates liver regeneration, which correlates with changes in the transcriptional program at 24 h after PH, increased expression of *Myc* and other mitogenic-related genes and attenuation in the activation of the TGF-β pathway (Fig. 7, left). *In vitro* results indicate that hepatocytes from *Nox4* deleted mice show increased proliferative capacity, coincident with higher *Myc* and cyclins expression, in response to FBS or mitogenic signals, but they maintain the capacity to respond to TGF-β1 in terms of growth inhibition (Fig. 7, right).

4. Discussion

Liver regeneration is a complex process that, despite extensive study, is not completely understood. Numerous signaling pathways, as well as interactions among different cell types, make the process extremely attractive to glean molecular insights into the self-renewal of mature cells, a property frequently associated with stem cells. Hepatocytes appear to be cell autonomous in deciding their replication fate, which depends on reprograming different molecular events in different cell types [32]. Results here support a role for Nox4 in negatively regulating liver regeneration. Interestingly, similar results were observed in NOX4−/− and NOX4HepKO models, which indicates that the effect on liver regeneration is mostly due to *Nox4* function in hepatocytes. This is not surprising, since *Nox4* expression is two orders of magnitude higher in hepatocytes than in other liver cell types, such as stellate cells, and even one order of magnitude higher than the expression in

myofibroblasts, under fibrotic conditions [6]. In fact, residual *Nox4* expression in the livers of NOX4HepKO mice was barely detectable, lower than 0.5% when compared to the corresponding WT mice (results not shown). *Nox4* expression is down-regulated after PH in mice, which is probably necessary for an efficient hepatocyte proliferation, due to its mitoinhibitory role [10]. Down-regulation of Nox4 might occur by the increase in proliferative signals, since both EGF and HGF inhibit its expression [33,34]. In the experimental animal models used in this study, where *Nox4* expression is deleted, hepatocytes were more "primed" to respond to mitogenic signals in a fastest way. An interesting aspect to be mentioned is that although a slight increase in the liver to body weight ratio was observed in NOX4−/− mice versus WT, long-term analysis revealed that proliferation was arrested, and the liver reached a size that did not overcome the initial one. Many signals contribute to the termination of liver regeneration and maintenance of standard liver mass [15] and *Nox4* does not appear to be essential for this process.

Trying to analyze the potential mechanism that could be regulated by *Nox4*, we found a stronger activation of the c-Myc pathway *in vivo*, as well as in hepatocytes in culture. c-Myc is a relevant regulator of the expression of cell-cycle related genes [35] and it has been suggested that hepatocytes require up-regulation of *Myc* after PH to efficiently exit G_0 [27]. Interestingly, c-Myc not only regulates hepatocyte proliferation, but also cell size [27]. Here, the increase in *Myc* expression in *Nox4* deleted mice correlated with a significant increase in hepatocyte cell size. It is well known that hypertrophy without cell division precedes proliferation after 2/3 PH and almost equally contribute to regeneration [36]. The increase in cell size observed at 24–36 h after PH in both mouse models of *Nox4* deletion correlated with the peak of *Myc* expression and preceded the peak of cell proliferation. Furthermore, c-Myc could also contribute to maintain lipid homeostasis, through
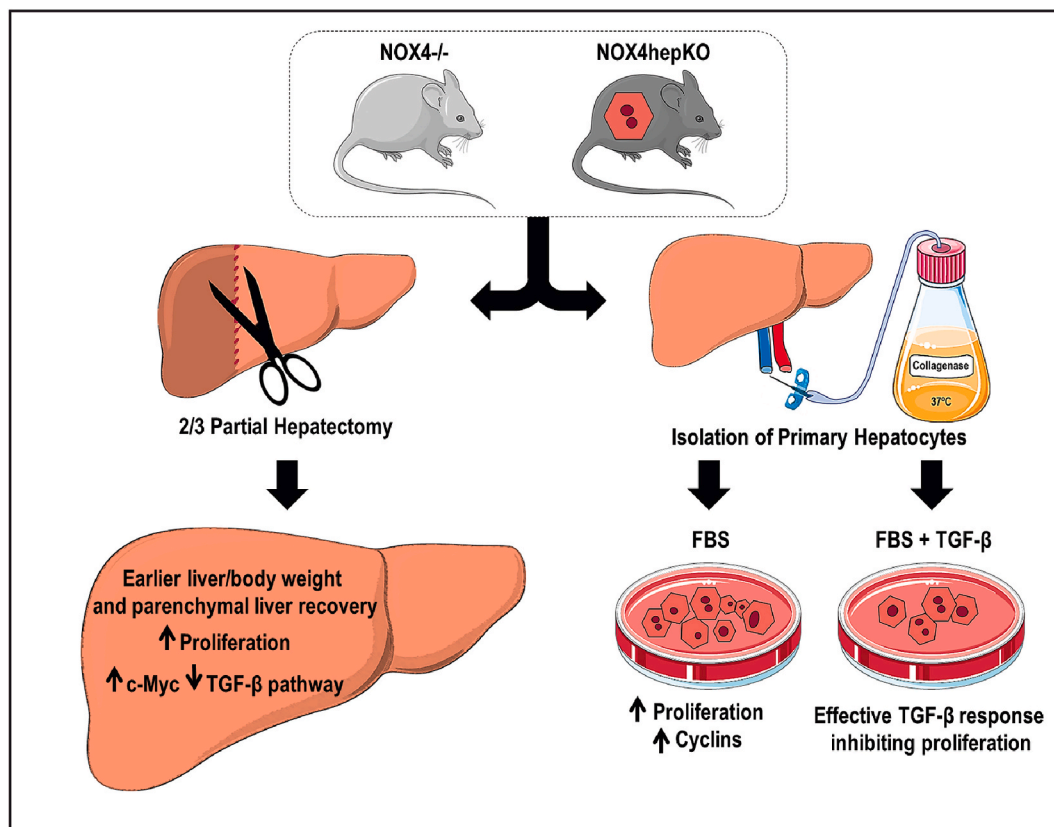

Fig. 7. Summary diagram. Left: After partial hepatectomy, Nox4 deleted mice show earlier liver/body weight recovery, concomitant with higher proliferation, up-regulation of Myc and down-regulation of the TGF-β pathway. **Right**: Primary hepatocytes from Nox4 deleted mice show higher proliferation in response to FBS, while maintaining TGF-β-induced growth inhibitory response.

activating fatty acid oxidation for energy demands [37]. Indeed, over-activation of c-Myc could also explain the faster recovery of regenerative liver steatosis observed in NOX4−/− mice.

RNA-seq analysis revealed significant differences at the transcriptional level after PH in NOX4−/− mice when compared to WT mice. The network of the top100 differentially expressed genes at 24 h from the "response to oxygen-containing compound" pathway located *Myc* in a node of proliferation-related genes whose expression decays at 24 h after PH in WT mice, but it is maintained, or even enhanced, at this same time in NOX4−/− mice. Significant increase in the expression of *Hbegf*, a member of the EGFR ligands family previously shown to have potent protective and mitogenic effects in liver regeneration [38], was observed specifically at 24 h after PH in NOX4−/− mice, as well as the expression of *Src*, a member of the cytosolic family of tyrosine kinase proteins.

Different evidences support a role for TGF-β inhibiting *Myc* expression [28]. In hepatocytes, TGF-β1 inhibits growth and induces apoptosis in hepatocytes [39,40] and one of its earlier effects is down-regulation of the mitogen-induced *Myc* early expression [41], without an effect on the expression of other proto-oncogenes, such as *Hras*. Here, we found that acceleration of liver regeneration and increased expression of *Myc* in both mice models of *Nox4* deletion could be attributed to the attenuation of the TGF-β pathway. It was proposed that transient escape of regenerative hepatocytes from TGF-β-induced growth inhibition and apoptosis is achieved through decrease in the expression of TGF-β receptors [42] and the acquisition of survival signals [43]. Nevertheless, a mitoinhibitory response to TGF-β is still present in regenerating hepatocytes, since intravenous TGF-β1/2 reversibly inhibits the proliferative response of the liver to PH [44] and inactivation of the TGF-β pathway results in an increased proliferative response after PH [45]. Anti-TGF-β molecular intervention also facilitates liver regeneration upon acute dimethylnitrosamine (DMN) or CCl4 induced injury [46,47]. Results here indicate that in the absence of *Nox4* expression, the TGF-β pathway was attenuated in hepatocytes, which could contribute to the acceleration of the liver regeneration.

Although it is well known that TGF-β up-regulates NOX4 in stellate cells and hepatocytes [6,7,9], it is less well recognized that NOX4 can reciprocally regulate TGF-β/SMAD signaling. The RNA-seq experiment revealed the potential mechanism responsible for this effect, which appears to be indirect, related to other cell-cell interactions and effects on extracellular matrix. On one side, TGF-β ligands, which are expressed in non-parenchymal liver cells, showed differences between WT and NOX4−/− mice. *Tgfb1* expression was significantly lower at 24 h after PH in NOX4−/− mice when compared to WT mice. Another member of the family, *Tgfb2*, by contrast, showed higher levels but its expression was much lower than that of *Tgfb1*. TGF-β2 up-regulation correlates with fibrotic markers and play a prominent role in biliary liver diseases [48, 49], but its expression during liver regeneration is 10 times lower than that of TGF-β1 [50]. Considering that Smad3 phosphorylation was clearly decreased in *Nox4* deleted mice, the decrease in *Tgfb1* expression appears to have a higher impact that the increase in *Tgfb2* expression. Furthermore, activation of the latent TGF-β1 at the extracellular matrix may be affected by the absence of *Nox4*. In support of this hypothesis, *Adamtsl2*, which interacts with latent LTBP1 and anchors it to the extracellular matrix, showed an increase in its expression in NOX4−/− mice at 24 h after PH. Mutations in *ADAMTSL2* have been described in human diseases and lead to dysregulation of TGF-β signaling correlating with increase in active TGF-β1 [29]. Furthermore, the expression of *Bmp1*, a metalloproteinase that cleaves LTBPs releasing the active form of TGF-β1 [30], is decreased at 24 h after PH in NOX4−/− mice. Altogether, these results reveal a mutual regulation between *Nox4* and the TGF-β pathway: TGF-β1 is the main up-regulator of *Nox4* expression and *Nox4* could contribute to modulate the process of TGF-β1 activation. A fine down-regulation of *Nox4* expression during the first hours after PH may be necessary for an efficient hepatocyte proliferation and liver regeneration.

Despite these *in vivo* observations, *in vitro* experiments in NOX4−/− hepatocytes indicated that they continue to respond to TGF-β1 in terms of growth inhibition, Smad2 phosphorylation or down-regulation of *Myc* levels, maintaining its suppressor function. Indeed, *Nox4* deletion increases the hepatocyte mitogenic response and modify the process of TGF-β1 activation *in vivo*, which increases the fastest and more efficient response of hepatocytes to mitogenic signals during liver regeneration. But the mechanism of response to extracellular TGF-β1 is not altered. *NOX4* does not appear to be required for TGF-β1-mediated *Myc* down-regulation, which was proposed to be a SMAD-4 dependent mechanism [51]. This could explain the arrest of proliferation *in vivo* long time after PH, when the expression/activation of TGF-β1, or other members of the family, increase.

5. Conclusions

NOX4 has been proposed as a potential therapeutic target in human liver chronic diseases [8], due to its role mediating TGF-β actions in liver fibrosis [5]. Results presented here would support the potential benefit of its inhibition also to favor liver regeneration from the remaining healthy hepatocytes. *Nox4* does not appear to be essential for the termination of liver regeneration, which reinforces its potential as therapeutic target, without adverse effects. Nevertheless, considering that inhibiting NOX4 could be detrimental under preneoplastic conditions, NOX4 inhibition must be considered at early stages of chronic inflammation and fibrosis in the liver.

Author contributions

I.F. and N.J.T. conceived and designed the study.

M.H.-I. acquired data, with the participation in some experiments of J.L.-L., E.C.-M., D.C.-D., E.G.-S and J.X.J.

M.G performed the RNA-seq.

B.M.-M. and A.E.-C. analyzed and interpreted the RNA-seq data.

M.H.-I., J.L.-L. and I.F. analyzed and interpreted data and drafted the article, which was revised it critically for important intellectual content by E.G.-S, N.J.T. and V.J.

All authors participated in manuscript revision and final approval of the version to be submitted.

Declaration of competing interest

The authors declare that they have no known competing financial interests or personal relationships that could have appeared to influence the work reported in this paper.

Acknowledgements

Appendix A. Supplementary data

Supplementary data to this article can be found online at https://doi.org/10.1016/j.redox.2020.101841.

References

[1] H. Buvelot, V. Jaquet, K.H. Krause, Mammalian NADPH oxidases, Methods Mol. Biol. 1982 (2019) 17–36.

[2] K.D. Martyn, L.M. Frederick, K. von Loehneysen, M.C. Dinauer, U.G. Knaus, Functional analysis of Nox4 reveals unique characteristics compared to other NADPH oxidases, Cell. Signal. 18 (1) (2006) 69–82.

[3] L. Serrander, L. Cartier, K. Bedard, B. Banfi, B. Lardy, O. Plastre, et al., NOX4 activity is determined by mRNA levels and reveals a unique pattern of ROS generation, Biochem. J. 406 (1) (2007) 105–114.

[4] J.X. Jiang, N. Török, NADPH oxidases in chronic liver diseases, Adv Hepatol 2014 (2014) 1–8.

[5] E. Crosas-Molist, E. Bertran, I. Fabregat, Cross-talk between TGF-β and NADPH oxidases during liver fibrosis and hepatocarcinogenesis, Curr. Pharmaceut. Des. 21 (41) (2015) 5964–5976.

[6] P. Sancho, J. Mainez, E. Crosas-Molist, C. Roncero, C.M. Fernández-Rodriguez, F. Pinedo, et al., NADPH oxidase NOX4 mediates stellate cell activation and hepatocyte cell death during liver fibrosis development, PloS One 7 (9) (2012), e45285.

[7] J.X. Jiang, X. Chen, N. Serizawa, C. Szyndralewiez, P. Page, K. Schröder, et al., Liver fibrosis and hepatocyte apoptosis are attenuated by GKT137831, a novel NOX4/NOX1 inhibitor in vivo, Free Radic. Biol. Med. 53 (2) (2012) 289–296.

[8] E. Crosas-Molist, I. Fabregat, Role of NADPH oxidases in the redox biology of liver fibrosis, Redox Biol. 6 (2015) 106–111.

[9] I. Carmona-Cuenca, C. Roncero, P. Sancho, L. Caja, N. Fausto, M. Fernández, et al., Upregulation of the NADPH oxidase NOX4 by TGF-beta in hepatocytes is required for its pro-apoptotic activity, J. Hepatol. 49 (6) (2008) 965–976.

[10] E. Crosas-Molist, E. Bertran, P. Sancho, J. López-Luque, J. Fernando, A. Sánchez, et al., The NADPH oxidase NOX4 inhibits hepatocyte proliferation and liver cancer progression, Free Radic. Biol. Med. 69 (2014) 338–347.

[11] E. Crosas-Molist, E. Bertran, I. Rodriguez-Hernandez, C. Herraiz, G. Cantelli, À. Fabra, et al., The NADPH oxidase NOX4 represses epithelial to amoeboid transition and efficient tumour dissemination, Oncogene 36 (21) (2017) 3002–3014.

[12] J. López-Luque, I. Fabregat, Revisiting the liver: from development to regeneration - what we ought to know!, Int. J. Dev. Biol. 62 (6–7-8) (2018) 441–451.

[13] N. Fausto, J.S. Campbell, K.J. Riehle, Liver regeneration, Hepatology 43 (S1) (2006) S45–53.

[14] G.K. Michalopoulos, Advances in liver regeneration, Expet Rev. Gastroenterol. Hepatol. 8 (8) (2014) 897–907.

[15] G.K. Michalopoulos, Hepatostat: liver regeneration and normal liver tissue maintenance, Hepatology 65 (4) (2017) 1384–1392.

[16] G.K. Michalopoulos, Liver regeneration after partial hepatectomy, Am. J. Pathol. 176 (1) (2010) 2–13.

[17] S. Carnesecchi, C. Deffert, Y. Donati, O. Basset, B. Hinz, O. Preynat-Seauve, et al., A key role for NOX4 in epithelial cell death during development of lung fibrosis, Antioxidants Redox Signal. 15 (3) (2011) 607–619.

[18] A. Bettaieb, J.X. Jiang, Y. Sasaki, T.-I. Chao, Z. Kiss, X. Chen, et al., Hepatocyte nicotinamide adenine dinucleotide phosphate reduced oxidase 4 regulates stress signaling, fibrosis, and Insulin sensitivity during development of steatohepatitis in mice, Gastroenterology 149 (2) (2015) 468–480, e10.

[19] G.M. Higgins, R.M. Anderson, Experimental pathology of liver: restoration of liver of white rat following partial surgical removal, Arch. Pathol. 12 (1931) 186–202.

[20] E. Gonzalez-Sanchez, D. Firrincieli, C. Housset, N. Chignard, Expression patterns of nuclear receptors in parenchymal and non-parenchymal mouse liver cells and their modulation in cholestasis, Biochim. Biophys. Acta (BBA) - Mol. Basis Dis. 1863 (7) (2017) 1699–1708.

[21] J. López-Luque, D. Caballero-Díaz, A. Martinez-Palacián, C. Roncero, J. Moreno-Càceres, M. García-Bravo, et al., Dissecting the role of epidermal growth factor receptor catalytic activity during liver regeneration and hepatocarcinogenesis, Hepatology 63 (2) (2016) 604–619.

[22] J. López-Luque, E. Bertran, E. Crosas-Molist, O. Maiques, A. Malfettone, L. Caja, et al., Downregulation of epidermal growth factor receptor in hepatocellular carcinoma facilitates transforming growth factor-β-induced epithelial to amoeboid transition, Canc. Lett. 464 (2019) 15–24.

[23] A. Dobin, C.A. Davis, F. Schlesinger, J. Drenkow, C. Zaleski, S. Jha, et al., STAR: ultrafast universal RNA-seq aligner, Bioinformatics 29 (1) (2013) 15–21.

[24] B. Li, C.N. Dewey, RSEM: accurate transcript quantification from RNA-Seq data with or without a reference genome, BMC Bioinf. 12 (1) (2011) 323.

[25] M.I. Love, W. Huber, S. Anders, Moderated estimation of fold change and dispersion for RNA-seq data with DESeq2, Genome Biol. 15 (12) (2014) 550.

[26] J. Reimand, M. Kull, H. Peterson, J. Hansen, J. g Vilo, Profiler—a web-based toolset for functional profiling of gene lists from large-scale experiments, Nucleic Acids Res. 35 (suppl_2) (2007) W193–200.

[27] E. Baena, A. Gandarillas, M. Vallespinos, J. Zanet, O. Bachs, C. Redondo, et al., c-Myc regulates cell size and ploidy but is not essential for postnatal proliferation in liver, Proc. Natl. Acad. Sci. Unit. States Am. 102 (20) (2005) 7286–7291.

[28] J.P. Frederick, N.T. Liberati, D.S. Waddell, Y. Shi, X.-F. Wang, Transforming growth factor -mediated transcriptional repression of c-myc is dependent on direct binding of Smad3 to a novel repressive Smad binding element, Mol. Cell Biol. 24 (6) (2004) 2546–2559.

[29] C.L. Goff, F. Morice-Picard, N. Dagoneau, L.W. Wang, Y.J. Crow, F. Bauer, et al., ADAMTSL2 mutations in geleophysic dysplasia demonstrate a role for ADAMTS-like proteins in TGF-β bioavailability regulation, Nat. Genet. 40 (9) (2008) 1119–1123.

[30] G. Ge, D.S. Greenspan, BMP1 controls TGFβ1 activation via cleavage of latent TGFβ-binding protein, J. Cell Biol. 175 (1) (2006) 111–120.

[31] R. Mayoral, L. Bosca, P. Martín-Sanz, Impairment of transforming growth factor beta signaling in caveolin-1-deficient hepatocytes: role in liver regeneration, J. Biol. Chem. 285 (6) (2010) 3633–3642.

[32] N. Fausto, J.S. Campbell, K.J. Riehle, Liver regeneration, J. Hepatol. 57 (3) (2012) 692–694.

[33] I. Carmona-Cuenca, B. Herrera, J.-J. Ventura, C. Roncero, M. Fernández, I. Fabregat, EGF blocks NADPH oxidase activation by TGF-β in fetal rat hepatocytes, impairing oxidative stress, and cell death, J. Cell. Physiol. 207 (2) (2006) 322–330.

[34] Z. Cao, T. Ye, Y. Sun, G. Ji, K. Shido, Y. Chen, et al., Targeting the vascular and perivascular niches as a regenerative therapy for lung and liver fibrosis, Sci. Transl. Med. 9 (405) (2017), eaai8710.

[35] G. Bretones, M.D. Delgado, J. León, Myc and cell cycle control, Biochim. Biophys. Acta Gene Regul. Mech. 1849 (5) (2015) 506–516.

[36] Y. Miyaoka, K. Ebato, H. Kato, S. Arakawa, S. Shimizu, A. Miyajima, Hypertrophy and unconventional cell division of hepatocytes underlie liver regeneration, Curr. Biol. 22 (13) (2012) 1166–1175.

[37] L.R. Edmunds, P.A. Otero, L. Sharma, S. D'Souza, J.M. Dolezal, S. David, et al., Abnormal lipid processing but normal long-term repopulation potential of myc-/-hepatocytes, Oncotarget 7 (21) (2016) 30379–30395.

[38] N.C. Khai, T. Takahashi, H. Ushikoshi, S. Nagano, K. Yuge, M. Esaki, et al., In vivo hepatic HB-EGF gene transduction inhibits Fas-induced liver injury and induces liver regeneration in mice: a comparative study to HGF, J. Hepatol. 44 (6) (2006) 1046–1054.

[39] B.I. Carr, I. Hayashi, E.L. Branum, H.L. Moses, Inhibition of DNA synthesis in rat hepatocytes by platelet-derived type β transforming growth factor, Canc. Res. 46 (5) (1986) 2330–2334.

[40] A. Sánchez, A.M. Álvarez, M. Benito, I. Fabregat, Apoptosis induced by transforming growth factor-β in fetal hepatocyte primary cultures: involvement of reactive oxygen intermediates, J. Biol. Chem. 271 (13) (1996) 7416–7422.

[41] A. Sanchez, A.M. Alvarez, M. Benito, I. Fabregat, Transforming growth factor-beta modulates growth and differentiation of fetal hepatocytes in primary culture, J. Cell. Physiol. 165 (2) (1995) 398–405.

[42] R.S. Chart, D.T. Price, S.R. Sue, W.C. Meyers, R.L. Jirtle, Down-regulation of transforming growth factor beta receptor type I, II, and III during liver regeneration, Am. J. Surg. 169 (1) (1995) 126–132.

[43] B. Herrera, A.M. Álvarez, J. Beltrán, F. Valdés, I. Fabregat, M. Fernández, Resistance to TGF-β-induced apoptosis in regenerating hepatocytes, J. Cell. Physiol. 201 (3) (2004) 385–392.

[44] W.E. Russell, R.J. Coffey Jr., A.J. Ouellette, H.L. Moses, Type β transforming growth factor reversibly inhibits the early proliferative response to partial hepatectomy in the rat, Proc. Natl. Acad. Sci. Unit. States Am. 85 (14) (1988) 5126–5130.

[45] J. Romero-Gallo, E.G. Sozmen, A. Chytil, W.E. Russell, R. Whitehead, W.T. Parks, et al., Inactivation of TGF-β signaling in hepatocytes results in an increased proliferative response after partial hepatectomy, Oncogene 24 (18) (2005) 3028–3041.

[46] T. Nakamura, T. Ueno, M. Sakamoto, R. Sakata, T. Torimura, O. Hashimoto, et al., Suppression of transforming growth factor-β results in upregulation of transcription of regeneration factors after chronic liver injury, J. Hepatol. 41 (6) (2004) 974–982.

[47] S. Karkampouna, M.-J. Goumans, P. ten Dijke, S. Dooley, M. Kruithof-de Julio, Inhibition of TGFβ type I receptor activity facilitates liver regeneration upon acute CCl4 intoxication in mice, Arch. Toxicol. 90 (2) (2016) 347–357.

[48] A. Dropmann, T. Dediulia, K. Breitkopf-Heinlein, H. Korhonen, M. Janicot, S. N. Weber, et al., TGF-β1 and TGF-β2 abundance in liver diseases of mice and men, Oncotarget 7 (15) (2016) 19499–19518.

[49] A. Dropmann, S. Dooley, B. Dewidar, S. Hammad, T. Dediulia, J. Werle, et al., TGF-β2 silencing to target biliary-derived liver diseases, Gut 69 (9) (2020) 1677–1690.

[50] S.B. Jakowlew, D. Danielpour, J. Wu, A.B. Roberts, N. Fausto, Transforming growth factor-β (TGF- β) isoforms in rat liver regeneration: messenger RNA expression and activation of latent TGF- β, Cell Regul. 2 (7) (1991) 535–548.

[51] M.J. Calonge, J. Massague, Smad4/DPC4 silencing and hyperactive ras jointly disrupt transforming growth factor-beta antiproliferative responses in colon cancer cells, J. Biol. Chem. 274 (47) (1999) 33637–33643.